DuRSAAM

Proceedings of the
DuRSAAM 2023 Symposium

ADVANCING ALKALI-ACTIVATED MATERIALS

Edited by Stijn Matthys and Alessandro Proia

Advancing Alkali-Activated Materials

Proceedings of the DuRSAAM 2023 Symposium

The PhD Training Network on Durable, Reliable and Sustainable Structures with Alkali-Activated Materials

This project has received funding from the European Union's Horizon 2020 research and innovation programme under grant agreement No 813596 DuRSAAM.

ISBN 9789082526844

D/2023/15076/01

Visit the DuRSAAM web site at
http://www.dursaam.eu

Contents

Preface

Concrete is a popular and efficient building material. However, being used that widely all over the world, its environmental impact sums up to large numbers, among which 8% of the carbon dioxide emissions and over 20% of earth's natural resources excavated for use as construction minerals. The upside of this observation is that when improving the environmental impact of concrete, significant improvements can be made in terms of reducing carbon dioxide emissions and using less primary raw materials. This in line with the goals set forth internationally in terms of Circular Economy and Green Deal policies. In the family of greener concrete solutions, alkali-activated concrete is emerging rapidly being compatible with current solutions for structural concrete and whereby pilot projects and applications have already been realized in various countries. The characterization and application of alkali-activated concrete remains however less advanced than traditional concrete, stressing the importance to provide a forum for researchers, professional practitioners, and governmental staff to share ideas and be challenged. This is the main goal behind organizing this DuRSAAM 2023 Symposium.

During the COVID crisis people longed for an improved social life and in response we opted to organize the DuRSAAM 2023 Symposium as an in-person event. Though the COVID crisis is gradually diminishing, the world is not free from other crises and our feeling of 'normality' has no doubt changed. So apologies to those who requested for a hybrid event, but we strongly felt to opt for collaborative participation through face-to-face interactions and to organise this event at a scale avoiding parallel sessions. Research on alkali-activated materials did not stop over the last years, rather the contrary, so that we were confident to excite many researchers to participate in-person, despite everyone being very busy. With more than 100 participants in this symposium, our expectations were met for a lively event of 3 days in exchanging knowledge, facilitating alkali-activated concrete more widely into practice, and jointly moving forward the agenda for more circular concrete.

The DuRSAAM 2023 Symposium in fact celebrates the end of an exciting and successful EU-project, titled 'PhD Training Network on Durable, Reliable and Sustainable Structures with Alkali-Activated Materials (DuRSAAM)' and coordinated by Ghent University. In line with the scope of this European project, that has run from 2018 till 2023, the DuRSAAM2023 Symposium focusses on new developments in all aspects of alkali-activated concrete, sometimes also referred to as geopolymer concrete. The programme is focussed on bringing stakeholders together along the triple helix academia – industry – government, to foster developments in circular concrete. As such we are proud that we have about equal amount of participants from academia versus industry and government, joining from 8 till 10 February 2023 at this symposium hosted by Ghent University and all the DuRSAAM project partners. This highlights the growing and wider interest in alkali-activated concrete and bringing alkali-activated research & technology into practice.

As coordinators of the DuRSAAM project and chairs of this symposium, we can happily say that the organization of the DuRSAAM 2023 Symposium has been made possible with the help of a motivated organizing team and scientific committee. You can find their names as part of these proceedings and we are grateful for their enthusiasm and support. Furthermore, this symposium was only feasible with the help from our partners fwo, *fib* and RILEM, next to the assistance provided by Ghent University, the City of Ghent and the North West Europe Interreg project URBCON. The latter being a sitter project of DuRSAAM, focussed on demonstration of alkali-activated concrete products in the urban environment. A special word of thanks goes to the DuRSAAM PhD fellows, who truly made the DuRSAAM project unique and who will without any doubt make a difference for the future.

These open source proceedings collect the short papers, as presented by the participants during the symposium, and provides researchers, building professionals and stakeholders recent insights on advancing alkali-activated materials. Enjoy reading!

Prof. Stijn Matthys, symposium chair
Dr. Alessandro Proia, symposium co-chair
Ghent, 2023

Scientific and organizing committees

SCIENTIFIC COMMITTEE

Prof. Stijn Matthys, Ghent University, Belgium (Chair)

Dr. Alessandro Proia, Ghent University, Belgium (Co-chair)

Prof. Guang Ye, Technische Universiteit Delft, The Netherlands

Prof. Geert De Schutter, Ghent University, Belgium

Prof. Frank Dehn, Karlsruhe Institute of Technology, Germany

Prof. John Provis, University of Sheffield, UK

Prof. Marijana Serdar, University of Zagreb, Croatia

Prof. Thanasis Triantafillou, University of Patras, Greece

Prof. Catherine Papanicolau, University of Patras, Greece

Prof. Guillaume Habert, ETH Zurich, Switzerland

Prof. Hubert Rahier, Vrije Universiteit Brussel, Belgium

Dr. Emanuela Manolova, Aurubis Group, Bulgaria

Yubo Sun, Ghent University, Belgium

Zhiyuan Xu, Technische Universiteit Delft, the Netherlands

Luiz Cesar Miranda de Lima Junior, Technische Universiteit Delft, the Netherlands

Laura Rossi, Karlsruhe Institute of Technology, Germany

Ivana Krajnovic, Ghent University, Belgium

Lazar Azdejkovic, University of Patras, Greece

Cassandre Le Galliard, University of Sheffield, UK

Dr. Antonino Runci, University of Zagreb, Croatia

Olivera Bukvic, University of Zagreb, Croatia

Richard Caron, Karlsruhe Institute of Technology, Germany

Andres Arce, University of Patras, Greece

Tamara Chidiac, University of Sheffield, UK

Anastasija Komkova, ETH Zurich, Switzerland

LOCAL ORGANISING COMMITTEE

Prof. Stijn Matthys, Ghent University, Belgium (chair)

Dr. Alessandro Proia, Ghent University, Belgium (co-chair)

Ms. Marijke Reunes, Ghent University, Belgium (co-ordinator)

Prof. Geert De Schutter, Ghent University, Belgium

Prof. Hubert Rahier, Vrije Universiteit Brussel, Belgium

Dr. Beibei Sun, Ghent University, Belgium

Ir. Ivana Krajnovic, Ghent University, Belgium

Ir. Yubo Sun, Ghent University, Belgium

Ir. Saeid Ghorbani, Ghent University, Belgium

Mr. Jens Mortier, Ghent University, Belgium

Symposium program

Day 1: Wednesday 8 February 2023

08:15 – 08:45	**Arrival and registration**
08:45 – 09:00	Welcome and opening
09:00 – 09:45	**Keynote lecture 1 by Prof. Barbara Lothenbach (EMPA)** **Topic: "Mix design and microstructure"**
09:45 – 10:45	**Session 1.1 (focused on "Mix design and microstructure" and "Durability performance")**
09:45 – 10:00	Influence of temperature on the kinetics of formation of sodium aluminosilicate hydrate gel *L. Miranda de Lima, J. L. Provis and G. Ye*
10:00 – 10:15	Benzoic acid derivates as admixtures for low alkaline activated BFS *S. Bagheri, T. Luukkonen and J. Yliniemi*
10:15 – 10:30	Influence of pre-saturation regime on the scaling resistance of alkali-activated slag concrete *O. Bukvić and M. Serdar*
10:30 – 10:45	Shrinkage and creep of alkali-activated slag and applicability of the *fib* MC 2010 *R. Caron, R. A. Patel and F. Dehn*
10:45 – 11:15	*Coffee break*
11:15 – 12:15	**Session 1.2 (focused on "Mix design and microstructure" and "Durability performance")**
11:15 – 11:30	Background for the mix proportioning of alkali-activated materials *V. Bílek Jr, J. Koplík, J. Hajzler and B. Kucharczyková*
11:30 – 11:45	Effect of water to binder and solution to binder ratio on the hydration kinetics of waterglass activated slag/fly ash blends *M. Mutti, S. Joseph and Ö. Cizer*
11:45 – 12:00	Chloride ingress and carbonatation resistance of ternary blend alkali activated concrete *S. Ghorbani and S. Matthys*
12:00 – 12:15	Study on the influence of solution composition on shrinkage of low calcium fly ash geopolymers *M. Hanumananaik and K. V L Subramaniam*
12:15 – 13:15	*Lunch break*
13:15 – 14:00	**Keynote lecture 2 by Prof. Aleksandra Radlinska (Pennsylvania State University)** **Topic: "Durability performance"**
14:00 – 15:15	**Session 1.3 (focused on "Mix design and microstructure" and "Durability performance")**
14:00 – 14:15	Reaction of carbonate minerals in alkaline medium *R. Firdous and T. Hirsch*
14:15 – 14:30	Effect of mixing methods on workability and ultrasound measurements of alkali-activated materials *L. Hertwig, B. H. Tekle and K. Holschemacher*

14:30 – 14:45	Preparation of precursors for alkali-activated materials by remelting *T. Hirsch, A. Buchwald, R. Firdous and D. Stephan*
14:45 – 15:00	Preservation of embodied carbon with sustainable resilience corrosion protection systems *G. Jones, C. Van Nguyen, P. Mangat and P. Lambert*
15:00 – 15:15	Impact of carbonation and other chemical attacks on alkali activated slag materials *C. Le Galliard, D. A. Geddes, B. Walkley and J.L. Provis*
15:15 – 15:45	*Coffee break*
15:45 – 17:00	**Session 1.4 (focused on "Mix design and microstructure" and "Durability performance")**
15:45 – 16:00	The relationship between mixture design and efflorescence formation in geopolymers made of iron ore tailings *Rafaela K. R. Silva, Polyana F. F. Martins, Márlon A. Longhi and Fernando S. Lameiras*
16:00 – 16:15	Freeze-thaw behaviour of hemp reinforced geopolymer *Y. Lu, A. Darby, A. Heath and X. Ke*
16:15 – 16:30	Immobilization of Cesium and Strontium-based waste by metakaolin geopolymer: Effect of waste loading and water-binder ratio on the properties of the host matrix *E. Mukiza, Quoc Tri Phung, S. Seetharam, L. Frederickx, G. De Schutter*
16:30 – 16:45	Influence of zinc sulphate on the setting and rheological properties of alkali activated binders *A. Sai Surya Sree Nedunuri and S. Muhammad*
16:45 – 17:00	Liquid release from superabsorbent polymer in alkali-activated slag and the mitigation of autogenous shrinkage *H. Dong, B. Chen, Z. Li and G. Ye*

Day 2: Thursday 9 February 2023

08:30 – 09:00	**Arrival and registration**
09:00 – 09:45	**Keynote lecture 3 by Prof. Jannie S.J. van Deventer (Zeobond)** **Topic: "Structural behaviour and design"**
09:45 – 10:45	**Session 2.1 (focused on "Mix design and microstructure" and "Durability performance")**
09:45 – 10:00	Air-entraining additive effect on geopolymer mortar workability *P. Prochoń, M. Kępniak, K. Załęgowski*
10:00 – 10:15	Efficient use of calcium in developing sustainable high-strength geopolymer for in-situ applications *K. K. Ramagiri and K. V. L. Subramaniam*
10:15 – 10:30	The effect of phosphorus oxide content in precursor on setting time and freeze-thaw resistance of alkaline-activated binders *P. Prochoń and D. Stańczak*
10:30 – 10:45	Effects of Mg on the reactivity of CaO-MgO-Al2O3-SiO2 glasses in the sodium silicate activated system *T. Kim, A. Hamdan and A. Hajimohammadi*

10:45 – 11:15	*Coffee break*
11:15 – 12:15	**Session 2.2 (focused on "Mix design and microstructure" and "Structural behaviour and design")**
11:15 – 11:30	Mechanical, microstructure and durability properties of alkali-activated mortar based on phosphate mining waste rocks, fly ash and metakaolin raw materials *S. Sbi, S. Mansouri, Y. Tamraoui and J. Alami*
11:30 – 11:45	Use of lime kiln dust as a waste-based reagent in fly ash Class C-based alkali-activated materials *P. Shoaei, S. Pilehvar and R. Pamies*
11:45 – 12:00	Influence of the fibre addition on shrinkage and pull-off bond strength of binary alkali-activated repair mortar made of blast furnace and copper slag *I. Krajnović and S. Matthys*
12:00 – 12:15	Stress-strain response of FRP-confined rubberised one-part alkali-activated concrete *M. Elzeadani, D. V. Bompa and A. Y. Elghazouli*
12:15 – 13:15	*Lunch break*
13:15 – 14:00	**Keynote lecture 4 by Prof. José Dinis Silvestre (Universidade de Lisboa)** **Topic: "Greening concrete with circular practices: environmental, toxicological, and economic benefits and challenges"**
14:00 – 15:15	**Session 2.3 (focused on "Mix design and microstructure" and "Structural behaviour and design")**
14:00 – 14:15	Performance of alkali-activated metakaolin at high H2O/Na2O ratios *F. Souayfan, E. Rozière, C. Justino, M. Paris, D. Deneele, A. Loukili*
14:15 – 14:30	Effects of activator compositions on the rheology of alkali-activated slag concrete *Y. Sun, G. Ye, G. De Schutter*
14:30 – 14:45	Behavior of alkali-activated slag mortar incorporated with other supplementary cementitious materials *S. Tavasoli, A. W. Sadeed and W. Breit*
14:45 – 15:00	Seismic Retrofitting of clay-brick masonry walls with AAM-TRM *L. D. Azdejkovic, T. C. Triantafillou and C. G. Papanicolaou*
15:00 – 15:15	Experimental investigation on long-term flexural behaviour of prestressed alkali-activated concrete (AAC) girders with cast-in-situ AAC topping *Z. Qian, G. Ye, S. Matthys and M. Luković*
15:15 – 15:45	*Coffee break*
15:45 – 17:00	**Session 2.4 (focused on "Mix design and microstructure" and "Service life and life cycle assessment")**
15:45 – 16:00	Calcined clay minerals as precursors for geopolymers and the influence of solubility on mixing ratios *N. Werling, F. Dathe, F. Dehn and K. Emmerich*
16:00 – 16:15	Chloride transport in alkali-activated slag paste under the exposure of wetting and drying cycles *Z. Xu and G. Ye*
16:15 – 16:30	Novel findings of pore shapes for hardened 3D printed concrete with silica fume by X-CT scanning *Y. Chen and H. Rahier*

16:30 – 16:45	Sensitivity analysis for a probabilistic service life prediction of alkali-activated concrete *T. J. Chidiac, N. Ukrainczyk, D. P. Prentice, Z. Zhang, T. Soetens, B. Van Belleghem and J.L. Provis*
16:45 – 17:00	The environmental impacts of alkali activated concretes: examining contribution of variability in constituents and of service life time to the uncertainty of LCA *A. Komkova, T.J. Chidiac, J.L. Provis and G. Habert*
19:30 – 22:30	**Symposium dinner**

Day 3: Friday 10 February 2023

08:30 – 09:00	**Arrival and registration**
09:00 – 09:45	**Keynote lecture 5 by Dr. Vilma Ducman (ZAG)** **Topic: "Industry perspective and application cases"**
09:45 – 10:45	**Session 3.1 (focused on "Durability" and "Industry perspective and application cases")**
09:45 – 10:00	Degradation of alkali activated slag mortars subjected to accelerated leaching *T. N. Nguyen, Q. T. Phung, L. Frederickx, D. Jacques, A. Dauzeres, J. Elsen, Y. Pontikes*
10:00 – 10:15	Design and tendering experiences of a geopolymer concrete bridge *C.B.M. Blom, W.D. Schutte, A.P. Allaart and J.L.M. van Leeuwen*
10:15 – 10:30	Removal of ammonium from wastewater with metakaolin based-geopolymer sorbents *M. Otero, L. Freire, S. Gómez-Cuervo and P. Villar*
10:30 – 10:45	Additive manufacturing of geopolymer-stones to replicate natural sandstones with low availability *S. Partschefeld, A. Tutal and A. Osburg*
10:45 – 11:15	*Coffee break*
11:15 – 12:15	**Session 3.2 (focused on "Structural behaviour and design" and "Industry perspective and application cases")**
11:15 – 11:30	Alkali-activated slag-based concrete incorporating single and multiple hooked-end steel fibers: mechanical behaviour and limitations to field applications *L. Rossi and F. Dehn*
11:30 – 11:45	Performance at load-bearing reinforced concrete with treated Cu slag as cement replacement *P. Sivakumar, M. A. Yaqub and S. Matthys*
11:45 – 12:00	Self-compacting alkali-activated concrete (AAC) for precast prestressed bridge girders - from lab research to industrial production *S. Zhang, M. Luković, Y. Yang, H. Herder, A. Scharringa and G. Ye*
12:00 – 12:15	URBCON - By-products for sustainable concrete in the urban environment *W. Crijns*
12:15 – 12:30	**Closure and intro to site visit**

12:30 – 13:30	*Goodbye lunch*
13:30 – 15:00	**Site visit to City of Ghent "Zonnepoort" pilot**

Keynote speakers

Prof. Barbara Lothenbach

EMPA

Barbara Lothenbach is a professor and head of the group cement chemistry and thermodynamics at EMPA (Switzerland). PhD. at the Institute of Terrestrial Ecology, Soil Protection, Swiss Federal Institute of Technology (ETH) Zürich in 1996, she has worked as a project leader and consultant scientist for nuclear wastes at BMG Engineering Ltd, Schlieren, Switzerland. In 2002, she has joined the Laboratory Concrete & Asphalt at EMPA. Her current research topics include hydration mechanisms of cementitious materials, thermodynamic modelling, characterization techniques, pore solutions and supplementary cementitious materials and non-Portland cement binders. She is author of more than 150 scientific journal articles and 170 conference papers.

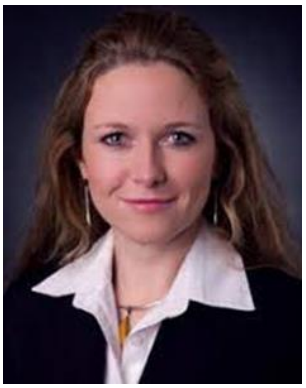

Prof. Aleksandra Radlinska

The Pennsylvania State University

Aleksandra Radlińska is an associate professor at the Pennsylvania State University. She holds a Ph.D. degree in civil engineering from Purdue University (2008). Her research interests include developing innovative materials to enhance infrastructure durability and reduce CO_2 impact. To date, she has focused her research on mechanisms and mitigation of shrinkage and carbonation in alkali-activated concrete, prediction and reduction of the probability of early-age cracking in concrete, cement solidification in the microgravity environment, and binders for Moon and Mars infrastructure, as well as pyrrhotite reactivity in concrete and 3D printing of concrete. In 2017 and 2018, Aleksandra as part of the Penn State Team team won a second-place award at the NASA 3D-Printed Habitat Challenge. She is the author of more than 80 publications including scientific journal articles, conference proceedings, and books.

Prof. Jannie S.J. van Deventer

Zeobond

With three doctorates in chemical engineering, mineral processing and business economics, Jannie has a track record of commercialising technology in cement, concrete, mineral processing, waste valorisation and biotechnology. He is Director of Zeobond that is developing cement and concrete with ultra-low CO2 emissions. He is an honorary professorial fellow at the University of Melbourne, where he was Dean of Engineering until 2007.

With a Scopus h-index of 89, Jannie is a highly cited researcher in cement science. Also, he is ranked number 2 in the world in mining and metallurgy research by Stanford University. He has received several awards for his research and has been listed three times as one of Australia's most influential engineers. He is a frequent plenary and keynote speaker at research and industry conferences.

Prof. José Dinis Silvestre

Instituto Superior Tecnico - Universidade de Lisboa

Associate Professor with Habilitation at the Department of Civil Engineering, Architecture and Georesources of Instituto Superior Técnico from Universidade de Lisboa, Portugal, where he is also a researcher at the 'Civil Engineering Research and Innovation for Sustainability' (CERIS). PhD in Civil Engineering from the same institution, being since 2009 an expert on assessing the sustainability of materials, construction systems and buildings. Carried out Life Cycle Assessment studies with more than 25 national manufacturers of construction materials and in national and international projects. Co-authored 90+ ISI journal papers and 3 books, coordinated 2 research projects with foreign partners, participated in 4 international research projects and participates in 13 national research projects (and in 5 more already concluded), related to sustainability and energy efficiency of building materials and construction solutions. Supervised 3 PhD Theses and co-supervised 6 others and supervised 10 Integrated Master Theses and co-supervised 4. Was President of the national Standardisation Commission CT 171 «Sustainability in Buildings» between 2017 and 2019 and is a member of the Technical Commission and verifier of the DAPHabitat System – Registration System of Environmental Product Declarations (EPD) for Habitat.

Dr. Vilma Ducman

ZAG

Head of the Laboratory for Cements, Mortars and Ceramics at ZAG (Slovenian National Building and Civil Engineering Institute), has been involved in research related to circular economy and upcycling in the construction sector, with particular emphasis on:

(i) development and technical evaluation of alkali-activated products ("geopolymers") based on different waste materials (fly ash, slags, calcined clay...), (ii) use of different waste materials (ashes, sediments, CDW...) in the construction sector (ceramics, concrete, mortar), (iii) processing of various wastes into artificial (lightweight) aggregates.

She has published (alone or as co-author) over 80 articles in SCI indexed journals and prepared over a hundred conference contributions. She has obtained 5 national patents on recycling.

In recent years, she has led or been involved in several national and international projects related to alkali activation technology or recycling in the construction sector such as Horizon Europe AshCycle (2022-2026), H2020 Wool2Loop (2019 -2022) , ERA-MIN 2: FLOW (2018-2021), H2020 InnoWEE (2016-2020), EIT KIC RawMaters projekt GEORIS (2022- 2025), EIT KIC RawMaters projekt RECOVER (2017-2019), EIT KIC RawMaters projekt MIN-PET (2016-2018), etc.

1. Mix design and microstructure

LIST OF CONTRIBUTIONS

Keynote lecture:

Extended abstracts:

Alkali activated materials: Mix design and microstructure

Prof. Barbara Lothenbach[1]

[1] Cement chemistry and thermodynamics, EMPA, SWITZERLAND.
(E-mail: Barbara.Lothenbach@empa.ch)

KEYNOTE SUMMARY

Alkali-activated binders based on ground granulated blast-furnace slag, fly ash or glasses can be a viable and sustainable alternative to Portland cement, since they use by-products of other industrial manufacturing processes. The presentation aims to summarise recent investigations on pore solution composition, on the effect of composition on the reactivity of the glassy phases and the changes occurring during carbonation. In addition, the effect of MgO and Al_2O_3 content of slags on the hydrate assemblage, and on compressive strength is discussed and compared with thermodynamic modelling predictions. The effectiveness of slag, fly ash or glass activation and thus the hydration kinetics depends on the activator used, on the mineralogical composition and the fineness of the glassy phase. The addition of alkalis stimulates the dissolution of glasses and thus the formation of hydration products. Alkali activated slags form mainly calcium silicate hydrates incorporating significant amounts of aluminium (C(-A)-S-H), hydrotalcite-like phase and strätlingite, while in alkali activated fly ashes or glasses rather N-A-S-H gels are formed.

Influence of temperature on the kinetics of formation of sodium aluminosilicate hydrate gel

Luiz Miranda de Lima[1], John L. Provis[2] and Guang Ye[3]

[1,3] Delft University of Technology, Faculty of Civil Engineering and Geosciences. Delft, the Netherlands. (E-mail: L.MirandadeLima@tudelft.nl, G.Ye@tudelft.nl)

[2]University of Sheffield, Department of Materials Science and Engineering. Sheffield, United Kingdom. (E-mail: J.Provis@sheffield.ac.uk)

HIGHLIGHTS

- At room temperature, degree of reaction of alkali-activated pastes is linearly correlated with chemistry of the binder.
- Combination of secondary electrons grayscale images with selective dissolution treatments allows the quantitative determination of sodium aluminosilicate hydrates in hardened alkali-activated matrixes.
- Acceleration periods observed in isothermal calorimetry tests performed at 60 ºC are indications of conversion of initial precipitates into ordered zeolite-like structures.

Keywords: phase assemblage, degree of reaction, sodium aluminosilicate hydrate gel

INTRODUCTION

The implementation of alkali-activated materials (AAMs) is one of the most suitable alternatives to ordinary Portland cement (OPC), in both structural and non-structural applications within the construction field. The similar-to-superior performance and durability characteristics, the lower embodied energy and lower CO_2 emission involved in the process, and the reutilization of industrial byproducts as raw-materials [1], [2] are among the advantages of this class of alternative building materials.

The initial mineralogy and chemical composition of the precursors used in these systems have a direct impact in their dissolution and further hardening reactions of AAMs [3]. However, the extensive list of potential precursors described in the literature imposes obstacles to the estimation of behavior of these materials. The evolution of the performance of AAMs is directly correlated with the phase assemblage within the hardened microstructure. The nature and the quantity of reaction products are among the main factors controlling the in-service behavior of these building materials, such as mechanical properties and durability characteristics. Hence, the possibility of quantitatively determining the solid phases formed during alkali-activating reactions is extremely desired, as it would allow accurate structural calculations and service life predictions, among other characteristics, to be modeled.

The present study investigated quantitatively the formation of sodium aluminosilicate hydrate (N-A-S-H) gels during the alkali-activation of synthetic glasses resembling blast furnace slags and coal fly ashes. A correlation of binder chemistry and phase precipitation is achieved at room temperature. The reaction mechanism is slightly modified when higher curing temperatures are applied. With the use of different experimental tools such as isothermal calorimetry, scanning electron microscopy, and selective chemical dissolution, corrections to the quantitative analysis of N-A-S-H gel have been applied and validated.

MATERIALS & METHODS

The synthetic glasses of simplified chemical compositions, comprising for Al_2O_3, CaO and SiO_2, were designed aiming for a resemblance with siliceous fly ash, calcareous fly ash, and blast furnace slags. Reagent grade Al_2O_3 and SiO_2, and $CaCO_3$ as a source of CaO, were mixed, melted using alumina crucibles with an ultimate temperature of 1600 ºC, and quenched in water after 2 h of dwell time. Glasses were dried and ground until reaching a D_{50} value of approximately 20 µm. Table 1 displays the chemical compositions obtained with X-ray fluorescence, and the D_{50} values obtained with laser diffraction analysis.

Table 1. Experimental chemical composition and particle properties of synthetic glasses.

Glass	Glass type	Atomic ratios				D_{50} (µm)
		Si/Ca	Si/Al	Al/Ca	Ca / (Si +Al)	
S4	Siliceous Fly ash	4.16	1.51	2.75	0.15	22.1
S2	Calcareous fly ash	2.04	1.47	1.39	0.29	17.2
S1	Blast furnace slag	1.00	1.56	0.64	0.61	21.5
S0.9	Blast furnace slag	0.93	2.05	0.46	0.72	16.6

A total of 8 different pastes were prepared by alkali-activation of the four synthetic glasses. Each glass was activated with solutions composed of sodium hydroxide (N8S0 – 8 g of Na_2O per 100 g of glass) and sodium silicate (N8S12 – 8 g of Na_2O per 100 g of glass and a silicate modulus of 1.5). The pastes were cured in sealed containers for 7 and 28 days at room temperature (mixtures prepared with all glasses), and at 60 ºC (mixtures prepared with fly ash-like glasses). Pastes were also prepared and analyzed through isothermal calorimetry for 7 days, at 20 ºC and 60 ºC, targeting the study of reaction kinetics according to the initial chemistry of the binder. Scanning electron microscopy (SEM) was used for the determination of the degree of reaction at different ages with the use of grayscale images [4]. In order to analyze N-A-S-H gel individually, 1g of each hardened paste was submitted to a selective dissolution procedure (combination of salicylic acid and methanol (SAM) [5]), which is able to eliminate low-ordered calcium containing phases. The weight loss during the dissolution experiments, normalized by reaction degree of the binder, was used to calculate the quantity of N-A-S-H gel formed in each paste. The characterization of the microstructure was performed with X-ray diffraction (XRD) measurements after 7 days of curing for each one of the eight paste mixtures.

RESULTS & DISCUSSION

The reactivity potential calculated for each paste, after 7 days of curing time at room temperature, indicated a direct correlation with binder chemistry, and more specifically with the Ca content of the mixture. As observed in Fig. 1a, the degree of reaction increased from 32.7 % for the paste S4-N8S12, to 48.2 % for the paste S0.9-N8S0 (Ca/(Si+Al) ratios of 0.16 and 0.85, respectively the lowest and highest values). Increased formation of N-A-S-H gel is also observed to be inversely proportional to the overall amount of Ca in the binder (Fig. 1b). Although it did not affect significantly the degree of reaction, the presence of aqueous silicate in the activator had a positive influence on inhibiting other Ca-based hydrates, as all glasses, except S0.9, showed residual N-A-S-H gel after selective dissolution. Although N-A-S-H gel is usually described in the literature as the dominant reaction product in fly ash-like systems [3], a great contribution of Ca was observed to the phase assemblage of these binders. As seen in Fig. 1, the maximum calculated quantity of N-A-S-H gel was only 61.7 % (S4-N8S12), indicating sufficient room for the growth of Ca-based phases.

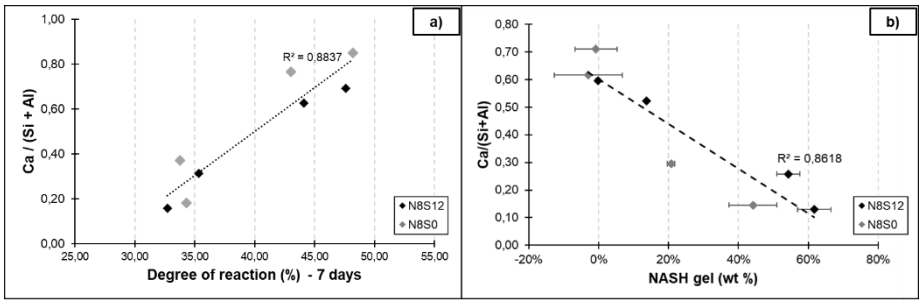

Figure 1. Influence of Ca content on the: a) overall degree of reaction; and b) quantity of N-A-S-H present in the microstructure of hardened pastes.

Ca has been proven to have significant impact on the initial reactivity of alkali-activated materials, since its release to the aqueous media occurs before the release of Si and Al during dissolution of the precursor [6]. The nucleation of Ca-based phases begins immediately after the initial contact of the precursor with the activating solution. Therefore, fly ash-based systems tend to present delayed N-A-S-H gel precipitation, as evidenced by the results from isothermal calorimetry tests shown in Fig. 2. After the dissolution peaks, an absence of acceleration peaks is observed in the calorimetry curves of S4-based pastes cured at room temperature (Fig. 2a), regardless of the activating solution. Combined with the non-negative low heat flow through the course of the experiment, this indicates a continuous, although slow and incomplete, process of N-A-S-H gel formation, yielding an unstable hardened matrix. Using a temperature curing regime of 60 ºC enhances the reaction potential of fly ashes-type glasses, as illustrated in Fig. 2b. Wider dissolution peaks are observed with the use of both activators, in addition to two distinct acceleration peaks for NaOH-activated glasses. These two peaks reflect the formation and transformations of N-A-S-H gel, as the implementation of increased temperatures is known to intensify its degree of structural ordering [7], converting it into zeolite-like solid phases without necessarily affecting the quantity of sodium aluminosilicate-based phases. Contrarily, waterglass-activated pastes display a broader dissolution peak with only one acceleration shoulder, as the presence of liquid silicate species in the activator favors a more disordered N-A-S-H gel structure, preventing its conversion into crystalline-like phases. The analysis of the cumulative heat release in both curing regimens, visualized in Figs. 2c and 2d, indicate that the reactions at room temperature are still under development after 7 days, as they present significantly lower values, while the microstructure after 7 days of curing at 60 ºC presents itself as more mature when compared to room temperature cured systems.

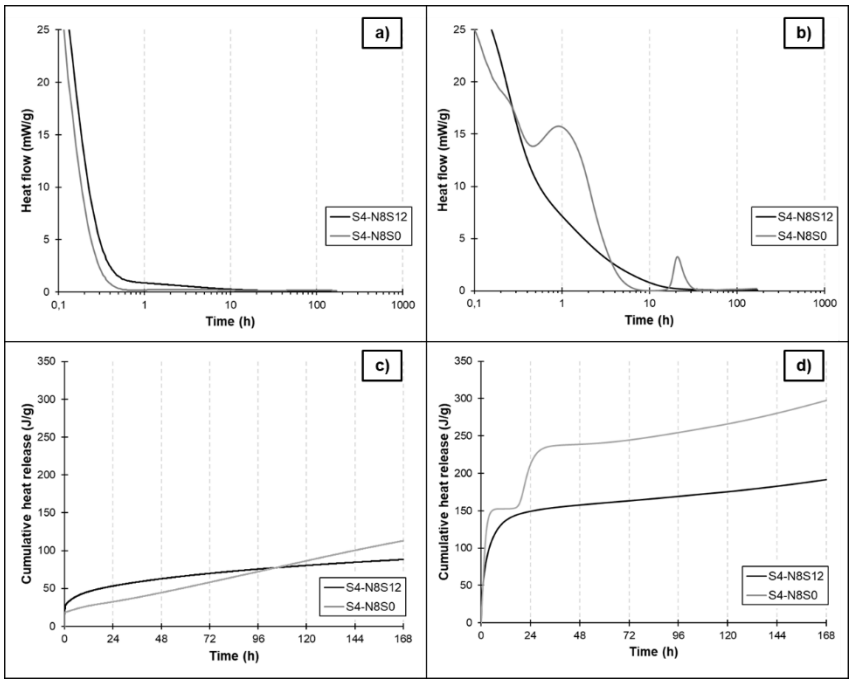

Figure 2. Isothermal calorimetry curves of glass S4-based pastes cured at: a) 20 ºC; and b) 60 ºC; and cumulative heat release curves of the same pastes at: c) 20 ºC; and d) 60 ºC.

The direct impact of temperature curing on the final microstructure of the hardened binders can be better visualized in the X-ray diffractograms of the four analyzed systems, displayed in Fig. 4. The use of waterglass as activator did not show any distinctive peaks in none of the curing regimens, as the high content of aqueous silicate species favours the precipitation and growth of reaction products with low-range degree of order. The influence played by temperature relies on the overall reactivity of the system, which can be qualitatively analyzed with cumulative heat release. On the other hand, sodium hydroxide-activated pastes were more susceptible to structural changes with implementation of elevated temperature curing. The observed acceleration periods observed for the system S4-N8S0 at 60 ºC promoted a more complex microstructure, as the diffractogram shows the presence of intense peaks of different zeolite structures (Faujasite-Y, Hydrosodalite, Na-P1), when compared to room temperature cured pastes, indicating the conversion of initially precipitated amorphous gels into reaction products with higher range of degree of order.

The observed differences in calorimetric response, due to the activating solution, combined with the microstructural characterization performed with XRD, illustrate the importance of the evaluation of the structure of reaction products present in a hardened matrix, in addition to quantitative determination of each of these phases.

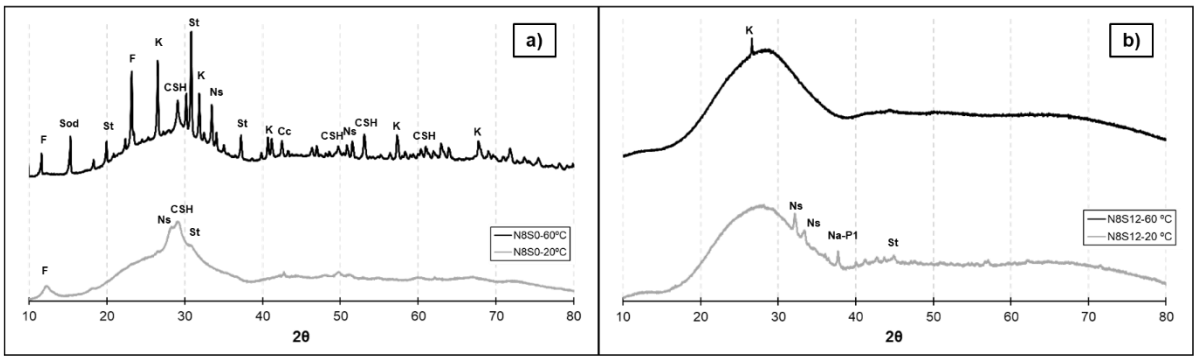

Ns – Sodium aluminosilicate hydrate (PDF # 01-089-0770) / Sod – Hydrosodalite (PDF # 01-072-2329) / St – Strätlingite (PDF # 00-029-0285) / F – Faujasite-Y (PDF # 00-039-1380) K – Katoite (PDF # 00-024-0217) / CSH – C-(A-)S-H (PDF # 04-012-1761) / Cc – Calcium carbonate (PDF # 00-005-0586) / Na-P1 – Zeolite Na-P1 (PDF # 01-089-6322)

Figure 3. X-ray diffractograms of S4-based pastes cured at room 20 ºC and 60 ºC: a) N8S0 systems; and b) N8S12 systems.

CONCLUSION

Based on this study, it can be concluded that Ca has a direct impact on the degree of reaction of alkali-activated materials and on the formation of sodium aluminosilicate hydrate (N-A-S-H) gel. A low Ca content hinders the dissolution of the precursor and the release of reactive species to the activating solution, thus delaying the process of formation of Ca-less phases. The use of waterglass as activating solution increases the quantity of N-A-S-H gel in the hardened matrix, even in slag-based systems, but does not have a significant impact on the degree of reaction. Implementation of increased temperature curing overcomes the lack of Ca on the binder, accelerating the precipitation of N-A-S-H gel which lead to an increased overall content. Lastly, the use of selective dissolution was proven to be successful in the quantitative determination of N-A-S-H gel, and further characterization of the solid residue of dissolution could provide valuable information over the activator effect on the reaction mechanism and on the structure of the gel.

ACKNOWLEDGEMENT

This project has received funding from the European Union's Horizon 2020 research and innovation programme under grant agreement No 813596 DuRSAAM. The opinions expressed in this document reflect only the author's view and reflect in no way the European Commission's opinions.

REFERENCES

[1] J. S. J. Van Deventer, D. G. Brice, S. A. Bernal, and J. L. Provis, "Development, standardization, and applications of alkali-activated concretes," *ASTM Spec. Tech. Publ.*, vol. 1566 STP, pp. 196–212, 2013, doi: 10.1520/STP156620120083.

[2] J. Rivera, F. Castro, A. Fernández-Jiménez, and N. Cristelo, "Alkali-Activated Cements from Urban, Mining and Agro-Industrial Waste: State-of-the-art and Opportunities," *Waste and Biomass Valorization*, vol. 12, no. 5, pp. 2665–2683, 2021, doi: 10.1007/s12649-020-01071-9.

[3] I. Garcia-Lodeiro, A. Palomo, and A. Fernández-Jiménez, "Ch. 2: An overview of the chemistry of alkali-activated cement-based binders," in *Handbook of Alkali-Activated Cements, Mortars and Concretes*, Woodhead Publishing Limited, 2015, pp. 19–47.

[4] Y. Zuo, M. Nedeljković, and G. Ye, "Coupled thermodynamic modelling and experimental study of sodium hydroxide activated slag," *Constr. Build. Mater.*, vol. 188, pp. 262–279, 2018, doi: 10.1016/j.conbuildmat.2018.08.087.

[5] S. Puligilla and P. Mondal, "Co-existence of aluminosilicate and calcium silicate gel characterized through selective dissolution and FTIR spectral subtraction," *Cem. Concr. Res.*, vol. 70, pp. 39–49, 2015, doi: 10.1016/j.cemconres.2015.01.006.

[6] R. Snellings, "Solution-controlled dissolution of supplementary cementitious material glasses at pH 13: The effect of solution composition on glass dissolution rates," *J. Am. Ceram. Soc.*, vol. 96, no. 8, pp. 2467–2475, Aug. 2013, doi: 10.1111/jace.12480.

[7] R. R. Lloyd, J. L. Provis, and J. S. J. Van Deventer, "Microscopy and microanalysis of inorganic polymer cements. 2: The gel binder," *J. Mater. Sci.*, vol. 44, no. 2, pp. 620–631, Jan. 2009, doi: 10.1007/s10853-008-3078-z.

Benzoic acid derivate as admixtures for low alkaline activated BFS

Sepideh Bagheri[1], Tero Luukkonen[1] and Juho Yliniemi[1]

[1] Fiber and Particle Engineering Research Unit, Faculty of Technology University of Oulu, Finland.
(E-mail: Sepideh.bagheri@oulu.fi)

HIGHLIGHTS

- Benzoic acid derivate ligands were studied as admixtures for sodium carbonate activated BFS
- Certain ligands showed promising acceleration of the hydration process
- The effect of ligand is sensitive depending on the dissolution and pore solution chemistry of the binder

Keywords: compressive strength, isothermal calorimetry, benzoic acid derivates

INTRODUCTION

Blast furnace slag (BFS) is a common material used as a Portland cement additive and as a calcium-rich precursor in AAMs [1–3]. As an alternative to traditional activators like sodium silicate and sodium hydroxide, sodium carbonate offers a way to generate more environmentally friendly AAM with less alkalinity, a smaller carbon footprint, and greater workability of the fresh paste [4]. The challenge with low alkaline activators such as sodium carbonate is the slow strength development. Here, we investigate how certain complexing agents affect strength development of sodium carbonate activated BFS.

Carboxylic acids are chemical molecules with the functional group carboxyl (-COOH) [5,6]. One of the most basic carboxylic acids, benzoic acid (BA) has a wide variety of derivatives, such as 4-aminobenzoic acid (ABA), salisylic acid (SA), and 3,4-dihydroxybenzoic acid (DHBA). Similar to amino acids, proteins, and many medicins, 4-aminobenzoic acid is an aromatic molecule with amino and carboxylic groups in the para position. salisylic acid and 3,4-dihydroxybenzoic acid (DHBA) are a phenolic acid with –COOH and –OH functionalities. Each functional group could form various complexes, for example, with Ca, Mg, and Al, which could potentially affect the dissolution and precipitation reactions of BFS hydration [7].

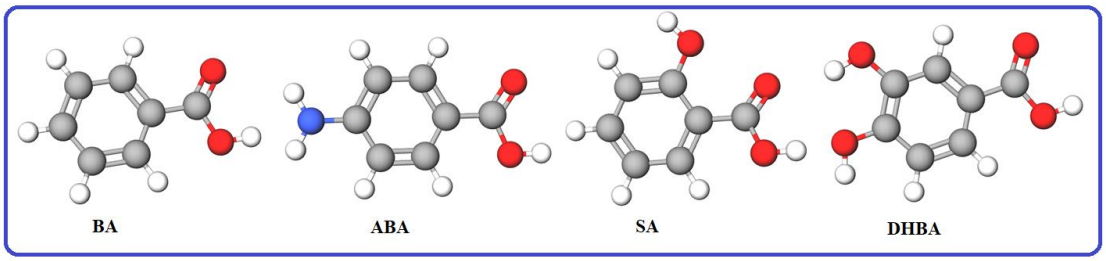

Figure 1. Benzoic acid (BA), 4-aminobenzoic acid (ABA), salisylic acid (SA) and ,4-dihydroxybenzoic acid (DHBA).

MATERIALS & METHODS

Ground granulated blast furnace slag is from Finnsementti, Finland (Table 1).

Table 1. Chemical composition of BFS (wt%).

	SiO2	MgO	Al2O3	Fe2O3	Na2O	CaO
BFS	33,8	10,1	9,9	0,37	0,56	37,7

Table 2. Mix design of the prepared samples, Na2CO3-solution molarity is 2.07 (mol/L).

Sample code	Blast furnace slag (g)	Na2CO3-solution (g)	Water-to-binder ratio	Type of ligand	Ligand dosage per binder mass (wt.%)
BFS_CO	40	18.3	0.35		
BFS_CO_DHBA0.1%	40	18.3	0.35	3,4-Dihydroxybenzoic acid	0.1
BFS_CO_ABA0.1%	40	18.3	0.35	4-Aminobenzoic acid	0.1
BFS_CO_SA0.1%	40	18.3	0.35	2-Hydroxybenzoic Acid	0.1
BFS_CO_DHBA0.3%	40	18.3	0.35	3,4-Dihydroxybenzoic acid	0.3
BFS_CO_ABA0.3%	40	18.3	0.35	4-Aminobenzoic acid	0.3

RESULT & DISCUSSION

Figure 2.a) shows the trends in compressive strength of hydrated BFS with different benzoic acid derivates after hardening for 1, 3, and 7 days. Many of the ligands decreased early-age strength development even with low dosages showing strong, but counterproductive, interaction in the hardening process. We also observed inconsistency on the effect of ligands when experiments were repeated (Figure 2.b).

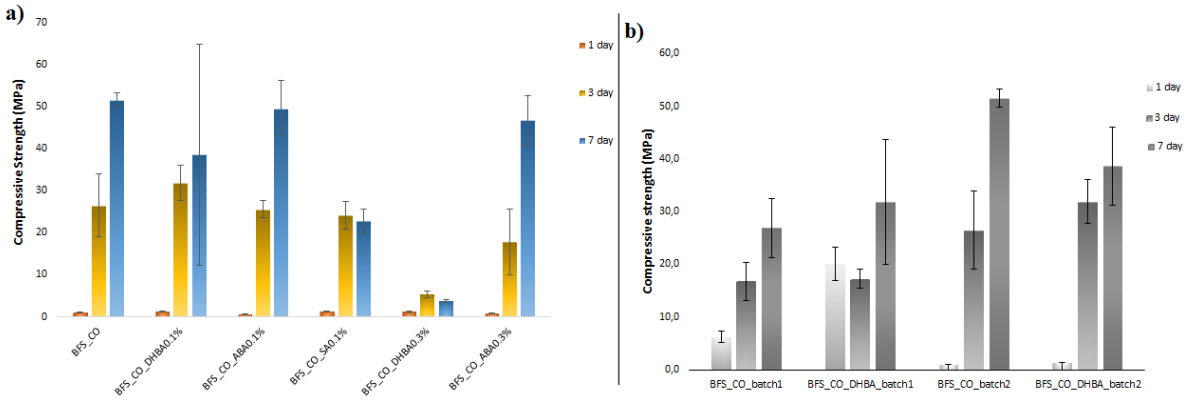

Figure 2. a) Compressive strength of the samples with benzoic acid derivates at different curing ages (1, 3 and 7 days), b) different results from multiple experiments as a function of ligands.

We believe this inconsistency is due to quality variation of BFS when different BFS batches were used, which consequently affected BFS differences in the BFS reactivity, and the effectivity of the ligand. We present chemical composition, BET surface area, and particle size distribution of both BFS batches

in the oral presentation and discuss about possible reasons for different results. Nevertheless, there was a clear acceleration in the reaction kinetics with certain ligands and dosages (Figure 3).

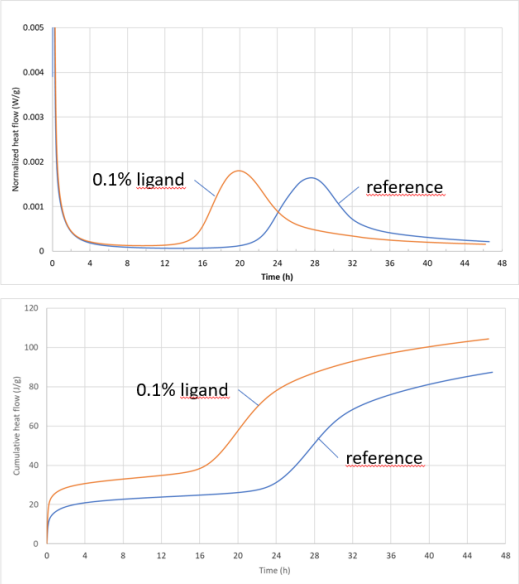

Figure 3. Isothermal calorimetry of activated BFS with and without 3,4-dihydroxybenzoic acid.

CONCLUSION

This work demonstrates that small amounts of benzoic acid derivates influence the early-age reaction kinetics of Na_2CO_3-activated BFS binder. The functional group of the ligand can affect the strength development, while retaining or improving the fluidity of the pastes. The effect was negative in most cases, but some promising results were obtained with BFS of certain quality.

ACKNOWLEDGEMENT

This research work was supported by the Faculty of Technology, University of Oulu, Finland.

REFERENCES

[1] Liu, Y., Zhu, W. & Yang, E.-H. Alkali-activated ground granulated blast-furnace slag incorporating incinerator fly ash as a potential binder. *Construction and Building Materials* 112 (2016), 1005–1012.

[2] Shi, C., Jiménez, A. F. & Palomo, A. New cements for the 21st century: The pursuit of an alternative to Portland cement. *Cement and concrete research* 41 (2011), 750–763.

[3] Wang, S.-D., Scrivener, K. L. & Pratt, P. L. Factors affecting the strength of alkali-activated slag. *Cement and concrete research* 24 (1994), 1033–1043.

[4] Al-Tabbaa, A., Abdalqader, A. & Jin, F. Performance of Magnesia-modified sodium carbonate-activated slag/fly ash concrete. *Cement and Concrete Composites* (2019).

[5] Rogers, J. R. & Bennett, P. C. Mineral stimulation of subsurface microorganisms: release of limiting nutrients from silicates. *Chemical Geology* 203 (2004), 91–108.

[6] Golubev, S. V, Bauer, A. & Pokrovsky, O. S. Effect of pH and organic ligands on the kinetics of smectite dissolution at 25 C. *Geochimica et Cosmochimica Acta* 70 (2006), 4436–4451.

[7] Yliniemi, J. Surface Layer Alteration of Multi-Oxide Silicate Glasses at a Near-Neutral pH in the Presence of Citric and Tartaric Acid. *Langmuir* (2022).

Background for the mix proportioning of alkali-activated materials

Vlastimil Bílek Jr. [1], Jan Koplík[2], Jan Hajzler[3] and Barbara Kucharczyková[4]

[1, 2, 3] Brno University of Technology, Faculty of Chemistry, Brno, CZECH REPUBLIC.
(E-mail: bilek@fch.vut.cz, koplik@fch.vut.cz, xchajzlerj@fch.vut.cz)

[4] Brno University of Technology, Faculty of Civil Engineering, Brno, CZECH REPUBLIC.
(E-mail: barbara.kucharczykova@vutbr.cz)

HIGHLIGHTS

- The mixing design of alkali-activated materials is recommended based on the activator molarity and the precursor volume fraction in the system (paste).
- The role of these two parameters, along with different types of activators, is illustrated on alkali-activated slag pastes from the perspective of microstructure and physical-mechanical properties.
- AAS with sodium hydroxide was found to be the most sensitive to changes in the slag volume fraction.

Keywords: microstructure, molarity, volume fraction

INTRODUCTION

Alkali-activated materials (AAMs) have considerable potential as a part of the sustainable toolkit of the inorganic binders [1]. Naturally, their properties are compared to those of binders based on ordinary Portland cement. The analogous expression of their composition is generally used based on the water-to-precursor (binder) weight ratio. The dose of the alkaline activator is then typically expressed as the content of Na2O or K2O with respect to the weight of the slag. The dry matter of the activator can but does not necessarily be incorporated in the expression of water content as a water-to-solids ratio. Furthermore, other expressions, such as the solution-to-precursor weight ratio, combined with activator molarity, are also quite common. Another critical variable arises in the silicate modulus when silicate activators are used. All of these aspects inherently lead to a still-growing jungle of compositions of AAMs over the scientific literature. It thus complicates the comparison of the results, further optimization of these promising materials, and their wider use in real applications.

In this abstract, we would like to discuss another approach based on the molarity of activating solution and the initial precursor volume fraction in the system. We are convinced that this approach is very reasonable, but it is surprisingly rarely used. The molarity of the activating solution dictates its pH, dissolution process, saturation of the pore solution with dissolved species, the stoichiometry of the arising solid products, etc. The solid volume fraction is vital for rheological properties, especially for concentrated suspensions. Still, it also affects hardened properties because of the different nature of the reaction products, depending on the activator type.

Therefore, the aim of this study, which is only a small part of our more comprehensive research, is to induce a change in thinking about the proportioning of AAMs. Alkali-activated slag (AAS) pastes were selected to illustrate the key aspects of the recommended mix design. Three of the most common alkali activators, sodium hydroxide, sodium waterglass (silicate modulus of 1.5), and sodium carbonate, were used. Unlike the vast majority of other studies, all results presented herein were obtained using the approach, according to which the paste is defined by the slag volume fraction and the molarity of the activator. Regardless of the activator type, its molarity is expressed as the molarity of sodium cations.

RESULT & DISCUSSION

Figure 1 illustrates the differences in the AAS pastes' microstructure with the most common activators, namely sodium hydroxide, sodium waterglass (silicate modulus of 1.5), and sodium carbonate. It corresponds to the findings in literature [2,3], i.e., relatively inhomogeneous and porous microstructure for the activation with sodium hydroxide, given by the presence of the reaction products close to the slag grains. On the contrary, sodium waterglass and sodium carbonate showed a homogenous matrix of reaction products among the slag particles with only rare signs of capillary porosity. The matrix is disturbed by cracking, which can partially originate from autogenous shrinkage during the curing period but is mainly affected by mechanical action during the sample preparation and severe conditions during its observation in SEM (vacuuming and exposure of the sample to the electron beam).

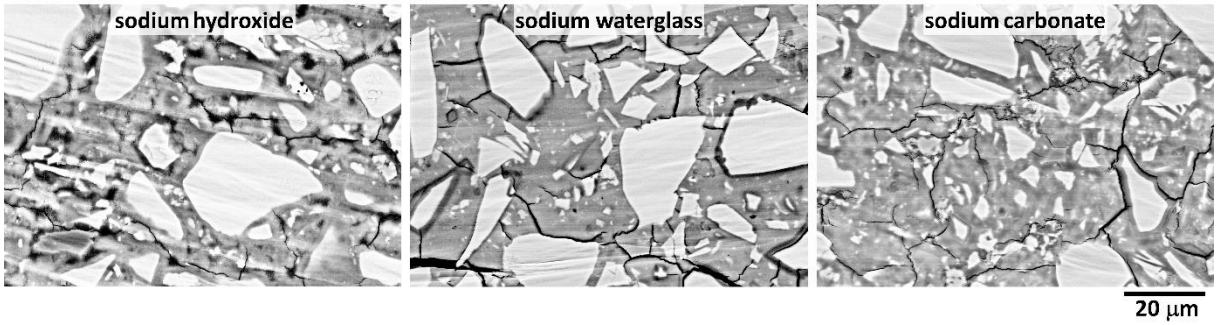

Figure 1. Comparison of the microstructure of alkali-activated slag pastes with three basic types of activators of the same molarity of 4M Na^+ and slag volume fraction of 0.52 after 28 days of reaction.

The differences in microstructure can also be observed by mercury intrusion porosimetry (MIP) for the pore sizes below 100 nm (Figure 2A), i.e., much finer porosity than shown by SEM. In this case, only the results for the pore entry diameters corresponding to the pores lower than 5 μm were considered. This corresponds well with the results of autogenous shrinkage (Figure 2B), which is 3 to 11 times higher for waterglass compared to sodium hydroxide, depending on the slag volume fraction. Another interesting phenomenon is a different evolution of autogenous shrinkage with decreasing slag volume fraction. The autogenous shrinkage of both sodium hydroxide and sodium carbonate-activated slag paste decreases with decreasing slag volume fraction, while the opposite (and not so pronounced) trend can be observed for waterglass. These differences are again due to the different nature of the reaction products. The increased shrinkage with an increase in the slag volume fraction points to the significant microstructure refinement and consequently to an increase in the driving force of shrinkage. The restraining effect of the slag particles, along with the likely marginal changes in pore sizes, explains the behaviour of the pastes with waterglass.

Microstructural differences are directly related to the effects of the slag volume fraction and molarity on compressive strength. Similar to autogenous shrinkage, the slag volume fraction had the most significant impact on the compressive strength of the sodium hydroxide-activated slag (Figure 3A). The same can be observed for the absolute values of the reference compressive strength used for this figure, which were 47, 104, and 72 MPa for sodium hydroxide, sodium waterglass and sodium carbonate, respectively. The magnitudes of the compressive strength are also affected by the molarity of the activator, which is demonstrated here on AAS with sodium hydroxide (Figure 3B). The highest compressive strength values were achieved with molarities of 2 to 4M. Reference pastes with 4M NaOH reached 8, 15, 23, and 31 MPa at the age of 1, 2, 7, and 28 days, respectively. This shows that there is an optimal range of molarities. A further increase in molarity beyond 4M resulted in a gradual decrease in the values of the compressive strength, while a rapid strength decrease was observed as the molarity decreased from 2 to 1M. More details about the results presented herein can be found in our previous papers [4,5]. The differences in strengths of 1 and 2M NaOH are the most significant at early ages (24 and 48 hours), which nicely illustrates another factor vital from both a scientific and

practical perspective. It is the effect of molarity on the reaction kinetics of AAS, to which the evolution of the microstructure and the physical-mechanical properties over time are inherently related.

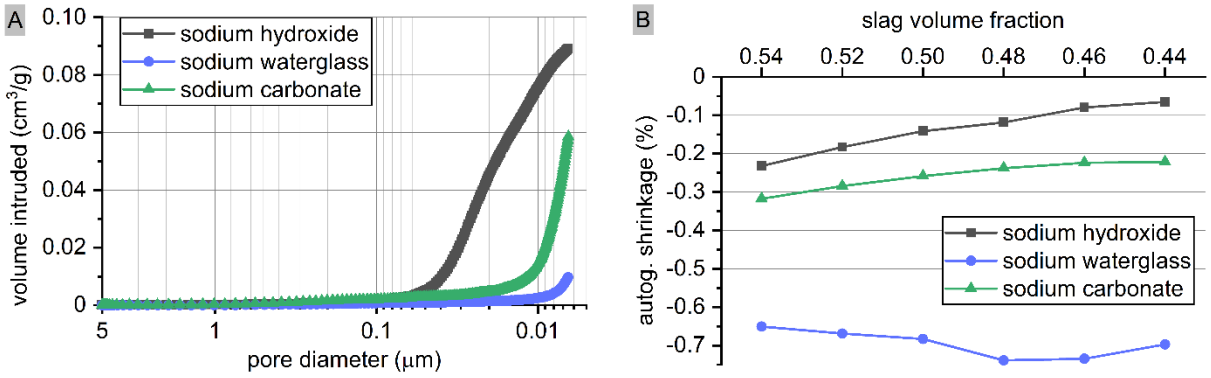

Figure 2. MIP response (A) and autogenous shrinkage (B) of alkali-activated slag pastes with three basic types of activators with the same molarity of 4M Na^+ after 28 days of reaction.

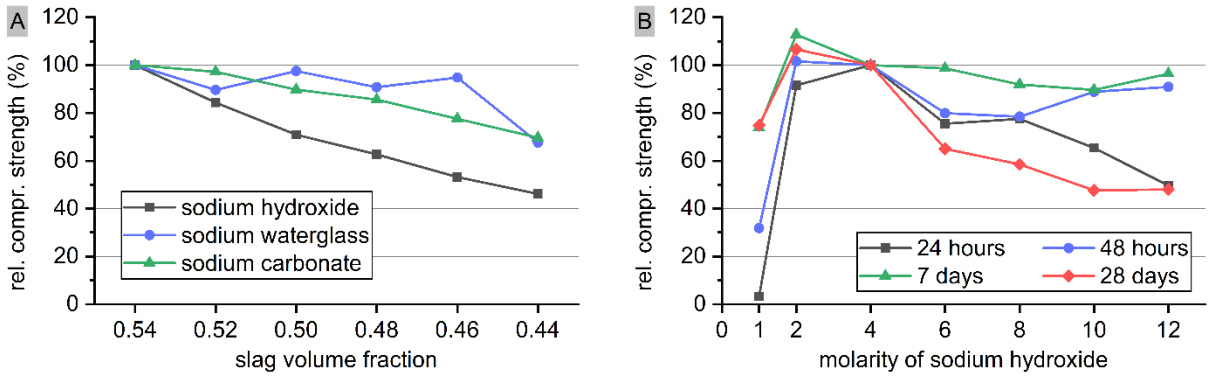

Figure 3. Effect of the slag volume fraction (A) and NaOH molarity (B) on the compressive strength of AAS pastes. The paste with the slag volume fraction of 0.54 for each activator and the paste with 4M at each time were taken as references.

CONCLUSION

The mix proportioning of AAMs based on the activator molarity and precursor volume fraction was proposed and discussed. In addition to the results presented here, the role of molarity in the reaction kinetics and temperature is of great importance. However, this is beyond the possibility of this short contribution and will be discussed in more detail in our subsequent publications and personally at the symposium.

ACKNOWLEDGEMENT

The authors would like to express their appreciation for the support of the Czech Science Foundation through project No 22-02098S.

REFERENCES

[1] Provis, J.L. Alkali-activated materials. *Cement and Concrete Research* 114 (2018) 517-521.

[2] Ben Haha, M., Le Saout, G., Winnefeld, F. and Lothenbach B. Influence of activator type on hydration kinetics, hydrate assemblage and microstructural development of alkali activated blast-furnace slags. *Cement and Concrete Research* 41 (2011) 301-310.

[3] Bernal, S.A., Provis, J.L., Myers, R., San Nicholas, R. and van Deventer, J.S.J. Role of carbonates in the chemical evolution of sodium carbonate-activated slag binders. *Materials and Structures* 48 (2014) 517-259.

[4] Hajzler, J., Bílek Jr., V., Kotrla, J. and Kucharczyková B. Influence of activator type and slag volume fraction on properties of alkali-activated slag pastes, *Journal of Physics: Conference Series* 2341 (2022) 012013.

[5] Hrubý, P., Bílek Jr., V., Iliushchenko, V. and Kalina, L. Dependence of Lignosulfonate Plasticizer Efficiency on the Activator Concentration in Alkali-Activated Blast Furnace Slag Paste. *Solid State Phenomena* 337 (2022)

Effect of water to binder and solution to binder ratio on the hydration kinetics of waterglass activated slag/fly ash blends

M. Mutti[1], S. Joseph[1] and Ö. Cizer[1]

[1] Civil Engineering Department, KU Leuven, Leuven, BELGIUM. (E-mail: marcello.mutti@kuleuven.be)

HIGHLIGHTS

- The water to binder ratio has a significant impact on the rate of the hydration process but does not affect the overall reactivity significantly.
- The solution to binder ratio, whilst only slightly affecting the rate of the hydration, exhibits a pronounced effect on the total heat release.

Keywords: alkali-activated materials, solution to binder ratio, water to binder ratio

INTRODUCTION

Alkali-activated materials (AAMs) are an alternative use of SCMs in combination with an alkali source to mimic cement hydration while actually ruling out ordinary Portland cement (OPC) itself from the formulation [1]. However, not all SCMs attracted the same interest as a potential precursor to be used in AAMs due to different reasons, on top of which there is their worldwide availability [2]. Ground granulated blast furnace slag (GGBFS) and fly ash (FA) nowadays represent the most investigated, and available, binders suitable for AAMs' formulations. These materials are barely reactive when mixed with water, hence the need of an alkali source that can provide the appropriate environment to trigger their hydration. Hydroxide and silicates are by far the most investigated activators, especially as sodium salts, due to the possibility to achieve mechanical properties comparable, when not superior, to OPC [3–5] Due to the presence of the alkaline activator, the mix design of AAMs is inherently more complex than that of a system based on OPC. In case of waterglass activation, parameters such as Na2O, SiO2, water to binder (w/b) and solution to binder (s/b) ratios need to be carefully evaluated as they can drastically change the hydration kinetics and the development of the mechanical properties of the material. Whilst being strictly dependent on each other and difficult to evaluate separately, the s/b and w/b ratios appear to differently affect the hydration kinetics of AAMs. The s/b ratio have been reported to exhibit effects similar to those of w/b in OPC based systems while the w/b appears to have an even more pronounced impact [6–9]. The objective of this study is thus to evaluate separately, taking into account their interdependency, the effects exhibited by s/b and w/b ratios on the hydration kinetics of AAMs. All the materials used in this study were procured commercially. GGBFS and FA were used as binder. The activating solutions were prepared beforehand starting from a waterglass solution (abcr, 8.3% Na2O 27.5% SiO2). Na2O and SiO2 contents were adjusted using NaOH(aq), prepared by dissolving NaOH pellets (VWR, ≥97%), and deionized water. A total of five compositions were designed either changing the s/b or the w/b ratio of a reference composition (Table 1). Isothermal calorimetry measurements were carried out using a TAM Air 8-channel kept at 20°C. The reported experimental results are normalized by the mass of binder. In the case of total heat curves, the first 30 minutes were discarded to not take into account the time necessary for the stabilization of the calorimeter after the sample insertion.

Table 2. Mixes composition.

ID	BFS/FA	s/b	w/b	Na_2O %	SiO_2 %	Ms (SiO_2/Na_2O)
Ref	50/50	0.55	0.42	5.26	7.56	1.44
HS	50/50	0.70	0.53	6.69	9.63	1.44
LS	50/50	0.48	0.36	4.54	6.53	1.44
HW	50/50	0.65	0.51	5.26	7.56	1.44
LW	50/50	0.52	0.37	5.26	7.56	1.44

RESULT & DISCUSSION

As widely reported in literature, the heat flow of AAMs activated with sodium silicate solutions exhibits, analogously to OPC, two well distinct peaks. The first peak is occurring as soon as the binder is mixed with the activating solution and it is associated to the wetting and initial dissolution of reactive particles while the second peak is associated to the formation of significant amount of reaction products and, as visible from the heat flow curves reported in Fig.1a, occurs between 20 and 40h for the compositions investigated in this study. The heat flow curves show that the s/b ratio has a rather limited influence on the hydration kinetics as both the occurrence of the hydration peak and its intensity appear close to those of the reference composition despite such parameter was modified up to around 30% (Ref to HS). In contrast to what observed in case of changes in s/b, the w/b ratio exhibits a much greater effect on the hydration kinetics. Despite being modified at a slightly lower magnitude, up to ~22%, the hydration peaks of HW and LW appear significantly shifted with respect to that of the reference composition and are also of significantly lower intensity in the case of HW. The differences evaluated in the heat flow curves are reflected in the total heat release, reported in Fig.1b, at least in the first few days of hydration. Here, it can be seen that the curves associated to all the compositions, with the exception of HW, almost overlap up to 24h from mixing time corresponding to the hydration peak maximum of HS. After that, the total heat release of both HS and LS starts to diverge from that of Ref. The heat release of LW also appears to diverge but to a lesser extent while that of HW gradually approaches the Ref one. These behaviours observed in the isothermal calorimetry measurements clearly indicate that the concentration of the activating solution plays a more significant role than the absolute amount of introduced species in defining the hydration kinetics of AAMs despite the almost identical pH of the activating solutions. The quicker occurrence of the hydration peak observed in LW compared to LS, and the opposite for what concerns HS and HW, might be inferred to the lower extent of dissolution of the binder necessary to reach saturation with respect to the hydration products. Moreover, the polycondensation of dissolved silicates eventually leads to their precipitation, thus favouring further hydrates precipitation by acting as nucleation seeds [10]. This phenomenon is once again promoted by the higher concentration of alkalis originated by reducing the w/b while keeping both Na_2O and SiO_2 constant. Whilst accelerating/decelerating the precipitation of hydrates, it does not appear that w/b exerts a significant influence on the extent of the hydration process; the opposite seems true for the s/b ratio. Assuming that analogous phase assemblages are formed in the investigated compositions, the gaps observed in the total heat release are thus associated to a different amount of hydrates that precipitates. Whilst exhibiting similar rate, the amount of volume available for the precipitation of products significantly changes between LS, Ref, and HS. This means that more products need to be precipitated in order to arrest the system and move towards a diffusion controlled process [9,11]. This is true also in the case of changes in w/b ratio but in that case the effects of the activator's concentration appear to prevail.

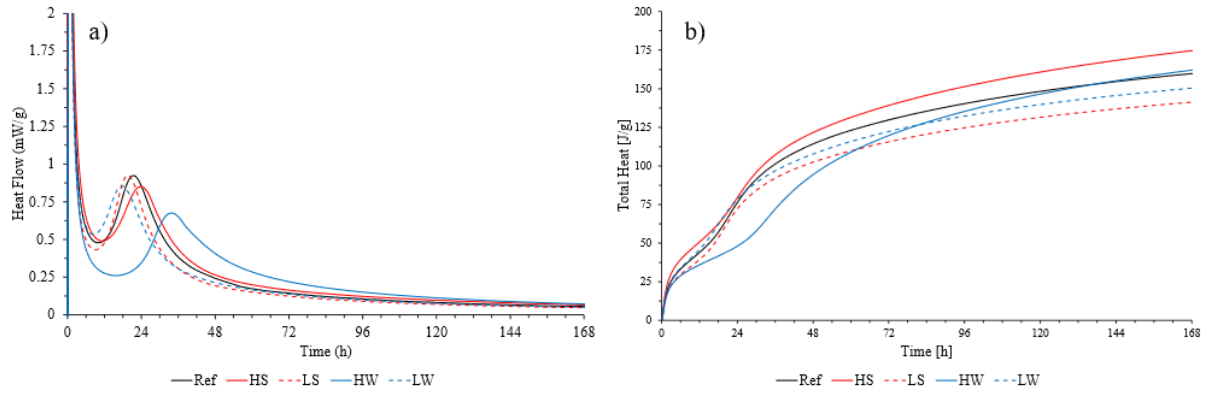

Figure 1. a) Heat flow curves b) Total heat release.

CONCLUSION

In this study we investigated the effect of s/b and w/b ratios on the hydration kinetics of waterglass AAMs. The experimental results clearly indicate that the w/b exerts more influence on the reactivity of the system. Affecting the concentration of the activating solution leads to significant shortening or lengthening of the induction period. This might be due to the different extent of binder's dissolution necessary to achieve the conditions for the products to precipitate, assuming a similar dissolution rate for the different compositions. Over longer periods it appears that the s/b ratio plays a greater role; it does not affect the rate at which the hydration occurs but it seems to influence the amount of hydrates that can precipitate. This is assumed to be due to both the volume availability as well as the amount of silicates introduced with the activating solution.

ACKNOWLEDGEMENT

This work is supported by the EOS-programme (The Excellence of Science) through research project 30439691.

REFERENCES

[1] Provis, J. L. Alkali-activated materials. *Cem. Concr. Res.* 114, 40–48 (2018).

[2] Snellings, R. Assessing, Understanding and Unlocking Supplementary Cementitious Materials. *RILEM Tech. Lett.* 1, 50 (2016).

[3] Ismail, I. *et al.* Modification of phase evolution in alkali-activated blast furnace slag by the incorporation of fly ash. *Cem. Concr. Compos.* 45, 125–135 (2014).

[4] Hojati, M. & Radlińska, A. Shrinkage and strength development of alkali-activated fly ash-slag binary cements. *Constr. Build. Mater.* 150, 808–816 (2017).

[5] Luo, X., Xu, J., Bai, E. & Li, W. Systematic study on the basic characteristics of alkali-activated slag-fly ash cementitious material system. *Constr. Build. Mater.* 29, 482–486 (2012).

[6] Chi, M. C. & Liu, Y. C. Effects of fly ash/slag ratio and liquid/binder ratio on strength of alkali-activated fly ash/slag mortars. *Appl. Mech. Mater.* 377, 50–54 (2013).

[7] Dai, X., Aydin, S., Yardimci, M. Y., Lesage, K. & de Schutter, G. Influence of water to binder ratio on the rheology and structural Build-up of Alkali-Activated Slag/Fly ash mixtures. *Constr. Build. Mater.* 264, 120253 (2020).

[8] Ruiz-Santaquiteria, C., Skibsted, J., Fernández-Jiménez, A. & Palomo, A. Alkaline solution/binder ratio as a determining factor in the alkaline activation of aluminosilicates. *Cem. Concr. Res.* 42, 1242–1251 (2012).

[9] Han, F., Zhang, Z., Liu, J. & Yan, P. Effect of water-to-binder ratio on the hydration kinetics of composite binder containing slag or fly ash. *J. Therm. Anal. Calorim.* 128, 855–865 (2017).

[10] Gebregziabiher, B. S., Thomas, R. & Peethamparan, S. Very early-age reaction kinetics and

microstructural development in alkali-activated slag. *Cem. Concr. Compos.* 55, 91–102 (2015).

[11] Rahimi-Aghdam, S., Bažant, Z. P. & Abdolhosseini Qomi, M. J. Cement hydration from hours to centuries controlled by diffusion through barrier shells of C-S-H. *J. Mech. Phys. Solids* 99, 211–224 (2017).

Reaction of carbonate minerals in alkaline medium

Rafia Firdous[1] and Tamino Hirsch[2]

[1, 2] Building Materials and Construction Chemistry, Institute of Civil Engineering, Technische Universität Berlin, Berlin, GERMANY. (E-mail: rafia.firdous@tu-berlin.de, t.hirsch@tu-berlin.de)

HIGHLIGHTS

- Anhydrous carbonate minerals react with NaOH and Na-silicate solutions.
- They can supply cations for formation of C-N-S-H gel.
- Formation of Na- and Ca-Na-carbonates can be detrimental for building products.

Keywords: carbonate minerals, alkali-activated materials, thermodynamics

INTRODUCTION

The environmental goals of the EU aim at achieving carbon neutrality by 2050 and therefore all the industrial processes must be re-thought. Reusing and recycling industrial, agricultural, and urban wastes to achieve a circular economy is one of these major goals. Building construction materials industry makes up to 10% of the anthropogenic CO2 emissions with the highest share originating from production of clinker for various types of Portland cement [1]. In a road map defined by cement technology authorities several ways from the manufacture to use of Portland cement have been defined in order to reduce these emissions [2]. Several types of cements show varying CO2 reduction potential based on their clinker content. Other alternative solutions include alkali-activated materials, which can be synthesized by the reaction of an aluminosilicate raw material with an alkaline source. Researchers have shown that depending upon the mixture design, type of materials and methods used, a lot of different strength classes and CO2 reductions can be observed [3]. The freedom of choice of raw material for these binders makes it possible to consider aluminosilicate-rich industrial, agricultural, or urban residues for production of such binders. This on the one hand shows a potential of recycling these materials, however, on the other hand this variation in materials leads to the fact that for each component of the raw material a detailed understanding should be developed. The minerals contained in these raw materials affect the mechanical, durability and micro-structural characteristics of these binders [4].

Carbonates are one of the mineral groups which are commonly available throughout the globe and can be not only a part of naturally occurring materials but can be also found in waste materials. Anhydrous carbonates containing various endmembers such as calcite, dolomite, siderite, ankerite, natrite are often observed in the raw materials. Previous work [5] on the reaction of calcite in alkaline medium showed that upon its reaction with sodium silicates, calcite can provide calcium for the formation of a sodium-containing calcium silicate hydrate. Whereas the carbonate can react with sodium and water from the solution to form water-containing sodium carbonate. Such a growth of the sodium carbonate was found to be detrimental for the binder, as precipitation of this phase in hardened binder was exhibiting an inner tensile pressure thus reducing the strength of the binder. Moreover, the formation of this phase was also depleting the system in alkalis and water.

The current work deals with determination of reactivity of two iron-magnesium-calcium carbonates (dolomite-ankerite solid solution) with sodium hydroxide and sodium silicate solutions. The carbonate samples milled in laboratory disk-mill are characterized by X-ray diffraction analysis (XRD) for their composition and are reacted with sodium hydroxide (16 mol/kg, labelled NH) and sodium silicate

(SiO2/Na2O = 1.1 mol/mol, labelled NS) solutions. Reaction kinetics are studied in an isothermal conduction calorimeter at 20 °C. The reaction products are tested with XRD and thermogravimetric analysis (TGA). Moreover, thermodynamic modelling is performed to predict the phase assemblage.

RESULTS & DISCUSSION

The characterization of the carbonate samples with XRD showed that both samples contain varying amounts of the endmembers. The sample named "D" contained more magnesium than iron and is by XRD approximately CaMg0.77Fe0.23(CO3)2. The other Fe-rich sample is named "S" and it is estimated to be CaMg0.32Fe0.68(CO3)2. The isothermal conduction calorimetry results for both samples with NH and NS are presented in Figure 1. The heat flow is normalized to the weight of the carbonate samples. Both sodium silicate and sodium hydroxide samples exhibit an exothermic reaction immediately at contact of liquid with solids. However, the samples reacted with NH solution show a second exothermic reaction. The time of the second exothermic reaction is different for both high- and low-iron samples. The Fe-rich carbonate (S) showed this peak in first 48 h, whereas the Mg-rich carbonate (D) showed this peak starting 24 h and continued till 144 h. Whereas samples reacted with NS showed no second exothermic reaction till 144 h.

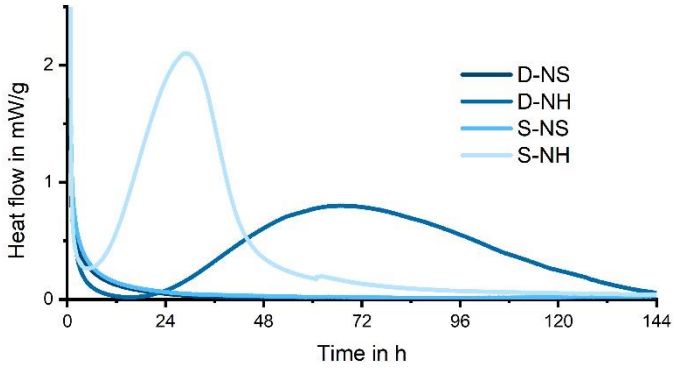

Figure 1. Isothermal conduction calorimetry curves for all samples.

The crystalline phase assemblage of reacted samples measured via X-ray diffraction analysis and complete phase assemblage predicted via thermodynamic modelling is tabulated in Table 1. The crystalline phases observed in XRD included gaylussite, brucite and pirssonite for NH reaction. Whereas for NS reacted samples thermonatrite and gaylussite are observed. Thermodynamic modelling performed via GEMS calculations is in fully oxidized conditions. The predicted phase assemblage is reported for 50% allowed degree of carbonate sample reaction. However, the actual degree of precursor reaction is so far not measured. For NH reacted samples compared to XRD, thermodynamic modelling showed additionally formation of ferrihydrite. Similarly for NS samples formation of amorphous C-N-S-H and M-S-H gels and ferrihydrite is predicted for the Mg-rich sample. Whereas for the Fe-rich sample at 50% allowed degree of reaction, formation of M-S-H, ferrihydrite and amorphous silica is predicted.

Table 1. Phase assemblage measured via X-ray diffraction and thermodynamic analysis

Sample ID	X-ray diffraction analysis	Thermodynamic analysis
D-NS	Ankerite, Thermonatrite, Gaylussite	Pore solution, CNASH, Gaylussite, MSH, Ferrihydrite, Unreacted precursor
S-NS	Ankerite, Thermonatrite, Gaylussite	Pore solution, Gaylussite, MSH, Ferrihydrite, amorphous silica, Unreacted precursor
D-NH	Ankerite, Gaylussite, Brucite, Pirssonite	Pore solution, Gaylussite, Ferrihydrite, Brucite, Unreacted precursor
S-NH	Ankerite, Gaylussite, Brucite, Pirssonite	Pore solution, Gaylussite, Ferrihydrite, Brucite, Unreacted precursor

The TGA conducted on NH reacted samples (Figure 2) showed a characteristic water loss from gaylussite in temperature range of 100-200 °C, whereas the carbonate decomposition is observed around 600-700 °C. A mass loss around 300 °C could be due to brucite. For NS reacted samples (Figure 2) a mass loss around 100 °C could be due free and partially bound water. Here also carbonate mass loss can be observed around 500-700 °C. Additionally in Mg-rich carbonate (D) a mass change observed around 800 °C could be due to C-N-S-H type phases.

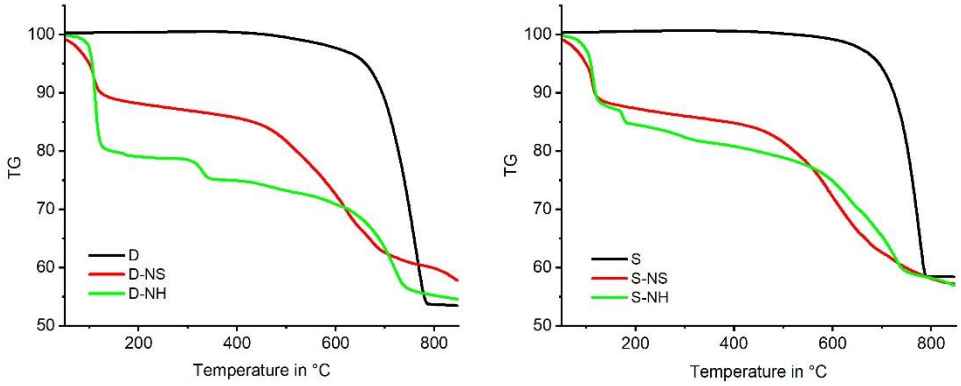

Figure 2. Thermogravimetric analysis for all samples.

CONCLUSION

The findings show that upon reaction of mineral samples from the dolomite-ankerite solid solution series under alkaline conditions with sodium hydroxide and sodium silicate formation of C-N-S-H gel like phases can be observed. Whereas the carbonate can lead to formation of other carbonate phases. Inclusion of Ca-Mg-Fe carbonates in aluminosilicate material for alkali-activation could not only enhance the formation C-N-A-S-H type gel but can also supply free carbonate for formation of other carbonate phases which could be detrimental for durability. Further work should be conducted to clarify this effect. Moreover, the limitations of the thermodynamic database should be improved in future to make better predictions.

ACKNOWLEDGEMENT

This study is supported by Bundesministerium für Bildung und Forschung under grant number 01LJ2006C.

REFERENCES

[1] United nations environment programme (2021). 2021 Global status report for buildings and construction: Towards a zero-emissions, efficient and resilient buildings and construction sector. Nairobi.

[2] International Energy Agency, World Business Council for Sustainable Development, Cement Sustainability Initiative. Technology Roadmap - Low-Carbon Transition in the Cement Industry. France; 2018.

[3] Firdous, R. Nikravan, M. Mancke, R. Vöge, M. Stephan, D. Assessment of environmental, economic and technical performance of geopolymer concrete: a case study. Journal of Material Science57(40) (2022),18711–25. https://doi.org/10.1007/s10853-022-07820-6.

[4] Firdous, R. Alkali activated natural pozzolans for geopolymer cement. https://doi.org/10.14279/depositonce-11551.

[5] Firdous, R. Hirsch, T. Klimm, D. Lothenbach, B. Stephan, D. Reaction of calcium carbonate minerals in sodium silicate solution and its role in alkali-activated systems. Minerals. Engineering, 165(3) (2021):106849. https://doi.org/10.1016/j.mineng.2021.106849.

Effect of mixing methods on workability and ultrasound measurements of alkali-activated materials

L. Hertwig[1], B. H. Tekle[2] and K. Holschemacher[1]

[1] Leipzig University of Applied Sciences, Structural Concrete Institute, Leipzig, GERMANY.
(E-mail: ludwig.hertwig@htwk-leipzig.de, klaus.holschemacher@htwk-leipzig.de)

[2] Federation University, Institute of Innovation, Science and Sustainability, Ballarat, AUSTRALIA.
(E-mail: b.tekle@federation.edu.au)

HIGHLIGHTS

- Ultrasonic measurements of alkali-activated materials
- Speed, mixing time and rest time affects workability and setting behaviour

Keywords: alkali-activated material, mixing methods, workability, ultrasonic testing, setting time

INTRODUCTION

As a new construction material, alkali-activated binders are attracting considerable research. This is due to the use of by-products or waste materials, environmental promises, and comparative performance with ordinary Portland cement binders. Most research in this area is limited to the investigation of mechanical and durability behaviours. A better understanding of their fresh properties and mixing procedures is paramount for better acceptance and application of alkali-activated materials in the construction industry.

Alrefaei et al. found that the choice of the mixing device, the mixing regime, and the mixing order effects the fresh and hardened concrete properties [1]. Puertas et al. suggested increasing the mixing time to improve the setting behaviour and increase workability [2]. In their study on Na2SiO3-anhydrous-activated binder, Alrefaei et al. compared one-part and two-part mixing techniques and proposed a hybrid mixing method where the mixing water is divided into two parts [1]. Their results showed that the mixing technique adopted affects the fresh and hardened concrete properties, with no change in chemical composition. Rasuli et al. observed that storing ingredients at a higher temperature of 45 °C and mixing them at a constant temperature of 24 – 26 °C results in a significant improvement in the flow and rheology of the mixture [3].

In this paper, four factors: the total mixing speed, the total mixing time, the length of a rest time, and the time at which the superplasticizer (SP) was added are investigated to understand the effects of the mixing on alkali-activated materials. Three variations are studied for each factor. A self-compacting fine-grained mortar with a maximum grain size of D = 3.15 mm was used. A mixed precursor system containing fly ash (FA), ground-granulated blast-furnace slag (GGBS), and silica fume (SF) is used. The chemical composition of the precursors can be found in [4]. The activator solution was a mix of sodium silicate and sodium hydroxide. The sodium silicate solution includes 26.82 % silicate, 8.2 % sodium oxide, and 64.98 % water. The sodium hydroxide is a 50 % by-weight solution. The amount of the sand, water, FA, GGBS, SF, sodium silicate, and hydroxide solutions in kg/m3 are 1180, 113, 357.5, 260, 32.5, 165, and 66. A SP (Geo-1, Sika Deutschland GmbH, Stuttgart, Germany) was applied to increase the workability and improve the setting time. The planetary mixing device (mortar mixer, 5 l, Testing Bluhm & Feuerherdt GmbH, Berlin, Germany) with two rotational speeds and complying with EN 196-1 was used. The low speed is 140 rpm with a planetary rotation of 62 rpm, and the high speed is 285 rpm

with a planetary rotation of 125 rpm.

no.	factor	slump	a_{max} [a]	$t_{a=max}$ [b]
		mm	$\cdot 10^3$(m/s)/min	min
1	control	264 ± 2	27 ± 4	84 ± 7
2	speed	280	32	70
3	speed	275	25	97
4	time	273	28	97
5	time	293	30	85
6	rest	283	26	90
7	rest	288	28	87
8	SP	268	24	87
9	SP	275	25	88

[a] ultrasonic, max acceleration
[b] ultrasonic, time of max acceleration

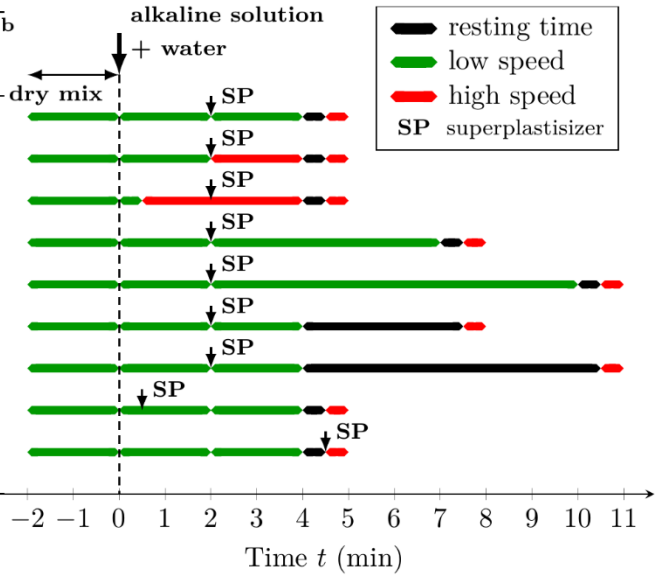

Figure 1. Experimental results (left) and illustration of used mixing regimes (right).

All mixtures were dry mixed for 120 s prior to adding the alkaline solution and extra water. The alkaline solution was premixed before the mixing day, and the extra water was added to the solution. The mix of alkaline solution and water was added slowly during mixing for about 30 s. The SP was slowly poured during the mixing process. At the beginning of the rest period, the vessel and paddle were scraped and manually checked for agglomeration for 10 – 15 s. The mixing regime of each sample can be found in Figure 1. The investigated parameters include the slump flow using the Hägermann cone and the ultrasonic parameters such as maximum acceleration and the time at which maximum acceleration was attained. The ultrasonic measurement was performed using IP-8, UltraTest GmbH, Achim, Germany. The slump tests started 3 – 6 min after finishing the mixing process. The ultrasonic measurements started within 5 – 8 min after mixing.

RESULT & DISCUSSION

Within the investigated ranges, the mixing regime showed different effects more pronounced on the workability than on the ultrasonic parameters. The ultrasonic velocity measurement typically shows three stages. In the beginning, there is a dormant stage with low velocity development. The second stage is the acceleration stage, where the ultrasonic velocity increases very fast due to the formation of reaction products transitioning from the liquid to the solid phase. In the third stage, the ultrasonic velocity increases more slowly over time. A previous study by the authors showed a good relationship between the time of the maximum acceleration and the initial and final setting times of the Vicat needle test [5].

To study the effects of mixing parameters on workability and setting time, the slump flow, the maximum acceleration amax and the time of the maximum acceleration ta=max were analyzed. Each measurement of the investigated factor is compared to a common control mix. The factor ranges were selected keeping a realistic mixing regime. To simplify the interpretation of the results only one property of the mixing regime was changed at once. The properties of the control mix were measured on five different batches to provide an uncertainty window. Figure 2 illustrates a summary of the investigated factors and the measured results. The increase in mixing time from 5 min to 11 min led to an increase in the slump by about 15 mm. Increasing the resting time from 0.5 min to 4.5 min also increased the workability. The factor "speed" is displayed by the total mean of rotations per minute (rpm). The slump generally increased with a higher mean rotation rate. Regarding the setting behaviour the time of the maximum acceleration and the maximum acceleration were analyzed. In

general the acceleration maximum was not affected much by the different factors. Only the increase of speed led to a higher amax until the mean rotation rate of 200 rpm. At 240 rpm amax was lower than the control mix, but increased ta=max by 13 min. The ultrasonic parameters are usually inversely proportional. Samples with higher ta=max had lower amax and vice versa. An exception is the mixing time (c.f. Figure 2f). The acceleration maximum at a mixing time of 8 min did not change, however the time when it was reached was prolonged (Figure 2j). A further increase of the mixing time to 11 min led to a decrease. Fernández-Jiménez and Puertas linked the initial pH of the alkaline solution with the setting time [6]. As the amount of the alkaline solution was kept constant this may explain why the mixing regime affected the workability more than the setting behaviour.

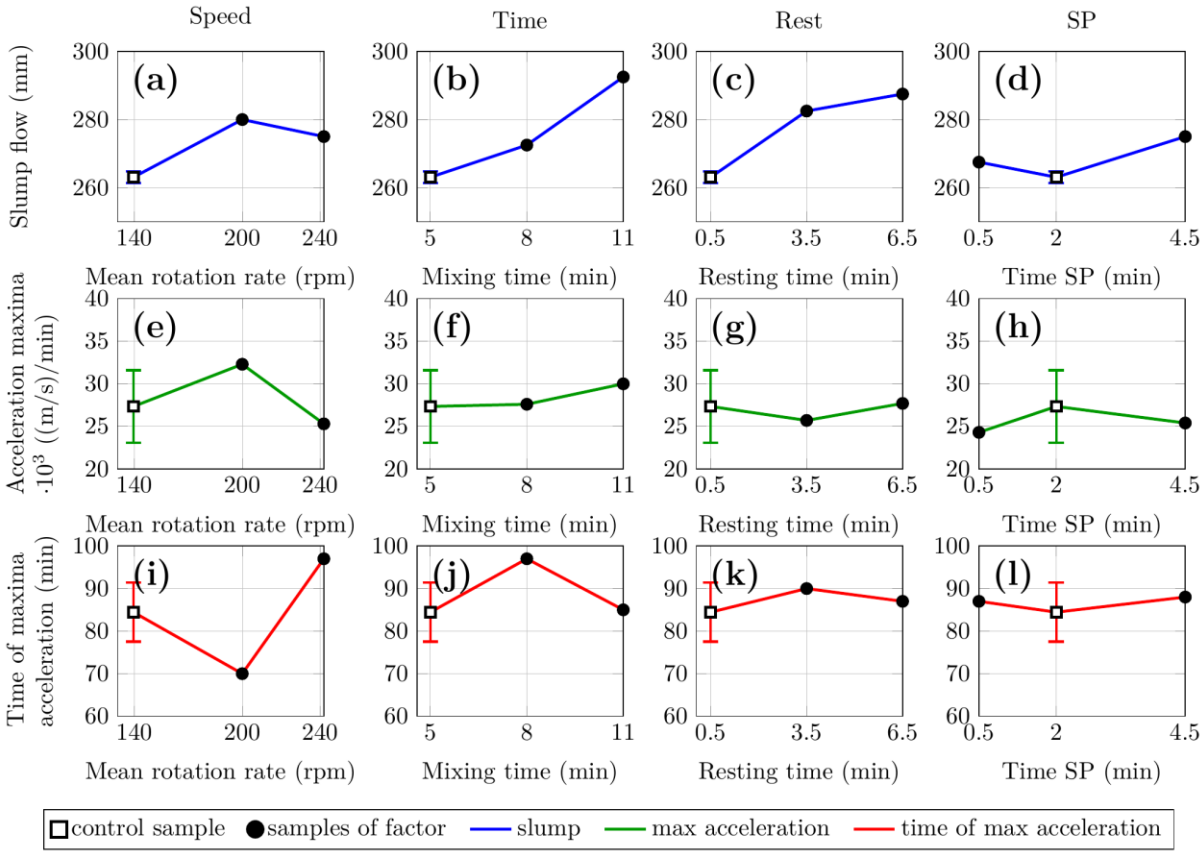

Figure 2. Results of slump, maximum acceleration and the time of maximum acceleration according to investigated factors. The standard deviation is only available for the control mix.

CONCLUSION

The method of mixing alkali-activated materials affects the fresh concrete properties. Mixing speed, mixing time, rest period, and the time of addition of the SP are investigated as parameters. Based on the results observed, the following conclusions can be drawn:

- the investigated parameters showed different effects on workability and setting behaviour,
- the mixing methods mainly affect the workability, the time of maximum acceleration is slightly affected by the mixing speed and the mixing time,
- the investigated parameters showed inverse effect on maximum acceleration and time at which this acceleration is attained,
- the investigated parameters showed no major effects on the acceleration maximum,
- the workability increase with the mixing speed, mixing and rest time,
- longer mixing and resting time led to the highest workability increase.

REFERENCES

[1] Alrefaei, Y., Wang, Y.-S. and Dai, J.-G. Effect of mixing method on the performance of alkali-activated fly ash/slag pastes along with polycarboxylate admixture. Cement and Concrete Composites 117, 103917 (2021).

[2] Puertas, F., Varga, C. and Alonso, M.M. Rheology of alkali-activated slag pastes. Effect of the nature and concentration of the activating solution. Cement and Concrete Composites 53 (2014), 279–288.

[3] Rasuli, M.I., Tajunnisa, Y., Yamamura, A. and Shigeishi, M. A consideration on the one-part mixing method of alkali-activated material: problems of sodium silicate solubility and quick setting. Heliyon 8, e08783 (2022).

[4] Tekle, B.H., Hertwig, L. and Holschemacher, K. Rheology of Alkali-Activated Blended Binder Mixtures. Materials 14, 5405 (2021).

[5] Tekle, B.H., Hertwig, L. and Holschemacher, K. Setting Time and Strength Monitoring of Alkali-Activated Cement Mixtures by Ultrasonic Testing. Materials 14, 1889 (2021).

[6] Fernández-Jiménez, A. and Puertas, F. Setting of alkali-activated slag cement. Influence of activator nature. Advances in Cement Research 13 (2001), 115–121.

Preparation of precursors for alkali-activated materials by remelting

Tamino Hirsch[1], Anja Buchwald[2], Rafia Firdous[1] and Dietmar Stephan[1]

[1] TU Berlin, Institute of Civil engineering, Berlin, GERMANY.
(E-mail: t.hirsch@tu-berlin.de, rafia.firdous@tu-berlin.de, stephan@tu-berlin.de)

[2] ASCEM B.V., Dodewaard, NETHERLANDS. (E-mail: a.buchwald@ascem.nl)

HIGHLIGHTS

- Preparation of highly reactive precursor glass by remelting waste
- Characterization of the glass in alkali activation
- Thermodynamic modelling of reaction products

Keywords: alkali activation, artificial glass, waste utilization, thermodynamic modelling

INTRODUCTION

Due to the urgent need to decrease the CO2 emissions of humanity and to reduce waste, the use of secondary raw materials for the production of building materials is increasing [1]. Such inorganic secondary raw materials can be used as a substitute for Portland cement and as a raw material for alternative binders like alkali-activated materials (AAM). Common secondary raw materials as precursors for AAM are ground granulated blast furnace slag and fly ash [2]. However, both materials are already virtually completely in use [2]. Furthermore, the substitution of coke in iron production and the closedown of coal power plants lead to changes in the reactivity of ground granulated blast furnace slag and a decrease in fly ash production, respectively.

On the other hand, large quantities of inorganic wastes are used for low-requirement applications or are even currently unused [3]. These less common secondary raw materials include mine tailing material, slags of metal production with lower annual turnover than iron, waste burning ashes and multiple more [2]. Some of these materials may already be reactive, but most possess a low reactivity and can vary in composition over time.

These issues might be overcome by remelting these materials to obtain more reactive, homogeneous materials. This is the target of the project PHöMixBeton. The current publication deals with the basic characterization of such a remolten material used to produce an alkali-activated material.

MATERIALS AND METHODS

The glass precursor for the alkali-activated material was prepared by the fusion of ferrochrome slag with several wastes and additives in an industrial electric arc furnace. The melt was granulated and ground in a ball mill with air classification. The composition of the glass is given in Table 1.

Table 1. Composition of the glass as determined by X-ray fluorescence [wt%].

Al_2O_3	CaO	Cr_2O_3	Fe_2O_3	K_2O	MgO	Na_2O	SiO_2	SO_3	TiO_2	LOI
18.5	41.6	0.6	1.4	0.2	6.5	0.9	28.3	0.8	0.6	0.2

Geopolymer pastes were prepared with several activating solutions. These alkaline solutions include sodium hydroxide solutions with 3 to 25 wt% sodium hydroxide and sodium as well as potassium water glass solutions.

The heat generation of the pastes was observed by isothermal conduction calorimetry using an MC-CAL/100P (C3 Prozess- und Analysentechnik GmbH) at a glass-to-solution ratio of 0.5. The pastes were externally prepared by mixing 1 min with a vortex mixer.

Thermodynamic calculations were performed with GEMS 3.7 [4] and the databases PSI-Nagra12/07 [5] and Cemdata18 [6]. The “CNASH solid solution” model was chosen in the calculations as C-S-H model.

RESULT & DISCUSSION

As can be seen in Figure 1, the artificial glass shows with variable alkaline solutions a strong reaction. In the case of sodium hydroxide solutions, not only an initial peak but one or more additional heat release events can be observed. These later events shift to an earlier time with increased sodium hydroxide content. With a sodium hydroxide solution of 25 wt%, these events are so strongly accelerated that they overlap indistinguishable with the initial peak. The activation of the artificial glass with waterglasses of sodium and potassium resulted in a flash set due to the high reactivity of the glass.

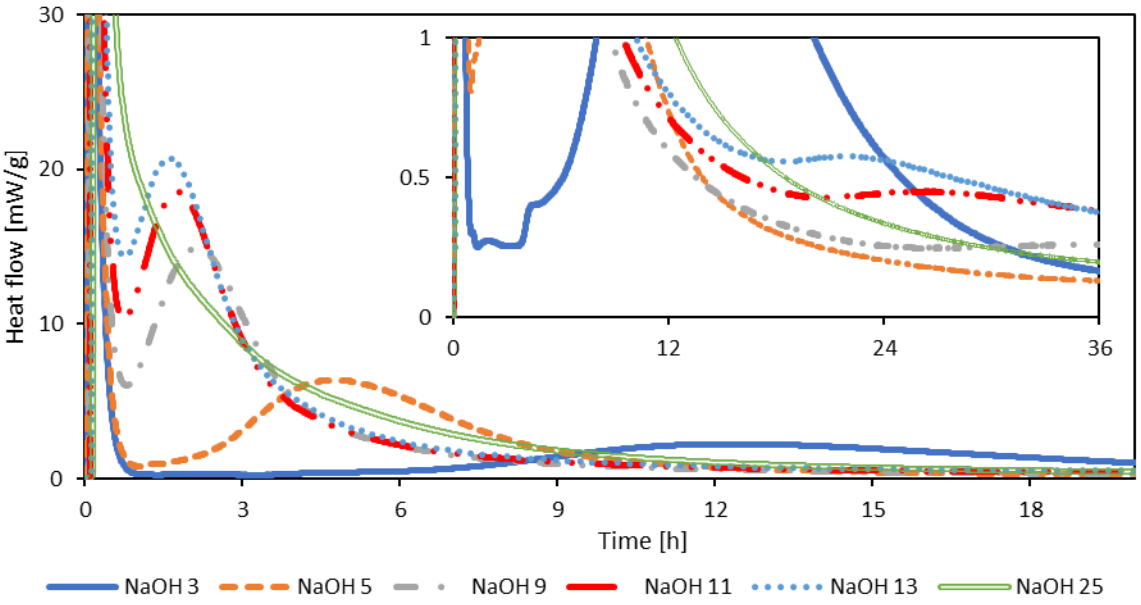

Figure 1. Heat flow by the alkali-activated artificial glass.

Thermodynamic modelling was performed so that it mimes a congruent gradual reaction of the slag. The reaction products with sodium hydroxide solution are majorly C-S-H (containing sodium and aluminum), strätlingite and hydrotalcite (MgAl-OH-LDH) (Figure 2), which is quite similar to alkali-activated blast furnace slag [7].

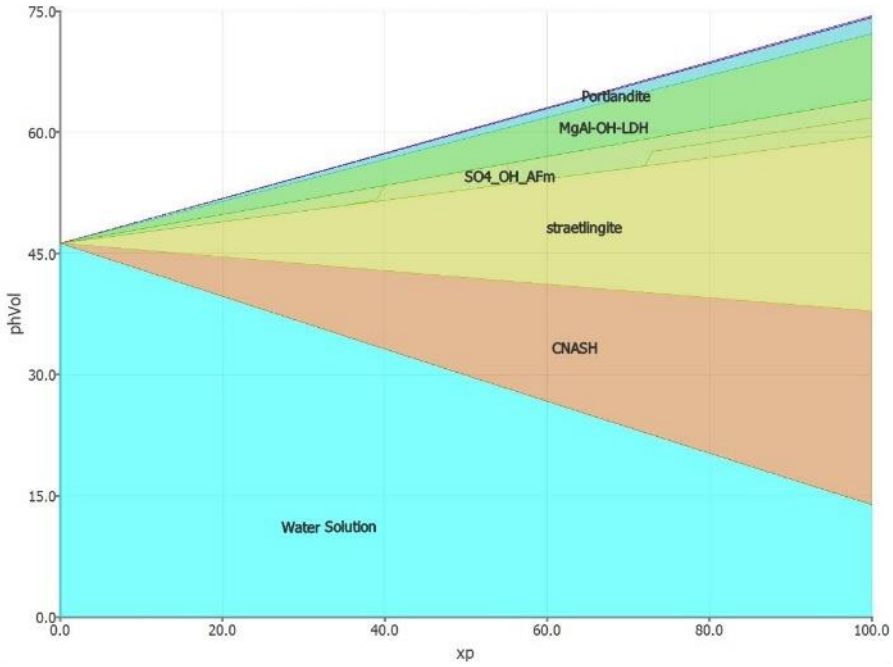

Figure 2. Reaction products of the activation of the artificial glass by the addition of low-concentrated sodium hydroxide solution. The unreacted slag is not shown. The horizontal axis indicates the degree of reaction of the artificial glass.

CONCLUSION

It is possible to produce a highly reactive precursor for alkali activation based on ferrochrome slag, which can be activated by very low-concentrated alkaline solutions. The expected reaction products are comparable to blast furnace slag.

ACKNOWLEDGEMENT

The authors are thankful to the German Bundesministerium für Bildung und Forschung for supporting this work in the scope of the project PHöMixBeton (Grant numbers 01LJ2006C).

REFERENCES

[1] United nations environment programme (2021). 2021 Global status report for buildings and construction: Towards a zero-emissions, efficient and resilient buildings and construction sector. Nairobi.

[2] J. L. Provis, J. S. J. van Deventer, Alkali Activated Materials, State-of-the-Art Report, RILEM TC 224-AAM. Springer, Dordrecht, Heidelberg, New York, London, 2014

[3] K.S. Al-Jabri, Research on the use of ferro-chrome slag in civil engineering applications, MATEC Web Conf. 149 (2018) 1017

[4] T. Wagner, D.A. Kulik, F.F. Hingerl, S.V. Dmytrieva, GEM-Selektor geochemical modeling package: TSolMod library and data interface for multicomponent phase models, Can. Mineral. 50 (2012) 1173–1195.

[5] T. Thoenen, W. Hummel, U. Berner, E. Curti, The PSI/Nagra Chemical Thermodynamic Database 12/07: PSI report 14-04, Villigen, Switzerland, 2014.

[6] B. Lothenbach, D.A. Kulik, T. Matschei, M. Balonis, L. Baquerizo, B. Dilnesa, G.D. Miron, R.J. Myers, Cemdata18: A chemical thermodynamic database for hydrated Portland cements and alkali-activated materials, Cem. Concr. Res. 115 (2019) 472–506.

[7] B. Lothenbach, A. Gruskovnjak, Hydration of alkali-activated slag: thermodynamic modelling, Advances in Cement Research 19 (2007) 81–92.

The relationship between mixture design and efflorescence formation in geopolymers made of iron ore tailings

Rafaela K. R. Silva[1], Polyana F. F. Martins[2], Márlon A. Longhi[3] and Fernando S. Lameiras[4]

[1, 2, 4] Nuclear Technology Development Center, CDTN, Minas Gerais, BRAZIL.
(E-mail: rkassia93@gmail.com, polyfabri@yahoo.com.br, fsl@cdtn.br)

[3] Circlua, Minas Gerais, BRAZIL. (E-mail: marlon.longhi@circlua.com.br)

HIGHLIGHTS

- The iron ore sand from the beneficiation of the iron ore in the Iron Ore Quadrangle (Minas Gerais, Brazil) was used to produce solid sodium silicate for the synthesis of a one-part geopolymer.
- The iron ore sand was also used as fine aggregate to produce a one-part geopolymer mortar.
- A simplex centroid mix design of metakaolin, solid sodium silicate, and iron ore sand (as aggregate), with the addition of water as a process variable, was performed to study the efflorescence of the geopolymer mortar.

Keywords: geopolymer, iron ore sand, efflorescence formation

INTRODUCTION

Iron ore tailings are available in large amounts in the state of Minas Gerais, especially in the Iron Ore Quadrangle area, which concentrates some of the most important iron ore mines in Brazil. After the collapse of two dams with huge social and environmental impacts, new applications for these tailings are required to reduce their disposal in the environment. The tailings result from the iron ore beneficiation process, which separates the quartz particles from the iron oxide ones in a flotation cell or column (Duarte & Lameiras, 2022), and can be used in geopolymer mortar as fillers. They can also be used as a raw material to produce an anhydrous solid sodium silicate after a thermal process at 400-450°C (Vogt & Lameiras, 2019) to synthesize a one-part geopolymer. This solid sodium silicate produced with iron ore sand is a new material and not reported in the literature currently available, so this work also aims to achieve more information on the use of this material in geopolymer composition.

Geopolymers are a type of cement with low content of calcium obtained by the reaction of an aluminosilicate source, such as ground natural rocks or industrial by-products, and an alkali activator, such as sodium or potassium hydroxide or silicate (Provis, 2017). Geopolymerization consists of the formation of a ceramic-like structure composed of chains of covalent-bonded molecules, resulting in an inorganic polymer, with properties like high mechanical strength, and resistance to fire and acid attack. The applications include civil construction, aviation, and art pieces, amongst others (Davidovits, 2017). This material can be synthesized by the mixture of a liquid activator with a powder precursor (two-part geopolymer), or by a mixture of solid precursor and activator with the addition of water (one-part geopolymer), which amplifies the scale of the in-site applications of the geopolymers (Provis, 2017).

Nonetheless, geopolymers present issues that may affect their durability, such as efflorescence. Efflorescence is visually identified as a white formation on the geopolymer surface and originates from the growth of salts at the surface and in the pores by the transport of alkalis through the pore matrix and reaction with atmospheric carbon dioxide. It may affect the geopolymer aesthetically and

decrease the mechanical strength, when in excess (Longhi et al., 2021). The availability of free alkalis in the geopolymer framework is an important factor for efflorescence formation. Therefore, the porosity and the improvement of the reaction extent are relevant to mitigate and control the efflorescence formation in geopolymers (Longhi et al. 2020). This work aims to understand the relationship between the mix design parameters of geopolymers in efflorescence formation.

This study used “iron ore sand”, a tailing from the iron ore concentration process (Matiolo et al., 2020), analyzed by energy-dispersive X-ray spectroscopy (EDX), with 80% of SiO_2 and 13.42% of Fe_2O_3, and the solid sodium silicate produced with it, with 52.65% of Na_2O, 42.46% of SiO_2, and 3.86% of Fe_2O_3 as main components. The kaolin clay used had a mean particle size of 12.17 µm and was calcined at 800ºC for 4 h, which resulted in an amorphous and highly reactive material (metakaolin). The metakaolin sample was analyzed by the X-ray fluorescence and showed 48.99% of SiO_2, 40.80% of Al_2O_3, 2.74% of CaO, and other oxides with concentrations lower than 1%.

The experiment design was based on the simplex centroid mixture designs of three components (Montgomery, 2013), resulting in 20 mixtures (Figure 1). The three components were iron ore sand, solid sodium silicate, and metakaolin, which were mixed to obtain a homogeneous dry mixture. The water was considered a process variable and its amount was coded into two levels: low (-1), corresponding to 19wt% of the dry mixture, and high (+1), corresponding to 23wt%. It was added to the dry mixture and mixed to form a uniform paste.

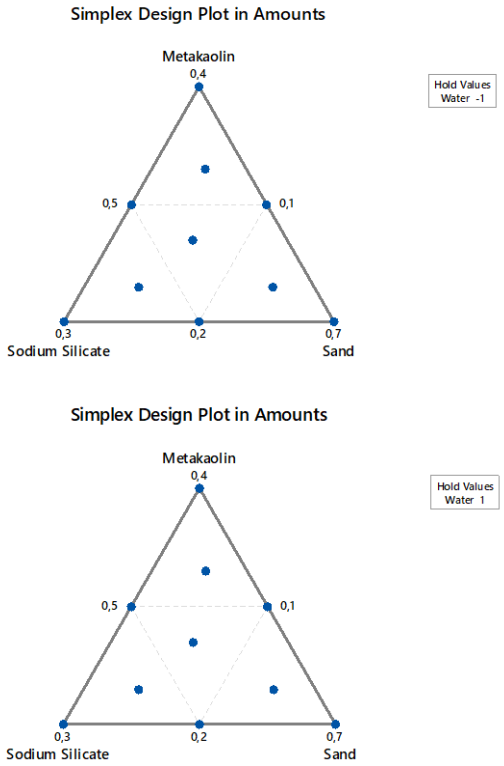

Figure 1. Centroide simplex design to study the influence metakaolin, sodium silicate, iron ore sand, and water on the properties of geopolymers.

The samples were cast in cylindrical molds with dimensions (100mm x 50mm), based on the Brazilian standard ABNT NBR 7215 (ABNT, 2019), to perform the compressive strength and efflorescence susceptibility tests after 7 and 28 days of curing in temperature and humidity of the environment. They were demolded after 24 hours of hardening. The density and open porosity were measured with the xylol immersion and penetration method. The efflorescence tests consisted first of a visual inspection, where the cylindrical samples were inserted on plates with a 5 mm column of water, and the water was replaced daily until the 14th day, while the samples were photographed from 0 to 28 days. The

efflorescence potential was measured by the pH registered by two cylindrical samples of the same composition immersed in different recipients with deionized water for 24 h. Before immersion, the samples were weighed and dried in an oven at 60°C for 3 h. After the immersion, they were dried at 60°C for 24 h and weighed again, and the difference between the final and the initial mass divided by the initial mass is the percentage of the mass loss, which represents the potential for efflorescence formation by mass loss. These tests were adapted from Longhi et al. (2021).

RESULT & DISCUSSION

Visual analysis of cylindrical samples showed that the content of solid sodium silicate is a significant factor for efflorescence formation. Samples with higher content of solid sodium silicate (30%) showed more efflorescence with deleterious effects, such as the disintegration of samples at 28 days. All the samples had some efflorescence as shown in Figure 2. The compositions and test results of four samples of the simplex design of Figure 1 are shown in Table 1.

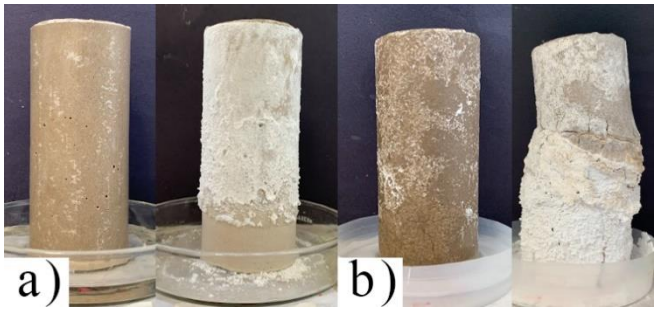

Figure 2. Geopolymer samples of two mix designs. **a)** Geopolymer sample of composition 2 with 20% of solid sodium silicate at 0 and 28 days. **b)** Geopolymer sample of composition 4 with 30% of solid sodium silicate at 0 and 28 days.

Table 1. Results for geopolymer samples (MK = Metakaolin, SS = Sodium Silicate, IOS = Iron Ore Sand).

Sample	Composition (wt%)				Molar Na/Al	Molar Si/Al	Maximun Compressive Strength (MPA)		pH (24 h)	Na_2O content (wt%)	Mass loss (wt%)
	MK	SS	IOS	Water			7 days	28 days			
1	0.23	0.13	0.64	19	0.77	1.39	33	35	12	6.84	15.30
2	0.30	0.20	0.50	23	0.91	1.45	40	38	12	10.53	19.46
3	0.20	0.30	0.50	19	2.05	2.02	6	10	12 - 13	15.80	18.01
4	0.20	0.30	0.50	23	2.05	2.02	6	11	12 - 13	15.80	61.44

The efflorescence susceptibility by pH measurement showed that the higher content of solid sodium silicate, the higher the pH after 24 hours. The same effect was observed in the loss of mass test, where samples with more than 15wt% of Na2O content had a loss of mass higher than 60wt% (highest Na/Al molar relation), the sample with less loss of mass had 6.84wt% of Na2O content and 15.30wt% of mass loss. The porosity measurements revealed that all the porosity in the samples is open, which also contributed to the efflorescence susceptibility. Compressive strength tests with cylindrical samples resulted in compression resistance from 6 MPa to 40 MPa, and the samples of mix designs with more content of solid sodium silicate had the lowest values.

CONCLUSION

The content of solid sodium silicate is a significant factor for efflorescence formation, as the pH measurement indicated. The mix designs with more content of sodium present more leachability of alkalis, as shown by loss of mass measurements. The best result were obtained with the Na/Al molar ratio close to 1, which is in accordance with the Literature. Regarding the water level as a process variable, no influence was observed in the range studied. The efflorescence phenomenon may lead to geopolymer structure degradation, as visual analysis showed during the accelerated test. The mechanical properties were higher for geopolymers with lower content of Na2O. All geopolymer samples showed only open porosity, which also contributes to efflorescence formation.

ACKNOWLEDGEMENT

This research is funded within the scope of the partnership between Vale and CDTN.

REFERENCES

Associação Brasileira de Normas Técnicas. ABNT NBR 7215 – Portland cement – Determination of compressive strength. RJ, Brazil, 2019.

Associação Brasileira de Normas Técnicas. ABNT NBR 15270-2 – Clay blocks and bricks for masonry – Part 2: Test methods. RJ, Brazil, 2017.

Davidovits, J. Geopolymers: Ceramic-like inorganic polymers. Journal of Ceramic Science and Technology 08 [3] (2017), 335-350.

Duarte, G. M.; Lameiras, F. S. Challenges for the destiny of Iron ore mining tailings in the Iron Quadrangle of Minas Gerais, Brazil. Revista Virtual de Química 14 [3] (2022), 552-559.

Longhi et al. Metakaolin-based geopolymers: Relation between formulation, physicochemical properties and efflorescence formation. Composites Part B 182 (2020), 1-15.

Longhi et al. Strategies for control and mitigation of efflorescence in metakaolin-based geopolymers. Cement and Concrete Research 144 (2021), 1-14.

Matiolo et al. Improving recovery of iron using flotation of iron ore slimes. Minerals Engineering 158 (2020), 106608.

Montgomery, D. C. Design and Analysis of Experiments. John Willey & Sons, Inc., Hoboken, NJ, USA, 2013.

Provis, J. L. Alkali-activated materials. Cement and Concrete Research 114 (2017), 40-48.

Vogt, J. C.; Lameiras, F. S. Patent number EP3992148A1.

Immobilization of Cesium and Strontium-based waste by metakaolin geopolymer: Effect of waste loading and water-binder ratio on the properties of the host matrix

Emile Mukiza[1,2], Quoc Tri Phung[1], Suresh Seetharam[1], Lander Frederickx[1], Geert De Schutter[2]

[1, 2] Institute for Environment, Health and Safety, Belgian Nuclear Research Centre, 2400 Mol, BELGIUM. (E-mail: emile.mukiza@sckcen.be, quoc.tri.phung@sckcen.be, suresh.seetharam@sckcen.be, lander.frederickx@sckcen.be)

[2] Department of Structural Engineering and Building Materials, Ghent University, 9052 Ghent, BELGIUM. (E-mail: Geert.DeSchutter@UGent.be)

HIGHLIGHTS

- High water-binder ratio showed detrimental effects on the performance of MK geopolymer.
- Cs and Sr exert negative influence on properties of host matrix with more effects observed with Sr.
- MK geopolymer preserved sufficient strength even at high content of Cs and Sr-simulated waste.

Keywords: geopolymer, Cs and Sr waste, immobilization

INTRODUCTION

The first-generation nuclear power plants and reprocessing facilities are approaching the end of their service lives [1]. As a result, spent nuclear fuel (SNF) and radioactive waste, generated by both the normal operations and decommissioning of nuclear power plants will undoubtedly rise significantly [2]. Reprocessing of SNF has long been regarded as a viable solution to address existing disposal issues. Under the Belgian waste management framework; the ASOF (Advanced Separation for Optimal management of spent Fuel) Project is advancing the development of new, innovative processes for the separation of minor actinides (Americium) and fission products Cesium (Cs) and Strontium (Sr) to optimise SNF disposal. In parallel, approaches for conditioning Cs and Sr are being investigated. Alkali-activated materials (AAMs) have been intensively studied in recent years and are considered as one of the potential alternatives to ordinary Portland cement (OPC) for waste immobilization. Geopolymer, a class of AAMs with a low calcium system and consisting of alkali aluminosilicate gel as the main product; offers a good immobilization and binding capacity of cations due to the pseudo-zeolitic structure of its amorphous network as well as high alkalinity. However, only one study exists to date in the literature concerning the possibility of co-immobilization of Cs and Sr into one single matrix. Li et al (2016 & 2018) investigated the immobilization of Cs and Sr by paper sludge (PS) ash-based geopolymer bearing 1% wt $Sr(NO_3)_2$ and $CsNO_3$ to address the issue of Cs and Sr present in contaminated water from Fukushima Daiichi NPP [3,4]. However, the reported mechanical properties were very low (Flexural strength < 1MPa) which potentially limits its wide adoption and application in other countries. This work aims to develop a metakaolin (MK)-based geopolymer mortar bearing high Cs and Sr loading and exhibiting high mechanical properties. The focus was to evaluate the effect of the water-binder (W/B) ratio and simulated Cs and/or Sr waste loading on the properties of MK geopolymer.

MATERIALS AND METHODS

MK was used as the aluminosilicate source and the activating solution (SiO2/Na2O=2) consisted of a mix of sodium hydroxide (NaOH 10 M) and sodium disilicate (Na2Si2O5). MK geopolymer mortars were designed with W/B of 0.55 and 0.75. Water refers to the overall amount of water including water in sodium hydroxide solution, water in solid Na2Si2O5 as well as additional water. MK geopolymer with W/B=0.75 initially designed to suit liquid wastes with high water content [5] was adopted and lowered to 0.55 to evaluate the effect of W/B ratio on the properties of Cs/Sr-bearing MK waste forms. Radioisotopes Cs-137 and Sr-90 were simulated by stable Cs and Sr incorporated as CsNO3 and Sr(NO3)2 and waste loading varied between 0 and 4%. The choice of nitrates was based on the fact that Cs/Sr waste stream contains significant nitrate content originating from HNO3 used in Cs/Sr partitioning from SNF. The activating solution was prepared 24h before casting by dissolving solid Na2Si2O5 into a mix of additional water and 10M NaOH solution. Then CsNO3 and/or Sr(NO3)2 were mixed with the activating solution and the resulting solution was mixed with MK precursor and sand. The MK geopolymer slurry was cast into 40×40×160 mm moulds and cured at 20°C and relative humidity of 95% for at least 24h and then demoulded and cured in the same conditions until 28d before testing. MK geopolymer formulations investigated in the present study are presented in Table 1.

Table 1. MK Geopolymer formulations.

Recipe Code	W/B ratio	$CsNO_3$	$Sr(NO_3)_2$
MK-0.55-Ref	0.55	0	0
MK-0.75-Ref	0.75	0	0
MK-0.55-Cs	0.55	4	0
MK-0.55-Sr	0.55	0	4
MK-0.75-Cs	0.75	4	0
MK-0.55-Cs-Sr	0.55	4	4
MK-0.75-Cs-Sr	0.75	4	4

RESULTS & DISCUSSION

Compressive strength

The findings of compressive strength are presented in Figure 1. The compressive strength varied between 21 MPa and 54 MPa and satisfies the minimum requirement of 8 MPa as per Belgian waste acceptance criteria (ACRIA). It was noticed that increasing W/B in MK waste forms only benefits the workability of the geopolymer (observed during mixing) but negatively affects the mechanical properties for both reference MK geopolymer and Cs and or Sr-bearing MK waste forms as shown in Figure 1. The compressive strength of MK-075-Ref was published in [5] and was quoted in the presented work for the sake of having a complete overview of the effect of Cs and Sr in matrices with different W/B ratios.

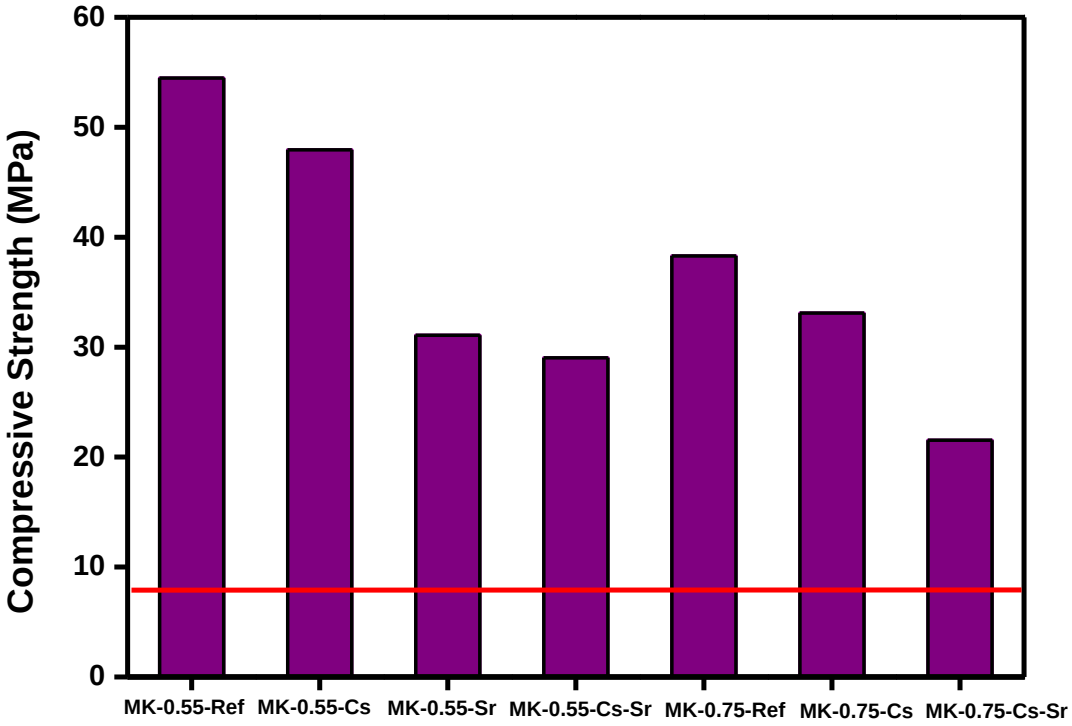

Figure 1. Effect of W/B ratio and Cs and Sr on mechanical properties.

Similarly, the incorporation of $CsNO_3$ and $Sr(NO_3)_2$ negatively impacted the compressive strength of MK geopolymers and a higher strength loss was observed for Sr-bearing geopolymer than comparable Cs-containing MK matrices with a similar W/B and waste loading. This could be attributed to the behavior of Sr^{2+} in the system. After adding $Sr(NO_3)_2$ into the activating solution, a white precipitate of $Sr(OH)_2$ (which was visually noticeable) was formed immediately as a result of the interaction of Sr^{2+} and OH^- ions and this decreased the OH^- content available for dissolution of metakaolin. As a consequence, Sr-bearing MK geopolymer systems contained lower amounts of dissolved silicate and aluminate groups and higher amount of unreactive MK binder compared to reference MK geopolymer and Cs-containing MK waste forms. As dissolution is the limiting step of the entire geopolymerization process [6], the low dissolution degree of MK binder certainly reduced the geopolymerization degree and negatively affects the strength development.

Porosity

The pore volumes determined by the water-accessible porosity test are presented in Table 2. It is evident that the volume of water-accessible pores increased significantly with increasing W/B ratio.

Table 2. Water-accessible porosity of MK geopolymer matrices.

Recipe	Water-Accessible Porosity (%)
MK-0.55-Ref	34.72
MK-0.55-Cs	34.09
MK-0.55-Sr	35.52
MK-0.55-Cs-Sr	33.61
MK-0.75-Cs-Sr	46.251

On the other hand, the volume of water-accessible pores slightly decreased with the incorporation of Cs while it increased with Sr addition. The high porosity in Sr-bearing matrices could be explained by the interaction of Sr^{2+} with the activating solution. As highlighted earlier, Sr^{2+} consumes part of the alkali activator thereby lowering the dissolution extent of MK precursor and leading to low amount of geopolymeric gel (N-A-S-H) formed. This leads to more unreacted particles in Sr-bearing MK system

and consequently, more gaps between N-A-S-H gel and unreacted particles.

CONCLUSION

This work intended to design the MK geopolymer suitable for the solidification of Cs and Sr. Based on the interaction of Cs and Sr with MK geopolymer. Findings showed that MK geopolymer is promising as a host of Cs and Sr since it preserved sufficient strength even when loaded with high content of Cs and Sr-simulated waste. However, a high W/B ratio was detrimental to the performance of MK geopolymer. Equally, Cs and Sr exert a negative influence on the properties of the host matrix with more effects observed with Sr. Since Cs-137 and Sr-90 are high heat generating and radiation emitting radioelements, future studies should focus on understanding the effect of irradiation and decay heat on the properties of Cs/Sr-based metakaolin waste forms.

ACKNOWLEDGMENT

The authors would like to express their appreciation for funding from the Belgian Energy Transition Fund (ASOF project).

REFERENCES

[1] De Felice, P., Bogucarska, T., Raiola, F. & Pedersen, B. Good Practice Guide for Validation of a Waste Characterisation System for Very Low , Low and Intermediate Level Radioactive Waste. (2021) doi:10.2760/748464.

[2] Gual, M. R. & Zucchetti, M. A gamma dose rate estimation model for radioactive waste containers. in Transactions of the American Nuclear Society vol. 111 1135–1137 (2014).

[3] Li, Z., Nagashima, M. & Ikeda, K. Treatment technology of hazardous water contaminated with radioisotopes with paper sludge ash-based geopolymer-stabilization of immobilization of strontium and cesium by mixing seawater. Materials (Basel). 11, 1–22 (2018).

[4] Li, Z., Ohnuki, T. & Ikeda, K. Development of paper sludge ash-based geopolymer and application to treatment of hazardous water contaminated with radioisotopes. Materials (Basel). 9, (2016).

[5] Frederickx, L., Nguyen, T. N. & Phung, Q. T. Strength and Microstructure Characteristics of Metakaolin-Based Geopolymer Mortars with High Water-to-Binder Ratios. Sustain. 14, 1–14 (2022).

[6] Zhu, X., Yan, D., Fang, H., Chen, S. & Ye, H. Early-stage geopolymerization revealed by 27Al and 29Si nuclear magnetic resonance spectroscopy based on vacuum dehydration. Constr. Build. Mater. 266, 121114 (2021).

Influence of zinc sulphate on the setting and rheological properties of alkali activated binders

Aparna Sai Surya Sree Nedunuri[1] and Muhammad Salman[2]

[1, 2] Department of Civil Engineering, Indian Institute of Technology Bombay, Mumbai, INDIA.
(E-mail: naparna@iitb.ac.in, msalman@iitb.ac.in)

HIGHLIGHTS

- $ZnSO_4.7H_2O$ is an effective retarder that can prolong the setting times of alkali activated materials.
- The rate of evolution of storage modulus decreased with an increase in the dosage of $ZnSO_4.7H_2O$.
- The initial storage modulus increased with an increase in the dosage of $ZnSO_4.7H_2O$.

Keywords: retarder, storage modulus, setting time

INTRODUCTION

The production of ordinary Portland cement (OPC) increased from 1.6 billion metric tons in 2000 to 4.3 billion metric tons in 2021 [1], accounting for 7-8% of global CO2 emissions [2]. To reduce these emissions from the cement sector, it is necessary to explore alternative cementitious materials. Alkali activated materials (AAM) are considered one such alternative. The widespread usage of these materials is limited by their drawbacks, such as quick setting [3], rapid loss of workability and high drying shrinkage [4–6]. This study attempts to address the issue of quick setting in AAM. The quick setting phenomenon in AAM is due to the predominant rigidification of the network caused by the precipitation of hydration products [7]. Therefore, to address the quick setting, it is necessary to use a retarder that can retard the precipitation of early hydration products and prolong the setting time. In this study, zinc sulphate heptahydrate (ZnSO4.7H2O) was used as a retarder. The influence of retarder on the setting time and the evolution of storage modulus with hydration time of AAM was investigated.

MATERIALS & METHODS

Ground granulated blast furnace slag (GGBFS) was used as a precursor along with the volume replacement by 50% fly ash. Sodium silicate of molar modulus 1.5 was used as an activator. The activator dosage (% of Na2O by weight of precursors) and water to precursor (w/p) ratio were maintained at 6% and 0.40, respectively. ZnSO4.7H2O was added at 0.0, 1.0, 2.0 and 3.0% by the weight of precursor. Since zinc sulphate heptahydrate does not dehydrate at temperatures lower than 88 oC [8], the water content of zinc sulphate heptahydrate was not considered in the mixture design. The required amount of zinc sulphate was dissolved in the mix water (the water required to maintain the water to precursor ratio). Both the activator solution and the mix water with dissolved zinc sulphate were added to the precursors for the preparation of paste mixtures. The mixing protocol mentioned in ASTM C305 [9] was followed for the preparation of paste mixtures. Setting time of paste mixtures was determined as per the procedure in IS 4031 part 5 [10]. Small amplitude oscillatory shear (SAOS) test was carried to understand the rate of evolution of the flocculated network with hydration time. A preshear with a shear rate of 300 s-1 was applied for 90 s, followed by a rest period of 60 s. Storage modulus was measured by subjecting the sample to a sinusoidal strain of 0.01% at a frequency of 1 Hz for a period of 60 min. Data was collected every 30 s.

RESULT & DISCUSSION

The initial and final setting times of AAM with 0, 1, 2 and 3% of ZnSO4.7H2O are shown in Figure 1. An increase in both the initial and final setting times was observed with an increase in the proportion of fly ash and dosage of ZnSO4.7H2O. A significant increase in initial and final setting times was observed with an increment in the dosage of ZnSO4.7H2O (2100% and 900%, respectively) when compared to an increase in the fly ash proportion from 0 to 50% (250% and 133%, respectively). The incorporation of a 50% fly ash and a 3% dosage of retarder prolonged the initial and final setting times by 2500% and 1100%, respectively. An increase in the amount of fly ash, containing relatively less reactive calcium [11], would slow down the hydration reactions and thus exhibit prolonged setting times [12]. The prolonged setting times obtained with an increase in the dosage of ZnSO4.7H2O can be attributed to the retardation in the formation of early reaction products by encapsulating the reactive ions such as Ca2+ and SiO_4^{4-} in the form of complexes [13,14].

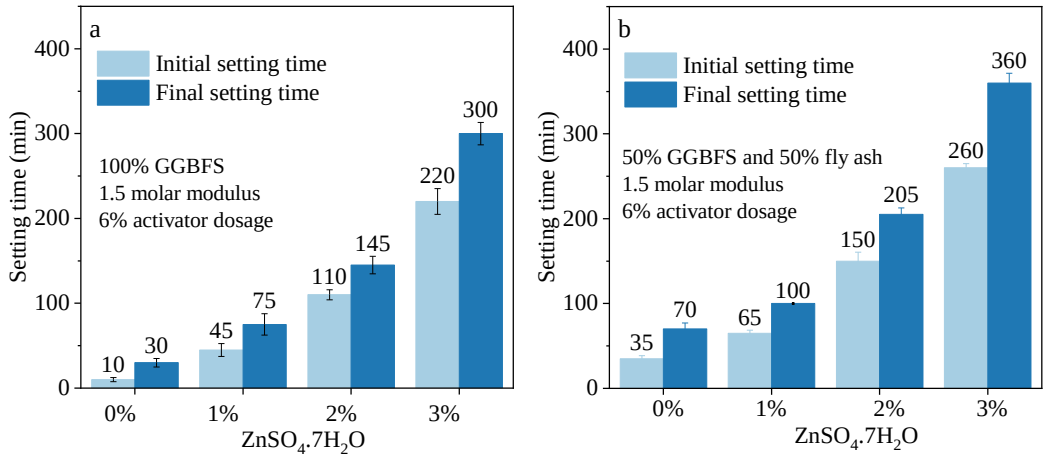

Figure 1. Initial and final setting time of AAM with increase in the dosage of $ZnSO_4.7H_2O$.

The evolution of the storage modulus of AAM with an increase in the dosage of ZnSO4.7H2O from 0 to 3% in 100% GGBFS mixtures with progress in hydration time is provided in Figure 2. At 0% ZnSO4.7H2O, the storage modulus was observed to increase rapidly. This rapid increment can be attributed to the structure formed by the precipitation of hydration products [7,15]. Increase in the dosage of ZnSO4.7H2O from 0% to 3%, decreased the rate of increment in storage modulus and the secondary increment in storage modulus was not observed in the mixture with 3% ZnSO4.7H2O. This can probably be due to retardation in the hydration reaction with the addition of zinc sulphate. The absolute value of storage modulus was observed to increase with an increase in the dosage of ZnSO4.7H2O from 0 to 3%. The possible formation of calcium-zinc [14] and zinc-silicate [13] complexes would have resulted in the formation of more coagulated contact points, which is reflected by the higher storage modulus values.

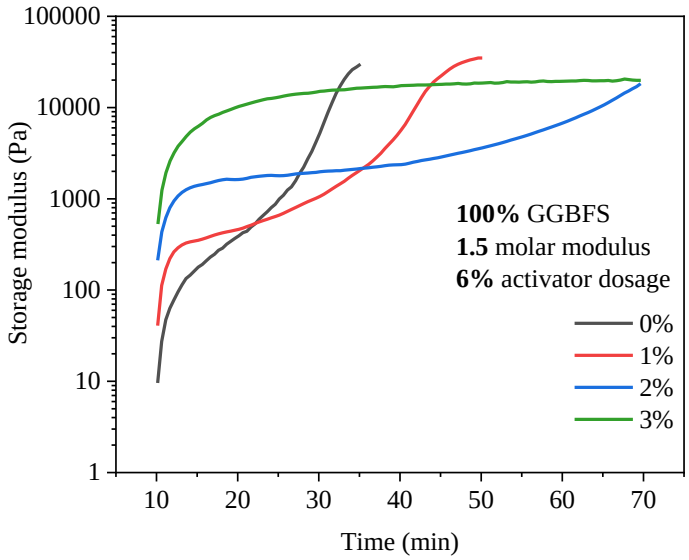

Figure 2. Evolution of storage modulus with progress in hydration time in AAM with increase in the content of $ZnSO_4.7H_2O$.

CONCLUSIONS

1. The increment in the proportion of fly ash from 0% to 50%, prolonged the initial and final setting times of AAM by 250% and 133%, respectively. $ZnSO_4.7H_2O$ was found to be an effective retarder in prolonging the initial and final setting times of AAM by 2100% and 900%, respectively**.**
2. The addition of $ZnSO_4.7H_2O$ decreased the rate of evolution of storage modulus in 100% GGBFS mixtures due to retardation in the hydration reaction.
3. At higher dosage of $ZnSO_4.7H_2O$ (3%), secondary evolution of storage modulus was not observed indicating a minimal rigidification of the network.
4. The absolute value of the initial storage modulus increased with an increase in the dosage of $ZnSO_4.7H_2O$.

REFERENCES

[1] M. Garside, Global cement production 1995-2021, (2022). https://www.statista.com/statistics/1087115/global-cement-production-volume (accessed September 19, 2022).

[2] P.J.M. Monteiro, S.A. Miller, A. Horvath, Towards sustainable concrete, Nat Mater. 16 (2017) 698–699. https://doi.org/10.1038/nmat4928.

[3] J.J. Chang, A study on the setting characteristics of sodium silicate-activated slag pastes, Cem Concr Res. 33 (2003) 1005–1011. https://doi.org/10.1016/S0008-8846(02)01096-7.

[4] N.K. Lee, J.G. Jang, H.K. Lee, Shrinkage characteristics of alkali-activated fly ash/slag paste and mortar at early ages, Cem Concr Compos. 53 (2014) 239–248. https://doi.org/10.1016/j.cemconcomp.2014.07.007.

[5] S. Hanjitsuwan, B. Injorhor, T. Phoo-ngernkham, N. Damrongwiriyanupap, L.-Y. Li, P. Sukontasukkul, P. Chindaprasirt, Drying shrinkage, strength and microstructure of alkali-activated high-calcium fly ash using FGD-gypsum and dolomite as expansive additive, Cem Concr Compos. 114 (2020) 103760. https://doi.org/10.1016/j.cemconcomp.2020.103760.

[6] C. Detphan, P. Kaeorawang, B. Injorhor, K. Chompoovong, S. Hanjitsuwan, T. Phoo-ngernkham, P. Chindaprasirt, Improving drying shrinkage and strength development of alkali-activated high-calcium fly ash using commercial-grade calcium sulfate as expansive additive, Engineering and

Applied Science Research. 49 (2022) 58–64.

[7] A.S.S.S. Nedunuri, S. Muhammad, Fundamental understanding of the setting behaviour of the alkali activated binders based on ground granulated blast furnace slag and fly ash, Constr Build Mater. 291 (2021). https://doi.org/10.1016/j.conbuildmat.2021.123243.

[8] J. Straszko, M. Olszak-Humienik, J. Mozejko, Kinetics of thermal decomposition of ZnSO4.7H2O, Thermochim Acta. 292 (1997) 145–150.

[9] ASTMC305, Standard Practice for Mechanical Mixing of Hydraulic Cement Pastes and Mortars of Plastic Consistency, ASTM International, 100 Barr Harbor Drive, PO Box C700, West Conshohocken, PA 19428-2959. United States, 2014. https://doi.org/10.1520/C0305-14.

[10] IS4031(Part 5), Methods of physical tests for hydraulic cement Part 5 Determination of initial and final setting times, Bureau of Indian Standards, New Delhi, India, India, 1988.

[11] A.S.S.S. Nedunuri, S. Muhammad, Influential parameters in rheology of alkali-activated binders, ACI Mater J. 117 (2020) 75–85. https://doi.org/10.14359/51724593.

[12] N. Li, C. Shi, Q. Wang, Z. Zhang, Z. Ou, Composition design and performance of alkali-activated cements, Mater Struct. 50 (2017) 178. https://doi.org/10.1617/s11527-017-1048-0.

[13] M.R. Anseau, J.P. Leung, N. Sahai, T.W. Swaddle, Interactions of silicate ions with zinc(II) and aluminum(III) in alkaline aqueous solution, Inorg Chem. 44 (2005) 8023–8032. https://doi.org/10.1021/ic050594c.

[14] N. Garg, C.E. White, Mechanism of zinc oxide retardation in alkali-activated materials: an in situ X-ray pair distribution function investigation, J Mater Chem A Mater. 5 (2017) 11794–11804. https://doi.org/10.1039/C7TA00412E.

[15] M. Palacios, S. Gismera, M.M. Alonso, J.B. d'Espinose de Lacaillerie, B. Lothenbach, A. Favier, C. Brumaud, F. Puertas, Early reactivity of sodium silicate-activated slag pastes and its impact on rheological properties, Cem Concr Res. 140 (2021) 106302. https://doi.org/10.1016/j.cemconres.2020.106302.

Liquid release from superabsorbent polymer in alkali-activated slag and the mitigation of autogenous shrinkage

H. Dong[1], B. Chen[2], Z. Li[3] and G. Ye[4]

[1, 2, 3, 4] Microlab, Delft University of Technology, Delft, The Netherlands.
(E-mail: H.Dong@tudelft.nl, B.Chen-4@tudelft.nl, Z.Li-2@tudelft.nl, G.Ye@tudelft.nl)

[4] Magnel Laboratory for Concrete Research, Ghent, Ghent University

HIGHLIGHTS

- Highlight 1. The liquid release from superabsorbent polymer (SAP) in alkali-activated slag pastes was studied by calculating the particle size of SAP before and after internal drying based on reconstructed 3-dimensional CT-image.

Keywords: superabsorbent polymer, particle size, autogenous shrinkage, alkali-activated slag

INTRODUCTION

Superabsorbent polymer (SAP) has a high capacity of liquid absorption, and has been proven efficient in mitigating autogenous shrinkage with the internal curing effect both in cement-based materials [1] and in alkali-activated materials [2,3]. The liquid absorption and release of SAP depend on its molecular structure, and further determines the efficiency in autogenous shrinkage mitigation [4]. This study evaluated the effects of SAP on compressive strength, internal relative humidity and autogenous shrinkage of alkali-activated slag pastes. The particle size of SAP in alkali-activated slag pastes before and after internal drying (i.e., self-desiccation) was calculated based on the reconstructed 3-dimensional CT image. The calculation results give insight into a deeper understanding on internal curing process of alkali-activated materials by SAP.

EXPERIMENTAL

Materials and paste formulation

The precursor used in this study was BFS provided by ECOCEM, chemical composition can be found in [5]. The alkali activators were NaOH solution from Brenntag (50% concentration) and water glass solution from PQ Corporation (Na2O·2SiO2, 44,1% concentration). SAP (Floset 27cc, a cross- linked copolymer of acrylamide and acrylate) was provided by SNF SAS. The absorption capacity of the SAP in the alkali activator solution used in this study was 21, 25 and 35 times after 15 min, 1 hour and 24 hours, respectively. SAP particles with the size of 63-125 μm were obtained by sieving and used for preparation of pastes, at a dosage of 0, 0,15% and 0,3% by weight of BFS.

Paste formulation and preparation

The paste formulation of the mixtures is listed in Table 1. The alkali activator solution was prepared 1 hour before mixing. All dry materials (i.e., BFS and/or SAP) were mixed for 1 min in a Hobart mixer. Then the alkali activator solution was added to the mixture, followed by another 2min mixing. The mixtures were cast in 40 mm × 40 mm × 160 mm moulds, demoulded after 1 day and cured under sealed condition at 20 ℃ until compressive strength tests. The mixtures were cast in corrugated tubes for autogenous measurements. For CT-scan tests, the mixtures were cast in ϕ4 mm × 10 mm tubes, and sealed at 20 ℃ until testing at 7 days.

Table 1. Paste formulation* of alkali-activated slag with/without SAP.

	BFS	NaOH (solid)	$Na_2O{\cdot}SiO_2$ (solid)	SAP	Water
Ref	1	0,026	0,059	0	0,412
SAP15				0,0015	
SAP30				0,0030	

*Na_2O% = 4% by weight of BFS, modulus of alkali solution SiO_2/Na_2O = 1, water-to-binder (BFS + solid alkali activators) ratio = 0,38.

Methods

The final setting time of the pastes was determined using a Vicat apparatus. The compressive strength was tested at 7 and 28 days. The autogenous shrinkage was recorded after mixing until 7 days according to ASTM C1968-09. The samples were scanned at 7 days using a Phoenix Nanotom Nano-CT-Scanner at 120 kev/60 mA. Reconstruction of the CT images was carried out with VG Studio Max, with a spatial resolution of 3 μm. The particle size of SAP in the pastes before and after internal drying was analyzed using an in-house numerical tool based on the CT images.

RESULTS AND DISCUSSION

The final setting time of Ref, SAP15 and SAP 30 is 13h25min, 12h50min, 12h35min, respectively. The addition of SAP shortened the setting time of paste. It can be explained by the reduced water-to-binder ratio caused by water absorption of SAP. The compressive strength ([MPa]) of Ref, SAP15 and SAP 30 is 59 $\pm$ 0,8, 53 $\pm$ 1,4 and 50 $\pm$ 0,7 at 7 days, 71 $\pm$ 0,9, 66 $\pm$ 0,7 and 61 $\pm$ 0,8 at 28 days. The addition of SAP reduced the compressive strength of paste due to the induced voids. The self-desiccation caused a reduction in internal relative humidity of Ref sample over time (Figure. 1). The incorporation of SAP significantly increased the relative humidity of “SAP15” and “SAP30” compared to “Ref” due to the internal curing effect (Figure. 1). The efficiency increased with the increasing dosage of SAP. As a result, “SAP30” showed the lowest autogenous shrinkage, compared to “SAP15” and “Ref” (Figure. 2). Fig. 3 shows the CT image of a cross-section of “SAP15” at 7 days. Due to water release from SAP for internal curing, the SAP particles shrank to a certain extent and left air voids in the paste. Based on reconstructed 3-dimensional CT image, the equivalent size (i.e., the diameter of spherical SAP particles with the same volume) of SAP particles in “SAP15” and “SAP 30” before and after internal drying (at 7 days) was calculated and shown in Figure. 4. Note that the original size (i.e., before drying) of each SAP in the pastes was calculated based on the total volume of SAP particle and air void (see Figure. 3). The maximum size SAP particles shrank from 306 μm to 258 μm for “SAP15”, and from 342 μm to 240 μm for “SAP30”, respectively. With the water release from SAP particles, the volume of SAP particles decreased from 1,1% to 0,6% for “SAP15” 2.5% to 1,6% for “SAP30”, indicating the water release from SAP particles of 0,5% (by volume of paste) for “SAP15” and 0,9% for “SAP30” respectively. This explains the higher efficiency of SAP in “SAP30” compared to that in “SAP15”. Based on the original size (i.e., 63-125 μm) of SAP particles before internal drying, there is still potential of SAP particles to mitigate autogenous shrinkage of pastes after 7 days.

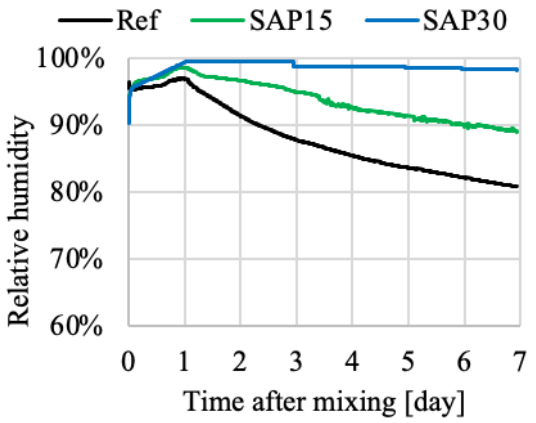

Figure 1. Internal relative humidity of AAM pastes with/without SAP.

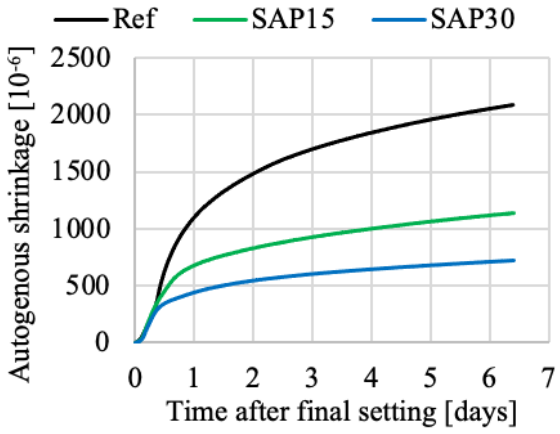

Figure 2. Autogenous shrinkage of AAM pastes with/without SAP.

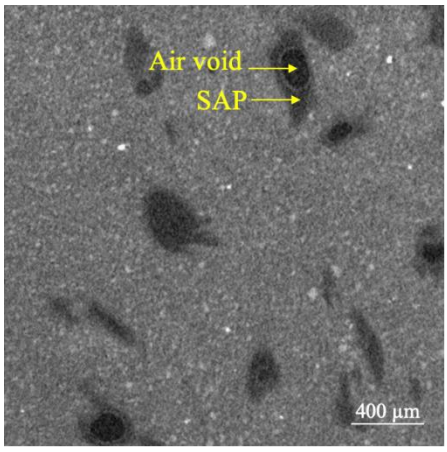

Figure 3. CT image of SAP15 at 7 days.

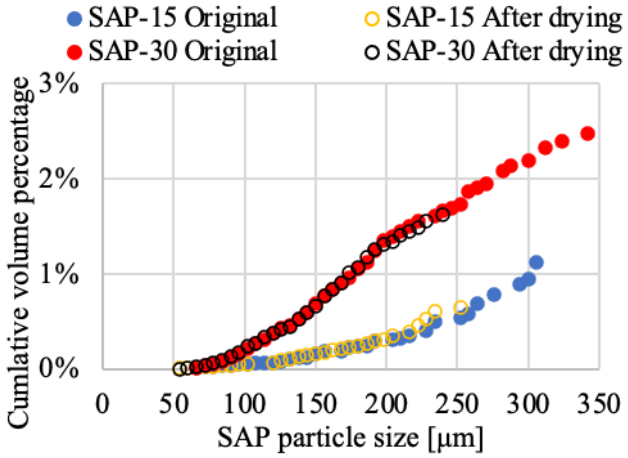

Figure 4. SAP particle size distribution in the pastes before and after internal drying.

SUMMARY

Akali-activated slag pastes were prepared with 0, 0,15% and 0,30% of SAP particles by weight of slag. With higher dosage of SAP, the compressive strength at 7 days and 28 days was lower due to the induced voids, the internal relative humidity in the pastes was higher, and the autogenous shrinkage was lower due to the internal curing effect of SAP. The size of SAP particles in the pastes before and after drying was calculated. The reduction of SAP size after drying of pastes provided quantitative information for explaining the efficiency of SAP in mitigating autogenous shrinkage of alkali-activated pastes.

ACKNOWLEDGEMENT

Support by the Northwest Europe Interreg project URBCON is gratefully acknowledged.

REFERENCES

[1] Abu, A.B. and Zakaria, B. Title of the manuscript in journal. *Applied Materials and Mechanics* 185 (2013), 517-521.

[2] Klemmer, R.S., Thomsen, M., Phelps-Goodman, E., Lee, R. and Landay, J.A. Where do web sites

come from? Capturing and interacting with design history. In *Proc. CHI 2002*, ACM Press (2002), 1-8.

[3] Schwartz, M. *Guidelines for Bias-Free Writing*. Indiana University Press, Bloomington, IN, USA, 1995.

[4] Choo, S.M. Title of a master's or PhD thesis. Universiti Teknologi Malaysia, Ph.D. Thesis, 2012.

[5] Li, Z., et al., Mitigating the autogenous shrinkage of alkali-activated slag by metakaolin. Cement and Concrete Research, 2019. 122: p. 30-41.

Air-entraining additive effect on geopolymer mortar workability

Piotr Prochoń[1], Maja Kępniak[2], Kamil Załęgowski[3]

[1, 2, 3] Faculty of Civil Engineering, Warsaw University of Technology, POLAND.
(E-mail: piotr.prochon@pw.edu.pl, maja.kepniak@pw.edu.pl, kamil.zalegowski@pw.edu.pl)

HIGHLIGHTS

- It is possible to modify a geopolymer composite with components that increase its thermal insulation without critically affecting workability.
- Perlite sand dosage is statistically insignificant for affecting the consistency of the composite.
- Perlite powder dosage decreases the workability.

Keywords: geopolymer, workability, air-entraining additive

INTRODUCTION

Production of ordinary Portland cement (OPC) is a carbon-intensive process that generates significant amounts of carbon dioxide (CO2) from the combustion of fossil fuels and thermal decomposition of limestone [1].

The recent advent of geopolymers shows great potential to reduce carbon footprint by utilizing the industrial by-products and converting them into a binding material [2,3]. Besides the low-carbon emissions, geopolymers are well known for their prominent properties, such as superior compressive strength, low permeability, chemical resistance, exceptional fire and heat resistance, and high durability [4,5].

In the presented research, an attempt is made to increase the thermal insulation properties of the geopolymer composite. In order to obtain a geopolymer composite with enhanced thermal insulation, attempt was made to introduce additives that could potentially improve the thermal performance of the material. Waste perlite powder perlite sand and cenospheres were used to modify the composite composition. The introduction of a porous fine-grained material with an increased specific surface area could significantly impair the workability of the composite. A verification experimental plan was prepared to determine the limiting dosage of the additives and to assess their effect on the geopolymer composite.

RESULTS & DISCUSSION

The influence of geopolymer composite modification on the composite properties was analysed on the basis of three additives potentially increasing thermal insulation: perlite powder, perlite sand and cenospheres. The aim of the experiment was to optimize the dosage ranges of individual components with a critical impact on workability. For the factor analysis, three composition parameters were selected as factors: amount of perlite sand, perlite powder and cenospheres in kg per m3 of composite. Each of the variables was studied at one of three levels: lower, middle and upper (Tab.1).

The experiment was carried out using a randomized fractional factorial plan for three variables, which were assigned three levels of value. To estimate the error resulting from the study procedure, the experiment matrix was enriched with three processes with variables set at central levels.

In this study, the undesirable feature of the composite indicating the critical interaction of dependent variables was consistency measured by immersion of the cone less than 10 mm. The test was performed on 10 l mixture by immersion of a 300 g cone (slant height 150 mm, max. diameter 75 mm)

in 10 s.

Table 1. Test factors and assigned value levels.

	Factor		
	Perlite sand [kg] (PS)	Perlite powder [kg] (PP)	Cenospheres [kg] (C)
Upper level	30	50	50
Middle level	15	25	25
Lower level	0	0	0

The tests were carried out on geopolymer mortars with a composition per 1 m3: 50 kg of metakaolin, 50 g of zeolite, 400 kg of fly ash, 10 kg of redispersible powder, 5 kg of magnesium formate, 60 kg of limestone powder, 50 kg of hydrated lime, 275 kg of sodium hydroxide, 150 kg of water, 45 kg of water glass and perlite powder, perlite sand and cynospheres according to the experiment plan. The natural sand content was determined each time as to obtain 1m3 of the composite. The full experimental plan, composition variables, together with the measurement results are summarised in Tab. 2.

Table 2. Variable parameters of composite composition in the experiment plan and the experiment response.

No.	Components				Experiment response
	Natural sand [kg]	Cenospheres [kg]	Perlite powder [kg]	Perlite sand [kg]	Consistency [mm]
1	1100	0	0	0	150
2	400	0	25	30	105
3	443	0	50	15	80
4	515	25	0	30	150
5	560	25	25	15	115
6	601	25	50	0	100
7	670	50	0	15	125
8	715	50	25	0	100
9	17	50	50	30	15
C1	560	25	25	15	95
C2	560	25	25	15	100
C3	560	25	25	15	95

For all of the analysed compositions the critical value of workability measured by consistency was achieved. The statistical significance of the independent variables was determined using the results obtained through Pareto analysis (Fig. 1) [6]. The Pareto analysis allows the calculation of correlation coefficients for individual independent variables and the calculation of the limiting coefficient at the assumed level of confidence (marked with a red line in Figure 1). Exceeding the limiting factor means that the independent variable has a significant impact on the analyzed dependent variable. The results of the analysis indicate that the modification with perlite powder (PP) and cenospheres (C) are statistically important for the workability of the composite.

As the perlite powder content increases, the workability of the composite decreases significantly, which is related to the grain size and shape of the filler grains. The effect of cenospheres content on workability is lower (Fig.2).

CONCLUSION

The presented research indicates that it is possible to modify a geopolymer composite with components that increase its thermal insulation without critically affecting workability. It is useful to note that modification with perlite sand, for which best results in terms of increased thermal insulation could be expected, is statistically insignificant for the consistency of the composite. Modification with perlite powder adversely affects workability, but within the maximum planned dosage it does not lead to exceeding the critical workability value.

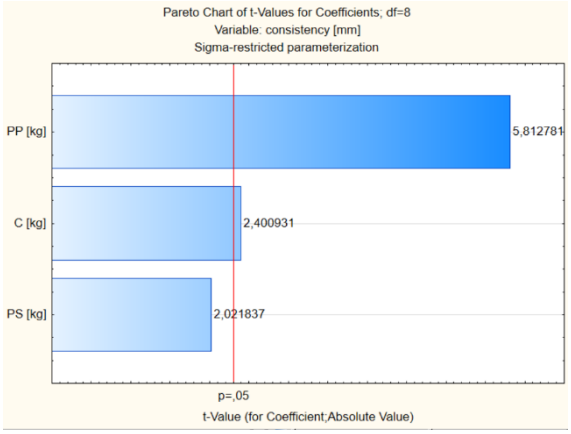

Figure 1. Pareto analysis of composite consistency.

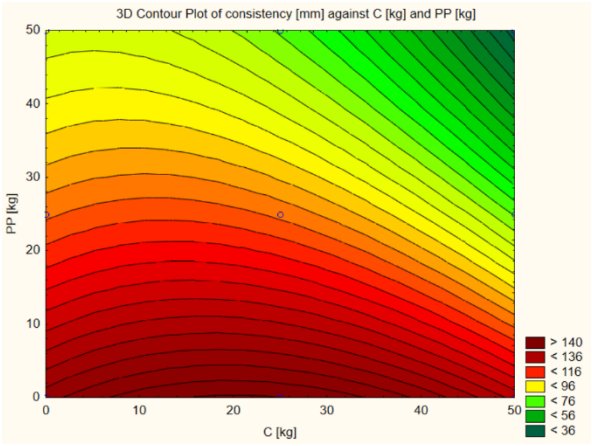

Figure 2. Consistency depending on perlite powder and cenospheres content.

ACKNOWLEDGEMENT

The authors would like to express their appreciation for the support of the sponsors the National Center for Research and Development Project Lider No LIDER/49/0187/L-11/19/NCBR/2020 “Sustainable materials – alkali-activated mortars - for specific shielding performance in civil engineering”

REFERENCES

[1] B.B. Das, S. Barbhuiya, R. Gupta, P. Saha, Recent Developments in Sustainable Infrastructure, Springer Science and Business Media LLC, 2021

[2] K. Mermerdas, S. Manguri, D.E. Nassani, S.M. Oleiwi, Effect of aggregate properties on the mechanical and absorption characteristics of Geopolymer mortar, Eng. Sci. Technol. Int. J. (2017).

[3] K. Neupane, Evaluation of environmental sustainability of one-part geopolymer binder concrete, Cleaner Materials, Volume 6, 2022

[4] Xiaonan Ge, Xiang Hu, Caijun Shi, Impact of micro characteristics on the formation of high-strength Class F fly ashb-ased geopolymers cured at ambient conditions, Construction and Building Materials, Volume 352, 2022

[5] Ning Li, Caijun Shi, Zuhua Zhang, Hao Wang, Yiwei Liu, A review on mixture design methods for geopolymer concrete, Composites Part B: Engineering,Volume 178, 2019

[6] Global Analysis and Economics I: Pareto Optimum and a Generalization of Morse Theory, Dynamical Systems, Academic Press, 1973

Efficient use of calcium in developing sustainable high-strength geopolymer for in-situ applications

Kruthi K. Ramagiri[1] and Kolluru V. L. Subramaniam[2]

[1, 2] Department of Civil Engineering, Indian Institute of Technology Hyderabad, Hyderabad, INDIA.
(E-mail: ce22pdf01@iith.ac.in, kvls@ce.iith.ac.in)

HIGHLIGHTS

- Minimal supply of calcium ensues significant performance enhancement of geopolymer under ambient conditions.
- Mix proportioning is based on reactive oxide composition.
- Significantly high compressive strength associated with N-A-S-H gel formation.

Keywords: geopolymer, ambient curing, N-A-S-H gel

INTRODUCTION

From 2015-2021, the direct CO2 intensity of cement manufacturing grew by around 1.5% each year. To reach net zero emissions by 2050, annual declines of 3% are needed through 2030 [1]. A greater emphasis on producing binders from alternative source materials is required. Alkali-activated binder (AAB) utilizes industrial residues as raw materials, thereby lowering carbon footprint and addressing residue disposal. Because of their wide availability, low-calcium fly ash and ground granulated blast furnace slag (slag) are utilized as source materials in AAB [2]. In order to activate low-calcium fly ash, a curing temperature of 60-85 °C is generally required owing to its inadequate reactivity at room temperature [3]. Slag can improve properties of fly ash-based geopolymer owing to the presence of CaO which promotes dissolution of fly ash [4]. However, a higher slag content increases the autogenous and drying shrinkage. Furthermore, the performance of fly ash-based geopolymer is also governed by the activator type and concentration. The dissolution of fly ash and the subsequent leaching of Al3+ and Si4+ ions depend on the molarity of sodium hydroxide [5]. Previous research reported use of a high molarity of NaOH for requisite strength gain [6]. However, the high molarity of NaOH limits the in-situ applications of AAB in the construction sector.

In this study, the mechanical performance of fly ash-based geopolymer activated with a 3M sodium hydroxide and cured at ambient temperature is investigated. The compressive strength development with inclusion of 5% of slag and using the activator after different resting periods is examined. The reaction products are identified and quantified.

MATERIALS AND METHODS

Precursors used were low-calcium fly ash and ground granulated blast furnace slag meeting the requirements of ASTM C618 and ASTM C989/C989M specifications, respectively [7,8]. Table 1 shows the oxide composition of the precursors along with d50 and d90 values. The reactive SiO2 and Al2O3 contents of the fly ash were 23.98% and 13.00%, respectively, as determined by an XRD-based analysis [9].

Table 1. Oxide composition (%) and LOI (%) of fly ash and slag.

	CaO	SiO_2	Al_2O_3	Fe_2O_3	MgO	K_2O	SO_3	TiO_2	LOI	d_{50}	d_{90}
Fly ash	4.0	52.8	23.5	6.4	2.7	3.0	1.1	2.0	0.1	108.4	1115.4
Slag	43.1	29.7	16.4	0.9	4.7	0.8	2.2	1.1	1.5	15.9	48.3

The mix composition is outlined in Table 2. Sodium silicate (14.70% Na2O, 34.17% SiO2, and 51.13% H2O) and sodium hydroxide were used to make the alkaline activating solution. As previously reported, the molarity of sodium hydroxide was kept constant at 3M for complete dissolution of reactive components in fly ash [10]. A drum mixer was used to make the activated pastes. The NaOH solution was made by dissolving pellets in water. The activating solution is used at two different temperatures of 45 °C and immediately after cooling down to room temperature.

Table 2. Mix proportions of fly ash-based geopolymer.

Mix designation	Fly ash/slag	SiO_2/H_2O in the activating solution	Solution/binder	Activator temperature	Reactive oxide ratio in the activated paste	
					SiO_2/Al_2O_3	Al_2O_3/Na_2O
100 FA_45 °C	1	0.34	0.35	45 °C	2.4	2.5
95 FA_45 °C	0.95	0.34	0.35	45 °C	2.4	2.5
100 FA_R	1	0.34	0.35	ambient	2.4	2.5
95 FA_R	0.95	0.34	0.35	ambient	2.4	2.5

Compressive strength and X-ray diffraction

Standard 70.6 mm cubes conforming to IS 4031-1988 specifications were cast to evaluate compressive strength [11] and cured at 27 ± 1 °C in a sealed condition. The cubes were demoulded after 24 h and sealed cured until the day of testing at 27 ± 1 °C. The 100 FA specimens were not tested for 1 day owing to their longer setting times. The compression test was carried out in accordance with IS 516-1959 at a loading rate of 14 MPa/min [12]. Samples from the crushed cubed were ground to size finer than 60 µm, solvent exchanged using isopropanol, dried at 40 °C, and stored in sealed condition.

The X-ray diffraction (XRD) scans were recorded in a in a vertical Bragg-Brentano (θ/θ) geometry from 10° to 70° through a CuKα radiation source. The step size and speed were kept constant at 0.02° and 0.6 s/step, respectively. Direct decomposition technique is used to quantify the amorphous reaction product of fly ash-based geopolymer [9].

RESULTS & DISCUSSION

The compressive strength of fly ash-based geopolymer as a function of age is presented in Figure 1. The N-A-S-H content evaluated through direct decomposition technique is also presented in Figure 1. The incorporation of 5% slag provides a synergistic enhancement in the N-A-S-H content and improves both the early age strength gain and the compressive strength achieved at 28 days. The compressive strength of mixture with 5% slag (95 FA_R) improved by 121% and 33% at 7 and 28 days, respectively compared to 100 FA mixture cured at room temperature. The presence of Ca from slag promotes dissolution of vitreous phases in fly ash and subsequently the additional silica from slag contributes to geopolymerization. Ca elevates the pH locally, which increases the solubility of fly ash [13]. As presented in Figure 2, characteristic peaks of C-A-S-H gel are not observed in the intensity signature. C-A-S-H is semi-crystalline, distinct peaks centered near 29° 2θ [14]. The primary reaction product in the 95 FA mixtures is produced by geopolymerization of fly ash. The presence of 5% slag, therefore,

enhances the geopolymerization at room temperature for improved compressive strength. While using the activating solution at 45oC resulted in enhanced strength gain up to 7 days, the 28-day strength was slightly lower than the activating solution mixed at room temperature. There is no significant difference in the N-A-S-H contents in the mixtures made using activating solutions at the two different temperatures. The effect of the higher temperature mixing on the early strength gain is significant in the 100 FA. With the addition of 5% slag there is no significant difference between high temperature mixing and room temperature processing. High strength can therefore be achieved for room temperature processing under ambient curing conditions with the use of 5% slag in an activated fly ash.

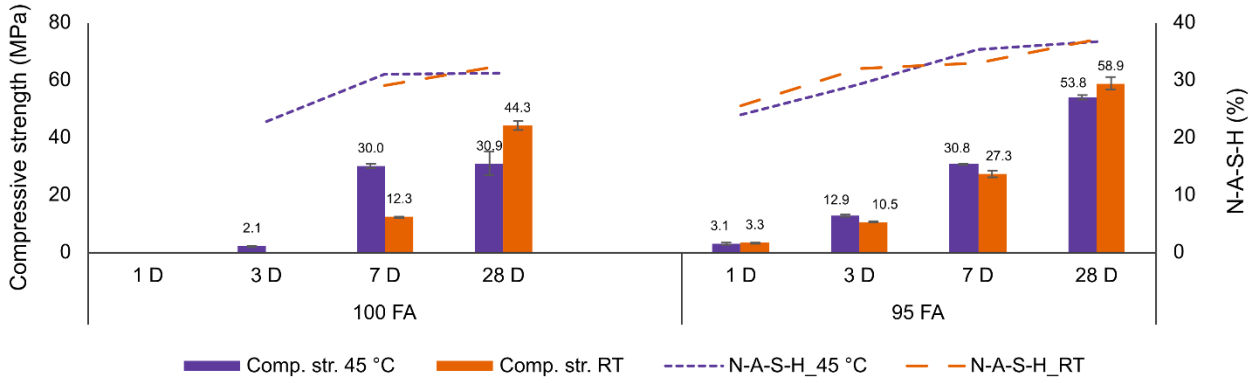

Figure 1. Variations in compressive strength and N-A-S-H content.

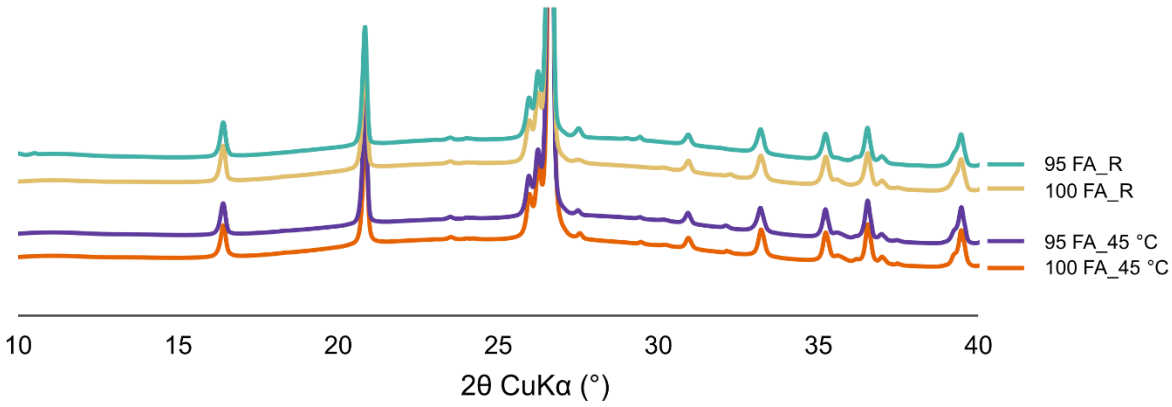

Figure 2. XRD pattern of activated fly ash mixtures.

CONCLUSION

The effect of incorporating 5% slag in fly ash-based geopolymer activated with low molarity activator and cured under ambient conditions is examined. A minimal addition of slag to the fly ash-based geopolymer produces a synergistic enhancement in strength. The strength gain is attributed to an increased formation of N-A-S-H gel. The incorporation of 5% slag promotes effective utilization of fly ash with enhancement in the final strength. Using activator at a higher temperature result in improved strength gain, while the final strength achieved is comparable to the room temperature. Ambient cured geopolymers are produced under room temperature processing with the incorporation of 5% slag in an activated fly ash mixture.

REFERENCES

[1] Cement – Analysis - IEA, (n.d.). https://www.iea.org/reports/cement (accessed October 26, 2022).

[2] J. Davidovits, Geopolymer Chemistry and Applications, 5th ed., Institut Géopolymère, Saint-Quentin, 2020.

[3] M.T. Junaid, A. Khennane, O. Kayali, A. Sadaoui, D. Picard, M. Fafard, Aspects of the deformational behaviour of alkali activated fly ash concrete at elevated temperatures, Cem Concr Res. 60 (2014) 24–29. https://doi.org/10.1016/J.CEMCONRES.2014.01.026.

[4] S. Puligilla, P. Mondal, Role of slag in microstructural development and hardening of fly ash-slag geopolymer, Cem Concr Res. 43 (2013) 70–80. https://doi.org/10.1016/J.CEMCONRES.2012.10.004.

[5] U. Rattanasak, P. Chindaprasirt, Influence of NaOH solution on the synthesis of fly ash geopolymer, Miner Eng. 22 (2009) 1073–1078. https://doi.org/10.1016/J.MINENG.2009.03.022.

[6] M.Z.N. Khan, F. uddin A. Shaikh, Y. Hao, H. Hao, Synthesis of high strength ambient cured geopolymer composite by using low calcium fly ash, Constr Build Mater. 125 (2016) 809–820. https://doi.org/10.1016/J.CONBUILDMAT.2016.08.097.

[7] ASTM C618-17a, Standard Specification for Coal Fly Ash and Raw or Calcined Natural Pozzolan for Use in Concrete, in: ASTM International, West Conshohocken, PA, 2017. https://doi.org/10.1520/C0618-17A.

[8] ASTM C989 / C989M-18, Standard Specification for Slag Cement for Use in Concrete and Mortars, in: ASTM International, West Conshohocken, PA, 2018. https://doi.org/10.1520/C0989_C0989M-18.

[9] G.V.P. Bhagath Singh, K.V.L. Subramaniam, Direct decomposition X-ray diffraction method for amorphous phase quantification and glassy phase determination in binary blends of siliceous fly ash and hydrated cement, Http://Dx.Doi.Org/10.1080/21650373.2016.1177478. 6 (2016) 111–125. https://doi.org/10.1080/21650373.2016.1177478.

[10] G.V.P. Bhagath Singh, K.V.L. Subramaniam, Effect of active components on strength development in alkali-activated low calcium fly ash cements, Https://Doi.Org/10.1080/21650373.2018.1520657. 8 (2019) 1–19. https://doi.org/10.1080/21650373.2018.1520657.

[11] B. of Indian Standards, IS 4031-5 (1988): Methods of physical tests for hydraulic cement, Part 5: Determination of initial and final setting times, n.d.

[12] B. of Indian Standards, IS 516 (1959): Method of Tests for Strength of Concrete, n.d.

[13] G.M. Canfield, J. Eichler, K. Griffith, J.D. Hearn, The role of calcium in blended fly ash geopolymers, J Mater Sci. 49 (2014) 5922–5933. https://doi.org/10.1007/S10853-014-8307-Z/METRICS.

[14] K.C. Reddy, K.V.L. Subramaniam, Investigation on the roles of solution-based alkali and silica in activated low-calcium fly ash and slag blends, Cem Concr Compos. 123 (2021) 104175. https://doi.org/10.1016/J.CEMCONCOMP.2021.104175

Mechanical, microstructure and durability properties of alkali-activated mortar based on phosphate mining waste rocks, fly ash and metakaolin

S. Sbi[1], S. Mansouri[2], N. Semlal[3], Y. Tamraoui[4] and J. Alami[5]

[1,2,4,5] Materials Science, Energy and Nano Engineering Department MSN, Mohammed VI Polytechnic University, Benguerir, Morocco.

[3]OCP SA, Innovation, BP 118, 24000, El Jadida, Morocco
(E-mail: Sanae.SBI@um6p.ma, Said.MANSOURI@um6p.ma, n.semlal@ocpgroup.ma, Youssef.TAMRAOUI@um6p.ma and Jones.ALAMI@um6p.ma)

HIGHLIGHTS

- Alkali activation PMWRs is a viable and promising technology for the sustainable management of these industrial by-products.
- Introducing FA and MK improve the mechanical strength and the durability performance of PMWRs mortars.
- PMWR/FA/MK alkali activated mortars showed better mechanical and durability properties compared to PCM mortar.

Keywords: alkali activated mortar, phosphate mining waste rocks, microstructure, durability

ABSTRACT

Each year, phosphate mining industry generates a significant amount of phosphate mining waste rocks (PMWRs) which usually deposited on large areas as stockpiles within the mine site, leading to high ecological costs and environmental challenges. In this research, a feasibility study is performed on alkali activation of phosphate mining waste rocks so that they can be recycled and utilized as construction material. Considering the extremely high silicon to aluminum (Si/Al) ratio for these waste rocks, metakaolin and fly ash are used to adjust the Si/Al ratio. Sodium hydroxide (NaOH) solution and silicate sodium (Na_2SiO_3) are used as alkaline activator. Replacements of 50% of PMWRs by FA/MK were carried out and compressive strengths in the range 35–57 MPa were obtained after 28 curing days, which is promising for construction applications. Microstructural studies are investigated using X-ray diffraction (XRD), Fourier-transform infrared (FTIR), Scanning Electron Microscopy (SEM) and Energy-Dispersive X-ray spectroscopy (EDX). The results show the formation of C-(A)-S-H and N-(A)-S-H gels as the main reaction products, with the formation of a hybrid C-(N)-A-S-H gels. The durability of alkali-activated mortars was compared to ordinary Portland cement (OPC) mortar in term of sulfuric acid resistance, fire resistance and water absorption. The behavior of alkali-activated mortars was better than that found for plain OPC mortars for all durability tests. However, the increase of metakaolin content appears to have a strong enhancement on the mechanical and microstructural properties of the synthesized mortars. As a general conclusion, phosphate mining waste rocks (PMWRs) show good cementing properties as a rich calcium precursor blended with metakaolin (MK) and fly ash (FA) in alkali-activated systems.

INTRODUCTION

Alkali-activated materials (AAMs) have emerged as most promising alternative to conventional ordinary Portland cement (OPC)[1]. In addition to superior strength and durability performance[1]–[3], AAMs can offer substantial environmental and social-economic benefits such as, lower CO_2 emission and less energy consumption[1]. AAMs are generally manufactured through alkali-activation of aluminosilicate raw materials with an alkaline solution (e.g., sodium hydroxide and sodium silicate solutions). A wide range of aluminosilicate materials can be used as AAM precursors which are generally wastes or industrial by-products, such as blast furnace slag (BFS) and coal fly ash (FA)[4]–[6]. For instance, class F fly ash is the most widely utilized industrial by-products in AAMs synthesis, and this is due to its high content of reactive silica and alumina along the low Ca-content, low water demand and worldwide availability[4], [6], [7]. The formation process of alkali-activated fly ash (AAFA) system consists of the dissolution of Si and Al species from FA in strong alkali solution, yielding in the formation of amorphous aluminosilicate gel known as sodium aluminosilicate hydrate (N-A-S-H) gels[7], [8], which is attributed to the same or higher mechanical strength performance than calcium silicate hydrate (C-S-H) in OPC[3].

One challenge for wide application of AAFA materials is the requirement of curing at elevated temperature[9]. In the strive towards improving the AAFA cured at ambient condition, several studies have attempted to enhance the reactivity of fly ash by adding some calcium containing materials, such as slag and OPC[4], [6], [10]. The addition of calcium source into AAFA system was reported to largely affect the fresh and hardened properties of this materials due to an additional C-S-H or C-A-S-H gel formation in the presence of N-A-S-H[4], [6].

Phosphate mining waste rocks (PMWRs) constitute one of the industrial solid by-products generated in huge amounts in many countries. In Morocco only, phosphate mining sites generate approximately 780 Mt to 3120 Mt of PMWRs every year[11], which are often deposited in stockpiles within the site mine. Consequently, the challenge of a sustainable disposal or valorization of these wastes is becoming considerably more critical. PMWRS are generally composed of clays and Ca-rich marls with high chemical and environmental stability[12], [13], that make them as excellent alternative secondary raw material in constructure sector. Serval studies have demonstrated that PMWRs are promising source material in road construction[13], fired brick manufacturing[14], as well as in alkali-activation process[12], [15]. In our recent study[12], PMWRs demonstrated high reactivity toward alkaline activation, resulting in the formation of C-S-H gel as the main reaction product with the coexistence of some trace of C-(A)-S-H and N-A-S-H gels and/or the possibility of formation C-(N-A)S-H gels. Therefore, the incorporation of PMWRs in AAFA can results in the high material performance in short- and long-term.

Metakaolin are different from other pozzolanic materials due to their fineness and high reactivity[16]. The inclusion of metakaolin in different alkali activated systems has been proven to improve their mechanical strength and final performance[3], [17], [18].

Incorporating cementitious additives into AAFA is expected to yield various changes in mechanical and microstructure characteristics due to different chemical reactions among constituents. This study aims to investigate the impact of substituting 50% of fly ash with different cementitious additives such as PMMWRs and metakaolin on compressive strength, structure/microstructure development, water absorption, efflorescence test, thermal stability and sulfuric acid resistance alkali activated mortars mixtures cured at moderate (55°C) conditions. The effects of binder composition on compressive strength development were monitored at different curing ages.

MATERIALS AND METHODS

Materials

The raw materials used in this study were the following:

- Portland cement (CPJ 45) was used to formulate the standardized Portland mortar.

- Metakaolin (MK) from calcination of kaolinitic clay (SIBILCO, France) at 750 °C/2h
- Fly ash (FA) from JORF LASFAR (El-Jadida, Morocco).
- Phosphate mining waste rocks from the cover layer (milled and calcined at 900°C/2h [12]) (Khouribga phosphate mine site, Morocco)
- Standardized sand was used for mortar formulation
- Sodium hydroxide (NaOH), with 97% of purity, was mixed with commercial sodium silicate solution (SiO_2/Na_2O=3.1) to achieve the desired molar ratio.

Mix design method and experimental approach

Alkali activated mortars (AAMs) were prepared according to the requirement of NF EN 196–1. OPC standardized mortar (PCM) was also formulated in order to have a clear insight on the difference between alkali activated based materials and Portland cement in term of mechanical strength and durability performance.

The effect of PMWRs/MK incorporation as partial substitution of 50% wt. FA was investigated, using three different PMWRs/MK proportions 25/75, 50/50 and 75/25. However, the total water to solid ratio, NaOH concentration and the molar ratio of the alkaline solution were maintained constant (W/S=0.5, NaOH 12M, SiO_2/Na_2O=1.33). Fig 1, illustrates the different mixture proportions of the AAMs at three replacements ratios of FA by PMWRs and MK.

The calculated amount of FA, Mk and PMWRs were dry mixed together for 2 minutes, followed by the addition of activator solution containing sodium hydroxide 12M and sodium silicate at fixed molar ratio, and mixed for another 10 minutes. The standardized sand was added to the mix and the resultant mixture was mixed for 5 min. The mixture obtained was then filled in molds of side 4 cm each and compacted with the help of a vibrating table to expel the air bubbles. The casted cubes were first cured at 55 °C in sealed bags for 24 h, followed by standard curing at ambient conditions (25 ± 0.5 °C) until testing. The purpose of implementing 55 °C as the curing temperature at an early age is to facilitate the alkali activation reaction of NaOH-activated FA/MK/PMWRs paste systems.

Fig.1. Alkali activated mortars AAMs preparation protocol.

Tests and characterization method

Raw materials (PMWRs, MK and FA) and AAMs mineralogical composition was evaluated by X-ray diffraction (XRD) using Bruker D8 Advance X-ray diffractometer (Cu Ka radiation). Raw materials chemical composition was evaluated by X-ray fluorescence (XRF) using a Malvern Panalytical energy-dispersive, Epsilon 4. Fourier Transform Infrared Spectroscopy (FTIR), with the brand name of PerkinElmer Frontier FT-IR Spectrometer, was used to assess the functional group of raw materials and AAMs with 4 cm^{-1} of resolution and scanned from 400 cm^{-1} to 4000 cm^{-1}. Particle size distribution was

determined by laser diffraction (Mastersizer 2000, Malvern Instruments). The morphological and microstructure analysis of AAMs was investigated using Scanning Electron Microscopy (SEM) coupled with Energy Dispersive X-ray Analysis (EDX) (Gemini scanning electron microscope, ZEISS 300). The compressive strength test was conducted on AAMs prism samples 4x4x4 cm (ASTM C 109) at 7 and 28 days of curing, using Cyber-Plus Progress (CONTROLAB) with max load of 500 KN.

Efflorescence formation on AAMs was evaluated by visual analysis. The principle of the test is to partially immerse an AAM specimen in distilled water to provoke efflorescence. Thereafter, when all the water evaporated, the intensity of precipitated efflorescence can be evaluated. For this purpose, AAM specimens were partially submersed in a glass Petri dish containing 40 ml of distilled water. The test was performed under ambient temperature (25 °C). It is considered completed when all the water evaporated.

Water absorption and fire resistance of AAMs were investigated after 28 days of curing. The water absorption tests were measured following the protocol described in ASTM D2216-05 2005. However, for fire resistance the AAMs cubes were put into an electric furnace in room temperature and subjected to heat treatment in the furnace at 400, 600, 800 and 1000°C for 2 hours at an incremental rate of 4°C per minute from 25°C. Then the specimens were allowed to cool down for 24 hours at room temperature inside the furnace for weight loss measurements and compressive strengths.

The durability of AAMs was investigated by accelerated erosion tests on AAMs specimens. The program consisted of immersion of specimens in solutions of 5% Sulfuric acid to a long time period and evaluation of its resistance in terms of surface corrosion, residual alkalinity, changes in weight and compressive strength at regular intervals. The acid sulfuric solution was replaced with a fresh solution every 10 days.

RESULTS AND DISCUSSION

Raw materials characterization

Fig. 2 shows the XRD pattern of the FA, MK and PMWRs, their chemical compositions are presented in Table 1. XRF analysis reveals of high calcium content of PMWRs. The XRD patterns of MK and FA reveal their amorphous nature, as denoted by the hump centered at around 25° 2θ. Nevertheless, the presence of some crystalline phases, mainly quartz and mullite, was detected. On the other hand, calcined PMWRs is much more crystalline than MK or FA, being quartz, periclase, calcite, lime and periclase group mineral (this latter would justify the presence of high calcium content detected via XRF), however, minor amount of amorphous phase cannot be excluded.

Fig.3 presents the particle size distribution of the solid components (FA, MK, and PMWRs). The PMWRs and FA show a broader particle size distribution when compared with MK (uniform particle size distribution around 6 μm).

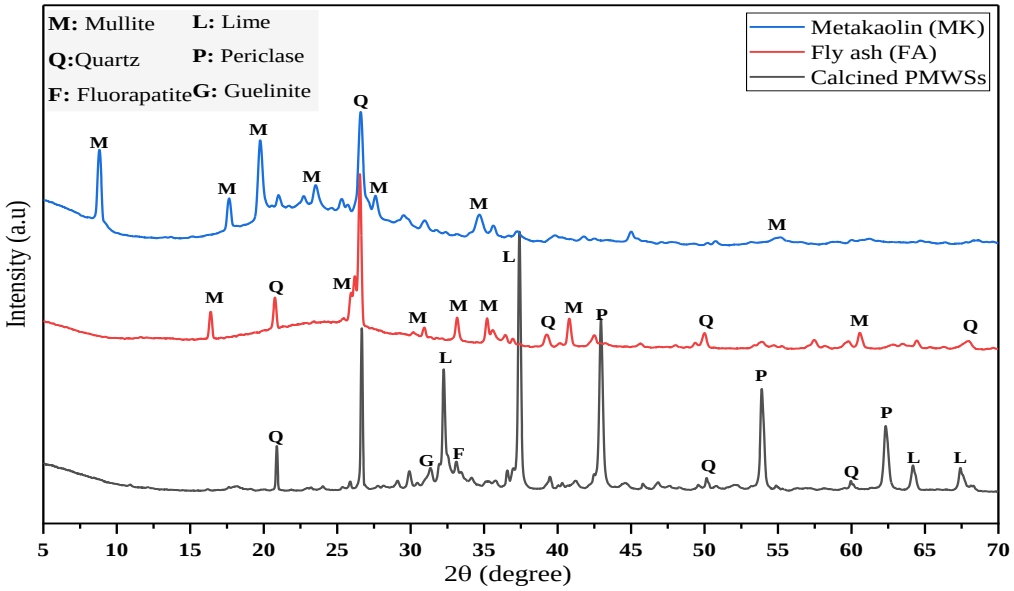

Fig.2. XRD analysis raw materials.

Table 1. Chemical properties of raw materials from XRF analysis.

Chemical Composition, wt. %	SiO_2	Al_2O_2	CaO	MgO	Fe_2O_3	K_2O	P_2O_5	SO_3	Other
FA	55,59	13,78	6,41	0.24	16,72	2,85	1,33	0,94	2.14
PMWRs	20.42	2.60	41.67	5.86	2.60	0.73	1.78	0.13	0.86
MK	63.64	30.47	------	------	1.45	3.60	0.37	-----	0.47

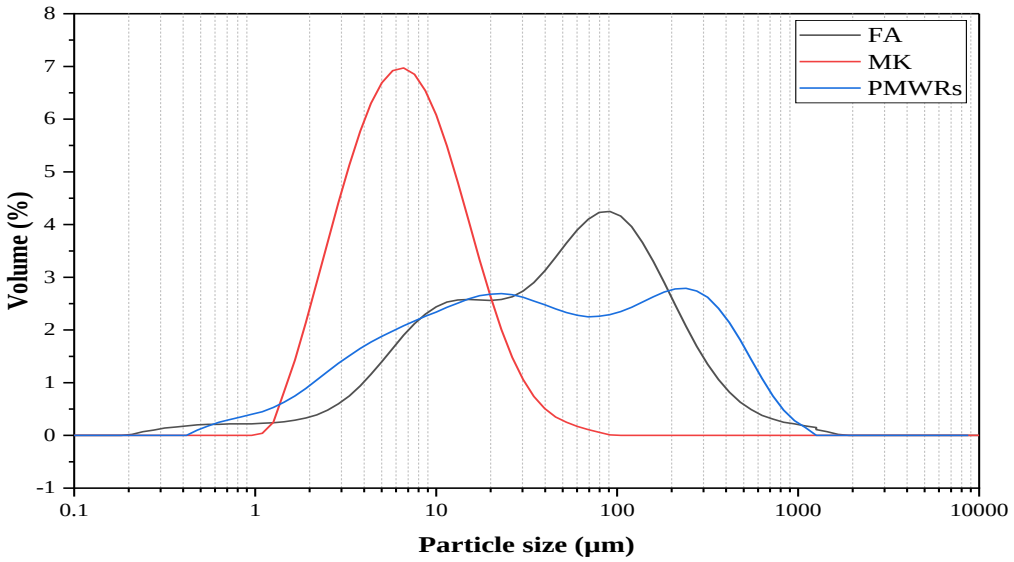

Fig.3. Particle size distribution of raw materials.

Alkali activated mortars characterization

Compressive strength

The effect of the different combinations FA/PMWRs/MK on the compressive strength of AAMs at the ages of 7 and 28 days is given in Fig. 4. For AAM specimens, a significant increase of the compressive strength is observed when the PMWRs/MK ratio decreased. In fact, decreasing the MK content results

in reducing the high reactive amorphous content in the binder which leads to this weakening in AAM system. It is important to note that all mixes of Alkali-Activated Materials (AAMs) have competitive mechanical resistances when compared to PCMs. The highest compressive strength was observed in the AAM-F3 mix, reaching a value of 56 MPa.

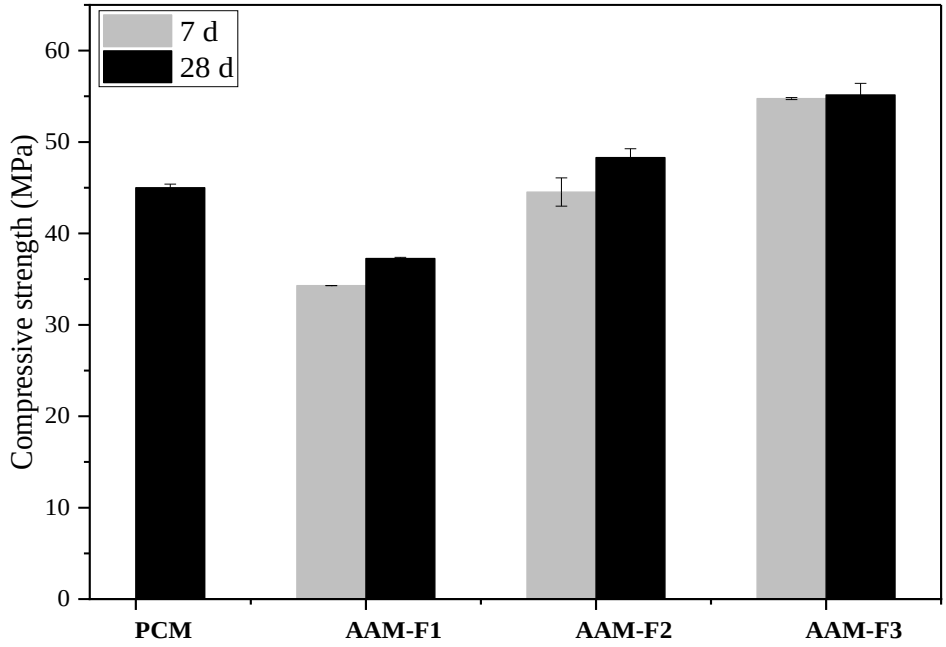

Fig.4. Compressive strength of all AAMs after 7-28 days (PCM represent compressive strength of Portland Cement Mortar specimens after 28 days).

XRD analysis

The XRD patterns of all AAM mixtures at the age of 28 days are shown in Fig. 5. The XRD patterns of all AAMs mixtures exhibited a broad hump in the range of 20°–40° 2θ, which corresponds to the amorphous aluminosilicate framework, suggesting that the products of AAMs are mainly aluminosilicate gels (coexistence of C-(A)-S-H and N-A-S-H gels) [19]. The broadness of the amorphous hump increased with the increase of MK content in the mix. These results indicate that increasing MK content from 15 to 35% by weight results in more amorphous aluminosilicate gels, which can explain the compressive strength test results reported earlier.

It can also be seen that some mineral phases from raw materials are still present in the hardened AAMs, but with decreased intensity, such as calcite, quartz, and periclase. These crystalline phases mainly come from unreacted PMWRs particles, where with changes in the formulation, an increase in PMWRs content leads to an increase in the intensity of these phases.

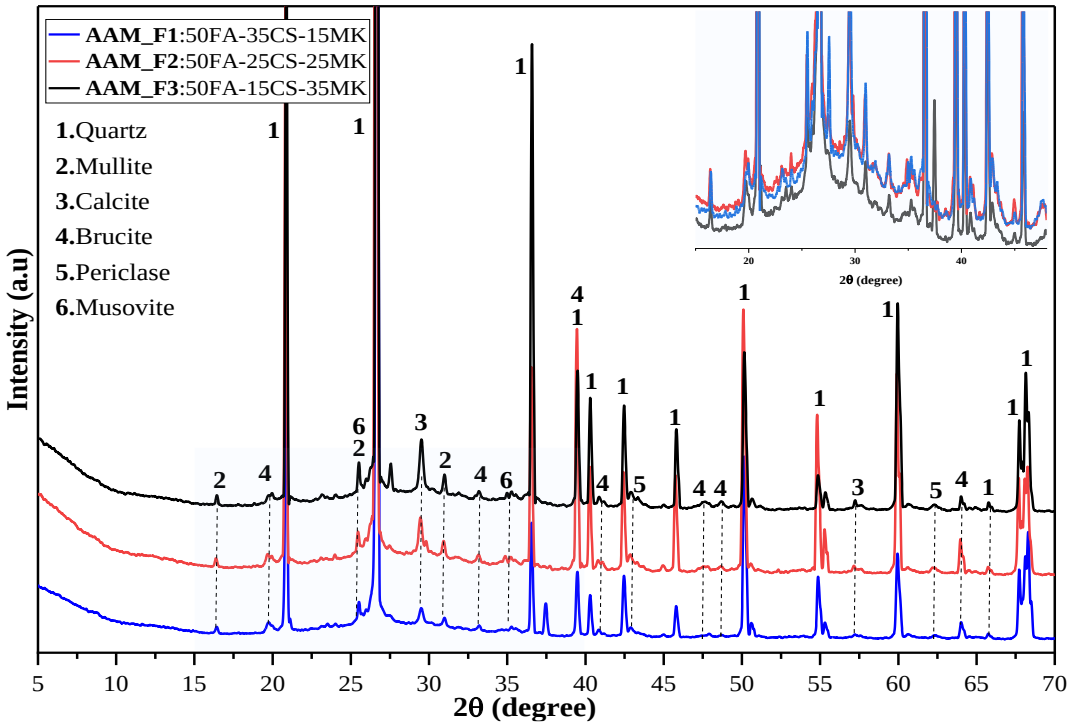

Fig.5. XRD analysis results of AAMs after 28 days of curing.

FT-IR analysis

Fig. 6 illustrate the FTIR spectra of all AAMs specimens at age of 28 days curing. The main band at around 1000 cm^{-1} is attributed to the asymmetric stretching vibration of Si-O-T where (T is Si or Al) [20], which is the typical structure of aluminosilicate chains contained in C-A-S-H or N-A-S-H type gel [21], [22]. The band at around 682 cm^{-1} and at 460 cm^{-1} corresponding to Al-O-Si bending vibration [23], and Si-O-Si bending vibration [24], respectively.

The same locations of the detected bands in different AAMs specimens indicate that the same type of reaction product, probably C-A-S-H and N-A-S-H gel, was formed in the pastes, irrespective of the raw material proportion. However, the broad bands at around 1000 cm^{-1} become more intensive with the incorporation of MK, indicating that the amount of reaction products increased when more MK was present in the AAMs mix. This is in line with the XRD results and the results of [25].

Water absorption bands were recorded at 3388 cm^{-1} and 1642 cm^{-1} which are assigned to the stretching vibrations of H–O–H and the bending vibration of O–H group [24], [26]. The small band at 1486 cm^{-1} attributed to O–C–O asymmetric stretching band in calcite [23], [27].

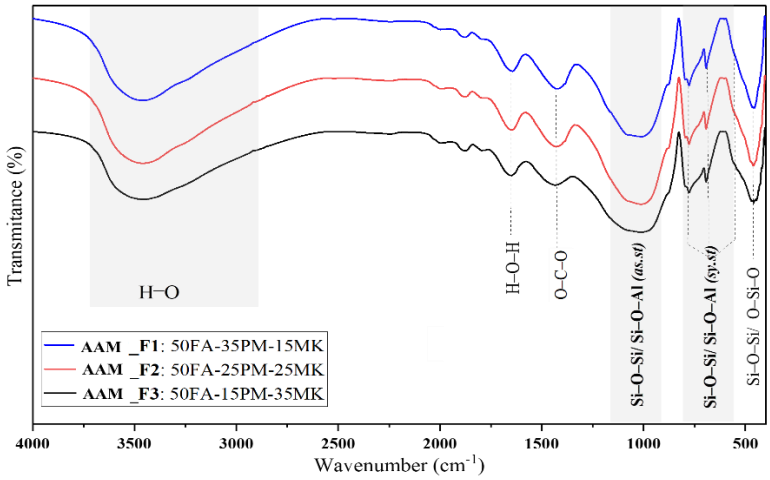

Fig.6. FTIR analysis results of AMMs after 28 days of curing.

SEM/EDS analysis

The 28 d micrographs and EDS analysis for all AAMs are represented in Fig. 7 and 8. It can be seen from all SEM images a similar morphology between the differently AAMs mixes.

All AAMs samples exhibited: partially unreacted and partially attacked spherical fly ash particles, sand particles and a dense and compact alkali activated matrix resulting from N–A–S–H and C-(N)-A-S-H gel precipitation.

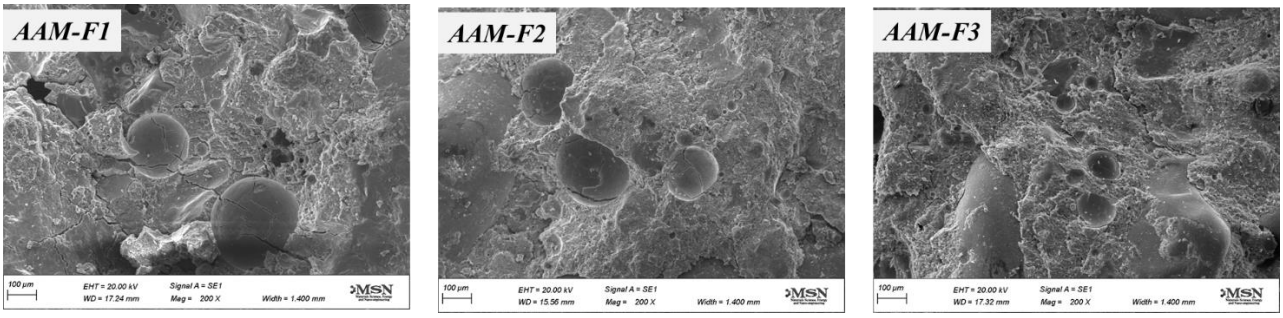

Fig. 7. Micrographs analysis of AAMs after 28 days of curing.

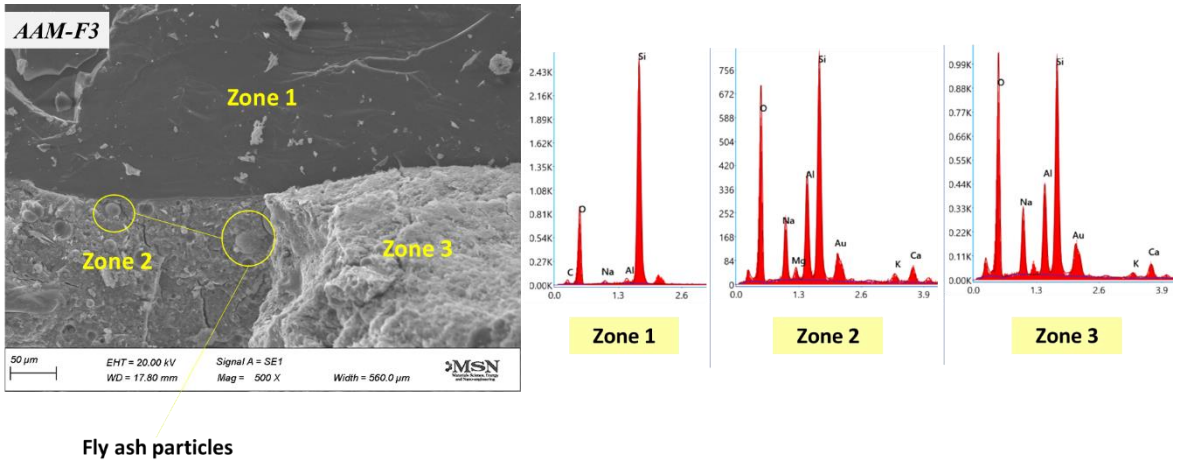

Fig. 8. EDX analysis of AAMs after 28 days of curing.

Thermal stability of AAMs

TGA analysis results

It can be seen from the TGA curves Fig. 9, a massive mass loss for all AAMs mixtures arises at about 100 °C, in part as the result of the evaporation of free water heated to under 100 °C, which is believed to have been wholly removed at 120 °C. After a significant mass loss between 105 and 180 °C all samples show a gradual decrease in mass until a temperature of 600 °C, followed by a stable curve with remarkably low mass loss (0.5 to 1.43%) between 600 and 1000 °C. This may indicate that the de-hydroxylation of hydrated gel namely C-A-S-H and N-A-S-H gels and removal of entrapped water inside the pore gel structure[28], [29].

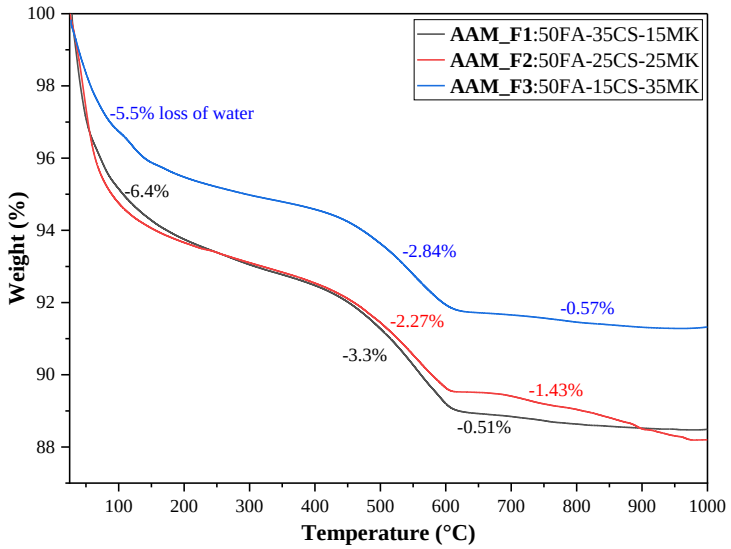

Fig. 9. TG analysis of AAMs after 28 days of curing.

Fire resistance test

Fire resistance of AAMs was determined in terms of visual appearance, weight loss, residual compressive strength, and structure change by XRD and FT-IR. The influence of high temperatures on the properties of AAMs was investigated at temperatures of 400, 600, 800 and 1000°C. One sample was kept sealed without heating, as reference, up to the characterization analysis was performed.

Physical appearance

Typical photographs in Fig.10 (b) show the physical appearance of the AAM specimens that depicted the color changes after being subjected to the different elevated temperatures.

AAMs specimens turned to grey from black after exposure to 400 °C, to brown after 600 °C, to pink after 800°C and then to beige after 1000°C as shown in Fig.10 (b). The color changes in these AAMs mixtures are slight similar to that observed in PCM after high temperature exposure, which primarily results from gradual dehydration of AAMs binder and microstructural transformations occurring within the matrix.

It can be also clearly seen that there is no visible effect on the surface or changing in the size or shape of all AAMs specimens heated up to 1000°C. However, the PCM specimens show a major damage and total deterioration after being exposed to 800°C (Fig.10 (a)). This can be attributed to the decomposition of binding phases.

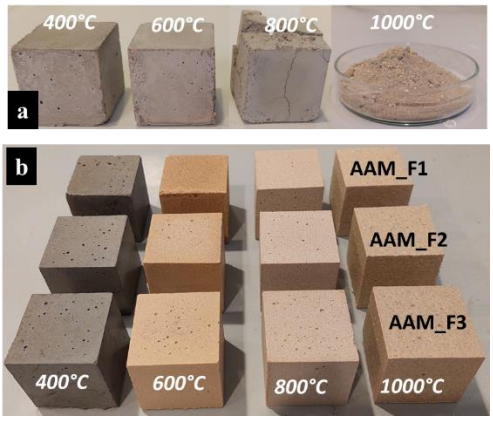

Fig .10. (a) Photos of PCM and (b) AAMs -28 days of curing after post-exposure to elevated temperatures of 400°C, 600°C, 800°C, and 1000°C**.**

Residual mass loss and compressive strength

Fig.11(a) shows the evolution of the relative residual mass (mT/m25) with the temperature of AAMs specimens. The trend of all AAM specimens is identical. A constant residual weight of approximately 0.9 was observed for all AAMs specimens at each heating temperature. This is probably due to dehydration of free water and water from aluminosilicate gel, as it is showed in TGA analysis results (Fig.9). However, sample prepared with PCM present the highest loss of mass of all (20% of loss), which can indicate the high thermal stability of AAMs at higher temperature.

Fig.11 (b) shows the evolution of the relative residual compressive strength (RCT/RC25) of AAMs after the exposure to different temperatures. The trend of both AAMs (AAM-F2 and AAM-F3) is identical. There is a continuous loss of compressive strength after heating at 400°C. However, AAM-F1 (containing 35% PMWRs) showed a gain of compressive strength after the exposure at high temperature of 1000°C. This may a good indication of the positive attribution of PMWRS addition for a high thermal stability of AAMs specimens.

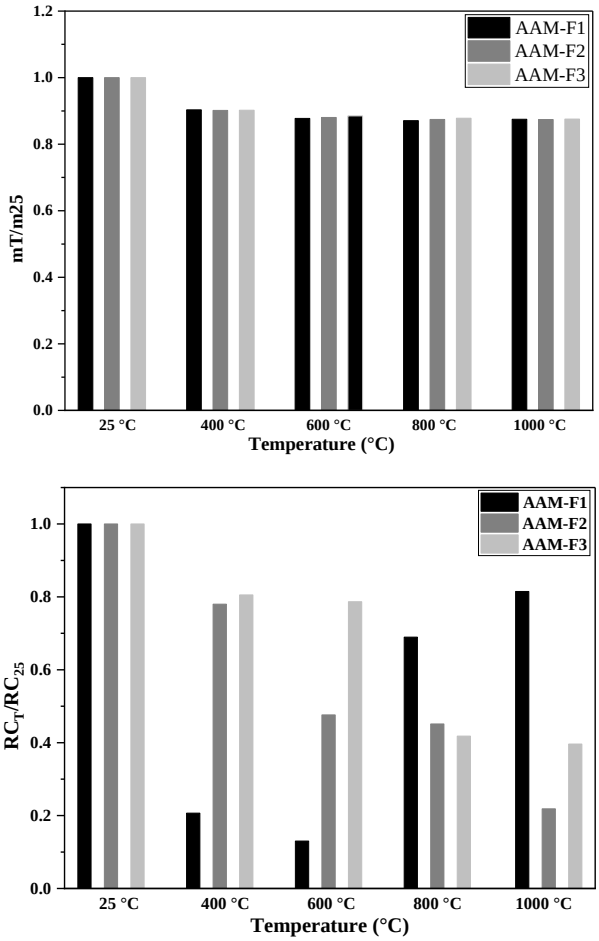

Fig.11. (a) Evolution of relative residual mass and (b) relative residual compressive strength of AAMs with the temperature.

Structure development (XRD analysis)

Fig. 12 (a, b, c) shows that all the XRD patterns of all alkali activated mortar mixtures exhibited similar crystalline phases before and after exposure to 400°C, with a slight reduction of the amorphous hump. New phases, which were jadeite and nepheline, were identified after exposure to 600°C in all the XRD patterns. However, no calcite phase was detected at this temperature [30]. Basically, the formation of jadeite ($NaAlSi_2O_6$) and nepheline ($NaAlSiO_4$) was originated from Na_2O and Al_2O_3 in each mixture [18], [31].

Fig. 12 (d) shows the XRD results of PCM before and after exposure to high temperatures. In the PCM samples heated up to 400°C, a reduction in the intensity of the lime peak (and calcium silicate hydrate (C–S–H) peak (around 29.4° 2θ). The intensity of these peaks also decreased as the temperature increased with no detection at the high temperature up to 600 °C. This is mainly due to the chemical deteriorations occurring at high temperatures where both chemically bound and intercalated water are lost with the decomposition of lime and C–S–H, accounting governing the strength loss of PCM with the increasing exposure temperature.

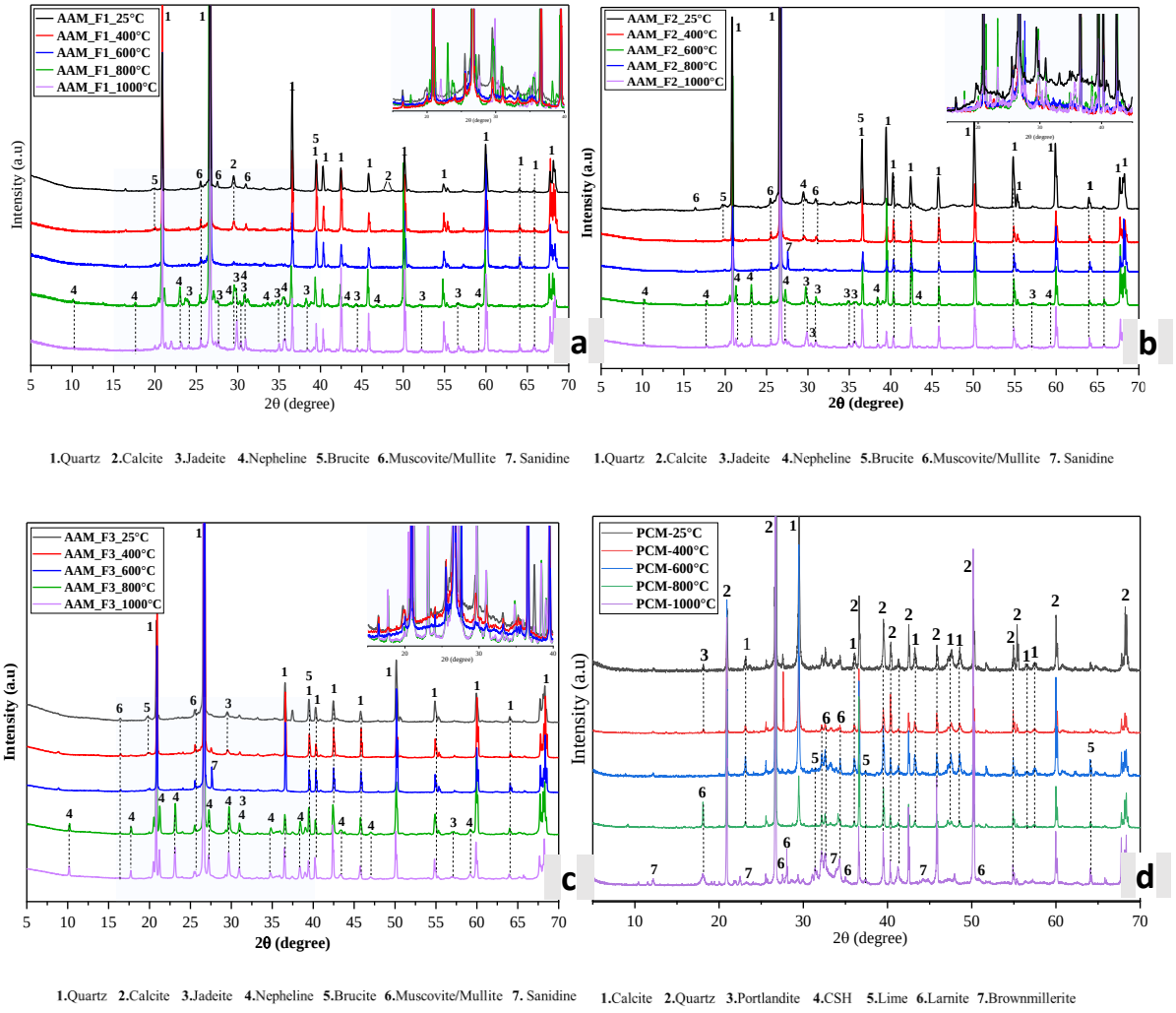

Fig. 12. XRD analysis of (a, b, c) AAMs and (d) PCM before and after exposure to high temperatures.

According to Fig. 13 (a, b, c) when the AAMs specimens was subjected to elevated temperatures the intensity of the diffuse band at 3200 cm^{-1} decreased and at 400 °C it completely disappeared. This proves that first free water and then constitutional water is released from the structure of AAMs. The number of carbonate species is also reduced due to their decomposition, which starts at about 400 °C and is completely finished at 800 °C. It can be also noted that upon exposure to 400°C, all AAM samples show a sharp reduction in intensity of the Si-O-Si/ Al-O-Si band. This may be related to the decrease in the chain length of AAMs, which account for the regression of compressive strength between 200 and 400°C as mentioned in section above. After raising the temperature to 1000°C, it can be noticing a pronounced increase in the intensity of this band for all AAMs specimens. This could be related to the further polymerization of unreacted metakaolin which promotes the densification of AAMs, which also is reflected in the residual strength values. A new peak can be also seen at 1087 cm^{-1} for the same temperature, related to the formation of new crystalline phases likely, nepheline and jadeite, which is emphasized by XRD patterns.

On the other hand, the FT-IR spectra of PCM heated at high temperature 25-1000°C (Fig. 13, d) shows a significant reduction of the main band related to the C-S-H gel, which reflected the total deterioration of cement matrix at higher temperature.

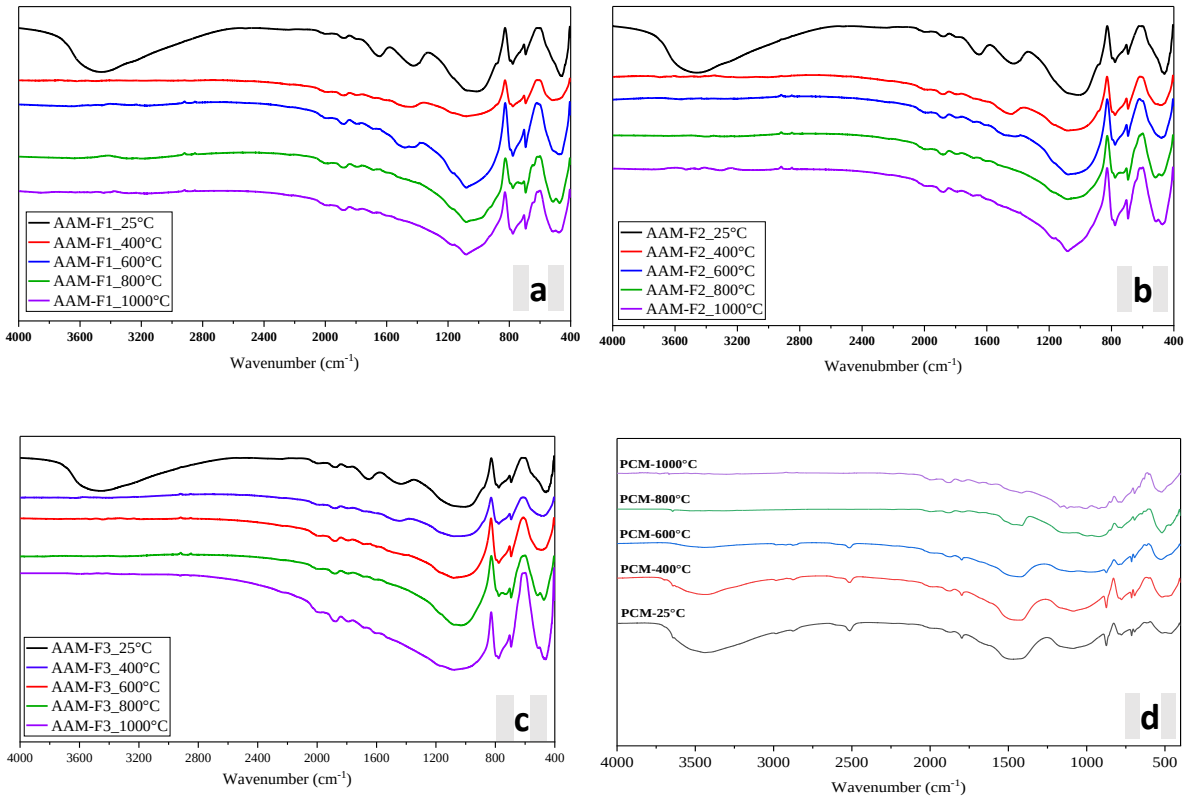

Fig. 13. FTIR analysis of (a, b, c) AAMs and (d) PCM before and after exposure to high temperatures.

Efflorescence test of AAMs

Efflorescence is the formation of white salt deposits on or near the surface of concrete. It is generally harmless in Portland cement-based products but can be a big issue in AAM products, when are exposed to humid air or in contact with water. The prepared AAMs samples (Fig. 14) show smooth surface and efflorescence occurs on the surface when they contact with water. It can be also seen from the figure an excessive efflorescence formation in AAM-F1 specimens compared to the others, which is reasonably due to the low Al availability in this system (High PMWRs content) that cause high mobility of excessive alkalis and such efflorescence formation.

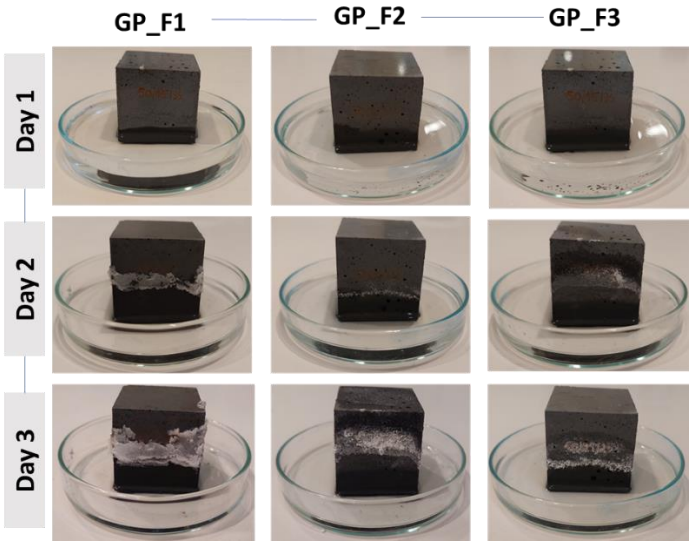

Fig.14. Efflorescence of AAMs in contact with water for 3 days.

Water absorption test of AAMs

To determine the water absorption of mortar specimens, the AAMs cubes from each mixture were oven dried at a temperature of 105°C for 24 hours and its weight determined as initial weight. The samples were then immersed in water and its saturated surface dry weight was recorded as the final weight at each time interval measurement. Water absorption of specimens is reported as the percentage increase in weight.

The following equation was used to calculate the water absorption.

$$\text{Water absorption of AAMs (\%)} = [(Mw-Md)/ (Md)] \times 100\%$$

Where Mw = weight of specimen after immersion in water

Md = Weight of specimen after oven drying at 105°C for 24 hours.

The results of water absorptions of mortars are shown in Fig.15. Regarding the PMWRs/MK variation, evolution of water absorption does not reveal a clear tendency. AAM-F1(with high PMWRs content) shows the lowest water absorption at the range of 2.9-3.12% for all time exposure. However, the AAMs specimens with high MK content (25-35%) show the highest water absorption (9-14%) for all time immersion. It should be noted that the water absorption of AAMs is deeply affected by the specific surface and pore volume inside the matrix, though these results would require further investigation and analysis.

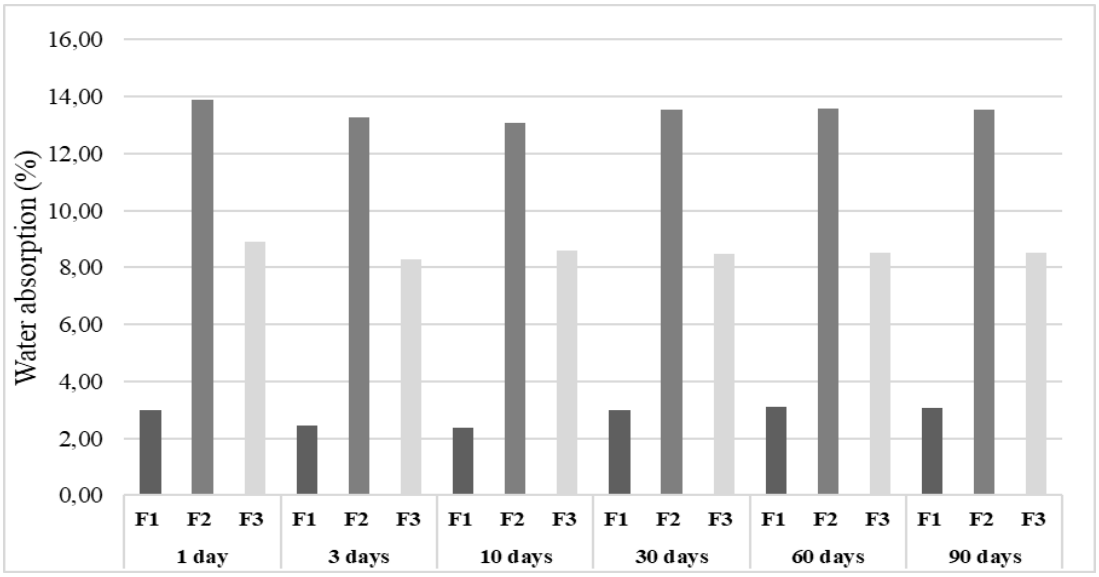

Fig.15. Water absorption of AAMs mortar with time.

Acid attack test

The impact of long-term exposure to acid solution (5% H_2SO_4) on Alkali-Activated Materials (AAMs) was evaluated using AAM-F1 specimens, as they have high calcium content (35% wt. PMWRs) and thus have a higher tendency to acid attack (such as visual deterioration and loss of compressive strength, among others).

Physical appearance

Fig.16 displays the appearance of the AAMs after exposure to 5% solutions of sulfuric acid for 10, 30 and 60 days. AAMs mortars have suffered limited visible damage in general, with almost no deterioration visible. However, at 60 days of acid sulfuric immersion, AAMs show some alkali activated paste loss and the exposure of sand particles that increase with the time exposure.

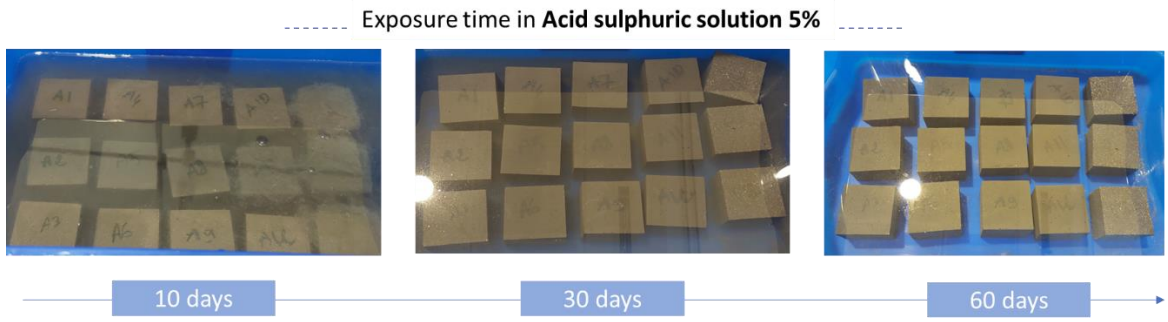

Fig.16. Typical appearances of AAM specimens after 5% acid sulfuric attack.

Residual Alkalinity

The residual alkalinity of the AAMs specimens was approximately determined after cutting the specimens into halve and spraying a 1% Phenolphthalein solution on the freshly cut surface. On spraying, de-alkalized part of specimen showed colorless while remaining part exhibited a pink color indicating its residual alkalinity. This provides an indication of how far the acid has penetrated or how far into each mix significant ion exchange with the acid solution has taken place.

Figure 17 illustrates the residual alkalinity of AAM-F1 specimens in acid solutions. It can be observed that the GP-F1 specimens (after 30 days of acid sulfuric exposure) show a pink section within the matrix, indicating a residual alkalinity of about 60%. This could be due to the acid resistance of the material, which slows down acid migration, providing a high degree of protection against aggressive agents and reducing permeability. However, the AAM-F1 specimen (after 60 days of acid sulfuric exposure) shows total dealkalization, indicating that the acid solution has fully migrated into the AAM matrix**.**

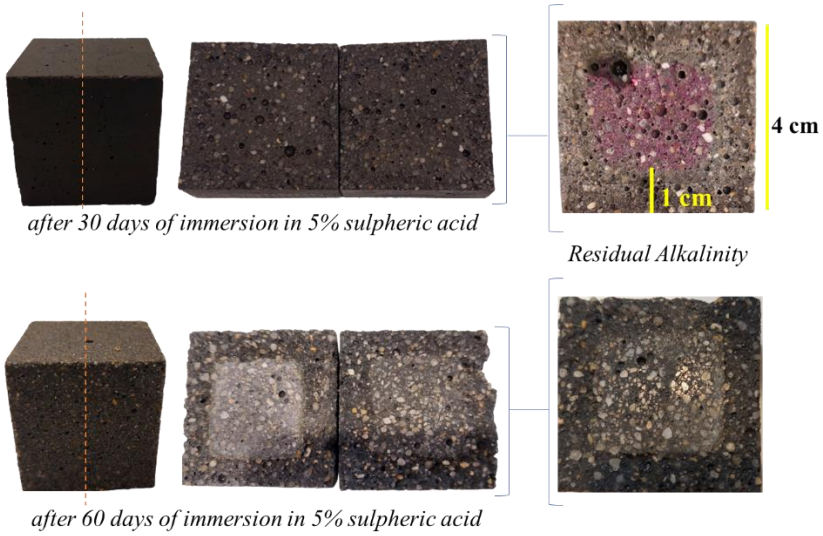

Fig.17. Residual alkalinity of AAM-F1 specimen after 30 to 60 days in 5% Sulfuric acid.

Change in Compressive strength

AAM-F1 specimens after 30 days of acid exposure, showed very little loss in strength initially (27 MPa). However, even after a long-time acid solution exposure (60 days), AAM-F1 specimens still possessed substantial residual compressive strength (7 MPa).

Change in structure (XRD analysis)

Fig. 18 shows the XRD pattern of AAM-F1 specimen before and after acid sulfuric immersion. When these specimens were exposed to sulphuric acid for 30 days, the AAM-F1specimen showed the

presence of quartz with high peak intensity, and with the addition of new peaks attributed to anhydrite phase. Anhydrite corresponds to calcium sulfate which tends to develop in the PMWRs based alkali activated system due to the reaction between sulfuric acid and the calcium based hydrated products whereas calcite refers to the co-existence of free calcium in the geo-polymeric system.

The formation of calcium sulfate may have a negative impact on the compressive strength of exposed specimens and can be considered as a significant factor for the concrete deterioration. This calcium sulfate either can reacts further to form gypsum or can be deposited as a weak layer on the concrete surface which decreases its density and softens the matrix. Therefore, the addition of high amount of PMWRs which considered as calcium rich precursor can results in quicker failure of concrete and causes its deterioration. Similar deterioration due to calcium sulfate layer deposition was also reported in previous studies.

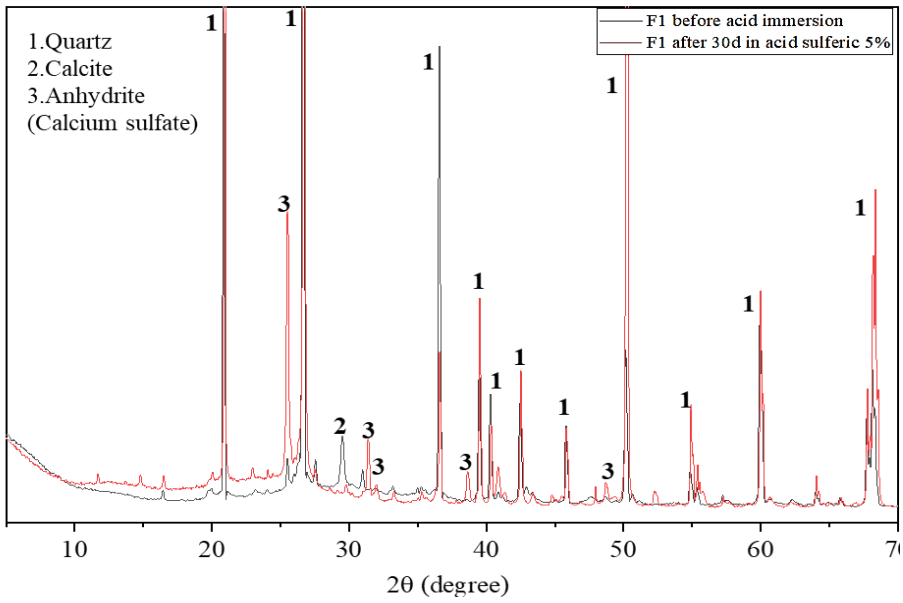

Fig.18. XRD patterns of AAM-F1 before and after 30 days of sulfuric acid attack.

CONCLUSION

This study presents an investigation of the microstructure properties, mechanical strength and durability behavior of alkali activated mortars based on the combination of FA/ PMWRs/MK. The following conclusions have been drawn from the experimental results and previous discussion:

- All AAMs show good mechanical properties (35–57 MPa) compared to PCM mortar.
- The performance of developed alkali activated mortars is considerably higher than that in PCM mortars.
- Visual observation of specimens after exposure to high temperature shows a severe deterioration in the PCM specimens, while in alkali activated mortars, no sign of deterioration was detected for all performed tests.
- The XRD, FTIR and SEM/EDX show a probable formation of C–(A) –S–H and N–A–S–H gels as the main reaction products with the coexistence of some trace of gels C–(N–A)S–H gels.
- The microstructure observation of all AAMs show a denser and high compact matrix, which results in the good mechanical properties of these materials.
- AAMs containing 35% of PMWRS pastes gained strength after thermal exposure to 600°C which may be due to the further polymerization of initially un-reacted materials leading to the formation of a dense matrix and improved the strength properties.

- All AAMs show a good durability performance under high thermal exposition and aggressive solution compared to conventional cement.

Therefore, more advanced tests and research on these materials may accelerate the standardization process and consequently increase their application in the civil construction market.

ACKNOWLEDGEMENT

This work was support by OCP-SA, Morocco, under the specific agreement OCP/UM6P #AS03#. The authors would like to show their gratitude to the OCP-SA collaborators for the highly valuable contribution concerning the sampling.

REFERENCES

[1] E. Adesanya et al., "Opportunities to improve sustainability of alkali-activated materials: A review of side-stream based activators," J. Clean. Prod., vol. 286, p. 125558, Mar. 2021, doi: 10.1016/j.jclepro.2020.125558.

[2] S. A. Bernal and J. L. Provis, "Durability of Alkali-Activated Materials: Progress and Perspectives," J. Am. Ceram. Soc., vol. 97, no. 4, pp. 997–1008, 2014, doi: 10.1111/jace.12831.

[3] O. Burciaga-Díaz and J. I. Escalante-García, "Comparative performance of alkali activated slag/metakaolin cement pastes exposed to high temperatures," Cem. Concr. Compos., vol. 84, pp. 157–166, Nov. 2017, doi: 10.1016/j.cemconcomp.2017.09.007.

[4] A. Aboulayt et al., "Alkali-activated grouts based on slag-fly ash mixtures: From early-age characterization to long-term phase composition," Constr. Build. Mater., vol. 260, p. 120510, Nov. 2020, doi: 10.1016/j.conbuildmat.2020.120510.

[5] T. A. Aiken, J. Kwasny, W. Sha, and M. N. Soutsos, "Effect of slag content and activator dosage on the resistance of fly ash geopolymer binders to sulfuric acid attack," Cem. Concr. Res., vol. 111, pp. 23–40, Sep. 2018, doi: 10.1016/j.cemconres.2018.06.011.

[6] T. Akçaoğlu, B. Cubukcuoglu, and A. Awad, "A critical review of slag and fly-ash based geopolymer concrete," vol. 24, pp. 453–458, Nov. 2019, doi: 10.12989/cac.2019.24.5.453.

[7] S. A. Bernal et al., "Gel nanostructure in alkali-activated binders based on slag and fly ash, and effects of accelerated carbonation," Cem. Concr. Res., vol. 53, pp. 127–144, Nov. 2013, doi: 10.1016/j.cemconres.2013.06.007.

[8] G. V. P. Bhagath Singh and K. V. L. Subramaniam, "Quantitative XRD study of amorphous phase in alkali activated low calcium siliceous fly ash," Constr. Build. Mater., vol. 124, pp. 139–147, Oct. 2016, doi: 10.1016/j.conbuildmat.2016.07.081.

[9] S. Wallah and B. Rangan, "Low-calcium fly ash-based geopolymer concrete: long term properties," Jan. 2006.

[10] I. García-Lodeiro, A. Fernández-Jiménez, and A. Palomo, "Variation in hybrid cements over time. Alkaline activation of fly ash–portland cement blends," Cem. Concr. Res., vol. 52, pp. 112–122, Oct. 2013, doi: 10.1016/j.cemconres.2013.03.022.

[11] Y. Taha, A. Elghali, R. Hakkou, and M. Benzaazoua, "Towards Zero Solid Waste in the Sedimentary Phosphate Industry: Challenges and Opportunities," Minerals, vol. 11, no. 11, Art. no. 11, Nov. 2021, doi: 10.3390/min11111250.

[12] S. Sbi et al., "An advance understanding of the alkali activation of cover layers waste rocks from phosphate mines: Mechanical, structure and microstructure studies," Constr. Build. Mater., vol. 346, p. 128472, Sep. 2022, doi: 10.1016/j.conbuildmat.2022.128472.

[13] M. Amrani, Y. Taha, A. Kchikach, M. Benzaazoua, and R. Hakkou, "Valorization of phosphate mine waste rocks as materials for road construction," Minerals, vol. 9, no. 4, p. 237, 2019.

[14] M. Loutou, Y. Taha, M. Benzaazoua, Y. Daafi, and R. Hakkou, "Valorization of clay by-product

from moroccan phosphate mines for the production of fired bricks," J. Clean. Prod., vol. 229, pp. 169–179, 2019.

[15] S. Mabroum, A. Aboulayt, Y. Taha, M. Benzaazoua, N. Semlal, and R. Hakkou, "Elaboration of geopolymers based on clays by-products from phosphate mines for construction applications," J. Clean. Prod., vol. 261, p. 121317, 2020.

[16] R. M. Barrer, "Chemistry of Soil Minerals. Part XII1.t Reactions of Metakaolinite with Single and Mixed Bases," 1972.

[17] M. C. Bignozzi, S. Manzi, I. Lancellotti, E. Kamseu, L. Barbieri, and C. Leonelli, "Mix-design and characterization of alkali activated materials based on metakaolin and ladle slag," Appl. Clay Sci., vol. 73, pp. 78–85, 2013.

[18] H. Y. Zhang, V. Kodur, S. L. Qi, L. Cao, and B. Wu, "Development of metakaolin–fly ash based geopolymers for fire resistance applications," Constr. Build. Mater., vol. 55, pp. 38–45, Mar. 2014, doi: 10.1016/j.conbuildmat.2014.01.040.

[19] S. M, J. R, and R. N. P, "Effect of change in the silica modulus of sodium silicate solution on the microstructure of fly ash geopolymers," J. Build. Eng., vol. 44, p. 102939, Dec. 2021, doi: 10.1016/j.jobe.2021.102939.

[20] S. Alehyen, M. Zerzouri, M. ELalouani, M. E. Achouri, and M. Taibi, "Porosity and fire resistance of fly ash based geopolymer," 2017.

[21] C. A. Rees, J. L. Provis, G. C. Lukey, and J. S. J. van Deventer, "In Situ ATR-FTIR Study of the Early Stages of Fly Ash Geopolymer Gel Formation," Langmuir, vol. 23, no. 17, pp. 9076–9082, Aug. 2007, doi: 10.1021/la701185g.

[22] I. Garcia-Lodeiro, A. Palomo, A. Fernández-Jiménez, and D. E. Macphee, "Compatibility studies between N-A-S-H and C-A-S-H gels. Study in the ternary diagram Na2O–CaO–Al2O3–SiO2–H2O," Cem. Concr. Res., vol. 41, no. 9, pp. 923–931, Sep. 2011, doi: 10.1016/j.cemconres.2011.05.006.

[23] H. Niu et al., "Recycling mica and carbonate-rich mine tailings in alkali-activated composites: A synergy with metakaolin," Miner. Eng., vol. 157, p. 106535, Oct. 2020, doi: 10.1016/j.mineng.2020.106535.

[24] R. A. Gado, M. Hebda, M. Łach, and J. Mikuła, "Alkali Activation of Waste Clay Bricks: Influence of The Silica Modulus, SiO2/Na2O, H2O/Na2O Molar Ratio, and Liquid/Solid Ratio," Materials, vol. 13, no. 2, Art. no. 2, Jan. 2020, doi: 10.3390/ma13020383.

[25] K. Kaya and S. Soyer-Uzun, "Evolution of structural characteristics and compressive strength in red mud–metakaolin based geopolymer systems," Ceram. Int., vol. 42, no. 6, pp. 7406–7413, May 2016, doi: 10.1016/j.ceramint.2016.01.144.

[26] S. A. Bernal, E. D. Rodríguez, R. Mejía de Gutiérrez, and J. L. Provis, "Performance of alkali-activated slag mortars exposed to acids," J. Sustain. Cem.-Based Mater., vol. 1, no. 3, pp. 138–151, Sep. 2012, doi: 10.1080/21650373.2012.747235.

[27] S. A. Bernal, R. M. de Gutierrez, J. L. Provis, and V. Rose, "Effect of silicate modulus and metakaolin incorporation on the carbonation of alkali silicate-activated slags," Cem. Concr. Res., vol. 40, no. 6, pp. 898–907, Jun. 2010, doi: 10.1016/j.cemconres.2010.02.003.

[28] S. K. Nath and S. Kumar, "Role of particle fineness on engineering properties and microstructure of fly ash derived geopolymer," Constr. Build. Mater., vol. 233, p. 117294, Feb. 2020, doi: 10.1016/j.conbuildmat.2019.117294.

[29] G. Görhan and G. Kürklü, "The influence of the NaOH solution on the properties of the fly ash-based geopolymer mortar cured at different temperatures," Compos. Part B Eng., vol. 58, pp. 371–377, Mar. 2014, doi: 10.1016/j.compositesb.2013.10.082.

[30] C. Rodriguez-Navarro, E. Ruiz-Agudo, A. Luque, A. B. Rodriguez-Navarro, and M. Ortega-Huertas, "Thermal decomposition of calcite: Mechanisms of formation and textural evolution of

CaO nanocrystals," Am. Mineral., vol. 94, no. 4, pp. 578–593, Apr. 2009, doi: 10.2138/am.2009.3021.

[31] S. Luhar, S. Chaudhary, and I. Luhar, "Thermal resistance of fly ash based rubberized geopolymer concrete," J. Build. Eng., vol. 19, pp. 420–428, Sep. 2018, doi: 10.1016/j.jobe.2018.05.025.

Use of lime kiln dust as a waste-based reagent in high calcium fly ash-based alkali-activated materials

Parham Shoaei[1,2], Shima Pilehvar[1] and Ramon Pamies[2]

[1] Faculty of Engineering, Østfold University College, P.O. Box 700, 1757, Halden, Norway. (E-mail: parhams@hiof.no, shima.pilehvar@hiof.no)

[3] Department of Materials Engineering and Manufacturing, Technical University of Cartagena, Cartagena, Murcia, Spain. (E-mail: ramon.pamies@upct.es)

HIGHLIGHTS

- High calcium fly ash can be successfully activated by using LKD.
- It could reach up to 28.2 MPa after 28 days of curing.
- Curing in water results in reduced mechanical strength.

Keywords: high calcium fly ash, lime kiln dust (LKD), alkali-activated materials

INTRODUCTION

Alkali activation facilitates utilization of industrial by-products as a binder in concrete mixes. The by-products suitable for use in alkali-activated concrete should be a source of aluminosilicates. The aluminosilicate source is mixed with silicates or alkali metals such as sodium silicate and sodium hydroxide to initiate geopolymerization. However, the production of silicates can be costly and energy intensive with high carbon footprint, which obstacles the widespread application of alkali-activated materials [1]. Therefore, it is important to find other materials with lower environmental impact to replace the silicates. Lime kiln dust (LKD) is a by-product of quick lime (QL) production, which is mostly landfilled. LKD is able to create a highly alkaline environment when mixed with water; hence, it can be used in alkali-activated concrete to dissolve Si and Al oxides. Previous studies have explored utilization of LKD in soil stabilization [2-4]; however, the use of LKD as a reagent in alkali-activated materials has been scarcely studied. Chee Ban et al. [5] studied the performance of fly ash (FA)-slag mixes incorporating LKD as the alkali activator. It was shown that using 10% LKD led to the optimal mix. In this study, LKD was used in alkali-activated mixes based on high calcium FA. For this purpose, mixes were made with different contents of LKD and the compressive strength of cube specimens cured in different conditions were measured at different ages.

MATERIALS AND METHODS

The binder used in this study was high calcium FA with the specific gravity of 2.5 and specific surface area of 3000 cm2/g. LKD was provided by the Nordkalk company in Sweden. The specific gravity and specific surface area of the LKD was 2.8 and 7990 cm2/g, respectively. Furthermore, the elemental composition of the FA and LKD was determined by X-ray fluorescence (XRF) analysis and the results are presented in Table 3.

Table 3. XRF analysis results.

Chemical compound	LKD	FA
CO_2	19.7	4.3
Na_2O	0.6	1.5
MgO	1.1	1.4
Al_2O_3	5.8	17.7
SiO_2	12.4	42.7
P_2O_5	0.25	0.9
SO_3	5.3	2.6
K_2O	3.1	2.1
CaO	48.8	18.9
TiO_2	0.3	0.9
Fe_2O_3	2.1	5.4
L.O.I (%)	19.7	5.3

Mix design and sample preparation

Three different FA/LKD mass ratios of 90:10, 80:20, and 70:30 were selected. The water-to-binder ratio was selected equal to 0.4 for all mixes. FA and LKD were poured into a mixing bowl and then the water was added. The materials were mixed for 2 minutes at 140 rpm, and then the mixer was stopped to scrape the walls of the bowl to make sure all powdery materials are in contact with water. Thereafter, the mixing was continued for another 2 minutes at 225 rpm. The fresh paste was poured into 30×30×30 mm3 cubes and was compacted by means of a vibrating table. A number of three samples were made from each mix and the average value was reported. The samples were pre-cured at ambient temperature for 48 h followed by demolding. The samples were cured in two different curing conditions including ambient and water at 20 °C. The compressive strength tests were performed after 7 and 28 days by using a Galdabini Quasar 100 Material Testing Machine with 5 mm/min loading rate. Furthermore, in order to investigate the effect of heat-curing on the strength development of mixes, a series of specimens were pre-cured in an oven at 60 ℃ for 24 h. Afterwards, the specimens were cured for 7 and 28 days in the ambient and water.

RESULT & DISCUSSION

Figure 2 shows the compressive strength of specimens cured in different conditions. In this figure, the mixes are named as FAC-X-Y where X denotes the water-to-binder ratio and Y denotes the percentage of LKD. It can be observed that the rate of strength development was low. According to the test results, the 28-day compressive strength of mixes was more than two times of the corresponding 7-day compressive strength. Furthermore, the water-cured samples showed about 43% lower compressive strength compared to the air-cured samples. The results showed that mixes containing 20% and 30% LKD had a lower compressive strength compared to that of the mix with 10% LKD. This could be due to the oversaturation of calcium ions in the mix when the LKD content exceeded 10% [5]. Thus, FAC-0.4-10 was the optimal mix and was selected for evaluating the effect of pre-curing with heat. It was shown that pre-curing increased the reaction rate. The pre-cured specimens showed a significantly higher compressive strength at 7 days compared to mixes without pre-curing. For example, the 7-day compressive strength of the pre-cured mix was about 40% higher than that of the counterpart air-

cured mix. The heat accelerates the reactions, and thereby it leads to a higher early-age strength [6]. However, it appears that pre-curing limited the strength development of the air-cured mixes, as the 28-day compressive strength was lower than that of the mixes without pre-curing. It has been reported that heat-curing may prevent the formation of a compact matrix [6]. On the contrary, pre-curing favored the compressive strength of water-cured specimens. Based on the test results, the 28-day compressive strength of the heated mix, which was cured in water, was about 19% higher than that of the counterpart mix without any pre-curing.

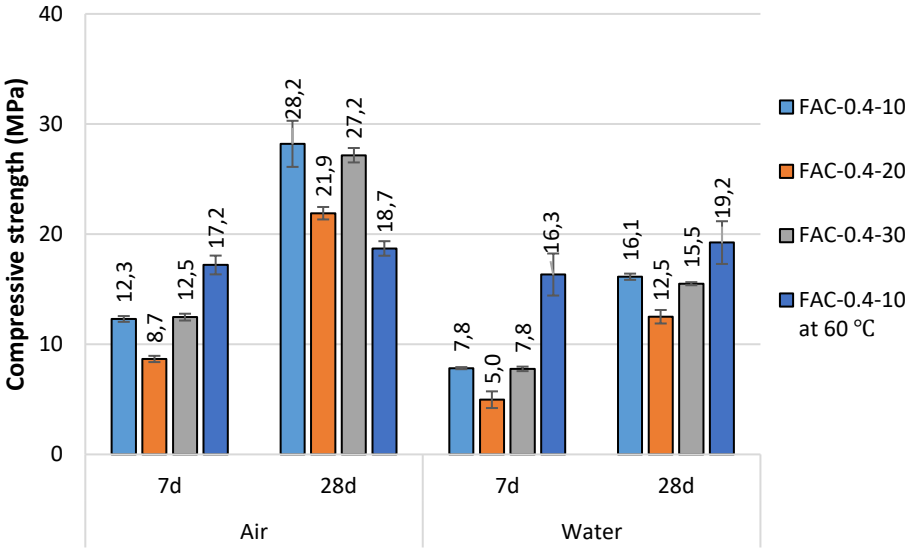

Figure 2. Compressive strength of mixes.

CONCLUSION

In this study, alkali-activated mixes based on high calcium FA and LKD were made and the strength development under different curing conditions was evaluated. The results showed that LKD can be successfully used as a waste-based reagent in alkali-activated materials based on high calcium FA. The product will have a lower environmental impact as it is exclusively made with industrial by-products. Also, it is possible to achieve a compressive strength value, which meets the requirements for structural concrete. Future studies should focus on finding the optimized mix design and a comprehensive mechanical performance and durability assessment of mortar and concrete mixes.

REFERENCES

[1] Rajan, H.S. and P. Kathirvel, *Sustainable development of geopolymer binder using sodium silicate synthesized from agricultural waste.* Journal of Cleaner Production, 2021. 286: p. 124959.

[2] Bandara, N., et al., *Pavement subgrade stabilization using recycled materials.* Airfield and Highway Pavements, 2015. 2015: p. 605-616.

[3] Jegandan, S., et al., *Sustainable binders for soil stabilisation.* Proceedings of the Institution of Civil Engineers-Ground Improvement, 2010. 163(1): p. 53-61.

[4] Sol-Sánchez, M., et al., *Stabilisation of clayey and marly soils using industrial wastes: pH and laser granulometry indicators.* Engineering geology, 2016. 200: p. 10-17.

[5] Ban, C.C., et al., *Properties and microstructure of lime kiln dust activated slag-fly ash mortar.* Construction and Building Materials, 2022. 347: p. 128518.

[6] Rovnaník, P., *Effect of curing temperature on the development of hard structure of metakaolin-based geopolymer.* Construction and building materials, 2010. 24(7): p. 1176-1183.

Performance of alkali-activated metakaolin at high H_2O/Na_2O ratios

Faten Souayfan[1], Emmanuel Rozière[1], Christophe Justino[2,] Michaël Paris[3], Dimitri Deneele[3,4], Ahmed Loukili[1]

[1] Civil engineering and Mechanics Research Institute (GeM), Nantes, France.
(E-mail: Faten.Souayfan@ec-nantes.fr)

[2] Soletanche Bachy, Montereau Fault Yonne, France.

[3] Université de Nantes, CNRS, Institut des Matériaux Jean Rouxel, IMN, F-44000 Nantes, France.

[4] GERS-LGIE, Université Gustave Eiffel, F-44344 Bouguenais, France.

HIGHLIGHTS

- Activated metakaolin with high H_2O/Na_2O ratios and constant Si/Al and Na/Al atomic ratio
- Influence of water on the reactivity of the precursor
- Decrease in compressive strength with H_2O/Na_2O

Keywords: geopolymer, water content, compressive strength, nuclear magnetic resonance

INTRODUCTION

Deep soilmixing allows improving the physical and mechanical properties of soil in-depth, by mixing in situ the soil with a diluted mixture called grout, using a specific tool. Currently, most of grouts are based on cement. Nevertheless, the durability of these materials exposed to aggressive medium has been questioned [1]. Geopolymers obtained from solid aluminosilicate sources (such as metakaolin) and an alkaline solution have opened new insights for soil improvement. Metakaolin can be used as precursor, due to its relatively low carbon footprint [2] and high durability [3]. Few studies have focused on the design of alkali-activated metakaolin mixtures used as grouts for soil improvement. The mixtures used as grouts have a high water-to-solid ratio; the water-to-solid ratio of the soilmix is even higher due to the initial water content of the soil. Grouts are expected to satisfy several specifications in fresh and hardened states. Grouts should be stable during storage before use and have relatively low viscosities, and these properties should be maintained during the entire duration of the process [4]. The hardened grout is expected to provide the soilmix with adequate mechanical properties and durability.

This study focused on the influence of high H2O/Na2O ratios on the properties of metakaolin-based grouts MK21, MK24, MK28 and MK34 defined respectively with H2O/Na2O ratios of 21, 24, 28 and 34 and constant Si/Al and Na/Al atomic ratios (1.8 and 1 respectively). Metakaolin was produced from the flash calcination of clay from Fumel, France. The proportion of the pure metakaolin Al2O3(SiO2)2 phase was 43 wt. %. The activation solution was prepared by diluting a sodium silicate solution with a fixed SiO2/Na2O ratio of 1.7 and 44% dry content in demineralized water. The advancement of geopolymerization reactions was studied through nuclear magnetic resonance (NMR) spectroscopy of Al and Si and the mechanical characterization was based on compressive strength at 7, 28, and 90 days. The 29Si spectra were decomposed into a formed phase and a signal representing remnant metakaolin. Remnant metakaolin was considered by fitting a scaled component spectrum calculated from the 29Si spectrum of raw metakaolin. The reaction degree of metakaolin RDmk was calculated using the silicon content from metakaolin of known chemical composition X(Si)mk and the remnant metakaolin deduced from 29Si RMN decomposition Rmk. (equation 1).

$$RD_{mk} = \frac{X(Si)_{mk} - R_{mk}}{X(Si)_{mk}} \quad (1)$$

RESULT & DISCUSSION

The 29Si spectra decomposition of two grouts MK21 and MK34 with H2O/Na2O ratios of 21 and 34 respectively is presented in Figure 3. The water content did not affect the structure of geopolymer-type phase as the peak position and full width at half height (FWHH) of the formed phase were the same at H2O/Na2O ratios of 21 and 34. Increasing this ratio resulted in higher content of unreacted metakaolin and a lower product fraction. The lower concentration of alkaline activator at high H2O/ Na2O content presumably resulted in a lower dissolution of silicates and aluminates from the raw material, resulting in fewer SiO4 and AlO4 tetrahedral units to form a geopolymer gel.

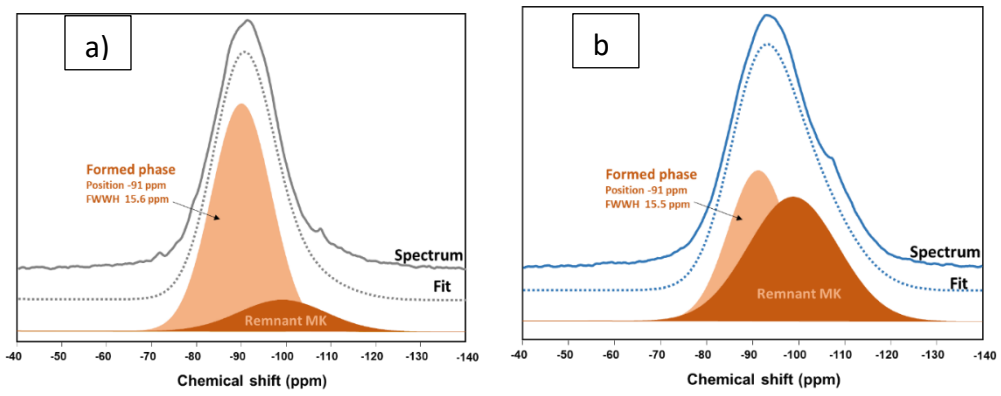

Figure 3. Decomposition of ^{29}Si MAS NMR spectra for a) MK21 and b) MK34 at 28 days.

The reaction degree of metakaolin RDmk $R_{mk}$is presented in Figure 4 for all mixtures. The time evolution of the reaction degree depended on the H2O/Na2O ratio. At H2O/Na2O ratios of 21 and 24, the degree of reaction nearly stabilized after 7 days, whereas at higher ratios, the degree of reaction significantly increased between 7 and 250 days. This shows that a higher amount of water delays the dissolution of the precursor without blocking the reaction progress. A significant amount of the amorphous fraction of metakaolin did not react even under highly alkaline conditions. About 20% of metakaolin did not react in MK21 and MK24 grouts after 250 days from an 29Si NMR perspective.

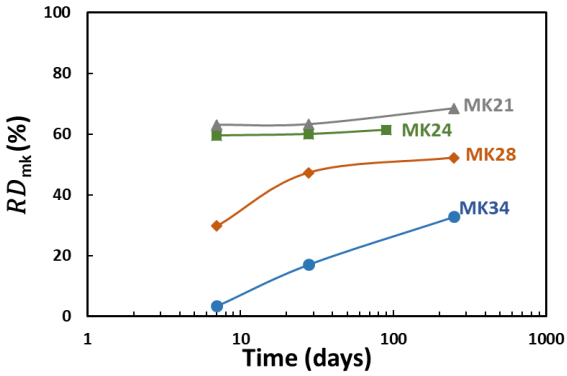

Figure 4. Reaction degree as a function of time calculated from ^{29}Si NMR spectroscopy.

Compressive strength decreased with H_2O/Na_2O ratio (Figure 5). The grout MK34 (defined by H_2O/Na_2O of 34) did not develop significant strength after 90 days. The minimum compressive strength

required in grouting specifications is 5 MPa at 28 days, which suggests that metakaolin is not suitable for applications requiring high water to solid ratios. The decrease in mechanical strength ca be due to the decrease in reactivity of precursor or change in structure of the reaction products depending on the amount of water available in the system and the concentration of alkali cations [5] [6]. Based on the analysis of nuclear magnetic resonance (NMR) spectra, the decrease in compressive strength with increasing H_2O/Na_2O ratio from 21 to 34 can be attributed to the influence of water on the reactivity of the precursor rather than the change of products structure.

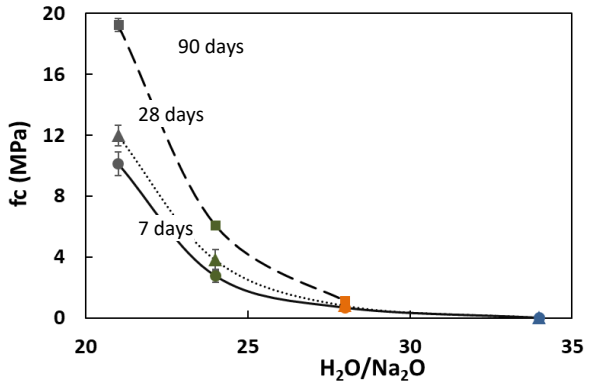

Figure 5. Evolution of compressive strength as a function of H_2O/Na_2O.

CONCLUSION

The H2O/Na2O ratio is likely to affect strength at two levels: the properties of binding phase and initial porosity. Results showed that the properties of binding phase (i.e. geopolymer phase) were not affected by the amount of water. The variations of strength can be explained by higher porosity related to higher water content and lower reactivity of metakaolin. The adjustment of water content remains critical to find a tradeoff between workability and strength when designing geopolymer grout. The introduction of admixtures or additions to increase the strength at a given H2O/Na2O ratio can constitute a major challenge to strengthen the position of geopolymers among possible choices for construction materials especially as grout systems.

ACKNOWLEDGEMENT

Funding: The authors would like to acknowledge financial and technical support of Soletanche Bachy France.

REFERENCES

[1] A. Wang *et al.*, «The Durability of Alkali-Activated Materials in Comparison with Ordinary Portland Cements and Concretes: A Review», *Engineering*, p. S2095809919306708, mai 2020, doi: 10.1016/j.eng.2019.08.019.

[2] J. Provis, *Alkali activated materials: state-of-the-art report, RILEM TC 224-AAM*, Springer Science&Business Media., vol. 13. New York: Springer, 2013.

[3] A. Cherki El Idrissi, E. Rozière, S. Darson-Balleur, et A. Loukili, «Resistance of alkali-activated grouts to acid leaching», *Construction and Building Materials*, vol. 228, p. 116681, déc. 2019, doi: 10.1016/j.conbuildmat.2019.116681.

[4] A. Aboulayt *et al.*, «Alkali-activated grouts based on slag-fly ash mixtures: From early-age characterization to long-term phase composition», *Construction and Building Materials*, vol. 260, p. 120510, nov. 2020, doi: 10.1016/j.conbuildmat.2020.120510.

[5] K. Juengsuwattananon, F. Winnefeld, P. Chindaprasirt, et K. Pimraksa, «Correlation between initial SiO2/Al2O3, Na2O/Al2O3, Na2O/SiO2 and H2O/Na2O ratios on phase and microstructure of reaction products of metakaolin-rice husk ash geopolymer», *Construction and Building*

Materials, vol. 226, p. 406-417, nov. 2019, doi: 10.1016/j.conbuildmat.2019.07.146.

[6] F. Souayfan, E. Rozière, M. Paris, D. Deneele, A. Loukili, et C. Justino, «29Si and 27Al MAS NMR spectroscopic studies of activated metakaolin-slag mixtures», *Construction and Building Materials*, vol. 322, p. 126415, mars 2022, doi: 10.1016/j.conbuildmat.2022.126415.

Effect of activator compositions on the rheology of alkali-activated slag concrete

Yubo Sun [1], Guang Ye [2], Geert De Schutter [3]

[1, 3] Magnel-Vandepitte Laboratory, Department of Structural Engineering and Building Materials, Ghent University, 9052 Ghent, Belgium. (E-mail: yubo.sun@ugent.be, geert.deschutter@ugent.be)

[2] Microlab, Section of Materials and Environment, Faculty of Civil Engineering and Geosciences, Delft University of Technology, Stevinweg 1, 2628 CN Delft, the Netherlands. (E-mail: g.ye@tudelft.nl)

HIGHLIGHTS

- Highlight 1: Rheology of alkali-activated slag concrete mixtures is assessed.
- Highlight 2: Herschel-Bulkley model is applied to reveal the non-linear rheological behavior.

Keywords: alkali-activated slag, concrete, rheology

INTRODUCTION

Alkali-activated material (AAM) is regarded as a green alternative binding material to replace Portland cement in concrete. With a proper mix design, AAM may provide equivalent or even better mechanical and long-term properties [1–3]. Compared to PC materials, the activator is applied as an additional phase in AAMs to raise the alkalinity of the solvent and promote the dissolution of precursors [4,5], which makes the solid-liquid interactions rather complex in the system. Accordingly, the flow of AAMs is not properly understood, with distinctive rheological behaviors being reported [6,7]. Moreover, existing literature has been focused more on paste and mortar levels, while studies on the rheology of AAM concrete are limited to date.

Therefore, this study aims to assess the rheological properties of alkali-activated slag (AAS) concrete. Stress growth and flow curve tests have been conducted with the ICAR Plus rheometer. Results have revealed the effect of silicate modulus (Ms) and sodium concentration (Na2O% by mass of precursor) on the rheology of AAS concrete.

MATERIALS AND METHODS

Ground granulated blast furnace slag (BFS, ECO2CEM from Ecocem Benelux B.V.,) with a specific gravity of 2.89 and a median particle size (d50) of 8.28 μm, was used in this study. Details of the chemical composition determined by X-ray fluorescence (XRF) and loss on ignition (LOI) are listed in Table 1.

Table 4. Chemical composition of BFS and LOI (wt.%).

Precursor	CaO	SiO_2	Al_2O_3	MgO	SO_3	TiO_2	K_2O	Fe_2O_3	MnO	ZrO_2	Other	LOI [a]
BFS	40.9	31.1	13.7	9.16	2.31	1.26	0.69	0.40	0.31	0.12	0.05	0.10

[a] LOI measured by TG analysis at 950℃

Sodium hydroxide and sodium silicate were used as activators in this study. Reagent-grade sodium hydroxide anhydrous pearls were provided by Brenntag N.V., and the sodium silicate solution (15% Na2O, 30% SiO2, and 55% water) was provided by PQ Corporation. River sand and gravel were used as the aggregate to prepare AAS concretes. The aggregates were air-dried before mixing.

Details of five AAS concrete mixtures tested in this study are given in Table 2.

Table 5. Mixture proportions of AAS concretes.

Mix	BFS (kg/m³)	Activator					w/b	Aggregate (kg/m³)		
		NaOH (kg/m³)	Sodium silicate solution (kg/m³)	Na_2O	Ms	Extra water (kg/m³)		0-4 mm	2-8 mm	8-16 mm
M1	400	13.55	10.00	3%	0.25	182.62	0.43	701	482	572
M2	400	11.61	20.00	3%	0.5	178.28		701	482	572
M3	400	7.74	40.00	3%	1.0	169.58		699	480	570
M4	400	15.48	26.67	4%	0.5	177.70		689	474	563
M5	400	19.35	33.33	5%	0.5	177.13		685	471	559

AAS concrete mixtures were prepared by mixing solid components with the activators in a planetary mixer. A dry mixing was first performed on the solid components (including precursor, fine and coarse aggregates) for 2 minutes. Afterwards, the activator was added and mixed for another 3 minutes to derive a homogeneous fresh concrete.

Rheological tests consisting of stress growth and flow curve steps were performed with an ICAR Plus rheometer. The rheometer van is consisting of 4 blades with 130 mm diameter and 130 mm height, while the cylindrical rheometer container has 390 mm depth and 286 mm inner diameter. In the beginning, about 20 L of fresh AAS concrete was loaded into the container. Afterwards, the rheometer vane was inserted, and the fresh concrete was left at rest for about 1 min since the end of remixing until the rheological test.

Stress growth test was first conducted at about 5 min after the contact between the activator and solid precursors with a constant rotational speed of 0.025 rev/s for 60 s. The maximum torque observed along the test was then converted into the static yield stress according to Eq. (1) [8].

$$\tau_S = \frac{2T_m}{\pi D^3(\frac{h}{D}+\frac{1}{3})} \quad (1)$$

where τ_s is the static yield stress (Pa), T_m is the maximum torque in Nm, D is the diameter of the vane m, and h is the height of the vane in m.

Flow curve tests were subsequently conducted. The fresh concrete was subjected to a 60 s pre-shear at 0.6 rev/s, followed by ascending and descending shear steps. The rotational speed was varied between 0.05 and 0.6 rps with a step size of 0.05 rps, where each step lasted for 10 s to reach an equilibrium state. The torque at each speed was recorded as the average value of the last 5 s. Downward portions of the torque-rotational speed relationship were fitted based on the Herschel-Bulkley model to derive the flow curves. Rheological parameters were derived based on the extension of Reiner-Riwlin equations [9,10].

RESULT & DISCUSSION

The static yield stress determined by stress growth tests is displayed in Fig. 1 (a). In 3% Na2O mixtures, the static yield stress of M2 and M3 declined 19.8% and 60.6% compared to M1 respectively, which indicates a fluidizing effect of higher Ms in activators. Similar trends have been observed by improving the sodium concentration. This might be ascribed to the reduction in solid concentration by applying more liquid activator content in the binder phase [11].

Downward portions of flow curves are illustrated in Figure 1 (b) and (c), and the rheological parameters obtained by fitting the Herschel-Bulkley model are summarized in Table 3. It was found that the evolution of dynamic yield stress and plastic viscosity in AAS concrete was following the same trend as the static yield stress, which was reduced with increased Ms and sodium concentrations in the activator. It is noteworthy that a shear thinning behavior was observed in M1 with a flow index smaller than 1. In specific, the slope of the torque profile first declined with an increased rotational speed, but later almost linearly increased at higher shear speed regions. It is indicated clusters formed in AAS mixtures were gradually broken down [12], and remained a steady flow with higher rotational speeds

[13,14]. Further, shear thickening was observed in M5 by applying higher Ms in the activator. This can be ascribed to the viscous nature of high Ms activators [6], which entraps more particles to form clusters and block the flow [15]. Similarly, the shear-thickening also became more pronounced with higher sodium concentrations in the activator.

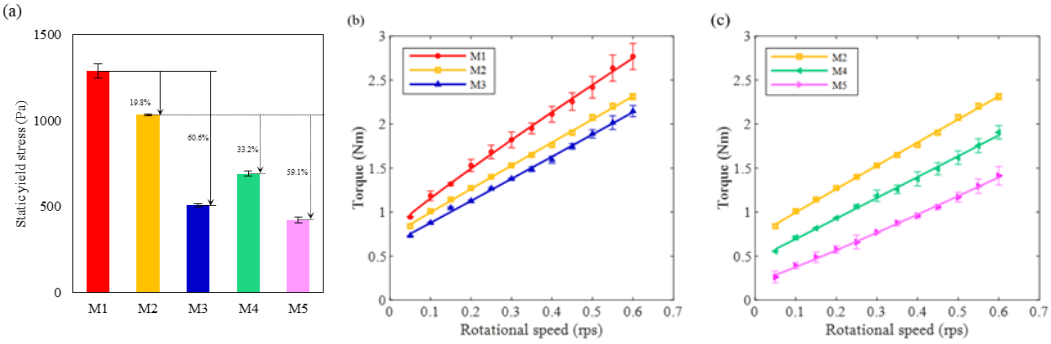

Figure 1. Rheology of AAS concrete. (a) Static yield stress. (b) (c).

Table 6. Dynamic rheological parameters of AAS concretes fitted with Herschel-Bulkley model.

Mix	Dynamic yield stress (Pa)	Consistency factor (Pa·s^n)	Flow index	R^2
M1	114.72	78.22	0.92	0.9988
M2	111.11	54.10	0.98	0.9986
M3	78.70	40.01	1.14	0.9993
M4	71.74	45.27	1.02	0.9976
M5	31.33	34.50	1.08	0.9984

CONCLUSION

This study aims to evaluate the rheological behavior of alkali-activated slag concretes with different compositions of activators. Results show that increases in silicate modulus (Ms) and sodium concentration (Na2O% by mass of precursor) have resulted in the reduction of yield stress and viscosity, indicating a fluidizing effect. Moreover, shear-thickening was observed in AAS concrete, which become more pronounced with higher alkaline doses in the activator.

ACKNOWLEDGEMENT

This paper presents the research results from the DuRSAAM project. The authors wish to acknowledge the financial support from the European Union's Horizon 2020 research and innovation programme (ETN DuRSAAM – H2020-MSCA-ITN-2018-813596).

REFERENCES

[1] J.S.J. Van Deventer, J.L. Provis, P. Duxson, Technical and commercial progress in the adoption of geopolymer cement, Miner. Eng. 29 (2012) 89–104. https://doi.org/10.1016/j.mineng.2011.09.009.

[2] S.A. Bernal, J.L. Provis, A. Fernández-jiménez, P. V Krivenko, E. Kavalerova, M. Palacios, C. Shi, Alkali Activated Materials, 2014. http://link.springer.com/10.1007/978-94-007-7672-2.

[3] T.A. Aiken, W. Sha, J. Kwasny, M.N. Soutsos, Cement and Concrete Research Resistance of geopolymer and Portland cement-based systems to silage ef fl uent attack, Cem. Concr. Res. 92 (2017) 56–65. https://doi.org/10.1016/j.cemconres.2016.11.015.

[4] J.L. Provis, J.S.J. Van Deventer, Alkali activated materials: state-of-the-art report, RILEM TC 224-AAM, Springer Science & Business Media, 2013.

[5] P. Krivenko, Why alkaline activation - 60 years of the theory and practice of alkali-activated materials, J. Ceram. Sci. Technol. 8 (2017) 323–333. https://doi.org/10.4416/JCST2017-00042.

[6] M.F. Alnahhal, T. Kim, A. Hajimohammadi, Distinctive rheological and temporal viscoelastic

behaviour of alkali-activated fly ash/slag pastes: A comparative study with cement paste, Cem. Concr. Res. 144 (2021) 106441. https://doi.org/10.1016/j.cemconres.2021.106441.

[7] A. Favier, J. Hot, G. Habert, N. Roussel, J.B. D'Espinose De Lacaillerie, Flow properties of MK-based geopolymer pastes. A comparative study with standard Portland cement pastes, Soft Matter. 10 (2014) 1134–1141. https://doi.org/10.1039/c3sm51889b.

[8] E.P. Koehler, D.W. Fowler, Development of a portable rheometer for fresh portland cement concrete, 2004.

[9] D. Feys, R. Verhoeven, G. De Schutter, Fresh self-compacting concrete, a shear thickening material, Cem. Concr. Res. 38 (2008) 920–929. https://doi.org/10.1016/j.cemconres.2008.02.008.

[10] G. Heirman, L. Vandewalle, D. Van Gemert, Ó. Wallevik, Integration approach of the Couette inverse problem of powder type self-compacting concrete in a wide-gap concentric cylinder rheometer, J. Nonnewton. Fluid Mech. 150 (2008) 93–103. https://doi.org/10.1016/j.jnnfm.2007.10.003.

[11] L. Struble, G.-K. Sun, Viscosity of Portland cement paste as a function of concentration, Adv. Cem. Based Mater. 2 (1995) 62–69.

[12] D. Feys, R. Verhoeven, G. De Schutter, Why is fresh self-compacting concrete shear thickening?, Cem. Concr. Res. 39 (2009) 510–523. https://doi.org/10.1016/j.cemconres.2009.03.004.

[13] J.R. Melrose, R.C. Ball, "Contact networks" in continuously shear thickening colloids, J. Rheol. (N. Y. N. Y). 48 (2004) 961–978.

[14] J.R. Melrose, R.C. Ball, Continuous shear thickening transitions in model concentrated colloids—The role of interparticle forces, J. Rheol. (N. Y. N. Y). 48 (2004) 937–960.

[15] R.G. Egres, N.J. Wagner, The rheology and microstructure of acicular precipitated calcium carbonate colloidal suspensions through the shear thickening transition, J. Rheol. (N. Y. N. Y). 49 (2005) 719–746.

Behavior of alkali-activated slag mortar incorporated with other supplementary cementitious materials

S. Tavasoli[1], A. W. Sadeed[1] and W. Breit[1]

[1] Institute of construction material technology, University of Kaiserslautern, Kaiserslautern, Germany. (E-mail: syamak.tavasoli@bauing.uni-kl.de)

HIGHLIGHTS

- Substitution of GGBS by calcined clay results in higher early age strength of alkali-activated GGBS mortar.
- Replacement of GGBS with CAC elongate the setting times of alkali-activated GGBS mortar.

Keywords: alkali-activated mortar, GGBS, metakaolin, calcined clay, fly ash, CAC

INTRODUCTION

Alkali-activated concrete (AAC) is considered as an alternative for ordinary Portland cement (OPC) concrete, due to its lower carbon footprint and energy consumption. Moreover, similar or higher performance of AAC is persuading researchers and engineers to bring it into practice. In this type of concrete ground granulated blast furnace slag (GGBS) for having higher potential of reactivity is the most used precursor among all common precursors [1,2]. However, due to the limited resources of GGBS, as well as not superior performance of AAC with GGBS in terms of carbonation, incorporating other supplementary cementitious materials, as well as binders can improve its behavior and reduce the costs. Due to the higher costs of AAC than OPC concrete in normal strength classes, using AAC in medium and higher strength concrete classes can be more beneficial [4]. For this purpose, using cheaper materials as activators or precursors are highly attended [4].

Substitution of GGBS with fly ash in alkali-activated fly ash/GGBS mortar, activated by sodium based activators, results in reduction of tensile strength, compressive strength and increase of setting times [4]. Calcined clay is considered as source of aluminosilicate and due to the lower cost of production, as well as CO2 production and vast availability globally is considered as a suitable alternative binder [2]. Alkali-activated metakaloin has longer setting times than pure alkali-activated GGBS paste and by increasing the replacement percentage of GGBS with metakaolin it will be shortened significantly [3]. Increasing the substitution parentage of metakaolin with GGBS will also reduce the compressive strength [3]. Calcium alumina cement (CAC) as the most important non-portlandit cement, despite its higher price than Portland cement is being used to improve the resistance of concrete mixture to chemical attack [5]. It also can be resulted in rapid hardening and increasing the 28 days compressive strength of concrete [6].

MATERIALS AND TESTING PROCEDURES

In this study, a primary alkali-activated mortar mix consisting of GGBS as precursor and ternary activator compound including NaOH solution (16M), Na2O.nSiO2 (n=1.7) und K2O.nSiO2 (n=2.1) with water to binder ratio of 0.5, was considered as a reference mixture. Mortar specimens were produced in prismatic molds and cured for 28 days in cling film in (20±2)°C according to EN 196-1. In other mixtures fly ash (F), calcined clay (CC), metakaolin (M) and CAC were substituted by 20% of GGBS presented in Table 1. Compressive strength, as well as tensile bending stress of prisms were tested after 1, 2, 3, 7 and 28 days according to EN 196-1. Corresponding pastes of mixtures in Table 1 were

also produced according to EN 196-3 for testing the setting times of the above mixtures. Moreover, consistency of fresh mortar (flow table) according to EN 1015-3 for mortar workability evaluation was carried out.

Table 1. Mortar mixture proportions.

Mixture	Sand (g)	Water (ml)	GGBS (g)	Metakaolin (g)	Fly ash (g)	CAC (g)	CC (g)	NaOH (g)	$Na_2O.nSiO_2$ (g)	$K_2O.nSiO_2$ (g)
100GGBS	1350	181.1	450					30.3	20	30
80GGBS 20F	1350	181.1	360	90				30.3	20	30
80GGBS 20M	1350	181.1	360		90			30.3	20	30
80GGB 20CAC	1350	181.1	360			90		30.3	20	30
80GGBS 20CC	1350	181.1	360				90	30.3	20	30

RESULT & DISCUSSION

Figure 1 shows the settings of the alkali-activated pastes produced according to Table 1. Replacement of fly ash, metakaolin and calcined clay with 20% GGBS resulted in reduction of both initial and final setting times. Nonetheless, substitution of CAC by 20% GGBS in 80GGBS20CAC led to increase of initial setting time about 54 minutes and the final setting time for 81 minutes.

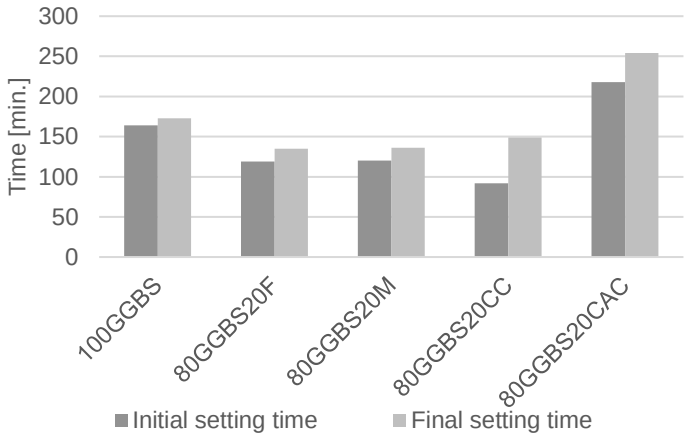

Figure 6. Initial and final setting times of mortar pasts.

Flow table test results of mixtures during the first 45 minutes after production are demonstrated in Figure 2. 80GGBS20F showed the highest flow range during the test period, incorporation of fly ash due its later reaction. On the other hand, 80GGBS20M indicated lower workability than 100GGBS during the testing procedure. The lowest workability among all mixtures were observed in 80GGBS20CC, which can be due to the higher reactivity potential of calcined clay, because of higher aluminum oxide content. Although 80GGBS20CAC had 3 cm lower flow than 100GGBS after 5 minutes, it demonstrated lower reduction in flow drop than 100GGBS, whereas after 45 minutes both demonstrated similar flow of 13 cm.

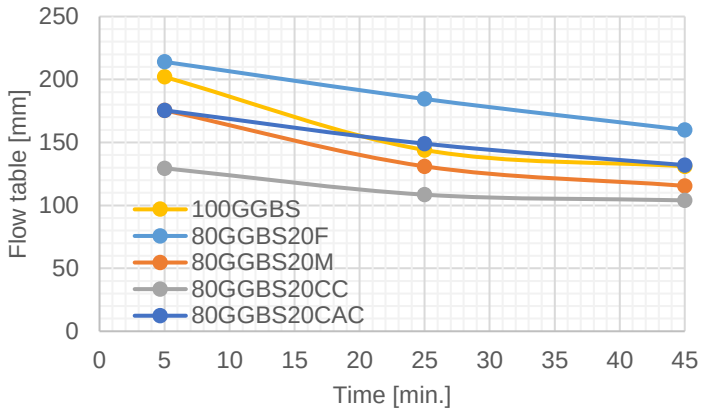

Figure 7. Flow table test results of mortar mixtures.

Tensile strength results of mixtures in Figure 3 show that except 80GGBS20CAC which had 2.8 MPa tensile strength after 3 days, other four mixtures showed considerably higher tensile strength over 4.8 MPa after 3 days. 80GGBS20CC which was consisted of GGBS combined with calcined clay experienced slight reduction of tensile strength after 3 days, while it obtained the highest tensile strength among others at this age. Despite 80GGBS20CAC experienced the lowest tensile strength at early ages, obtained almost 6.8 MPa after 7 days that was similar to the 100GGBS reached 7.8 MPa after 28 days as the highest strength among all five mixtures.

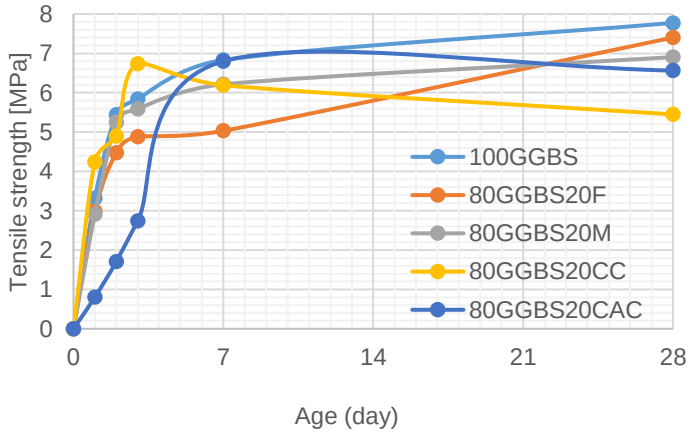

Figure 8 .Tensile strength of mortar mixtures.

Compressive strength results of the mortar mixtures are illustrated in Figure 4. All mixes except 80GGBS20CAC showed proper compressive strength of above 12 MPa after one day, and specifically 80GGBS20CAC experienced highest strength of 18 MPa. Compressive strength of 80GGBS20CAC could not reach this value even after 3 days, However, its trend of catching compressive strength accelerated after two days, whereas it reached 34 MPa after 7 days achieving the highest compressive strength at this age and later among all mixes. The compressive strength of 80GGBS20CAC reached 54 MPa after 28 days which was 10 MPa higher than 100GGBS. This behavior is due to the higher content of Al2O3 in CAC, that results in decreasing reaction rate of AAC with GGBS in early ages [7]. Lower compressive strength of 80GGBS20F due to the replacement of fly ash needs ambient pH ≥ 13 or curing over 100°C to compensate the loss of strength [8]. The blended GGBS with metakaolin mixture resulted in lowering the compressive strength. This behavior could be as result of new porous structure generation regarding the thermal processing of metakaolin [9].

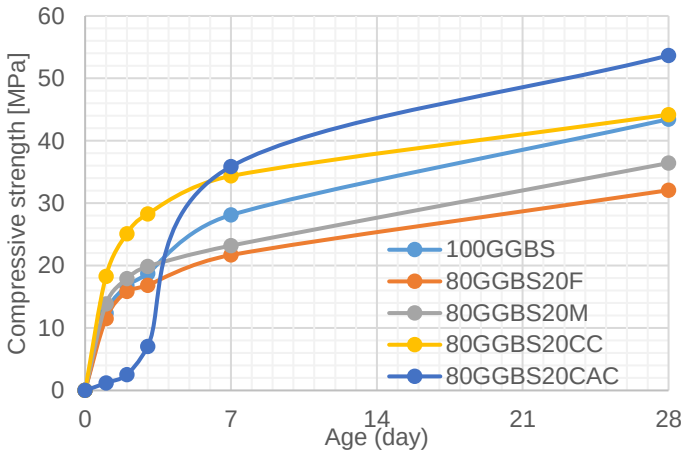

Figure 9 Compressive strength of mortar mixtures

CONCLUSION

Evaluation of experimental results obtained in this study shows that partly substitution of CAC with GGBS in alkali-activated GGBS concrete, not only increases compressive as well as tensile strength in later ages, provide more stable workability and longer setting times in order to be used in ready mix concrete. For the further study, partly substitution of CAC and calcined clay with GGBS can provide a better performance in terms of workability and early age strength of mortar.

ACKNOWLEDGEMENT

The authors acknowledged the partly financial support of INTERREG in the framework of URBCON project cooperated with the University of Kaiserslautern.

REFERENCES

[1] Passuello A., Rodríguez E. D., Hirt E., Longhi M., Bernal S. A., Provis J. L. et al. Evaluation of the potential improvement in the environmental footprint of geopolymers using waste-derived activators. Journal of Cleaner Production, 2017; 166:680–9. https://doi.org/10.1016/j.jclepro.2017.08.007.

[2] Bature A. S., Khorami M., Ganjian E., Tyrer M. Influence of alkali solution on compressive strength of calcined clay and GGBS alkali activated mortar. Proceeding of 38th Cement and Concrete Science Conference, 2018 (16).

[3] Cyr M., Samson G., Gao X. X. Thermomechanical performance of blended metakaolin-GGBS alkali-activated foam concrete. Construction and building materials, 2017; 157:982-993.

[4] Vinai R., Rafeet A., Soutsos M., Sha W. Guidelines for mix proportioning of fly ash/GGBS based alkali-activated concretes. Construction and building materials, 2017; 147:130-142.

[5] Newman J., Choo B. S.. Advanced Concrete Technology: Constituents properties. Butterworth-Heinemann, 2003.

[6] Cao Y.F., Tao Z., Pan Z., Murphy T., Wuhrer R. Effect of calcium aluminate cement on workability and compressive strength of fly ash geopolymer mortar cured at ambient temperature. Mechanics of Structures and Materials: Advancement and Challenges. Taylor & Francis Group, London, 2017.

[7] Ben Haha M., Lothenbach B., Le Saout G., Winnefeld F. Influence of slag chemistry on the hydration of alkali-activated blast-furnace slag - Part II: Effect of Al2O3.Cement and concrete research, 2012; 42:74-83.

[8] Humad A. M., Kothari A., Provis. J. L., Cwirzen A. The effect of blast furnace slag/fly ash ratio on setting, Strength and shrinkage of alkali-activated pastes and concretes. Frontiers in materials,

2019.

[9] Rashad A. M. Alkali-activated metakaoli: A short guide for civil engineer - An overview. Construction and building materials, 2013; 41:751-765.

Calcined-clay minerals as precursors for geopolymers and the influence of solubility on mixing ratios

N. Werling[1], F. Dathe[1], F. Dehn[1] and K. Emmerich[1]

[1] Institute for Concrete Structures and Building Materials (IMB/MPA/CMM), Karlsruhe Institute of Technology (KIT), Karlsruhe, GERMANY.
(E-mail: nadja.werling@kit.edu, felix.dathe@kit.edu, frank.dehn@kit.edu, katja.emmerich@kit.edu)

HIGHLIGHTS

- Calcined clay minerals for geopolymer production
- Solubility in NaOH metakaolinite > metasmectite > metaillite
- Micromechanical properties of geopolymers produced with different calcined clay minerals

Keywords: geopolymers, calcined clay minerals, thermal and alkaline activation

INTRODUCTION

Geopolymers produced with calcined clay minerals are a potential construction material of the future. The CO2 emissions of the construction industry could be reduced significantly (40 – 80% reduction of emitted CO2; McLellan et al., 2011; Davidovits, 2013). Geopolymers are inorganic binders with a 3-dimensional network of Si[OH]4 and Al[OH]4- oligomers. They are formed by the reaction of aluminosilicates with a highly alkaline activator solution. Calcined clay minerals are suitable as precursors since they contain large amounts of silicon (Si) and aluminum (Al). NaOH or KOH can be used as activator solutions. Natural clays, like so called common clays, could reduce the costs of geopolymer production. Common clays are very heterogeneous concerning the phase composition, structure and particle morphology of the clay minerals. Nevertheless, they are suitable as geopolymer precursors due to their chemical and mineralogical composition. So far, mainly metakaolinite was studied as a precursor. But, metakaolinite would lead to higher costs compared to cement. The aim of this project was to study the relationship between material properties and process parameters which influence the geopolymer properties. The thermal and alkaline activation of different clay minerals and the resulting properties of geopolymer mortars and concretes is not yet fully understood. Therefore, a combination of investigations on model clay minerals and mortars/concretes prepared with calcined common clay precursors was targeted. The following focuses on the experiments conducted with the model clay minerals. Raw materials containing dioctahedral clay minerals, with Si:Al ratios between 1:1 and 2:1 were used as precursors exclusively. For this project three different clay minerals (a kaolinite, a smectite, an illite) were investigated. The discoveries of the analysis of the three clay minerals, concerning the solubility of calcined clay minerals and micromechanical properties of the geopolymers, were used for a prediction of the behavior of mixtures of clay minerals, like in natural common clays.

MATERIALS & METHODS

The clays KBE-1 (kaolin), Ceratosil (bentonite), and Arginotec INX (illitic clay) were used to investigate the three different clay minerals. Each of the clays contained one main clay mineral, namely a kaolinite, a cis-cis-vacant dioctahedral smectite, and a trans-vacant dioctahedral illite (a detailed characterization of the materials can be found in Werling et al., 2022). As ancillary phases mainly quartz, silica polymorphs, and feldspars could be detected. As alkaline activator solutions NaOH was

used with concentrations in the range of 0.01 mol/L to 10.79 mol/L. The use of commercial waterglass (sodium silicate solutions) was avoided, since it would impair the environmental benefit of geopolymers. Therefore, an industrially produced crystalline aluminum hydroxide powder (Hydrafil®, HPF – The Minerals Engineers, Frechen, Germany) and an amorphous SiO2 powder (Amosil®, HPF – The Minerals Engineers, Frechen, Germany) were used for adjusting the Si:Al ratio in geopolymers. For all solubility experiments a solid/liquid (calcined clay mineral/activator) ratio of 0.02 was set. The solid/liquid ratio for geopolymer production was in the range of 0.8 – 1.44. Simultaneous thermal analysis, X-ray diffraction, inductively coupled plasma optical emission spectroscopy, mercury intrusion porosimetry and nanoindentation were used (Werling et al., 2022).

RESULT & DISCUSSION

The dissolution behavior of the calcined clay minerals in highly alkaline solutions (pH > 14) forms the basis for the polymerization of the binder.

It was shown that the solution of silicon (Si) and aluminum (Al) occurred congruently for the kaolinite for different concentrations of NaOH (Fig. 1; Werling et al., 2020). In addition, it was shown that the solubility of kaolinite increased with the concentration of the activator solution (Fig. 1). The uncalcined material showed hardly any solubility (< 5%) regardless of the reaction time and concentration of the activator solution. It was determined that 700 °C was the optimum calcination temperature for the kaolinite studied. At this calcination temperature, a solubility of 77% after 24 h and 88% after 7 d could be achieved after thermal activation. Complete dissolution of kaolinite could not be achieved, irrespective of the reaction time.

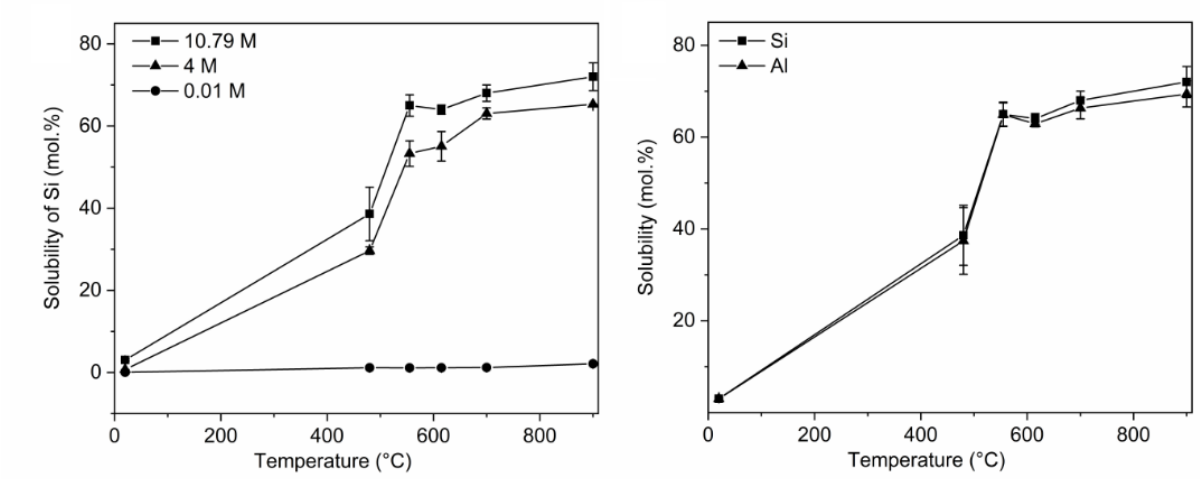

Figure 1. Solubility of Si (equal for Al) of metakaolinite in NaOH (10.79 mol/L, 4 mol/L, 0.01 mol/L) as a function of calcination temperature (reaction time 24 h) (left; from Werling et al., 2020). Solubility of Si and Al of metakaolinite (reaction time 24 h, NaOH 10.79 mol/L) (right; from Werling et al., 2022).

As before, it was shown that the solubility of the dioctahedral smectite and illite increased with the concentration of the activator solution (Fig. 2). For the selected smectite, the uncalcined material showed the lowest solubility. However, in contrast to the kaolinite, a significant decrease in solubility was visible at too high calcination temperature (900 °C; Fig. 2). The decrease in solubility at too high calcination temperatures is an expected phenomenon due to recrystallization of high temperature phases (Khalifa et al., 2020). However, the temperature at which recrystallization begins is individual to each clay mineral and cannot be confidently deduced from the study of a model clay mineral for the different groups. Maximum solubility for the smectite studied was achieved at a calcination temperature of 750 °C (63.5% Si after 24 h, 84.1% Si after 7 d). The solubility of this material was incongruent for Si and Al. The maximum solubility for Al was 67.9% after 7 d, which was lower than for Si.

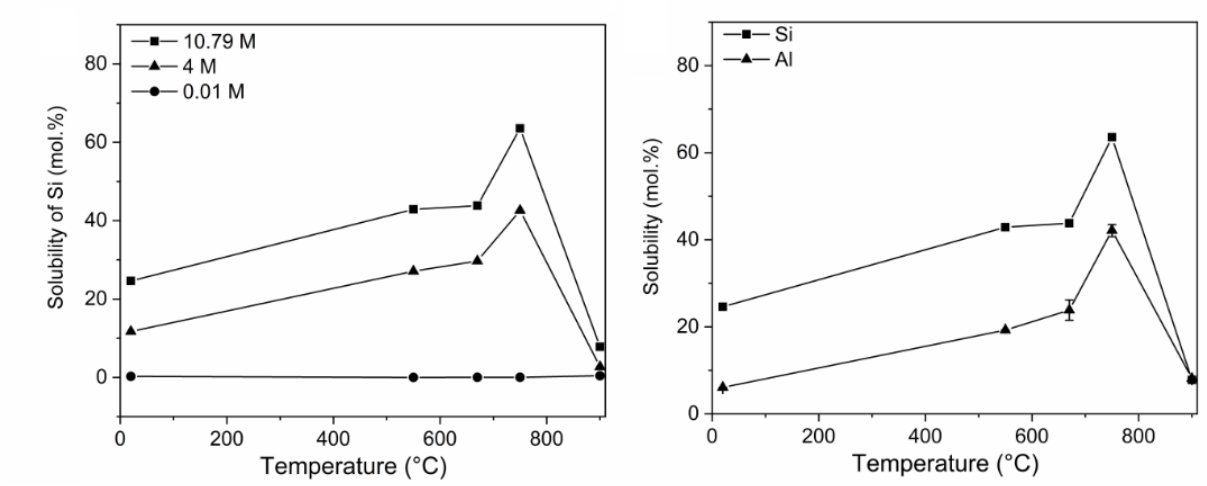

Figure 2. Solubility of Si (equal for Al) of metasmectite in NaOH (10.79 mol/L, 4 mol/L, 0.01 mol/L) as a function of calcination temperature (reaction time 24 h; left). Solubility of Si and Al of metasmectite (reaction time 24 h, NaOH 10.79 mol/L; right) (from Werling et al., 2022).

For the illite, the lowest solubility was found for the uncalcined material and the material calcined at 900 °C (Fig. 3). As for the smectite, the maximum solubility was obtained at a calcination temperature of 750 °C (44% after 24 h, 62% after 7 days). However, in contrast to the calcined smectite, the solution of Si and Al occurred congruently in the illite. By comparing the materials, it was shown that the solubility of clay minerals decreases in the order metakaolinite > metasmectite > metaillite. The optimum activation temperature of the smectite as well as the illite was 750 °C despite strongly different dehydroxylation temperatures (Werling et al., 2022) of the cis-vacant smectite and the trans-vacant illite.

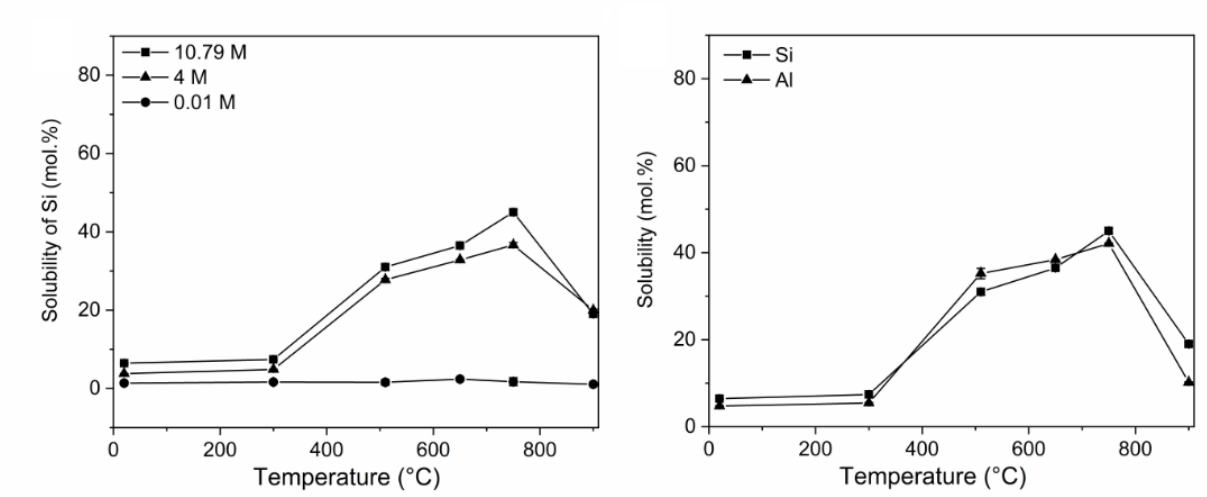

Figure 3. Solubility of Si (equal for Al) of metaillite in NaOH (10.79 mol/L, 4 mol/L, 0.01 mol/L) as a function of calcination temperature (reaction time 24 h; left). Solubility of Si and Al of metasmectite (reaction time 24 h, NaOH 10.79 mol/L; right) (from Werling et al., 2022).

In order to investigate the mechanical properties of geopolymers, produced from the calcined clay minerals of the preliminary solubility investigations, nanoindentation measurements were carried out. This method allows determination of the hardness and Young's modulus of the geopolymers even on small test specimens. This is particularly important to study the contribution of different meta clay minerals in calcined common clays. For geopolymer preparation, stoichiometric blends were calculated with varying Si:Al ratios and a fixed Na:Al ratio of 1:1. The natural Si:Al ratio of 1:1 of kaolinite (from KBE-1) was increased by the addition of amorphous SiO2 in some of the blends to

investigate the impact of the Si:Al ratio on the hardness of the geopolymer. The natural Si:Al ratio of 2:1 of smectite (from Ceratosil WG) and illite (from Arginotec INX) was either decreased to 1:1 by addition of Al(OH)3 powder or increased to 3:1 by amorphous SiO2. When preliminary tests were carried out, some of the calculated mixtures turned out to be unprocessable. The most common reason for failed processing was the high viscosity of the mixture, making homogeneous mixing impossible. The geopolymers that had been shown to be processable during the preliminary tests (solid/liquid ratio 0.8 – 1.44) were subsequently prepared for nanoindentation. Hardness was investigated on geopolymer discs (⌀ 2.5 cm; height ≈ 5 mm) prepared from the three different calcined clay minerals. Since a very smooth surface is required for nanoindentation, the geopolymers were ground and polished after complete hardening. In addition to the investigations of the mechanical properties, the porosity of the geopolymers (crushed fragments, 2 – 4 mm) was determined by mercury intrusion porosimetry. It could be shown for both hardness (10 MPa – 1.1 GPa) and porosity (20.3 – 31.6%) that the values of the produced geopolymers were in the same order of magnitude as for cement paste. Moreover, it was shown that not only geopolymers prepared with metakaolinite showed hardness and porosity in this order of magnitude, but also the geopolymers prepared with metasmectite and metaillite. Therefore, it is assumed that not only geopolymers can be produced from the different metaclay minerals, but also from mixtures of these clay minerals. However, in the future the manufacturing process has to be improved further, especially the processability is a crucial factor with regard to the application of geopolymers produced from calcined clay minerals.

The binders produced in this work may find application in the field of building materials science in the future. The reduced energy requirement for calcining the clays and extremely low CO2 emissions from the clays during calcination can contribute to the targeted CO2 neutrality of the cement industry by 2050 (GCCA, 2022). In addition, the high acid resistance and thermal stability of geopolymers is an enormous advantage over conventional cementitious systems. However, the use of geopolymers requires certification and standardization of the investigated materials as building materials.

CONCLUSION

Geopolymers can be produced from the different metaclay minerals, and also from mixtures of clay minerals. The production was possible with each calcined clay mineral tested. For geopolymer production it has to be taken into account that the Si:Al ratio of the evolving geopolymer will differ from the stoichiometric ratio of the precursors, due to incomplete and/or incongruent dissolution of the calcined clay minerals.

It is not possible to make general statements regarding activation and processing that are universally valid for every clay mineral (Khalifa et al., 2020). Activation procedures specifically tailored to individual clay minerals must be identified to achieve the desired geopolymer properties. The activation procedure for mixtures of clay minerals needs to be adapted based on what is known about individual clay minerals. Calcined clays have great potential as a starting material for CO2-neutral building materials. However, there are still a number of difficulties to be solved if this technology is to be deployed and used in the future. In particular, the development of admixtures for these systems is an important focus. For the practical use of geopolymers, a way must be found to control the setting time and flowability without having to accept qualitative losses in material quality. Research should focus primarily on durability and possible damage processes as well as the development of admixtures. The influences of the variability of the clay minerals in their groups as well as the by-product proportions in the clay deposits should also be further investigated.

ACKNOWLEDGEMENT

This project was funded by Deutsche Forschungsgemeinschaft (DFG) under EM79/8-1.

REFERENCES

Davidovits, J. (2013). Geopolymer cement. A review. *Geopolymer Institute, Technical papers*, 21, 1-11.

GCCA – Global Cement and Concrete Association (2022). GCCA Concrete Future – Roadmap to Net Zero. https://gccassociation.org/concretefuture/wp-content/uploads/2021/10/GCCA-Concrete-Future-Roadmap-Document-AW.pdf

Khalifa, A. Z., Cizer, Ö., Pontikes, Y., Heath, A., Patureau, P., Bernal, S. A., & Marsh, A. T. (2020). Advances in alkali-activation of clay minerals. *Cement and Concrete Research,* 132, 106050.

McLellan, B. C., Williams, R. P., Lay, J., van Riessen, A., and Corder, G. D. (2011). Costs and carbon emissions for geopolymer pastes in comparison to ordinary portland cement*. Journal of Cleaner Production*, 19(9), 1080-1090.

Werling, N., Dehn, F., Krause, F., Steudel, A., Schuhmann, R., & Emmerich, K. (2020). Solubility of precursors and carbonation of waterglass-free geopolymers. *Clays and Clay Minerals*, 68, 524-531.

Werling, N., Kaltenbach, J., Weidler, P.G., Schuhmann, R., Dehn, F., and Emmerich, K. (2022). Solubility of Calcined Kaolinite, Smectite, and Illite in High Molar NaOH and Suitability as Precursors for Geopolymers. *Clays Clay Minerals,* 70, 270–289.

Chloride transport in alkali-activated slag paste under the exposure of wetting and drying cycles

Zhiyuan Xu[1] and Guang Ye[2]

[1, 2] Department of Materials and Environment (Microlab), Faculty of Civil Engineering and Geoscience, Delft University of Technology, Delft, the Netherlands.
(E-mail: z.xu-6@tudelft.nl, G.Ye@tudelft.nl)

HIGHLIGHTS

- Chloride ion transport in alkali-activated slag paste is modeled under the exposure condition of wetting and drying cycles
- The microstructure degradation is considered using thermodynamic modelling
- The influence of microstructure degradation on chloride ingress is displayed

Keywords: chloride transport, wetting and drying cycles, structure degradation

INTRODUCTION

Chloride ions are considered one of the main agents that result in the degradation of steel-reinforced concrete. The penetrated chloride ions will destroy the protective passivity layer formed on the surface of embedded steel when a threshold chloride concentration is reached at the steel bar. Subsequently, the corrosion of steel rebar initiates [1]. The process of rebar corrosion is particularly accelerated in environments with wetting and drying cycles [2]. This is because, on the one hand, chloride ion transport is facilitated due to the convection in wetting and drying cycles. On the other hand, the concrete structure degrades in wetting and drying cycles. This paper developed a numerical model to simulate chloride transport in wetting and drying cycles with the influence of structure degradation for alkali-activated slag (AAS) paste.

METHODOLOGY

The chloride transport in drying-wetting cycles is a complex process. It involves liquid water transport, water vapor transport, liquid-vapor phase transition, chloride transport by diffusion and convection and structure degradation. The mechanisms and governing equation for these processes are presented.

Liquid water transport

The liquid water transport in unsaturated cementitious materials is a two-phase flow. Such two-phase flow can be described by Richard equation. With proper substitution and arrangement for Richard equation, the governing equation of liquid water transport is given as

$$\frac{\partial(\phi s)}{\partial t} = \nabla \cdot \left(D_l(s) \nabla s \right)$$
$$D_l(s) = -\frac{K}{\mu} k_r(s) \frac{dp(s)}{ds} \quad (1)$$

where s represents the saturation degree and $D_l(s)$ is liquid water diffusion coefficient. $k_r(s)$ and $p(s)$ are relative permeability and capillary pressure respectively, which can be obtained by Van

Genuchten (VG) model [3],

$$p(s) = a \cdot \left(s^{-\frac{1}{m}} - 1 \right)^{(1-m)}$$
$$k(s) = s^{0.5} \cdot \left(1 - \left(1 - s^{1/m} \right)^{m} \right)^{2} \quad (2)$$

In Eq. (2), a and m are fitting parameters dependent on the microstructure.

Water vapor transport

In cementitious materials, the moisture transfer is induced by water vapor pressure. The governing equation for the moisture can be expressed by

$$\frac{\partial \left(\phi_g \cdot w_v \right)}{\partial t} = \nabla \cdot \left(F(s) \cdot D_v \cdot \nabla w_v \right) \quad (3)$$

where ϕ_g is the volume fraction of gas-filled pores, w_v (kg/m^3) is the mass of water in the unit volume of gas. *F(s)* is the resistance factor and can be calculated by an empirical equation: $F\left(s\right) = \phi^{4/3} \cdot (1-s)^{10/3}$ where ϕ is the porosity. D_v is the water vapor diffusion coefficient (m^2/s). According to Eq.(3), the vapor flux is then written as $J_v = -F\left(s\right) \cdot D_{v-g} \nabla w_v$.

Liquid-vapor phase transition

The water liquid transport and water vapor transport in the cementitious materials are not independent. The phase transition between them always exists when liquid and vapor are not in equilibrium. The equilibrium state equation, which can be obtained by Kelvin equation and Young-Laplace equation, is derived as

$$RH = \exp\left(\frac{V_m}{RT} \cdot p(s) \right) \quad (4)$$

According to mass conservation, the changes of water liquid and water vapor follow

$$\Delta s \cdot \phi \cdot \rho_w = -\Delta w_v \cdot \phi \cdot (1-s) \quad (5)$$

where Δs and Δw are mass changes of water liquid and water vapor. The phase transition continues until the equilibrium state equation is met by updated saturation degree and humidity.

Chloride transport

Chloride transport subjected to drying-wetting cycle is controlled by both chloride diffusion in the pore solution and chloride convection due to liquid water transport. The chloride flux by diffusion J_{Cl}^{d} can be expressed by

$$J_{Cl}^{d} = -D_{Cl}^{a} D_{Cl}^{r}(s) \theta \nabla C \quad (6)$$

where D_{Cl}^{a} is apparent chloride diffusion coefficient, $D_{Cl}^{r}(s)$ relative chloride diffusion coefficient at saturation degree of s, C is chloride concentration. The chloride convection results from the liquid water transport and can be expressed by

$$J_{Cl}^{c} = -C \cdot D_l\left(s\right) \nabla s \quad (7)$$

According to the mass conservation of chloride ions, the chloride transport in drying-wetting cycles is presented as

$$\frac{\partial(\theta C)}{\partial t} = \nabla\left(C \cdot D_l(s)\nabla s + D_{Cl}^{a} D_{Cl}^{r}(s)\theta\nabla C\right) \quad (8)$$

Thermodynamic modelling

As the chloride ions enter the structure and other ions such as Ca^{2+}, Na^{+} and OH^{-} leave the structure in the wetting and drying cycles, the concrete structure is no longer in thermodynamic equilibrium. Therefore, chemical degradation reactions e.g., decalcification and dissolution of cement components take place. This process induces a gradual change in pore structure as the movement of solutes in the concrete structure. Such process is modelled based on thermodynamic equilibrium. A thermodynamic data set for AAS [4] together with GEM-Selektor v.3 software [5] is used to calculate the updated reaction products and pore solution in equilibrium.

RESULT & DISCUSSION

The chloride ion transport is simulated for N6M1W0.4 paste, where N represents weight percentage of Na2O respect to slag, M is the silica module and W is the w/b ratio. The wetting and drying period are both 12 hours. Figure 1 shows the volume ratio change ((a) and (b)) and porosity change (c) during the wetting and drying cycles. It is clear that the content of reaction products like CNASH and MA-OH-LDH is reduced. The degradation depth for the sample is increased from 8 mm to 13 mm for wetting and drying cycles from 90 days to 365 days. Figure 2 displays the chloride distribution inside the AAS paste sample with and without the consideration of structure degradation. It shows that the structure degradation obviously benefits the chloride ingress.

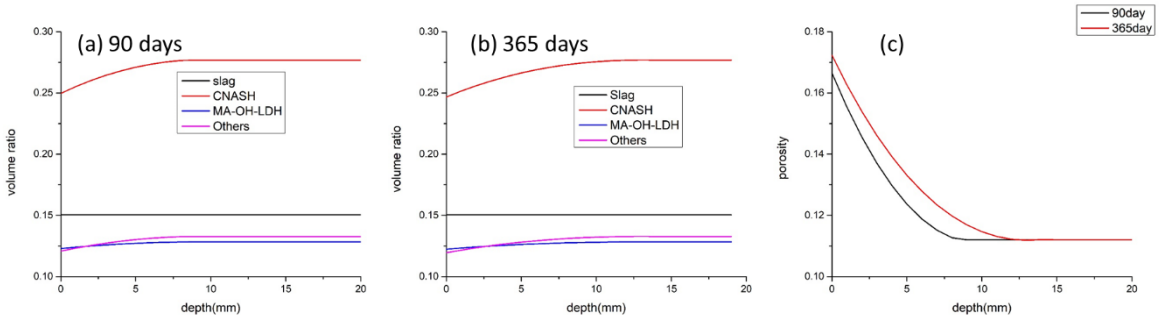

Figure 1. Simulated results for Structure degradation.

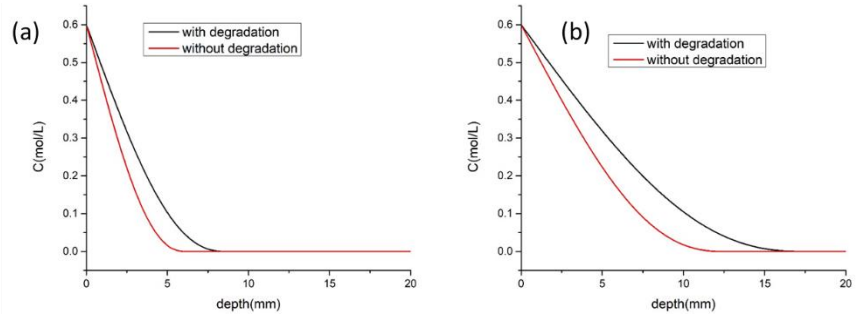

Figure 2. Chloride distribution after 90 days (a) and 365 days (b).

CONCLUSION

A model for chloride transport in wetting and drying cycles with structure degradation is developed in this paper. The model successfully modeled the increase of porosity due to structure degradation. The influence of structure degradation for chloride transport can be quantitively evaluated by the simulation results.

ACKNOWLEDGEMENT

This project has received funding from the European Union's Horizon 2020 research and innovation

programme under grant agreement No 813596 DuRSAAM. The opinions expressed in this document reflect only the author's view and reflect in no way the European Commission's opinions. The European Commission is not responsible for any use that may be made of the information it contains.

REFERENCES

[1] A. Neville, Chloride Attack of Reinforced-Concrete - an Overview, Mater Struct 28(176) (1995) 63-70.

[2] M. Medeiros, A. Gobbi, G. Réus, P. Helene, Reinforced concrete in marine environment: Effect of wetting and drying cycles, height and positioning in relation to the sea shore, Constr Build Mater 44 (2013) 452-457.

[3] M.T. van Genuchten, A Closed-form Equation for Predicting the Hydraulic Conductivity of Unsaturated Soils, Soil Science Society of America Journal 44(5) (1980) 892-898.

[4] R.J. Myers, S.A. Bernal, J.L. Provis, A thermodynamic model for C-(N-)A-S-H gel: CNASH_ss. Derivation and validation, Cement Concrete Res 66 (2014) 27-47.

[5] D.A. Kulik, T. Wagner, S.V. Dmytrieva, G. Kosakowski, F.F. Hingerl, K.V. Chudnenko, U.R. Berner, GEM-Selektor geochemical modeling package: revised algorithm and GEMS3K numerical kernel for coupled simulation codes, Computational Geosciences 17(1) (2013) 1-24.

Novel findings of pore shapes for hardened 3D printed concrete with silica fume by X-CT scanning

Yanjuan Chen[1], Hubert Rahier[2]

[1, 2] Physical Chemistry and Polymer Science, Vrije Universiteit Brussel, Brussel, Belgium.
(E-mail: yanjuan.chen@vub.be, Hubert.Rahier@vub.be)

HIGHLIGHTS

- The statistics analysis shows that the distribution curves of pore shapes follow similar trends, regardless of the printed concrete or casted concrete.
- The bigger voids with an equivalent diameter of more than 80 µm for casted concrete are more "equant" compared to printed concrete

Keywords: 3D printed concrete, pore shapes, aspect ratio

INTRODUCTION

Several studies have been carried out on the pore structure of 3D printed concrete. These studies suggest that the pores in 3DPC tend to be more irregular/elliptical due to the printing in layers compared to casting for conventional concrete. However, most of these conclusions are obtained by only visual inspection from several 2D images from X-CT [1,2]. Apparently, the visual inspection method has some limitations. Moreover, the visual inspection from 2D images obtained from X-CT is more subjective depending on individuals. Since many issues resulting from the pore structure of 3DPC are still open and need to be investigated sufficiently, it requires to describe the pore shape on a quantitative level.

This study aims to characterize the pore shape quantitatively with information obtained from X-CT. Statistical analysis was performed on pore shape parameters i.e., aspect ratio and relationship between elongation, flatness, and volume (bubble size) of particular voids in relation to the pore shapes.

In this research, a custom-designed printable mixture was adopted, containing Portland cement (CEM I 52.5 R) blended with silica fume, granite aggregates (particle size ≤ 2 mm), limestone filler, calcium formate as setting time modifier, PCE dispersants as rheology control additives, and a small amount (1.6 g/L(binder)) of PVA fibers. The water to binder ratio was 0.22 by volume, or 0.36 by weight. The concrete printer consists of a degree of freedom (DOF) gantry robot and a M-Tec Duomix 2000 mixer-pump with a linear displacement pump, that feeds concrete through a 25 mm diameter nozzle connected to a 10 m length hose. After printing, the slab was covered with a plastic sheet for 24 hours. At the same time, one casted concrete specimen with the same recipe was prepared as the reference. At an age of 50 days, three cores of 40 mm diameter and 100 mm height were drilled from the three different orientations of 3D printed concrete, while the same size core was drilled from casted concrete specimen as a reference. Typical samples are shown in Figure 1. Subsequently, these cores were scanned using the 240 kV microfocus tube with 0.5 mm of copper as a beam filter. Three-dimensional rendering of the internal structure is shown in Figure 2.

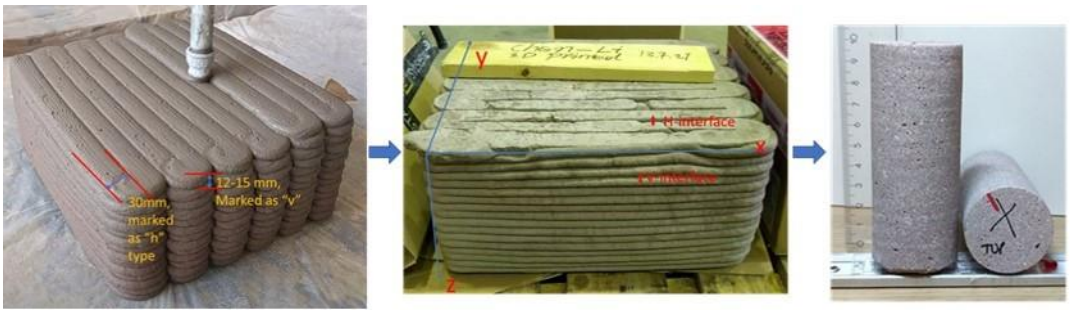

Figure 1. 3D printing and cores drilled (The X, Y and Z directions are indicated).

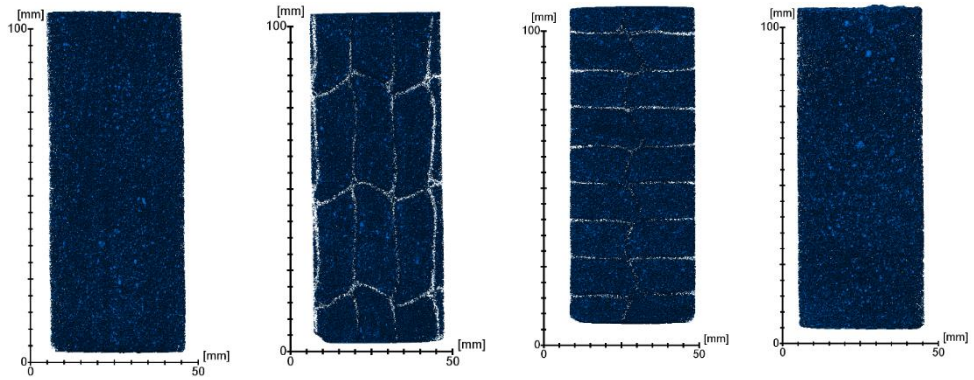

3DPC-X 3DPC-Y 3DPC-Z Casted

Figure 2. Three-dimensional rendering of internal structure from the X-CT data for samples.

RESULT & DISCUSSION

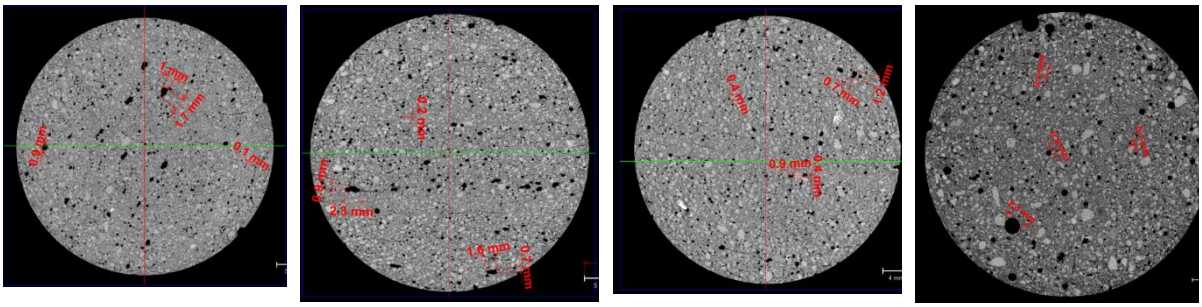

3DPC-X 3DPC-Y 3DPC-Z Casted-cross section

Figure 3. Two-dimensional CT scanning slice images.

As shown in Fig.3, it seems that the pores in casted samples exhibit circular shapes, while the pores in 3DPC samples mostly exhibit irregular shapes (approximately ellipsoidal). The observed pores in Fig.3 are categorized based on the size (marked in Fig.3). In this figure, it also looks like the casted sample has more large pores (with an equivalent diameter of more than 80 µm) compared to 3DPC samples. The aspect ratio (AR3D) of a 3D void, is used in this study as a parameter of shape descriptor, quantifying the shape of a pore/void. The aspect ratio is defined as the average value of elongation index (EI) and flatness index (FI) [3]. Elongation is the ratio between major and intermediate axes of the ellipsoid to a void; flatness is the ratio between intermediate and minor axes of the ellipsoid of a void [4]. Fig.4 shows the probability distributions of 3D voids' aspect ratio for concrete. The number of voids/pores for each sample is more than 100 million. The statistics show that the distribution curves follow similar trends, regardless of printing or casting of the concrete.

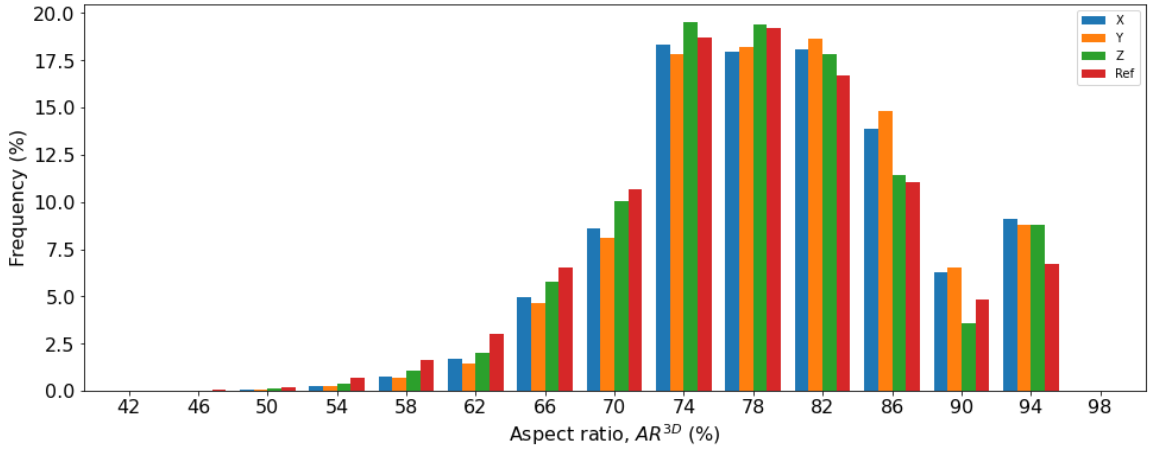

Figure 4. Statistic of probability distribution of the 3D aspect ratio for voids in concretes (Ref indicates casted sample).

Fig.5 exhibits the relationship between elongation, flatness, and volume (bubble size) of particular voids in relation to the pore shapes [5]. Statistics show that most of the voids are in the quadrant of "equant", regardless of printing or casting concrete. It suggests most of the voids are roughly spherical in shape. However, most of the bigger voids for casted concrete are more "equant" by comparison with printed concrete. This can explain why it seems that pores in casted samples exhibit circular shapes while the pores in 3DPC samples mostly exhibit irregular shape (approximately ellipsoidal shapes), especially for the larger pores (with an equivalent diameter of more than 80 µm) of casted concrete by visual inspection from 2D images. Because people tend to notice larger pores first during the visual inspection, this will result in an illusion that most pores look like the shape that larger pores are like. However, visual inspection is not always reliable. Statistical analysis might be more appropriate and reliable.

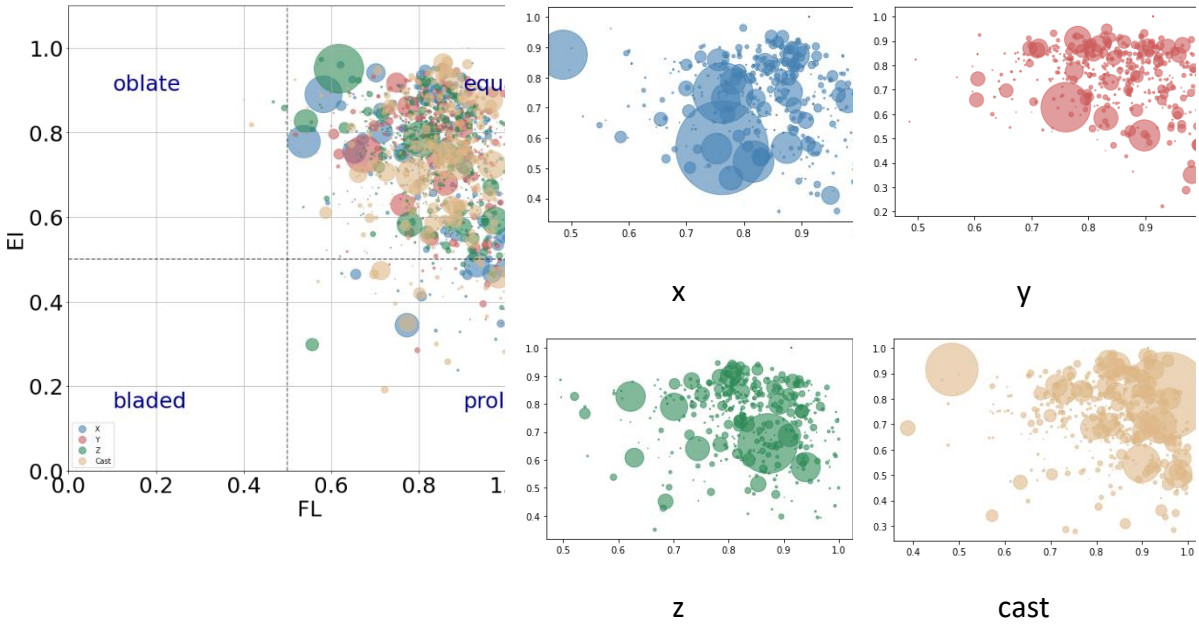

Figure 5. Relationship between elongation, flatness and volume (bubble size) of particular voids in relation to the pore shapes.

CONCLUSION

The statistics based on 3D analysis show that the distribution curves follow similar trends, regardless of printing or casting concrete. Statistical analysis was also performed on the relationship between

elongation, flatness, and volume (bubble size) of particular voids in relation to the pore shapes. It suggests that most of the voids are roughly spherical in shape regardless of printing concrete or casting concrete. The most obvious difference is that bigger voids in casted concrete are somewhat more "equant" compared with printed concrete. This can explain why casted samples exhibit somewhat more circular voids while in 3DPC samples they exhibit a more irregular shape (approximately ellipsoidal), especially for the bigger pores of casted sample by visual inspection from 2D images.

ACKNOWLEDGEMENT

This work was supported by the European Union Horizon 2020 research program under MSCA COFUND grant agreement 101034352 with cofunding from the VUB-Industrial Research Fund.

REFERENCES

[1] Liu, Chao, et al. Construction and Building Materials 314 (2022): 125572.

[2] Ma, Lei, et al. Construction and Building Materials 315 (2022): 125731.

[3] Su, D., and W. M. Yan Acta Geotechnica 15.6 (2020): 1533-1555.

[4] Zhao, Budi, and Jianfeng Wang. Powder technology 291 (2016): 262-275.

[5] Strzelecki, Piotr J., Adam Fheed, and Paweł Raczyński. AIP Conference Proceedings. Vol. 2209. No. 1. AIP Publishing LLC, 2020.

2. Durability performance

LIST OF CONTRIBUTIONS

Keynote lecture:

Extended abstracts:

Design, durability, and rapid curing of geopolymer lunar concrete

Prof. Aleksandra Radlinska[1]

[1] Concrete Research Group, The Pennsylvania State University, USA. (E-mail: azr172@psu.edu)

KEYNOTE SUMMARY

In order to construct safe and reliable infrastructure on the lunar surface, materials compositions designed using in-situ resources need to be researched and formulae developed that can be implemented via automated deposition. In this work, geopolymer lunar concrete has been created using various lunar soil simulants mixed with an alkaline solution, such as sodium silicate and sodium hydroxide, with all materials that can be mostly produced in situ. A circumscribed central composite design was utilized to understand the influence of three primary variables: the solution to simulant ratio (0.30 to 0.55), the modulus of the solution (SiO_2/Na_2O of 0.49 to 3.01), and the curing temperature (45°C to 95°C) on the mechanical properties of the lunar geopolymer. To encompass a large area of the lunar surface, lunar regolith simulants representing both the mare and highlands regolith regions of the Moon were used (OPRL2N and OPRH2N). A three-variable design resulted in 20 mixtures for each type of the simulant. All the samples were cured for three days at the various curing temperatures in the design, then demolded, and left in a standard laboratory environment until they were tested for compressive strength at 28-days. The results have shown, that viable binder formulations can be created using ISRU. Future work will focus on modifying the mixture design and curing variables in real-time to achieve the optimal rheology of these binders for 3D printing.

Influence of pre-saturation regime on the scaling resistance of alkali-activated slag concrete

Olivera Bukvić[1], Marijana Serdar[2]

[1, 2] Department of Materials, Faculty of Civil Engineering, University of Zagreb, Zagreb, CROATIA.
(E-mail: olivera.bukvic@grad.unizg.hr, marijana.serdar@grad.unizg.hr)

HIGHLIGHTS

- The scaling resistance of alkali-activated concrete was tested according to EN 12390-9 “slab test” procedure.
- Three pre-saturation regimes were tested: pre-saturation in de-ionized water for 3 days, and pre-saturation in 3% NaCl solution for 3 and 7 days.
- The scaling resistance was improved by introducing the pre-saturation with 3% NaCl and by increasing the pre-saturation period.

Keywords: scaling, freeze-thaw resistance, alkali-activated concrete

INTRODUCTION

Alkali-activated materials (AAMs) have been extensively researched in recent decades as a possible sustainable alternative to ordinary Portland cement (OPC) concrete. However, literature reports on the freeze-thaw resistance of AAMs are often inconsistent [1]. Freeze-thaw resistance with and without de-icing salts is of great importance for the durability of concretes in cold regions. While the parameters that are critical for freeze-thaw resistance, such as water to binder ratio, pore size and pore connectivity, and degree of saturation, are generally known [2,3], there is still a need for a better understanding of the mechanisms of freeze-thaw degradation of AAMs and the influencing factors.

Treatment of the concrete surface with de-icing salts causes scaling - peeling of the upper concrete layers [4]. The exact degradation mechanism is still under discussion, but it is known to be closely related to hydraulic pressure and osmotic pressure gradients [2].

The influence of pre-saturation on salt scaling resistance has been studied for the OPC concrete and OPC concrete with the supplementary cementitious materials [4,5], and for AAMs [1], according to different methods such as RILEM CDF test [1], ASTM C 672 or BNQ standard [4,5]. The longer pre-saturation period with freezing medium was found to be beneficial, when tested [4,5].

This paper presents the evaluation of the scaling resistance of alkali-activated slag concrete mix according to the EN 12390-9 "slab test" procedure [6] and the comparison with alternative pre-saturation regimes.

MATERIALS AND METHODS

For this experimental research, ground granulated blast furnace slag (GGBFS) provided by Ecocem, Benelux was used as a precursor. GGBFS was activated with sodium hydroxide (SH) pellets dissolved in water and commercially available sodium silicate (SS) solution Geosil 34417, produced by Woellner. Crushed dolomite aggregate with the maximum grain size of 16 mm was used, with the ratio of fine to coarse aggregate of 1:1.5. No air entrainers were used.

The mix design is presented in Table 7. Water to binder ratio (w/b) was calculated as the ratio of the sum of water in activator solutions and water added to attain satisfactory workability (add. water) and

the sum of GGBFS and solids in the activator solutions. The alkali content (Na2O) was calculated as weight percent of GGBFS, while the silica modulus of the mix (Ms) represents the ratio of silica and alkali content ($n(SiO_2)/n(Na_2O)$).

Table 7. Mix design of alkali-activated slag concrete.

GGBFS [kg/m³]	w/b	m(SH) - solid [kg/m]	m(SS) – solution [kg/m³]	Na_2O [%]	Ms	Add. water [kg/m³]	Aggregate (0-4mm) [kg/m³]	Aggregate (4-8mm) [kg/m³]	Aggregate (8-16mm) [kg/m³]
375	0.42	15.0	10.09	4.1	0.42	140.3	706.0	358.0	694.0

The scaling resistance of the mix was tested on three sets of four samples. The tests were conducted in accordance with the "slab test" procedure described in EN 12390-9 [6], except for the initial curing. Instead of curing in water for the first 7 days, the samples were cured sealed, due to their sensitivity to water curing [7]. While the set designated as S2 was pre-saturated in accordance with the EN 12390-9, the other two sets (S2/A and S2/B) were tested under alternative pre-saturation regimes. The test regimes for all sample sets are described in Table 8. At 28 days of age, the samples were subjected to the pre-saturation, followed by a freeze-thaw cycling (1 cycle=24h). Scaled material was collected and weighed after 7, 14, 28, 42 and 56 freeze-thaw cycles.

Table 8. Curing conditions and pre-saturation regimes - five sets of AA slag concrete samples.

Sample set	Curing	Pre-saturation period	Pre-saturation medium
S2	7 days sealed / 21 days in humidity chamber*	3 days	de-ionized water
S2/A	7 days sealed / 21 days in humidity chamber*	3 days	3% NaCl
S2/B	7 days sealed / 21 days in humidity chamber*	7 days	3% NaCl

*20±2°C and 65±5%, according to EN 12390-9

RESULTS & DISCUSSION

The results of the scaling resistance test are shown in Figure 1. The sample set S2, which was pre-saturated according to EN 12390-9, showed a steep increase in scaling material in the first 7 cycles and a moderation thereafter. A similar trend was reported in the RILEM TC 247-DTA report [1], with the explanation that the low scaling resistance at the beginning of the tests could be caused by the carbonation of the upper concrete layer. However, the other two pre-saturation regimes presented in this study resulted in a drastic reduction of the cumulative scaled material in the first 7 cycles, suggesting that the reason for the initial high scaling of the set S2 should be explained by degradation mechanisms other than carbonation.

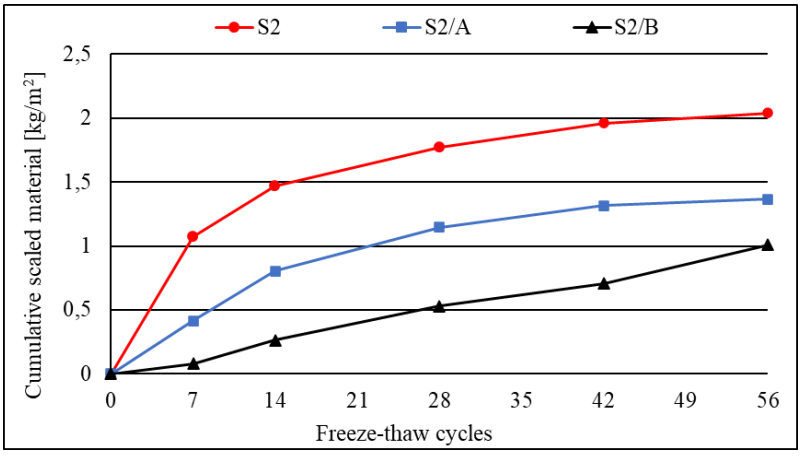

Figure 10. Cumulative scaled material of AA slag concrete mixes with different pre-saturation regimes.

The improvement of scaling resistance can be analyzed from two aspects: the influence of the pre-saturation period and the type of pre saturation medium on the scaling resistance. The pre-saturation of the samples with a NaCl solution instead of de-ionized water, as prescribed in EN 12390-9, resulted in significantly higher scaling resistance of the S2/A set. Extending the pre-saturation period with NaCl solution from 3 to 7 days increased the scaling resistance of the S2/B set even more (Figure 1). This set of samples almost met the durability requirements for exposure class XF2, which is defined in the Croatian National Annex as <0.5 kg/m3 of scaled material. The use of NaCl solution as a pre-saturation medium and the extension of the pre-saturation period could be explained by balancing the ions between the salt solution on top surface and the pores in the surface layers of the concrete, reducing the osmotic pressure gradients that cause scaling [2,4].

CONCLUSION

This research presents the results of the scaling resistance of alkali-activated slag concrete, tested according to EN 12390-9 and alternative pre-saturation regimes. The results show that both the pre-saturation period, and the type of the pre-saturation medium, have significant impact on the overall scaling resistance and its progression. The comparison of the pre-saturation period showed that for the 7-day sealed curing, the 7-day pre-saturation with 3% NaCl exhibited the highest increase in scaling resistance. Further research will focus on this phenomenon and understanding the prevalence of the different freeze-thaw deterioration mechanisms.

ACKNOWLEDGEMENT

This research has been conducted as a part of the project DuRSAAM - The PhD Training Network on Durable, Reliable and Sustainable Structures with Alkali-Activated Materials funded by the European Union's Horizon 2020 research and innovation programme under the Marie Skłodowska-Curie grant agreement No 813596. Research is also supported by the project "Alternative Binders for Concrete: understanding microstructure to predict durability, ABC", funded by the Croatian Science Foundation under number UIP-05-2017-4767.

REFERENCES

[1] Winnefeld F, Gluth GJG, Bernal SA, Bignozzi MC, Carabba L, Chithiraputhiran S, et al. RILEM TC 247-DTA round robin test: sulfate resistance, alkali-silica reaction and freeze–thaw resistance of alkali-activated concretes. *Materials and Structures* 53 (2020), 1-17.

[2] Cyr M, Pouhet R. *Chapter 11 - The frost resistance of alkali-activated cement-based binders. Handbook of Alkali-activated Cements*, Mortars and Concretes, Cambridge, UK: Woodhead Publishing, 2015.

[3] Neville AM, Brooks JJ. *Concrete Technology*. 2nd ed. n.d., Pearson Education Limited, England, UK, 2010.

[4] Ahani RM, Nokken MR. Salt scaling resistance – The effect of curing and pre-saturation. *Construction and Building Materials* 26 (2012), 558–564.

[5] Bouzoubaâ N, Bilodeau A, Fournier B, Hooton RD, Gagné R, Jolin M. Deicing salt scaling resistance of concrete incorporating supplementary cementing materials: laboratory and field test data. *Canadian Journal of Civil Engineering* 35 (2008), 1261–1275.

[6] EN 12390-9:2016 - Testing hardened concrete - Part 9: Freeze-thaw resistance with de-icing salts - Scaling 2016.

[7] Provis JL, van Deventer JSJ, editors. *Alkali Activated Materials - State of the Art Report TC 224-AAM*. RILEM State-of the-Art Reports 13, Dordrecht: Springer Netherlands, 2014.

Shrinkage and creep of alkali-activated slag and applicability of the fib MC 2010

R. Caron[1], R. A. Patel[1] and F. Dehn[1]

[1] Institute of Concrete Structures and Building Materials, Karlsruhe, GERMANY.
(E-mail: richard.caron@kit.edu, ravi.patel@kit.edu, frank.dehn@kit.edu)

HIGHLIGHTS

- Deformations of alkali-activated slag (AAS) are higher than the ones of ordinary Portland cement (OPC)
- The *fib* MC 2010 can be extended for AAS concrete for basic shrinkage, drying shrinkage and basic creep
- The drying creep evolution of AAS concrete is different from the one of OPC concrete

Keywords: alkali-activated slag, shrinkage, creep

INTRODUCTION

Slag is a waste generated produced by the steel industry. It can be mixed with an alkali solution to generate concrete with comparable mechanical properties to ordinary Portland cement (OPC) concrete. However, shrinkage and creep of AAS concrete have been reported higher compared to OPC concrete. Shrinkage refers to the deformations of concrete without any load, while creep corresponds to the deformations under sustained load. Both types of deformation can affect the serviceability and the durability of concrete structures. Some models, such as the fib MC 2010, have been developed to predict the deformations of OPC concrete [1]. In this contribution, shrinkage and creep properties of AAS concrete are investigated experimentally and the results are compared with predictions from the fib MC 2010.

MATERIALS AND METHODS

The composition of the slag used in this study was measured by energy-dispersive X-ray fluorescence (XRF) with a M4 Tornado spectrometer (Bruker GmbH Karlsruhe, Germany). It is composed of 38.8 % mass of CaO, 36.3 % mass SiO2, 12.8 % mass Al2O3 mass and 8.0 % mass MgO. Two mix designs were selected due to their promising behavior for structural applications [2]. The corresponding alkali solutions had a water-slag ratio (w/s) equal to 0.45, and an alkalinity coefficient (n) equal to 5.0 g Na2O / 100 g slag, and their silicate ratio (MS) equal to either 0.5 for the mix lS or 2.2 for the mix hS. The slag content in concrete was 450 kg/m3. The aggregate to slag content was 3.5 kg/kg. Sand accounted for 40 % volume of aggregates, middle-size gravels 30 % and big-size gravels 30 %.

Creep and shrinkage specimens were cylinders of 100 mm diameter and 285 mm height. For creep experiments, only the mix lS was investigated. In this case, additional specimens with the same geometry were cast to determine Young's modulus and compressive strength at the loading age. The loading was set to one-third of the compressive strength and was applied after 7 days. Both sealed and unsealed conditions were studied for creep and shrinkage. For shrinkage, samples were dried either from 1, 7 or 28 days. Drying creep was measured for an age of exposure to drying equal to seven days.

MODELING OF SHRINKAGE AND CREEP OF AAS

In the fib MC 2010, the total deformations of concrete εc(t) are modeled as:

$\varepsilon_c(t) = \varepsilon_{ci}(t_0) + \varepsilon_{cc}(t) + \varepsilon_{cs}(t) + \varepsilon_{cT}(t)$ where εci(t) is the initial strain at loading, εcc(t) is the creep strain at t > t0, with t0 the loading age, εcs(t) is the shrinkage strain and εcT(t) is the thermal strain. The shrinkage strain is discomposed into a basic shrinkage component εcbs(t) and a drying shrinkage component εcds(t):

$$\varepsilon_{cs}(t) = \varepsilon_{cbs}(t) + \varepsilon_{cds}(t)$$

To extend this model for AAS concrete, the same approach used by Tosic et al. [3] is applied:

$$\varepsilon_{cs}(t) = \xi_{cbs1} \cdot \varepsilon_{cbs}(t, \xi_{cbs2}) + \xi_{cds1} \cdot \varepsilon_{cds}(t, \xi_{cds2})$$

where the coefficients ξcbs1, ξcbs2, ξcds1 and ξcds2 must be calibrated.

The creep strain is modeled with the creep coefficient φ(t,t0):

$$\phi(t, t_0) = \frac{\varepsilon_{cc}(t)}{\varepsilon_{ci}(t_0)}$$

This creep coefficient is discomposed into a basic creep coefficient $\varphi_{bc}(t)$ and a drying creep coefficient $\varphi_{dc}(t)$:

$$\phi(t, t_0) = \phi_{bc}(t, t_0) + \phi_{dc}(t, t_0)$$

Following the approach of Tosic et al. [4] for recycled aggregate concrete, the proposed extension has the following form:

$$\phi(t, t_0) = \xi_{bc1} \cdot \phi_{bc}(t, t_0, \xi_{bc2}) + \xi_{dc1} \cdot \phi_{dc}(t, t_0, \xi_{dc2})$$

where the coefficient ξ_{bc1}, ξ_{bc2}, ξ_{dc1} and ξ_{dc2} must be calibrated. More information on the original model can be found in the fib MC 2010 [1].

For both shrinkage and creep, the parameters were calibrated using the least-square methods on the experimental results obtained in this study with the following objective function:

$$F_{obj}(\xi_1, \xi_2) = \sqrt{\sum_i \left(F_{model}(t_i, \xi_1, \xi_2) - F_{exp}(t_i)\right)^2}$$

where ξ_1 and ξ_2 are the parameters to optimize, t_i is the time of the experimental measure, $F_{exp}(ti)$ is the measure at t_i and F_{model} is the model function. Several starting points were chosen as initial guesses to obtain the global minimum of the optimized function. The tolerance of the relative error of the sum of the squares was lower than 1.5 e-10.

RESULT & DISCUSSION

The results of basic shrinkage and drying shrinkage for both mix lS and mix hS are given in Figure 1. The results of the calibrated parameters are given in Table 1. The experimental results can be compared with the original fib MC 2010 and the proposed calibrated model. First, basic shrinkage of AAS concrete is much higher than the one of OPC concrete as seen with the calibrated values for ξ_{cbs1} around 10. The speed of basic shrinkage is though comparable with the one predicted by the fib MC 2010. For drying shrinkage, if the samples are exposed to drying after one day, a higher shrinkage is observed for both mixes. However, if the samples are exposed later (at 7 or 28 days), ξ_{cds1} and the drying shrinkage are very low. Moreover, ξ_{cds2} is in almost all the configurations much lower than 1, indicating that the speed of drying shrinkage is very fast. Finally, the relative importance of basic shrinkage on the total shrinkage is around 70 % and higher than what is expected for OPC concrete.

Table 1. Obtained parameters of the calibration for shrinkage.

Sealed specimens	ξ_{cbs1}	ξ_{cbs2}
Mix lS – sealed	9.90	0.80
Mix hS - sealed	13.0	1.51
Unsealed specimens	ξ_{cds1}	ξ_{cds2}
Mix lS – unsealed after 1 day	0.85	0.041
Mix lS – unsealed after 7 days	0.36	2.6
Mix lS – unsealed after 28 days	0.083	0.17
Mix hS – unsealed after 1 day	3.5	0.002
Mix hS – unsealed after 7 days	0.44	0.0033
Mix hS – unsealed after 28 days	0.16	0.32

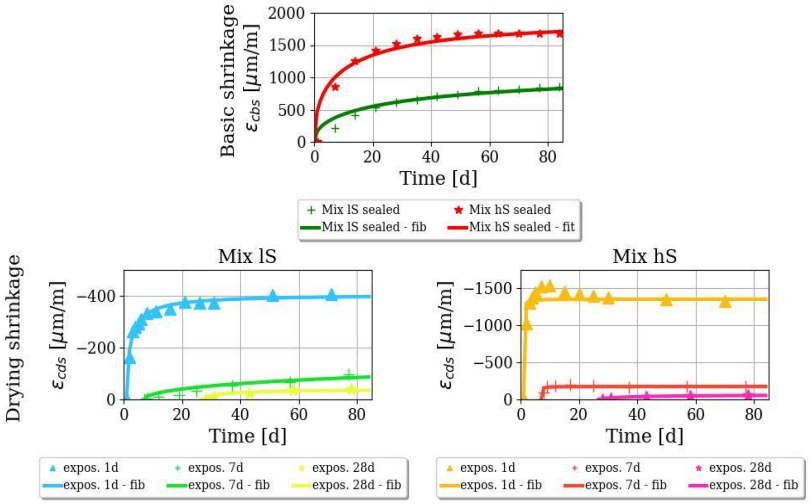

Figure 1. Results of shrinkage of AAS concrete. (left) basic shrinkage; (right) drying shrinkage. The points correspond to experiments and the plain lines to the calibrated models.

The Young's modulus after 7 days of the mix lS was 27.7 GPa. The compressive strength was 40.9 MPa. For this reason, a loading of 13.6 MPa was applied in both sealed and unsealed conditions to determine the basic creep and the drying creep of the mix lS. The experimental results, as well as the comparison with the original fib MC 2010 are provided in Figure 2. Basic creep is higher just after loading and its evolution is higher at later-age. For drying creep, the strains are lower in the first days after loading but the evolution is higher at later-age. For basic creep, it was possible to optimize the objective function presented above. ξ_{bc1} was found equal to 2.4 and ξ_{bc2} was found equal to 2.8. This confirms that the asymptotic creep evolution is much higher for AAS concrete than predicted by the fib MC 2010. For the drying creep, it was not possible to calibrate the objective function. This would mean that the drying creep model of the fib MC 2010 in its current form cannot capture the drying creep evolution of AAS concrete.

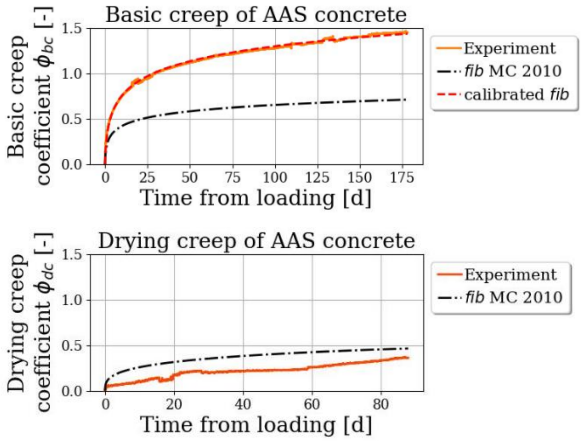

Figure 2. Results of creep of AAS concrete. (left) basic creep; (right) drying creep.

CONCLUSION

Basic shrinkage of AAS concrete is around ten times higher than that of OPC concrete. In comparison to OPC concrete, drying shrinkage depends a lot on the age of exposure to drying. In particular, drying shrinkage is very low when this age of exposure increases. The relative importance in the total shrinkage of basic shrinkage is higher than for OPC. Basic creep is around two times higher for AAS concrete. The drying creep of AAS differs from OPC and it was not possible to extend the fib MC 2010 for this creep component.

ACKNOWLEDGEMENT

This work was supported by the European Union's Horizon 2020 research and innovation program under the Marie Skłodowska-Curie grant agreement No 813596.

REFERENCES

[1] *fib* (2013): *fib* Model Code for Concrete Structures 2010. International Federation for Structural Concrete (*fib*), Lausanne.

[2] Caron, R.; Patel, R. A.; Dehn, F. Extension of the *fib* MC 2010 for basic and drying shrinkage of alkali-activated slag concretes. Structural Concrete 64 (2022), 106107

[3] Tošić, N.; de La Fuente, A.; Marinković, S. Shrinkage of recycled aggregate concrete: experimental database and application of *fib* Model Code 2010. Mater Struct 51 (2018) 125

[4] Tošić, N.; de La Fuente, A.; Marinković, S.: Creep of recycled aggregate concrete: Experimental database and creep prediction model according to the *fib* Model Code 2010. In *Construction and Building Materials* 195 (2019), 590–599

Chloride ingress and carbonation resistance of ternary blend alkali activated concrete

Saeid Ghorbani[1] and Stijn Matthys[2]

[1, 2] Department of Structural Engineering and Building Materials, Ghent University, Ghent, Belgium. (E-mail: Saeid.Ghorbani@UGent.be , Stijn.Matthys@UGent.be)

HIGHLIGHTS

- Ternary blend alkali activated concrete showed comparable chloride resistance to a reference mixture with CEM I.
- In reference to accelerated testing (1 % CO_2), the carbonation resistance of ternary blend alkali activated concrete is lower than that of PC based reference mixtures.

Keywords: alkali activated concrete, chloride ingress, carbonation, ground granulated blast furnace slag, copper slag, stainless steel slag

INTRODUCTION

In recent years, alkali activated materials (AAMs) have been of great attention due to their sustainability advantages compared to Portland cement (PC) such as reducing CO2 emission and lowering energy consumption [1, 2]. As reported in the literature [2-4], AAMs show comparable or even better structural properties compared to PC based materials. However, a thorough understanding in terms of their durability and long-term performance needs to be taken place and documented prior to their wide applications [5, 6]. The carbonation of cementitious materials is due to the reaction between the dissolved CO2 in pore solution and the reaction products, causing a drop-down in the pH of pore solution [7, 8]. It has been reported that the carbonation resistance of AAMs is lower than that of PC materials [9, 10]. In terms of chloride ingress, AAMs shows more or less comparable resistance compared to PC based materials due to their lower permeability, however, the chloride binding mechanism in AAMs is not sufficiently studied [8, 9, 11]. Through these years, the majority of investigations in alkali activated technology, especially in terms of their durability performance have been focused on ground granulated blast furnace slag (GGBFS) and fly ash (FA) based AAMs [12]. Given limted avavalibility of GGBFS and FA in some regions, exploring other by-products such as copper slag (CS) and stainless steel slag (SS) is of interest. The current study aims to investigate the durability performance of a ternary slag alkali actviated concrete (AAC), including three types of solid precursors namely GGBFS, CS and SS. The results of explorative studies done by the authors at the paste and mortar levels resulted in proposed ternary AAC. The ternary precursor blend considered for this study consists of 50 % CS, 35 % GGBFS and 15 % SS. This paper will report on the carbonation resistance and chloride penetration of the teranry blend AAC and its comparison with PC based refrence mixtures.

MATERIALS & METHODS

The GGBFS, CS and SS powders are type eco2cem (Ecocem), Koranel 419 (Aurubis) and Fillinox 3000 (Orbix), respectively. CEM I-52.5 N (Holcim) and CEM III-42.5 N (Heidelberg) were used for producing the PC based concrete reference mixtures. Chemical composition of precursors determined by X-ray fluorescence (XRF) are summarized in Table 1. The particle size distribution of precursors are presented in Figure 1.

Table 9. Chemical composition of precursors (mass% as oxide).

Precursor	Chemical composition (%)											
	SiO_2	CaO	Al_2O_3	Fe_2O_3	MgO	SO_3	K_2O	MnO	Na_2O	Cr_2O_3	ZnO	Others
GGBFS	31.10	40.90	13.70	0.40	9.16	2.31	0.68	0.31	-	-	-	1.44
CS	29.50	2.60	9.85	45.40	1.05	0.85	0.19	0.65	3.66	1.36	3.32	1.57
SS	28.00	44.20	6.30	2.04	4.41	0.49	0.05	2.65	-	9.90	0.01	1..95

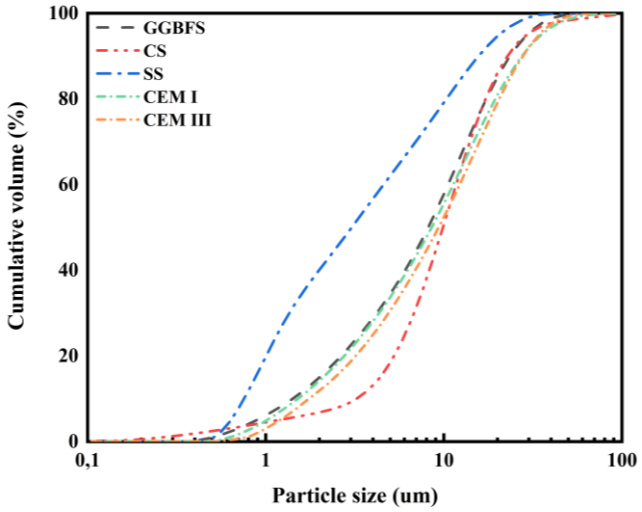

Figure 11. Particle size distribution of the precursors and Portland cements.

Sodium hydroxide and sodium silicate solutions are applied as alkaline activators. Reagent-grade sodium hydroxide anhydrous pearls (Brenntag), and sodium silicate solution (15% Na_2O, 30% SiO_2, and 55% water) (PQ Corporation) were used to obtain a molar ratio (SiO_2/Na_2O) of 1.30. In this study, fine sand (0-4 mm) and coarse aggregates (gravel 2-8 and 8-16 mm) were used to manufacture the concrete mixtures. Details of the mix proportion of AAC and PC mixtures are given in Table 2. AAC and reference PC concrete mixtures are designed with a fixed solid binder content of 400 kg/m^3.

Table 10. Mix proportions of the concrete mixtures (kg/m^3).

Group	GGBFS	CS	SS	CEM I	CEM III	Sodium silicate	NaOH	Water	Sand	Gravel 2-8mm	Gravel 8-16 mm	SP[1]
AAC	124	215	61	-	-	120	12.5	94	737	511	611	-
CEM I	-	-	-	400	-	-	-	159.5	753	523	624	1
CEM III	-	-	-	-	400	-	-	159.5	744	516	617	1

[1] Superplasticizer

A series of durability tests in terms of chloride penetration and carbonation according to NT Build 492 and EN 12390-12 have been conducted, respectively, on the three concrete mixtures listed in Table 2.

RESULT & DISCUSSION

The non-steady-state migration and accelerated carbonation (CO_2 =1 %) test results of the three concrete specimens are presented in Figure 2.

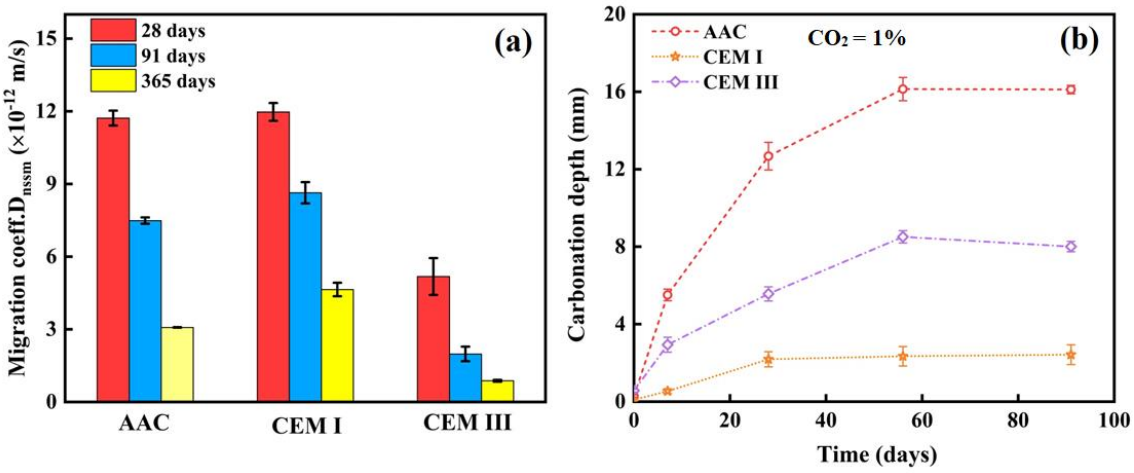

Figure 12. Durability performance of concrete mixtures: (a) chloride migration coefficient and (b) carbonation resistance.

The results show that the chloride migration coefficient of both AAC and PC mixtures decreased with curing time prior to starting the test. This is due to the pore structure densification. Compared to the chloride migration coefficient of AAC at 28 days, the chloride migration coefficient of AAC at 91 days and 365 days reduced by about 39 % and 69 %, respectively. While the decreasing chloride migration coefficient of the two types PC concrete shows different reduction rates with time, caused by the different chemical compositions. The 365 days chloride migration coefficient of CEM I and CEM III concrete mixtures decreases by 61 % and 83 %, respectively, compared to the 28 days chloride migration coefficient. It is observed that AAC specimens have similar resistance to chloride ingress as for the CEM I reference mixture, while both of them have lower resistance than that of CEM III reference specimens. A potential reasoning for this lower resistance next to differences in composition of hydration products and microstructure may be related to the larger amount of shrinkage-induced microcracks in alkali activated systems compared to PC based systems [13, 14].

As seen in Figure 2 (b), the carbonation depth in AAC is more severe compared to PC based specimens, whereby the 91 days carbonation depth of the AAC is about 14 and 8 mm larger than that of PC concrete with CEM I and CEM III, respectively. This could be attributed to the different carbonation mechanisms of AAMs and PC materials [8]. It is reported that the C-A-S-H gel in AAMs has a more vulnerable structure to carbonation (especially to accelerated carbonation) compared to C-S-H in PC based materials [15]. The carbonation process in PC based materials affect the pore structure of the matrix as a result of: 1) CH reaction with H_2CO_3 forming $CaCO_3$; 2) decalcification of C-S-H gel; 3) decomposition of ettringite. Conversely, for AAMs, H_2CO_3 dissolved in the aqueous phase directly consumes the Ca ions located in the interlayer of the C-A-S-H gel chains, disintegrating the structure, and leading to a larger shrinkage [8, 16]. The cracks generated by larger shrinkage AAMs facilitates the penetration of CO_2, which allows the H_2CO_3 to react with C-A-S-H gel deeper inside the specimens.

CONCLUSION

The chloride migration coefficient of both AAC and PC specimens decreased with curing time due to the pore structure densification. AAC specimens offer comparable and lower resistance to chloride ingress, compared with CEM I and CEM III reference specimens, respectively. The accelerated carbonation depth develops more rapidly in AAC specimens than in PC specimens.

ACKNOWLEDGEMENT

This research study was carried out in the frame work of the “By-products for sustainable concrete in the urban environment” project, funded by Interreg North-West Europe. Additionally, the authors wish to express their gratitude towards Ecocem, Aurubis and Orbix for providing the GGBS and CS and EAFS used within this study.

REFERENCES

[1] Y. Ding, J.G. Dai, C.J. Shi, Mechanical properties of alkali-activated concrete: A state-of-the-art review, Construction and Building Materials 127 (2016) 68-79.

[2] J.L. Provis, Alkali-activated materials, Cement and Concrete Research 114 (2018) 40-48.

[3] A. Noushini, F. Aslani, A. Castel, R.I. Gilbert, B. Uy, S. Foster, Compressive stress-strain model for low-calcium fly ash-based geopolymer and heat-cured Portland cement concrete, Cement and Concrete Composites 73 (2016) 136-146.

[4] R.J. Thomas, S. Peethamparan, Alkali-activated concrete: Engineering properties and stress–strain behavior, Construction and Building Materials 93 (2015) 49-56.

[5] J. Zhang, C. Shi, Z. Zhang, Effect of Na2O concentration and water/binder ratio on carbonation of alkali-activated slag/fly ash cements, Construction and Building Materials 269 (2021) 121258.

[6] K. Arbi, M. Nedeljkovic, Y. Zuo, G. Ye, A review on the durability of alkali-activated fly ash/slag systems: advances, issues, and perspectives, Industrial & Engineering Chemistry Research 55(19) (2016) 5439-5453.

[7] M.S. Badar, K. Kupwade-Patil, S.A. Bernal, J.L. Provis, E.N. Allouche, Corrosion of steel bars induced by accelerated carbonation in low and high calcium fly ash geopolymer concretes, Construction and Building Materials 61 (2014) 79-89.

[8] A. Wang, Y. Zheng, Z. Zhang, K. Liu, Y. Li, L. Shi, D. Sun, The durability of alkali-activated materials in comparison with ordinary Portland cements and concretes: a review, Engineering 6(6) (2020) 695-706.

[9] O.A. Mohamed, A review of durability and strength characteristics of alkali-activated slag concrete, Materials 12(8) (2019) 1198.

[10] P. Awoyera, A. Adesina, Durability properties of alkali activated slag composites: short overview, Silicon 12 (2020) 987-996.

[11] J. Zhang, C. Shi, Z. Zhang, Z. Ou, Durability of alkali-activated materials in aggressive environments: A review on recent studies, Construction and Building Materials 152 (2017) 598-613.

[12] Z. Yan, Z. Sun, J. Yang, H. Yang, Y. Ji, K. Hu, Mechanical performance and reaction mechanism of copper slag activated with sodium silicate or sodium hydroxide, Construction and Building Materials 266 (2021) 120900.

[13] C. Shi, Strength, pore structure and permeability of alkali-activated slag mortars, Cement and Concrete Research 26(12) (1996) 1789-1799.

[14] L.Y. Yang, Z.J. Jia, Y.M. Zhang, J.G. Dai, Effects of nano-TiO2 on strength, shrinkage and microstructure of alkali activated slag pastes, Cement and Concrete Composites 57 (2015) 1-7.

[15] C. Shi, D. Roy, P. Krivenko, Alkali-activated cements and concretes, CRC press (2003).

[16] S.A. Bernal, R.M. De Gutiérrez, J.L. Provis, Engineering and durability properties of concretes based on alkali-activated granulated blast furnace slag/metakaolin blends, Construction and Building Materials 33 (2012) 99-108.

Study on the influence of the activating solution composition on shrinkage of low calcium fly ash geopolymers

Mude Hanumananaik[1], Kolluru V L Subramaniam[2]

[1]Research Scholar, Department of Civil Engineering, Indian Institute of Technology Hyderabad, Hyderabad, TS 502285, INDIA. (Email: ce15m17p000001@iith.ac.in.)

[2] Professor, Department of Civil Engineering, Indian Institute of Technology Hyderabad, Hyderabad, TS 502285, INDIA. (Email: KVLS@ce.iith.ac.in)

HIGHLIGHTS

- Shrinkage of geopolymer concrete produced by alkali activation of low calcium fly ash with different activator compositions are studied.
- Decrease in water content resulted in increase in N-A-S-H decrease in porosity and critical pore size and increase in drying and autogenous shrinkage
- Increase in sodium content have no significant effect on N-A-S-H and compressive strength. The porosity and critical pore size is decreased with increase in sodium content and also the autogenous shrinkage and drying shrinkage is increased with identical moisture loss

Keywords: geopolymers, N-A-S-H, porosity, shrinkage

INTRODUCTION

In recent years, there has been an uptick in both the rate of cement production and cement utilization as a result of an increase in the pace at which infrastructure is being built. An increased emphasis is being placed on the research and development of new clinker-free binders that are friendly to the environment in order to reduce the negative effects that the cement industry has on the surrounding ecosystem. Alkali-activated binders are potential alternatives that produce superior mechanical and durability characteristics in addition to a lower carbon footprint [1, 2, 5, 21, 23]. According to the studies that have been done so far [1, 7, 8, 12, 13, 20, 22], the potential for warming the planet caused by AABs is between 45 and 80 percent lower than that of OPC. The use of alternative source materials, such as fly ash and slag, has garnered a significant amount of attention during the development of AABs [2, 5, 21, 23]. It is known that alkali-activated low-calcium fly ash, abbreviated as AAF, can form a three-dimensional network gel [4, 10, 14, 15, 16]. Heat curing is required for low-calcium fly ash in order to accelerate the geopolymerization process, which is necessary in order to achieve the desired mechanical properties [2, 3, 14, 17, 18, 19, 20].

The compressive strength, and setting time are mainly dependent on the activator concentration, [11]. The activating solutions used for AABs are typically proportioned for achieving high strength from the composites. The activator composition also contributes to shrinkage in the AABs [6]. Reducing the activator modulus reduces the drying shrinkage [9]. It is generally acknowledged that silica in the activator contributes to strength. The role of silica content in the activating solution on the shrinkage in AAFSB is not yet fully understood.

In this study the shrinkage of geopolymer concrete produced by alkali activation of low calcium fly ash with different activator compositions are studied. The activation solution is varied in terms of total water content in the system and sodium content of the activating solution. The activating solutions are proportioned for strength based on the reactive content in the fly ash for achieving aluminosilicates

of consistent composition [24]. The procedure developed previously for determining the activating solution composition for a given reactive oxide composition of fly ash was followed for deciding the mixture compositions. The shrinkage of the geopolymer is related to the reaction product content in the activated mixture.

MATERIALS AND METHODS

Sodium hydroxide (NaOH) and sodium silicate are the components of the alkaline solution used to activate the fly ash samples (Na_2OxSiO_2). Commercially available fly ash obtained from a thermal power plant located at NTPC Ramagundam in Telangana state, Indian is utilised. The oxide composition of the fly ash is determined by XRF spectroscopy and listed in table 1. The fly ash is classified as the silicious fly ash in accordance to IS 3812 and class F fly ash in accordance to ASTM C618. The fly ash is further classified as "low calcium fly ash" due to lack of calcium available in the material.

Table 1. Oxide compositions of binders.

Oxide	SiO_2	Al_2O_3	Fe_2O_5	CaO	TiO_2	K_2O	MgO	SO_3
Mass %	55.66	26	5.58	4.06	1.82	2.8	1.92	0.94

Commercially available Sodium silicate and sodium hydroxide were used for preparing the alkali silicate activating solution. The sodium silicate consisted of 14.70% sodium oxide (Na_2O), 34.17% silicon dioxide (SiO_2), and 51.13% water. The pH at 24°C and n-modulus (SiO_2/Na_2O ratio) of the sodium silicate were 12.98 and 2.32, respectively. The sodium hydroxide used was in pellets form with 98% purity. Deionized water with a pH range between 7 to 7.1 was used for preparing the activating solution.

Three mixes were selected to study the influence of water content and added sodium content. The mix labelled I was proportioned with the reactive SiO_2/Al_2O_3 and reactive SiO_2/Na_2O ratios in the activated paste of 2.0 and 5.0, respectively. Maintaining reactive SiO_2/Al_2O_3 ratio of 2 and reactive SiO_2/Na_2O ratio close to 5.0 has been shown to produce the highest compressive strength from the activated paste [24]. The reactive oxide ratios presented in the table result in the formation of a sodium alumino-silicate gel (N-A-S-H) with a Si/Al ratio of 2.0. [24]. The water to solids ratio (W/S) of the mix 1 was 0.25. Two additional mixtures were prepared to study the influences of water and added sodium contents in the activated paste. In the mix labelled as II, the reactive oxide ratios in the paste were kept constant, while the W/S was decreased to 0.22. Mix III was prepared by increasing the sodium content in the activated paste, while the water to solids ratio was maintained as 0.25. A detailed mix design was shown in table 1. After casting, the samples are moist cured for 24 hours at 60°C. After 24 hour, the samples were demolded and cured at 60°C and 50% relative humidity (RH).

Table 1. Alkali-activated fly ash mixture composition.

Mix Name	I	II	III
Si/Al	2	2	2
Si/Na	5	5	4
W/S	0.25	0.22	0.25

Compressive strength was determined from 70mm X70 mm cubes. The compressive strength was measured at 1, 3, 7, 14 and 28 days. The drying shrinkage was measured in accordance to ASTM C 596 [26]. A specimen with cross section of 25 mm and 285 mm length was used. The initial measurement was taken after 24 hours of casting, with a length comparator of 0.0025 mm accuracy. After the initial reading, the shrinkage measure was carried out every 2 hours for first 24 hours, and then one measurement was recorded for every day. Mass loss is also recorded on the same samples, after

measuring the drying shrinkage with a scale of 0.01 g accurate. The autogenous shrinkage of the AAF paste was measure in accordance to ASTM C1698 [27]. According to the standard a flexible corrugated pipe of 420±5 mm and a diameter of 29±5 mm was used. After casting, both the ends of the corrugated pipe was sealed with the rubber corks. Initial reading was measured after the final setting time. Linear variable differential transformers (LVDT) with an accuracy of 0.001 mm was used to record the data at 50 seconds interval for first three days. The LVDTs were removed after three days, and the measurements were performed with a length comparator of 0.0025 mm accuracy for the remaining curing age. Porosity was measured using mercury intrusion porosimetry (MIP).

RESULT & DISCUSSION

The compressive strength of all three mixes are shown in the figure 1. The measured strengths from the three mixtures indicates that nominally similar strengths are obtained from the two pastes which have identical water contents. The two pastes had a difference in the added sodium from a difference in the NaOH content. The higher sodium content in mix III does not appear to contribute to strength. The higher basicity in the paste does however contribute to a higher early reactivity, which leads to a faster rate of strength gain initially. While the NaOH molarity in the two pastes is different, the later age strengths are similar. The reduction in the water content in the paste contributes significantly to higher rate of strength gain and higher strengths at later ages. Comparing the two pastes with Si/Na=5.0, the reactive oxide ratio was identical, however, the lower water content produces a higher strength in II.

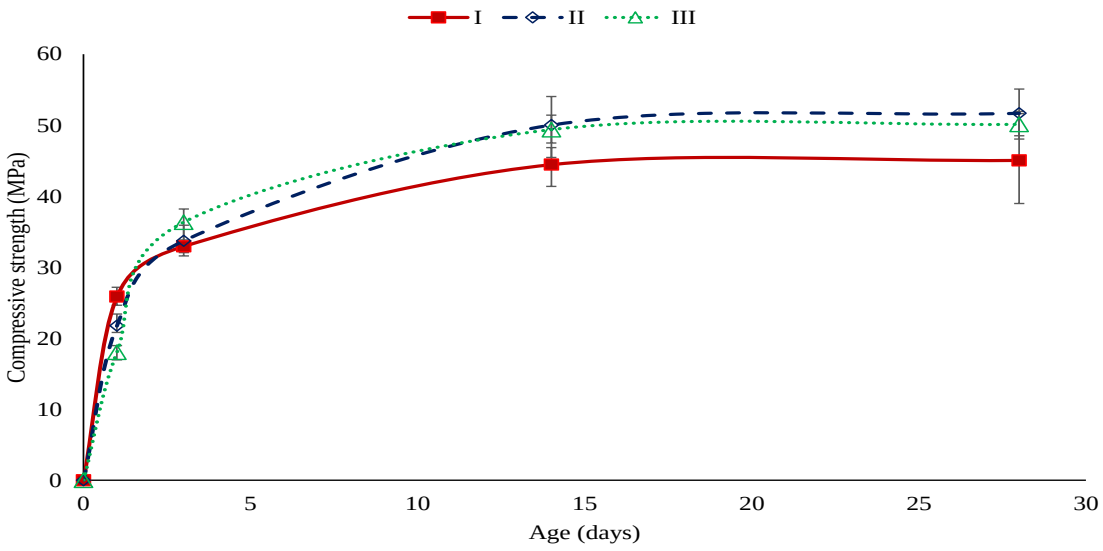

Figure 1. Compressive strength of AA paste with different activating solution composition.

The autogenous shrinkage of the AAF paste with different activating solutions are shown in the figure 2. The majority of autogenous shrinkage occurred with in first 24 hours. Decrease in water content resulted in increase in the autogenous shrinkage. Increase in sodium content with identical water content resulted in increase in autogenous shrinkage. Drying shrinkage of cement paste with w/c ratio of 0.41 is also plotted for the reference. The drying shrinkage of OPC and AAF paste is nominally identical up to three days. The drying shrinkage of AAF paste is lower than the cement pastes with time. In cement paste, the shrinkage continued for 28 days. The drying shrinkage of AAF paste is occurred within the first few days and attains a constant value with in ten days after the initiation of drying. Decrease in water content resulted in increase in the shrinkage strain and increase in sodium content resulted in increase in drying shrinkage [25].

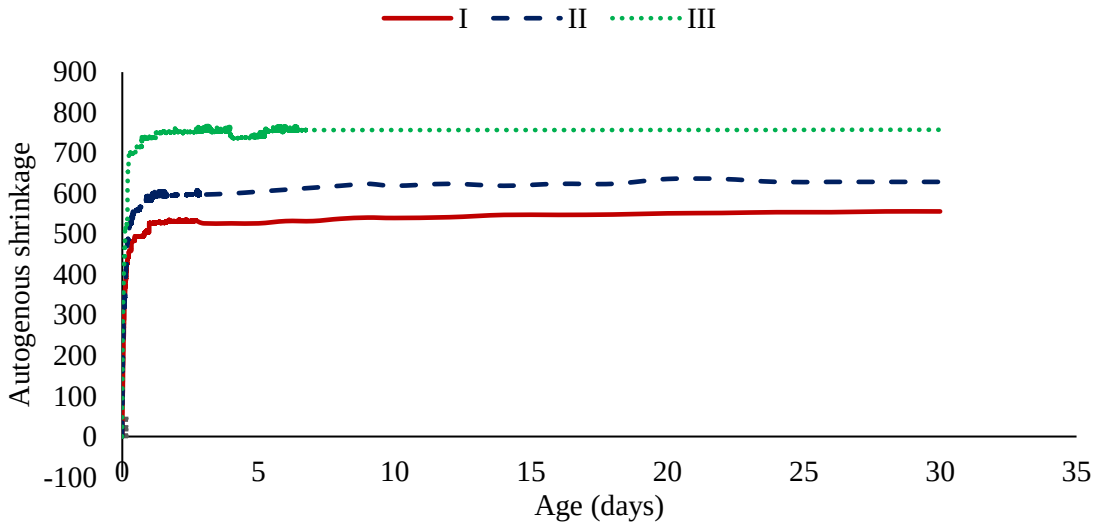

Figure 2. Autogenous shrinkage of AAF paste with different activating solution composition.

Figure 3(a) depicts the drying shrinkage of the AAF paste with different activating solution composition, while the Figure 3(b) depicts the mass loss of the AAF paste. For AAF, the majority of mass loss occurred with in first three days after initiation of drying and incase of OPC, the mass loss attained a constant value by 15 days after initiation of drying. The mass loss is decreased with decrease in water content of the AAF paste. The mass loss of the AAF mix with similar water content and varying added sodium content is nominally identical. Decrease in water content resulted in lowering the mass loss, and increase in drying shrinkage of AAF. Increase in added sodium content with constant water content, resulted in constant mass loss and increased drying shrinkage of AAF.

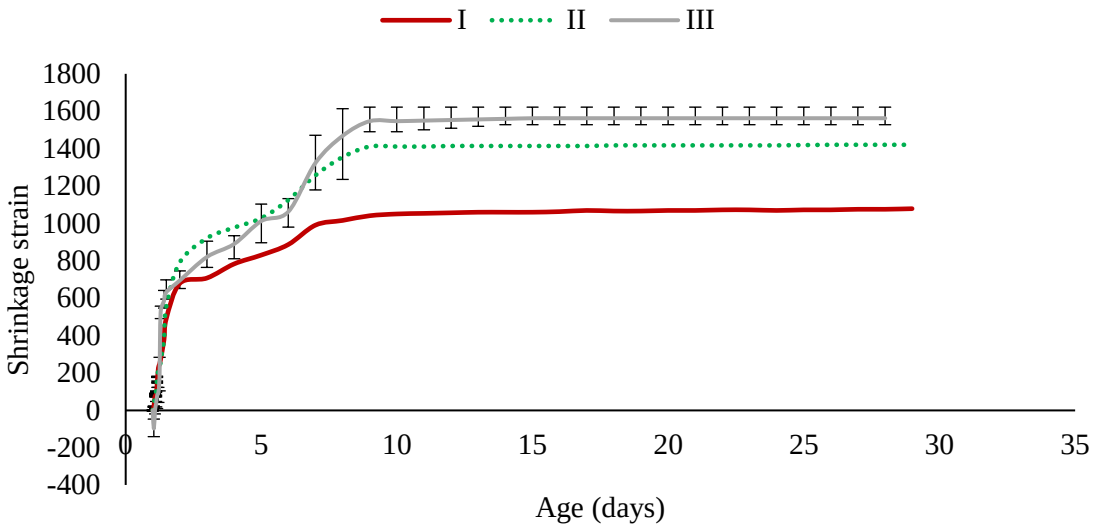

(a)

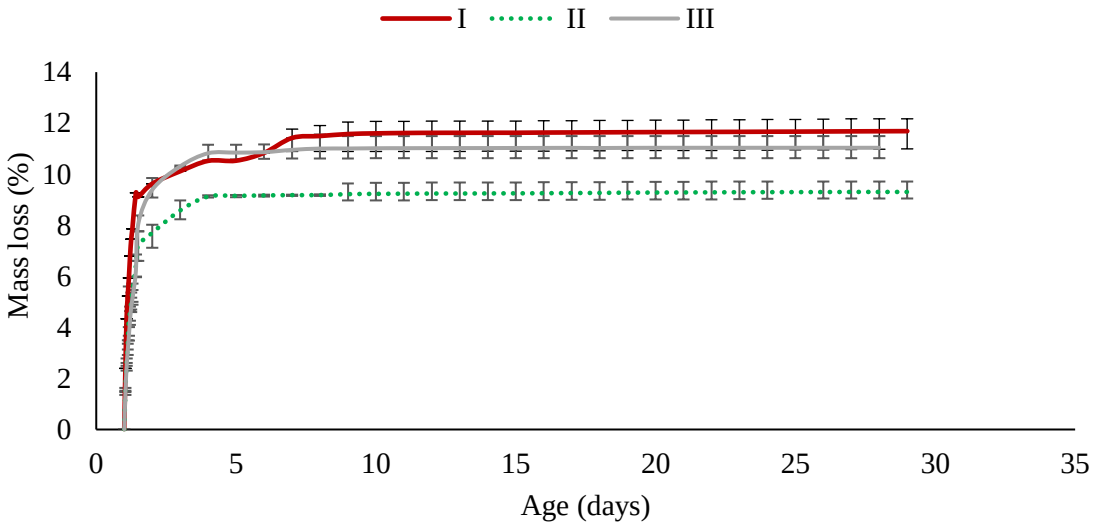

(b)

Figure 3. (a) Drying shrinkage and (b) mass loss of AAF paste with different activating solution composition.

The porosity and the pore structure of the AAF paste with different activating solution was shown in the figure 4. The total porosity is decreased with decrease in water content and also the critical pore size is also decreased, which resulted in increase in shrinkage strain of the AAF paste. Increase in sodium content resulted in decrease in porosity and critical pore size, which resulted in increase in shrinkage strain of AAF paste with identical water content and mass loss. Increase in sodium content with identical water content have no influence on strength, N-A-S-H content and mass loss of the AAF paste, while the shrinkage strain increased with increase in sodium content.

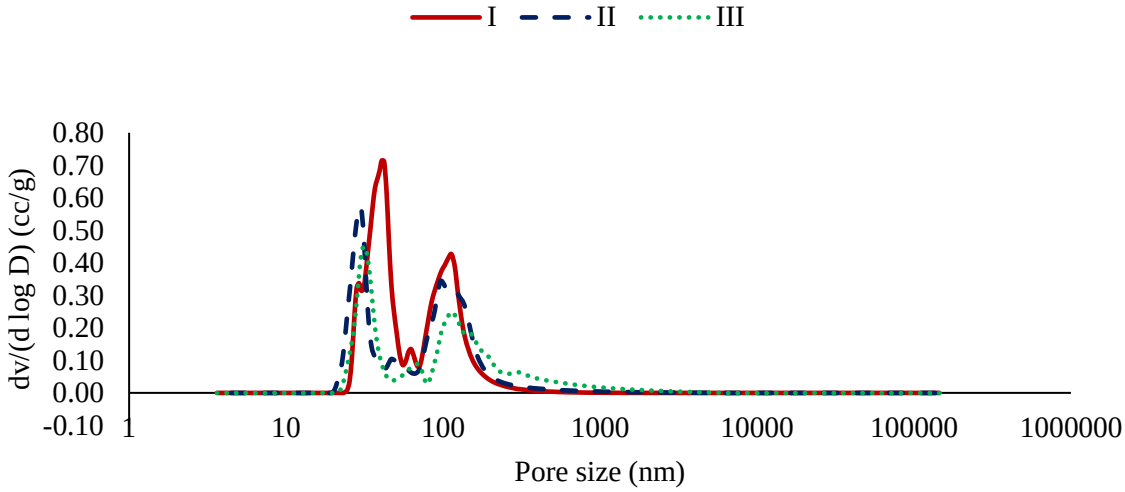

(a)

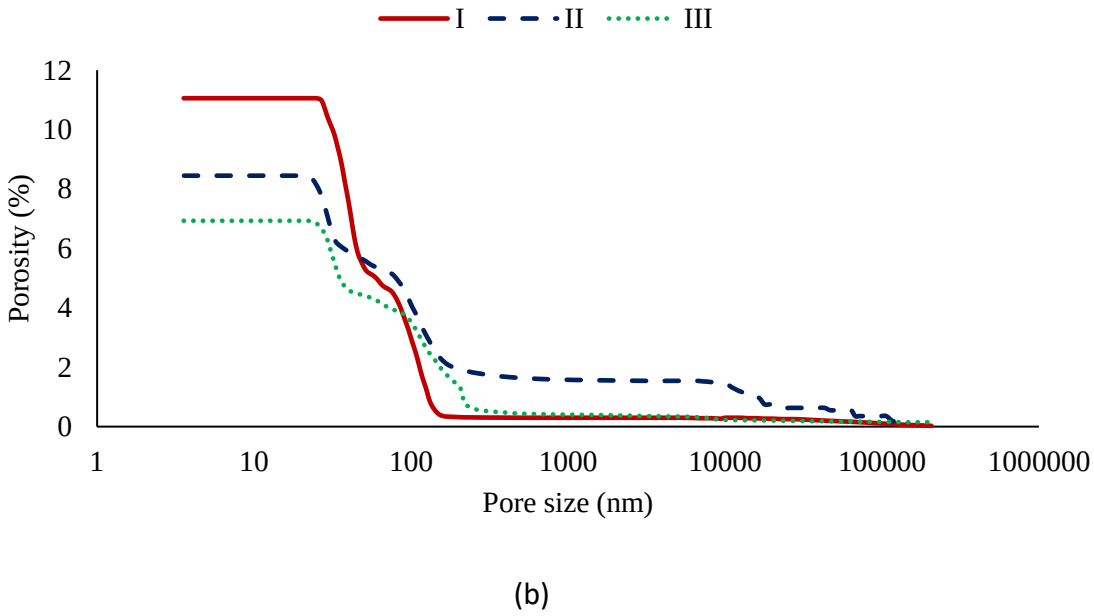

(b)

Figure 4. (a) Pore size distribution (b) Porosity of the AAF paste with different activating solution composition.

CONCLUSIONS

The influence of the activating solution composition on the compressive strength and shrinkage of AAF paste was studied. The shrinkage of the AAF paste was related to the porosity of the AAF paste. The conclusions of the work are

- Decrease in water content resulted in increase in decrease in porosity and critical pore size and increase in drying and autogenous shrinkage.
- Increase in sodium content have no significant effect on compressive strength.
- The porosity and critical pore size is decreased with increase in sodium content and the autogenous shrinkage and drying shrinkage is increased with identical moisture loss.

REFERENCES

[1] Adesanya, E., Perumal, P., Luukkonen, T., Yliniemi, J., Ohenoja, K., Kinnunen, P., and Illikainen, M. (2021). "Opportunities to improve sustainability of alkali-activated materials: A review of side-stream based activators." *Journal of Cleaner Production*, Elsevier Ltd, 286, 125558.

[2] Bakharev, T. (2005). "Geopolymeric materials prepared using Class F fly ash and elevated temperature curing." *Cement and Concrete Research*, 35(6), 1224–1232.

[3] Chithiraputhiran, S., and Neithalath, N. (2013). "Isothermal reaction kinetics and temperature dependence of alkali activation of slag, fly ash and their blends." *Construction and Building Materials*, Elsevier Ltd, 45, 233–242.

[4] Davidovits, J. (1991). "Geopolymers." *Journal of Thermal Analysis*, 37(8), 1633–1656.

[5] Fernandez-Jimenez, A., García-Lodeiro, I., and Palomo, A. (2007). "Durability of alkali-activated fly ash cementitious materials." Journal of Materials Science, 42(9), 3055–3065.

[6] Gao, X., Yu, Q. L., and Brouwers, H. J. H. (2016). "Assessing the porosity and shrinkage of alkali activated slag-fly ash composites designed applying a packing model." *Construction and Building Materials*, 119, 175–184.

[7] Habert, G. (2013). *Assessing the environmental impact of conventional and "green" cement production*. *Eco-Efficient Construction and Building Materials: Life Cycle Assessment (LCA), Eco-Labelling and Case Studies*.

[8] Habert, G., D'Espinose De Lacaillerie, J. B., and Roussel, N. (2011). "An environmental evaluation of geopolymer based concrete production: Reviewing current research trends." *Journal of Cleaner Production*, Elsevier Ltd, 19(11), 1229–1238.

[9] Hojati, M., and Radlińska, A. (2017). "Shrinkage and strength development of alkali-activated fly ash-slag binary cements." *Construction and Building Materials*, 150, 808–816

[10] Li, C., Sun, H., and Li, L. (2010). "A review: The comparison between alkali-activated slag (Si + a) and metakaolin (Si + Al) cements." *Cement and Concrete Research*, Elsevier Ltd, 40(9), 1341–1349.

[11] Marjanović, N., Komljenović, M., Baščarević, Z., Nikolić, V., and Petrović, R. (2015). "Physical-mechanical and microstructural properties of alkali-activated fly ash-blast furnace slag blends." Ceramics International, 41(1), 1421–1435.

[12] Mclellan, B. C., Williams, R. P., Lay, J., Riessen, A. Van, and Corder, G. D. (2011). "Costs and carbon emissions for geopolymer pastes in comparison to ordinary portland cement." Journal of Cleaner Production, Elsevier Ltd, 19(9–10), 1080–1090.

[13] Ouellet-Plamondon, C., and Habert, G. (2015). *Life cycle assessment (LCA) of alkali-activated cements and concretes*. *Handbook of Alkali-Activated Cements, Mortars and Concretes*, Woodhead Publishing Limited.

[14] Palomo, A., Krivenko, P., Garcia-Lodeiro, I., Kavalerova, E., Maltseva, O., and Fernández-Jiménez, A. (2014). "A review on alkaline activation: new analytical perspectives." *Materiales de Construcción*, CSIC-Instituto de Ciencias de la Construcción Eduardo Torroja (IETCC), 64(315), e022.

[15] Phoo-Ngernkham, T., Maegawa, A., Mishima, N., Hatanaka, S., and Chindaprasirt, P. (2015). "Effects of sodium hydroxide and sodium silicate solutions on compressive and shear bond strengths of FA-GBFS geopolymer." *Construction and Building Materials*, Elsevier Ltd, 91, 1–8.

[16] Provis, J. L. (2014). "Geopolymers and other alkali activated materials: why, how, and what?" *Materials and structures*, Springer, 47(1), 11–25.

[17] Singh, G. V. P. B., and Subramaniam, K. V. L. (2019). "Influence of processing temperature on the reaction product and strength gain in alkali-activated fly ash." *Cement and Concrete Composites*, Elsevier Ltd, 95, 10–18.

[18] Singh, G. V. P. B., Subrahmanyam, C., and Subramaniam, K. V. L. (2018). "Dissolution of the glassy phase in low-calcium fly ash during alkaline activation." *Advances in Cement Research*, 30(7), 313–322.

[19] Swanepoel, J. C., and Strydom, C. A. (2002). "Utilisation of fly ash in a geopolymeric material." Applied Geochemistry, Pergamon, 1143–1148.

[20] Turner, L. K., and Collins, F. G. (2013). "Carbon dioxide equivalent (CO_2-e) emissions: A comparison between geopolymer and OPC cement concrete." *Construction and Building Materials*, Elsevier Ltd, 43, 125–130.

[21] Wang, S. D., Scrivener, K. L., and Pratt, P. L. (1994). "Factors affecting the strength of alkali-activated slag." *Cement and Concrete Research*, 24(6), 1033–1043

[22] Yang, K. H., Song, J. K., and Song, K. Il. (2013). "Assessment of CO 2 reduction of alkali-activated concrete." *Journal of Cleaner Production*, Elsevier, 39, 265–272.

[23] Zhang, H. Y., Kodur, V., Qi, S. L., Cao, L., and Wu, B. (2014). "Development of metakaolin-fly ash based geopolymers for fire resistance applications." *Construction and Building Materials*, 55, 38–45

[24] Bhagath Singh, G. V. P., and Subramaniam, K. V. L. (2020). "Evaluation of Total Reactive Oxide Ratios and Working Solution Ratios on Strength Development in Fly Ash–Based Geopolymers." *Journal of Materials in Civil Engineering*, 32(4), 04020051.

[25] Ma, Y., and Ye, G. (2015). “The shrinkage of alkali activated fly ash.” *Cement and Concrete Research*, Pergamon, 68, 75–82.

[26] ASTM C596-18. (2007). “Standard Test Method for Drying Shrinkage of Mortar Containing Hydraulic Cement.” *Annual Book of ASTM Standards*, 11(5), 1–3.

[27] ASTM C1698 (2019). “Standard Test Method for Autogenous Strain of Cement Paste and Mortar”. Annual book of ASTM Standards.

Preservation of embodied carbon with sustainable resilience corrosion protection systems

Graeme Jones[1], Chinh Van Nguyen[2], Pal Mangat[3] and Paul Lambert[4]

[1] C-Probe Systems Limited, St Helens, UNITED KINGDOM (E-mail: gjones@c-probe.com)

[2] formerly Sheffield Hallam University now The University of Danang - University of Science and Technology, Danang, Viet Nam. (E-mail: nvchinh@dut.udn.vn)

[3] Materials & Engineering and Research Institute, Sheffield Hallam University, Sheffield, UNITED KINGDOM. (E-mail: p.s.mangat@shu.ac.uk)

[4] Materials and Corrosion Technology Department, Mott MacDonald, Altrincham, UNITED KINGDOM. (Email: paul.lambert@mottmac.com)

HIGHLIGHTS

- Decarbonization of corrosion protection products
- Repurposing of industrial wastes to retrofit resilience management solutions to protect structural assets
- Long-term control and reporting of performance using embedded service life tracking online.

Keywords: corrosion, cathodic protection, AACM, resilience, preservation, embodied carbon, whole life performance

INTRODUCTION

Corrosion is responsible for 70% of infrastructure problems at a cost of over 3% of GDP for industrialized countries [1]. This study has looked at using alkali-activated cementitious materials (AACMs) produced from repurposing industrial wastes to form conductive mortars that can act as an activator for galvanic protection of reinforcement steel and as an impressed current cathodic protection (ICCP) anode retrofitted to structures.

Collaborating with Sheffield Hallam University and Mott MacDonald, data are presented that demonstrate successful performance of these in the laboratory as well as commercial uses in both reinforced concrete and transitional steel frame masonry-clad buildings.

LABORATORY TESTING

Research and development of this AACM is an extension of previous work undertaken in the 1990s at SHU focusing on the refractory features of these materials and their formulation from industrial waste streams, especially slag from steel manufacturing. Later work at SHU provided insights to the durability [2] of the AACM and its pore properties [3].

C-Probe provided industrial support to a research project at SHU to investigate the feasibility of combining the structural strengthening and electric conductivity capabilities of carbon fibre reinforced polymers (CFRPs) to produce a dual function ICCP anode [4]. The success of this project saw the evolution of the AACM formulated within the project for its use as an anode mortar material. The physical and mechanical properties of the AACM [2,3,4,5] provided comparable workability, shrinkage and compressive strengths to conventional Portland cements and concrete. The superior properties were:

1. Pore properties
2. High acid resistance
3. Ultra-low resistivity (see Figure 1 below)
4. High current capacity to 128mA/ m^2 of steel.

Therefore, the AACM could be used as a mortar and concrete anode where the repurposing of wastes can be usefully aimed at preserving structures for whole life thereby maintaining their structural integrity, value, and whole life carbon sustainably. This also lends itself to decarbonization of the corrosion protection materials, with the limited use of rare earth metal oxides and consumption of zinc [6].

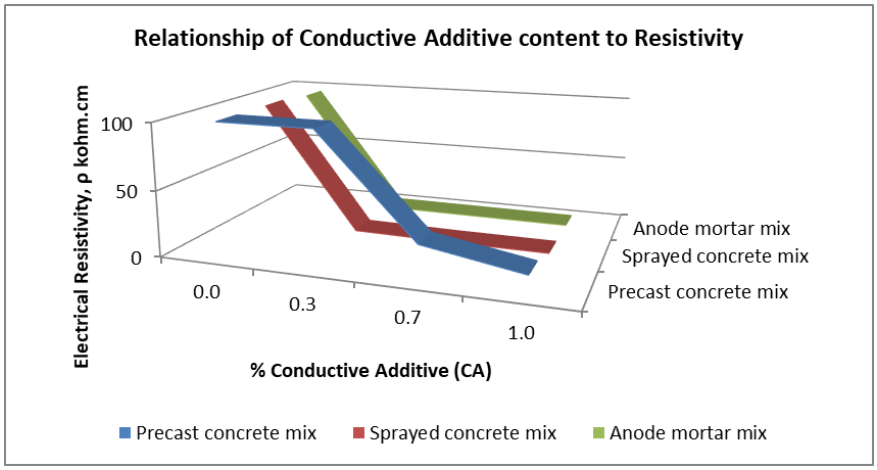

Figure 1. Measurement of resistivity of AACMs in conductive and non-conductive forms.

The site trials at Leeds Civic Hall and the first commercial use at The Commerce Bank in Kansas City to protect the main entrance using the AACM mortar within the bed joints of the stonework provided the platform for extended use on both masonry-clad and reinforced concrete structures. These case studies highlight an example from each type of construction in high profile applications of AACMs.

CASE STUDY #1 – The Helmsley Building

Transitional steel frame buildings were constructed in the era 1890 to 1950, between the lower-level load bearing masonry era and the evolution of curtain wall construction. They were designed in response to the desire to build higher than the limits of load bearing masonry as demand for city-based commercial space grew. Their construction typically allowed absorption of moisture into the stone or brick cladding and its subsequent release. However, performance was hampered by the trapping of moisture in loosely filled mason's mortar within the void space between the steel frame and the external masonry. Over time the protective coatings failed, corrosion propagated, consequently causing the movement and cracking of the masonry.

One such building to be protected from corrosion using the AACM anode mortar was The Helmsley Building on Park Avenue in New York City. Built in 1929 by Warren & Wetmore in the Beaux-arts style, it is a 35-level steel frame terracotta-clad construction with colonnades at the 29th to 32nd levels; it was these colonnades that were the target for the use of ICCP.

Performance is assessed using embedded corrosion rate probes. It is analyzed and remotely controlled in accordance with ISO12696:2022 in conjunction with service life tracking [7] by cumulative monitoring of rate of reduction of corrosion.

CASE STUDY #2 – OMNI Centre Underground Car Park

Parking structures are especially vulnerable to disrepair from the ingress of chloride ions within the concrete cover arising from the tracking-in of deicing salts from the street. Over time this causes the depassivation of the protective oxide film resulting in cracking and spalling of the structural concrete elements.

The OMNI Centre in Edinburgh is a 4-level underground reinforced concrete parking structure with an additional -5 level for incoming goods. It hosts traffic for the associated shopping centre and theatre.

A comprehensive condition survey led to the design and implementation of a multi-level corrosion management scheme targeting ICCP to Levels -2, -3 and ramps where corrosion was especially high in risk profile. The mixed use of in repair galvanic anodes with general use of surface-applied corrosion inhibitors to Levels -1 and -4 was made together with a waterproofing and trafficking membrane used for all levels for aesthetic and additional protection from future ingress of moisture and chlorides.

AACM anode mortar was used within chases grooved into the decks and ramps as well as utilizing its high alkalinity and conductive properties to activate the galvanic anodes. In addition, a localized structural beam area exposed to leaking water from street level to Level -1 was protected using a sprayed form of the AACM anode binder with aggregate to form a concrete encasement of the vulnerable beam.

All corrosion management options are monitored, remotely controlled, service life tracked and reported online to the owner on a continual basis.

CONCLUSION

A specialized development of AACMs as conductive anode materials has seen the commercialisation of laboratory tested R&D to protect assets from corrosion, for whole life value and preservation of embodied carbon in existing structures.

ACKNOWLEDGEMENTS

The authors would like to express their appreciation for the support of Sheffield Hallam University and Mott MacDonald as well as the Directors of C-Probe Group Limited for their funding of this project.

REFERENCES

[1] NACE Impact Report, Cost of Corrosion, 2016

[2] P.S. Mangat, O.O. Ojedokun, P. Lambert, Chloride-initiated corrosion in alkali activated reinforced concrete, Cem. Concr. Compos. 115 (2021). https://doi.org/10.1016/j.c

[3] P.S. Mangat, O.O. Ojedokun, Influence of curing on pore properties and strength of alkali activated mortars, Constr. Build. Mater. 188 (2018) 337–348. https://doi.org/10.1016/J.CONBUILDMAT.2018.07.180.

[4] PhD thesis, Dual function carbon fibre reinforced anodes system for concrete structures, Chinh van Nguyen, Sheffield Hallam University, 2014 and Enhanced Mentoring Internship, Sheffield Hallam University, 2015-2016

[5] Jones, G. and Lambert, P., Characterization of low-carbon AACM concrete and mortar, Concrete, The Concrete Society, November 2016.

[6] Jones G., Decarbonisation of Cathodic Protection for the Built Environment, Materials Performance, AMPP, April 2021

[7] Jones, G. and Lambert, P., Service life assessment using site accessible corrosion rate monitoring, Forensic Engineering, ICE Publishing, April 2018.

Impact of carbonation and other chemical attacks on alkali activated slag materials

C. Le Galliard[1], D. A. Geddes[2], B. Walkley[3] and J.L. Provis[4]

[1, 2, 4] Department of Materials Science and Engineering, Sir Robert Hadfield Building, University of Sheffield, Sheffield S1 3JD, UNITED KINGDOM. (E-mail: c.legalliard@sheffield.ac.uk, d.geddes@sheffield.ac.uk, j.provis@sheffield.ac.uk)

[1, 3] Department of Chemical and Biological Engineering, Sir Robert Hadfield Building, University of Sheffield, Sheffield S1 3JD, UNITED KINGDOM. (E-mail: b.walkley@sheffield.ac.uk)

HIGHLIGHTS

- This study highlights the impact of soft water leaching and carbonation on alkali activated slag microstructure.
- This study reveals the negative impact of efflorescence and carbonation on the alkali activated slag.
- This study gives new insight into ambient carbonation while explaining in detail the carbonation process for slag-based alkali activated materials.

Keywords: durability, carbonation, efflorescence, soft water leaching

INTRODUCTION

The carbonation reaction which takes place between cementitious paste in concrete and the atmospheric CO2, is an important threat to the durability of cementitious materials. It causes, in most cases, changes to the mechanical properties and a decrease of the pH which increases the risk of depassivation of the steel rebar, and its potential corrosion. This process is driven by the diffusion of CO2 in the cementitious matrix followed by its reaction with the cementitious phases. [1–3] Even though it is sometimes assumed that the chemical reactions, CO2 diffusivity as well as main controlling factors and output of the carbonation would be the same for alkali-activated materials (AAM) as for Portland cement based materials (PC), this is largely not the case. The main difference between the carbonation of PC based materials and of AAM is due to the differences in chemical composition, mainly the absence of portlandite in AAM, and the high alkali metal content in AAM pore solutions. [4] For AAMs, the CO2 diffuses first through the capillary pores of AAM. Then, the gas dissolves in the pore solution and reacts with the sodium rich phases, which leads to a drop of pH. Following this step, the calcium rich phases (if present) are decalcified and main hydrate products become carbonated, which could lead to a change of mechanical properties.[5,6]. Unfortunately, few studies have been done on the analysis of the natural carbonation of in-service alkali activated binders, due to the small amount of old in-service structures. [7]

AAMs are more likely to be subject to efflorescence than PC due to the high content of alkalis, which could be detrimental for their structures. [8] These materials are also prone to the leaching of calcium and sodium, which could affect their microstructure severely. [8,9] Although several studies have already studied the combined effect of efflorescence and leaching or efflorescence and carbonation in the laboratory, no studies have addressed the problem of the combined effects of carbonation and other chemical attacks such as leaching due to rain water or leaching in outdoor conditions, on these materials. [10] In this study, the combined effect of these attacks on the microstructure under outdoor

conditions have been compared to indoor natural carbonation.

MATERIALS AND METHODS

A ground granulated blast-furnace slag (GGBS) supplied by Ecocem (France) is used in this study. In order to perform accurate microstructural studies on the carbonation of the alkali activated slag, the samples are cement pastes. First, to prepare the alkali activator, NaOH pellets, provided by Sigma-Aldrich, are dissolved into water with sodium silicate. The ratio of activators used is 4 g NaOH/100 g GGBS and 3.86 g Na2SiO3/100 g GGBS. To achieve a water/binder ratio of 0.42, the water is added to the activators solution. The solution is then stirred at room temperature (20 ± 2°C) until the mix is homogenous before being cool down during 24 hours. The paste is mixed for 10 minutes before being set in the appropriate mould. This mould is sealed for 24 hours at 100% RH and 20 ± 2°C. After being demoulded, it is stored sealed at 20°C and 100% RH for 28 days depending on the experiments to be performed on the sample.

Finally, the samples were demoulded and placed into the different exposure conditions during a year. The samples have been carbonated in four different carbonation environments:

- Outside in Sheffield exposed to the rain, these samples were thus exposed to soft water leaching;
- Outside in Sheffield protected from the rain by a shelf, these samples were exposed to conditions causing efflorescence;
- Inside in the laboratory, where the temperature and the relative humidity (RH) were not precisely controlled (respectively 20 ± 5°C and 35 ± 15%);
- Inside a climate chamber, where the temperature and the relative humidity were controlled (respectively 20 ± 0.5°C and 30 ± 2%).

Analytical methods used to analyze the samples include X-ray diffraction (XRD) and thermogravimetry with mass spectroscopy (TG-MS), magic angle spinning (MAS) nuclear magnetic resonance (NMR) spectroscopy for aluminium (27Al) and silicon (29Si). To perform these tests, the hydration should be stop. According to Zhang et al., the most effective technique to preserve AAM microstructure while removing the free water is to exchange it by isopropanol. [11] Consequently, the samples are immersed into isopropanol for one week after being crushed into 10 mm pieces. The isopropanol solution is changed regularly during this week. Thereafter, the samples were dried in an ambient environment and then stored under vacuum at ambient temperature before performing the tests. The samples are crushed into 63 µm powder before being tested.

RESULT & DISCUSSION

The samples exposed to the weather and protected from the rain had a white deposit on their surfaces. The XRD analysis revealed that this deposit was composed of gaylussite, calcium carbonate and sodium carbonate. These products are due to the efflorescence reaction which happens when the samples sporadically have a small layer of water on their surface. This phenomenon can happen with the mist or the dew, for example. [12]

According to the XRD and TG-MS results, the non-carbonated parts of all the samples are principally composed of C-A-S-H gel and hydrotalcite. These phases are the main hydration phases for high calcium alkali activated materials. [13] According to the NMR results, the C-A-S-H present in the non-carbonated parts of the sample that was exposed to efflorescence was more cross-linked than the other samples. This result indicates that the processes causing efflorescence are also altering the main binding phase of all the sample, even the interior region that is not exposed to carbonation.

According to the XRD and TG-MS results, calcium carbonate is present in the carbonated parts of all the samples, in different polymorphs. For the sample exposed to soft water and carbonation, the XRD patterns clearly show that vaterite is the main calcium carbonate polymorph present, along with calcite in a lesser quantity. The other samples present calcite as the main carbonation products. The NMR results shows that the C-A-S-H gel is more cross-linked when carbonation is combined with soft water

leaching. The NMR results also shows that the third aluminate hydrate disappears after carbonation in every condition. This result is in agreement with observations from previous studies. [14]

CONCLUSION

The carbonation and the efflorescence leads to the formation of more cross-linked C-A-S-H and other siliceous gels. The carbonation leads to the formation of calcium carbonate with calcite as the main polymorph. Conversely, when the carbonation is combined with soft water leaching, the main polymorph is vaterite, and the C-A-S-H gel is more cross-linked than solely under carbonation.

The efflorescence under in-situ conditions leads to the formation of deposits composed of hydrated forms of calcium carbonate and sodium carbonate as well as gaylussite. The effects of efflorescence combined with carbonation are similar to the effect of carbonation alone on the carbonated part of the sample.

ACKNOWLEDGEMENT

This work was supported by the European Union's Horizon 2020 research and innovation program under the Marie Skłodowska-Curie grant agreement No 813596.

REFERENCES

[1] Hobbs, D. W. Concrete deterioration: Causes, diagnosis, and minimising risk. *Int. Mater. Rev.* 46, 117–144 (2001).

[2] Fernández Bertos, M., Simons, S. J. R., Hills, C. D. & Carey, P. J. A review of accelerated carbonation technology in the treatment of cement-based materials and sequestration of CO_2. *J. Hazard. Mater.* 112, 193–205 (2004).

[3] Papadakis, V. G., Vayenas, C. G. & Fardis, M. N. Fundamental modeling and experimental investigation of concrete carbonation. *ACI Mater. J.* 88, 363–373 (1991).

[4] Palacios, M. & Puertas, F. Effect of carbonation on alkali-activated slag paste. *J. Am. Ceram. Soc.* 89, 3211–3221 (2006).

[5] Bernal, S. A., Ke, X., Criado, M., Mundra, S. & Provis, J. L. Factors controlling carbonation resistance of alkali-activated materials. *ACI SP230*, American Concrete Institute, pp. 36.1-36.10 (2017).

[6] Shi, Z., Shi, C., Wan, S., Li, N. & Zhang, Z. Effect of alkali dosage and silicate modulus on carbonation of alkali-activated slag mortars. *Cem. Concr. Res.* 113, 55–64 (2018).

[7] Shi, C., Krivenko, P. V & Roy, D. *Alkali-Activated Cements and Concretes*. Taylor & Francis (2006). doi:10.4324/9780203390672.

[8] Yao, X., Yang, T. & Zhang, Z. Compressive strength development and shrinkage of alkali-activated fly ash–slag blends associated with efflorescence. *Mater. Struct.* 49, 2907–2918 (2016).

[9] František, Š., Vít, Š., Hlaváček, P., Kopecký*, L. & Cílová, Z. A weak alkali bond in (N,K)-A-S-H gels: Evidence from leaching and modeling. *Ceram.-Silik.* 56, 374–382 (2012).

[10] Srinivasamurthy, L., Chevali, V. S., Zhang, Z. & Wang, H. Phase changes under efflorescence in alkali activated materials with mixed activators. *Constr. Build. Mater.* 283, 122678 (2021).

[11] Zhang, J. & Scherer, G. W. Comparison of methods for arresting hydration of cement. *Cem. Concr. Res.* 41, 1024–1036 (2011).

[12] Pacheco-Torgal, F., Labrincha, J. A., Leonelli, C., Palomo, A. & Chindaprasirt, P. *Handbook of Alkali-Activated Cements, Mortars and Concretes*. Woodhead Publishing (2014). doi:10.1016/C2013-0-16511-7.

[13] Provis, J. L., Palomo, A. & Shi, C. Advances in understanding alkali-activated materials. *Cem. Concr. Res.* 78, 110–125 (2015).

[14] Sevelsted, T. F. & Skibsted, J. Carbonation of C-S-H and C-A-S-H samples studied by ^{13}C, ^{27}Al and ^{29}Si MAS NMR spectroscopy. *Cem. Concr. Res.* 71, 56–65 (2015).

Freeze-thaw behaviour of hemp reinforced geopolymer

Yuxi Lu[1], Antony Darby[1], Andrew Heath[1] and Xinyuan Ke[1]

[1] Department of Architecture & Civil Engineering, University of Bath, Bath, UK.
(E-mail: yl3639@bath.ac.uk, A.P.Darby@bath.ac.uk, A.Heath@bath.ac.uk, X.Ke@bath.ac.uk)

HIGHLIGHTS

- Hemp and other natural fibres can be used as low-carbon alternatives to synthetic fibres
- Adding hemp fibre can improve the freeze-thaw resistance of metakaolin geopolymers
- Adding hemp fibres can also improve ductility of metakaolin based geopolymers

Keywords: hemp fibre, geopolymer, freeze-thaw

INTRODUCTION

Geopolymer is an alternative sustainable binder to traditional ordinary Portland cement (OPC) materials, formed by reacting materials containing alumina and silica (such as metakaolin or other by-product materials) with alkali activators, such as sodium hydroxide and sodium silicate. However, similar to conventional building materials like OPC, while geopolymers are relatively strong in compression, they are weak in tension and have a brittle failure mode. One method to improve the ductility of a geopolymer material is to add fibres to it. There are two main types of fibre: synthetic and natural. Synthetic fibres include steel, inorganic, carbon-based and polymeric (plastic) fibres. While these fibres have high mechanical strength, they are expensive and generally have the high embodied carbon compared to the geopolymer binders. Natural fibres, on the other hand, such as animal hair, mineral, or plant fibres, can help reduce embodied carbon while still providing adequate strength and ductility enhancement. Animal fibres are difficult to collect, and mineral fibres require significant processing before application, with some having been shown to have serious health impacts (e.g. asbestos). In comparison, plant fibres can offer many benefits: low weight, low cost, low-carbon, widely available, biodegradable, renewable, non-hazardous, desirable aspect ratio, and good tensile strength.

There has been extensive research on the mechanical properties of different geopolymers. The existing research has shown the molar ratio in geopolymer paste directly influences the mechanical properties, such as strength, which subsequently affects freeze-thaw behaviour. For optimum mechanical strength, using a metakaolin precursor, Rowles and O'Connor (2003) advised that Si/Al ratio of 2-2.5 and Na/Al ratio of 1-1.5 can produce optimum mechanical properties while Lahoti et al. (2017) concluded Si/Al of 1.5-2.2 and Na/Al of 0.8-1.5 were preferable. It is shown by Yan et al., (2020) that after 50 freeze-thaw cycles, geopolymers with a Si/Al ratio of 2.62 and Na/Al ratio of 1.26 shows only a minor mass loss and strength loss but their research does not include a broad range of elemental ratios. In Yan et al.'s tests, the Si/Al ratio is varied within a fixed low-Na/Al ratio group and Na/Al is varied within a fixed higher Si/Al group. Two thirds of samples in the Si/Al group and one third of samples in the Na/Al groups broke and did not achieve any mechanical strength. To improve freeze-thaw performance, Kim and Park (2016) looked at adding plant fibre. Their research showed that compared to adding slag or latex to the mix, adding plant fibres resulted in highest residual strength after 100 freeze-thaw cycles.

The research presented in this paper investigates freeze-thaw behaviour of metakaolin based, alkali activated geopolymers. The focus is on investigating the influence of molar ratio of plain geopolymer and the optimal content of hemp fibre reinforcement for improved performance.

METHODOLOGY

Precursor and activator solutions. The geopolymer used in this research used metakaolin in the form of MetaStar® 501 from Imerys (50.5 wt.% SiO2, 45.5 wt.% Al2O3, 4.0 wt.% other minerals). Commercial sodium silicate solution (VWR) and commercial grade sodium hydroxide pellets with 98% purity and distilled water were used for the alkaline activator. The chemical composition of the sodium silicate was 9.03 % Na2O, 29.77 % SiO2 and 61.20 % water by mass. Alkaline solutions with molar ratios of SiO2/Na2O = 1.0 and H2O/Na2O = 13 were prepared by dissolving sodium hydroxide in the sodium silicate solution. Alkaline solutions were stored for a minimum of 24 h before use to allow them to cool.

Hemp fibre. Hemp fibres were used to reinforce the geopolymer. Several steps of processing were carried out before adding hemp fibres to the geopolymer paste. The first was to remove any coarse hemp shiv from the raw hemp fibres. Next, the hemp fibre was cut into lengths shorter than 12mm. After cutting, the hemp fibres were put into a commercial food blender to break down the hemp fibre bundle and produce shorter and finer hemp fibres. Finally, the blended hemp fibre was oven dried at 105 °C and then stored in sealed plastic bags to prevent deterioration from moisture or other sources.

Geopolymer synthesis. Plain (unreinforced) geopolymer samples were prepared by mixing metakaolin and activator with an SiO2/Al2O3 ratio of 1.5 used to form a homogeneous paste. During mixing, a low speed was used for the first 5 minutes followed by 5min at higher speed. For the hemp fibre reinforced samples, the paste was produced in the same manner. After mixing the metakaolin and the activator and obtaining a homogenous paste, the blended hemp fibres were added. The hemp reinforced geopolymer samples contains 5wt% hemp fibre by the mass of geopolymer paste. The composite was mixed for a further 10 min at low speed. The paste (reinforced or plain) was transferred into Nylon molds (with Teflon tape on the surfaces to prevent samples sticking to the molds, and to limit contamination from applying oil to the samples) and vibrated on a vibration table for a further 5 minutes. The samples were then sealed from the atmosphere in plastic bags. The plain activated geopolymer samples were cured at 20 °C and ambient pressure for 24 h before demolding and stored in plastic bags at ambient conditions (25–30 °C) until the date of testing. Two sample sizes were cast: thin plate samples (160 x 40 x 8 mm). The thin plate samples were cut widthwise into small cuboid pieces (40 x 15 x 8 mm) for flexural strength tests specimens.

Mechanical tests. For initial research, the small cuboid samples (40 x 15 x 8 mm), were used for both flexural (3-point bending) and compressive tests, conforming to BS EN 12467:2012 and BS EN 196-1:2016. This was done by using a 50kN displacement-controlled test machine and a 1kN load cell at their 7-day age. The applied force and displacement were recorded during both the flexural and compressive tests. A control group of small cuboid samples were tested for flexural and compressive strength. Next, following BS EN 12467:2012, another group of small cuboid samples were soaked in water for 48 hours to fully saturate the samples. After soaking, the samples were transferred into a freezer set to -20°C for 2 hours and put back into the water at 20 °C for another 2 hours. This freeze-thaw process was repeated for 100 cycles. After 100 cycles, the small cuboid samples were tested for flexural strength and compressive strength.

RESULT & DISCUSSION

Freeze thaw induced cracking

Figure 13. Images of plain, (a) and (b), and fibre reinforced, (c) and (d), alkaline activated geopolymer after freeze-thaw cycles.

Figure 13 contains the optical images of plain geopolymer (PG) and hemp reinforced geopolymer (HRG). It can be seen from Figure 13 (a) that some PG samples crack after only 2 freeze-thaw cycles (F-T cycles) and, in Figure 13 (b), all the PG specimens have cracked within 6 cycles. PG does not have any significant resistance against the F-T cycles. On the other hand, there are no visible cracks observed on HRG samples, as shown in Figure 13(c) and Figure **13**(d). Microscope images were also taken from an HRG sample at the same location after different F-T cycles. After 2 cycles, some very small cracks were visible, but the fibres limited the elongation and expansion of these cracks. With further F-T cycles, the number of small cracks increased and by 28 cycles no more cracks were generated; subsequent F-T cycles resulted only in cracks growing wider. Between 49 and 100 cycles, there was little additional growth of cracks. It is clear that the hemp fibres limited crack growth and maintained the integrity of the specimens.

MECHANICAL TESTS

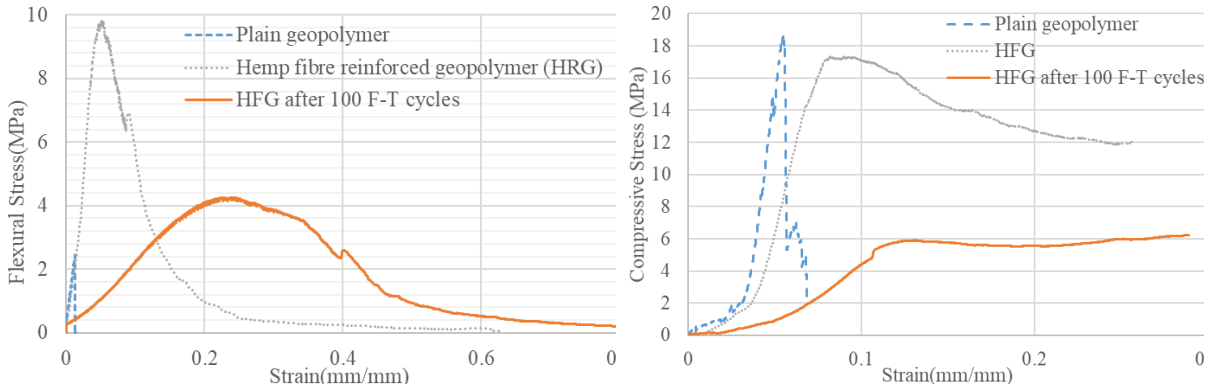

(a)Flexural stress-strain curves

(b)Compressive stress-strain curves

Figure 14. Mechanical behaviour between PG, HRG and HRG after 100 F-T cycles.

The results of flexural and compressive tests on samples before and after 100 F-T cycles are shown in Figure 14. As all the PG samples cracked and lost integrity after 6 F-T cycles, there was no mechanical testing of equivalent for PG after 100 F-T cycles. In Figure 14 (a), comparing PG and HRG before F-T cycles, the increase in flexural strength due to adding hemp fibres improves the flexural strength, with a 3-fold increase I 1n strength without affecting stiffness, and reducing brittleness after peak response. For samples with hemp fibre reinforcement subject to F-T cycles, the initial stiffness is much lower than the HRG without any F-T cycles, indicating that the geopolymer contributes significantly to the composite behaviour. Figure 14 (b) shows the results of compressive strength tests. The PG samples have a higher stiffness than the HRG samples, but the overall strength is similar with the HRG having a much more ductile failure mode. After F-T cycles, the HRG stiffness and strength reduce, but there remains significant post-peak ductility.

CONCLUSION

Adding hemp fibre to geopolymer can control crack growth and help improve the resistance to F-T action, from 6 cycles to over 100 cycles. There remains significant flexural and compressive capacity in hemp fibre reinforced geopolymer after freeze thaw cycles, and a change in failure mode from brittle to ductile, while the unreinforced geopolymer samples quickly failed under freeze thaw action. Freeze

Thaw durability is one of the main issues limiting geopolymers for sheet material applications (e.g., roofing sheets in cold climates). Adding plant fibre is therefore a promising method to maintain structural behaviour and improve durability, while ensuring low embodied carbon, using sustainable resources.

ACKNOWLEDGEMENT

Y. L. acknowledges receipt of scholarship from China Scholarship Council.

REFERENCES

Kim, H.-H.; Park, C.-G. Plant Growth and Water Purification of Porous Vegetation Concrete Formed of Blast Furnace Slag, Natural Jute Fiber and Styrene Butadiene Latex. *Sustainability* (2016), 8, 386.

Lahoti, M., Narang, P., Tan, K. H. & Yang, E.-H. Mix design factors and strength prediction of metakaolin-based geopolymer. *Ceramics International* (2017), 43, 11433-11441.

Rowles, M. & O'connor, B. Chemical optimisation of the compressive strength of aluminosilicate geopolymers synthesised by sodium silicate activation of metakaolinite. *Journal Of Materials Chemistry* (2003), 13, 1161-1165.

Yan, D., Xie, L., Qian, X., Ruan, S. & Zeng, Q. Compositional Dependence of Pore Structure, Strengthand Freezing-Thawing Resistance of Metakaolin-Based Geopolymers. *Materials* (2020), 13, 2973.

The effect of phosphorus oxide content in precursor on setting time and freeze-thaw resistance of alkaline-activated binders

Piotr Prochoń[1], Dominika Stańczak[2]

[1, 2, 3] Faculty of Civil Engineering, Warsaw University of Technology, POLAND.
(E-mail: piotr.prochon@pw.edu.pl, dominika.stanczak@pw.edu.pl)

HIGHLIGHTS

- Up to 3% addition of P_4O_{10} the freeze thaw resistance is not affected in AAMs.
- P_4O_{10} addition demonstrates its potential as an effective setting time accelerator for AAMs.
- The higher addition of P_4O_{10} to mortars causes a decrease of their freeze-thaw durability.

Keywords: AAMs, phosphorus oxide, setting time, freeze-thaw resistance

INTRODUCTION

As a result of increased use of biomass as a bioenergy source, the new type of waste materials derived from its solely combustion named biomass fly ash (BFA) occurred. Since BFA characteristics is directly related to the source and species of the biomass used as feedstock the composition of it will define properties, quality and application perspectives [1]. A possible beneficial reuse of BFA is to use it as a precursor for preparation of alkali-activated materials, an alternative binder with comparable mechanical and durability properties to OPC composites.

The effects of impurities in the chemical composition of geopolymerization precursors like P4O10 have not been fully studied. The current state of knowledge on the impact of phosphorus compounds on the geopolymerization process allows us to conclude that to date, no comprehensive program of fundamental studies, devoted to the analysis of the effects of phosphorus oxide on the properties of alkali-activated materials has been conducted.

MATERIALS & METHODS

Geopolymer mortars are prepared by mixing two types of Fly Ash (FA), from combustion of coal (RFA) and from combustion of wood biomass (BFA) in ratio 7:3 (see Table 1). FA is activated with an aqueous hydroxide solution with NaOH/Na2SiO3 ratio equal to 2.7. Tetraphosphorus decaoxide (P4O10) is added to FA before its alkali-activation. The standard sand is used as an aggregate. 40 x 40 x 160 mm beam samples are prepared and formed according to a modified procedure from PN-EN 196-1. Raw material is mixed in first 30s with sand and during next 30s an activating solution is added. Further procedure is similar to the description in the standard EN 196-1. Prepared samples are demoulded after 24 hours, cured firstly in an oven at 65°C for 48 hours and secondly kept in laboratory conditions until testing.

Table 1. Mortar composition in the experiment plan.

Sample	Components			
	FA (RFA + BFA) [g]	Alkaline Activator [g]	P_4O_{10} [g]	Natural sand [g]
P0	2250 (1575 + 675)	1464	0	3375
P1	2250 (1575 + 675)	1464	22.5	3375

P3	2250 (1575 + 675)	1464	67.5	3375
P5	2250 (1575 + 675)	1464	112.5	3375

The setting time is performed in accordance with EN 480-2. The time is measured from the moment the dry mortar components are mixed with the alkaline solution. Measurements of Vicat apparatus needle immersion are performed at a frequency not less than 3 per 1h.

The freeze-thaw resistance test is performed according to PN-85/B-04500. The saturated samples are placed in freeze-thaw chamber for 25 cycles. One complete cycle is 4h in water at temperature 20 ± 5 °C and 4h of freezing at temperature −20 ±5 °C. The freeze-thaw cycles are finalized when the samples showed in visual inspection degradation patterns. The freeze-thaw resistance is analyzed by either the number of cycles that mortar sustain or the compressive strength loss comparing to reference samples through equation:

$$R_m=(1-(R_f-R_r)/R_r\ )*100$$

Where,

R_m – residual compressive strength after freeze/thaw test, %,

R_f – compressive strength of sample after freeze/thaw test, MPa,

R_m – compressive strength of reference sample, MPa.

RESULTS & DISCUSSION

The initial setting time of the samples decreased with the increase of P4O10 content and changed from 310 min for the reference sample (P0) to 120 min for P5 sample (see Figure 1). Similar change is observed for the final setting time – from 410 min for P0 to 200 min for P5. The time reduction between those two mortars was more than 61% for the initial setting time and almost 52% for the final setting time. It can be connected with the change of mix temperature due to exothermic reaction of P4O10 with liquid alkaline solution. It was confirmed by other researchers that proper geopolymerization is at curing temperature between 60°C and 90°C and it promotes the formation of a more cross-linked binding, with a denser microstructure of the binder [2][3].

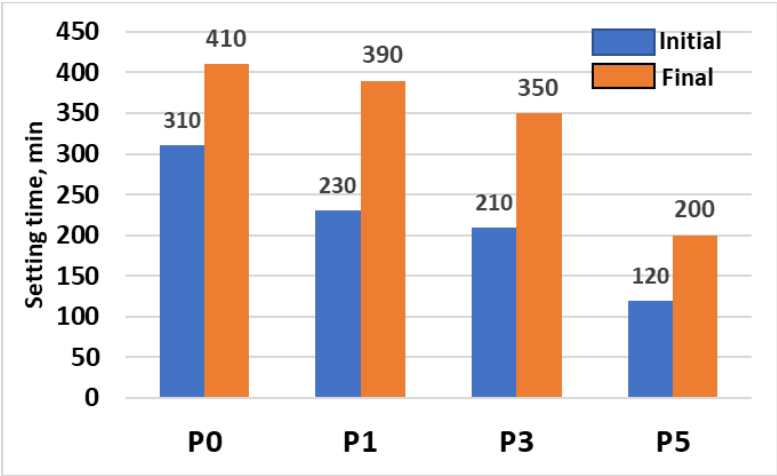

Figure 1. Setting time results for mortars with different level of P_4O_{10}.

After 25 freeze-thaw cycles, no disruption or deformation could be detected in the P0 and P1 mortars. The compressive strength losses for those samples were below 23% and 35%, respectively. Further addition of P4O10 to alkali-activated mortars caused a decrease of their freeze-thaw durability. The compressive strength values for P3 mortar were reduced by almost 50% after 25 cycles of freeze-thaw test. The largest influence of freeze-thaw test on the integrity of the samples structure was observed

for samples P5, which sustained only 21 cycles. The strength losses could not be measured as the P5 samples collapsed during removing them from the freeze-thaw apparatus. The weaker performance of samples with 3% and 5% of P4O10 can be connected with the existence of soluble chemical compounds in their matrix that increased the water permeability in the material structure affecting the frost resistance of the composite as mentioned by Temuujin et al [4].

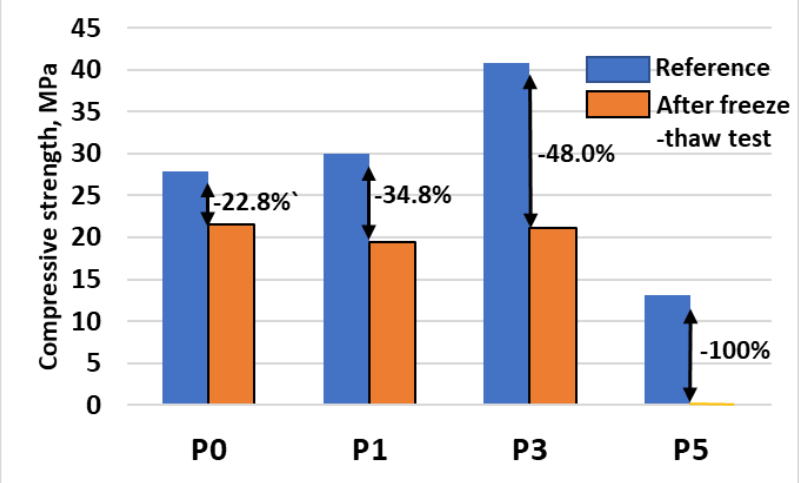

Figure 2. Results of freeze-thaw test with 25 cycles.

CONCLUSION

The alkali-activated samples containing P4O10 showed a substantial change in initial setting time in comparison to reference samples. The addition of P4O10 in the AAMs worked as accelerator due to its exothermic reaction with the liquid solution. Adding up to 3% of P4O10 to the AAMs increases strength, decrease the setting time and does not reduce freeze-thaw resistance. This P4O10 may be provided by the addition of biomass fly ash. The effect of phosphate content in the fly ash AAMs mixtures needs to be further investigated with different precursors.

ACKNOWLEDGEMENT

The authors would like to express their appreciation for the support of the National Science Center Project Preludium 16 No 2018/31/N/ST8/02276 and Faculty of Civil Engineering WUT.

REFERENCES

[1] Rajamma R., Ball R.J., Tarelho L.A., Allen G.C., et al. Characterisation and use of biomass fly ash in cement-based materials, J. Hazard. Mater., 172 (2), 2009, p. 1049-1060;

[2] Khale D., Chaudhary R., Mechanism of geopolymerization and factors influencing its development: A review, Journal of Materials Science, 42, 2007, p. 729-746;

[3] de Vargas A.S., Dal Molin D. C. C., Vilela A.C.F., et al., The effects of Na2O/SiO2molar ratio, curing temperature and age on compressive strength, morphology and microstructure of alkali-activated fly ash-based geopolymers, Cement and Concrete Composites, 33(6), 2011, p. 653-660;

[4] Temuujin J., Minjigmaa A., Davaabal B., et al., Utilization of radioactive high-calcium Mongolian flyash for the preparation of alkali-activated geopolymers for safe use as construction materials. Ceramics International, 40(PB), 2014, p. 16475–16483

Effects of Mg on the reactivity of CaO-MgO-Al_2O_3-SiO_2 glasses in the sodium silicate activated systems

Taehwan Kim[1], Abdelrahman Hamdan[2] and Ailar Hajimohammadi[3]

[1, 2, 3] Centre for Infrastructure Engineering and Safety, School of Civil and Environmental Engineering, UNSW Sydney, Australia.
(E-mail: taehwan.kim@unsw.edu.au, a.hamdan@unsw.edu.au, ailar.hm@unsw.edu.au)

ABSTRACT

Great attention has been paid to understanding and predicting the reactivity, microstructural development, and mechanical and durability properties of alkali-activated materials (AAMs). Numerous factors (including types of precursor, type of activator, modulus ratio, mix proportion, and curing method) can affect these properties of AAMs but one of the most important factors would be the physicochemical and mineralogical properties of precursors. The use of industrial slags to study the effect of glass chemistry on the reactivity of alkali-activated systems has shown contradictory results. In this study, a novel synthesis approach (organic steric entrapment) was used to synthesize chemically controlled CaO-MgO-Al2O3-SiO2 (CMAS) glasses. In these synthetic glasses, either Ca or Al was replaced with Mg to investigate the role of Mg on the reactivity and microstructure development. The effects of the substitution of Ca/Al by Mg on glass structures were characterised using 29Si and 27Al NMR. Sodium silicate-activated synthetic glasses were analyzed using isothermal calorimetry and in-situ Fourier transformation infrared (FTIR) spectroscopy. The microstructure development was studied using X-ray diffraction (XRD), thermogravimetric (TG) analysis and nitrogen gas adsorption (NGA) techniques.

When more Mg replaces Ca in the glass, the initial reactivity was delayed, and the reaction products (C-A-S-H) were highly polymerised disordered C-A-S-H. However, if Mg replaced Al (network former), the initial reaction rate was accelerated in the CMAS system and the types of reaction products also significantly changed as a function of the contents of Al2O3 and MgO. This indicates that the effect of MgO on the reactivity in AAMs has to be considered along with the variations of other oxides such as Ca, Al, and Si. This study provided a better understanding of the effect of the chemical composition of the CMAS phase by elucidating the effect of Al replacement by Mg.

Degradation of alkali-activated slag mortars subjected to accelerated leaching

Thi Nhan Nguyen[1,4], Quoc Tri Phung[1], Lander Frederickx[1], Diederik Jacques[1], Alexandre Dauzeres[2], Jan Elsen[3], Yiannis Pontikes[4]

[1, 2, 3, 4] Institute for Environment, Health, and Safety, Belgian Nuclear Research Centre (SCK•CEN), MOL, BELGIUM. (thi.nhan.nguyen@sckcen.be, quoc.tri.phung@sckcen.be, lander.frederickx@sckcen.be, jacques.diederik@sckcen.be)

[2] Institute of Radiation protection and Nuclear Safety (IRSN), FONTENAY-AUX-ROSES, FRANCE. (alexandre.dauzeres@irsn.fr)

[3] Department of Earth and Environmental Sciences, KU Leuven, LEUVEN, BELGIUM. (jan.elsen@kuleuven.be)

[4] Department of Materials Engineering, KU Leuven, LEUVEN, BELGIUM. (yiannis.pontikes@kuleuven.be)

HIGHLIGHTS

- The effect of water-to-binder ratios on the leaching resistance in 6M NH_4NO_3 of alkali activated slag mortars was investigated.
- C-A-S-H gel was much more siliceous, and the microstructure of the mortars was coarser after leaching.
- The higher the water-to-binder ratio, the more Ca-leaching, the more cross-linked gel, and the coarser the microstructure.

Keywords: alkali activated slag, leaching, water-to-binder ratio

INTRODUCTION

Alkali activated slag (AAS) is an amorphous aluminosilicate material consisting mainly of C-A-S-H gel with a considerably high pH of approximately 12-13. Alkali and earth-alkali ions (e.g., Na^+, K^+, and Ca^{2+}), besides contributing to the alkalinity of the pore solution, serve as the charge-balancing ions for the Al^{3+} in the C-A-S-H gel [1]. The alkali ions are potentially leached out of the AAS matrix when the materials are exposed to acidic or even neutral environments, leading to the dissolution and consequently degradation of the C-A-S-H gel. Because of the absence of portlandite, a lower Ca/Si ratio of C-A-S-H gel, and a low porosity of the matrix, AAS is expected to be much more stable in acidic media than conventional cementitious materials [2].

Few studies have published on the alteration in AAS properties immerged in a 6M NH_4NO_3 solution (pH ~ 4.25). For example, Komljenovic et al. [3] reported the leaching of sodium and the decalcification of C-A-S-H gel, and strength reduction of AAS paste after up to 90 days of leaching. Varga et al. [4] investigated the effect of slag composition on the evolution of the gel structure of AAS paste after 21 days of immersion in a 6M NH_4NO_3 solution, and found that the C-A-S-H gel was more stable if slag precursor contained a lower MgO and higher Al_2O_3 content. As a consequence of the decalcification, the microstructure potentially change after leaching; however, its alteration has not been widely reported in literature. Furthermore, although the leaching process also depends significantly on the

microstructure of AAS as it controls the diffusion of ions from the solution into the matrix, studies on how microstructure influencing the leaching process are still rare. Furthermore, the water-to-binder (w/b) ratio is known as one of the primary parameters affecting the microstructure of AASs, however, the effect of this parameter on the leaching resistance and microstructure after leaching of AAS remains a topic of active research.

In order to address the gap in understanding the correlation between the microstructure of AAS and its leaching resistance in the concentrated NH4NO3 solution, this study aims to investigate the alteration of the C-A-S-H gel and the microstructure of AAS mortars after 28 days of leaching in a 6M NH4NO3 solution, with a focus on the effect of the w/b ratio. Different of techniques, including inductive coupled plasma-optical emission spectrometry (ICP-OES), 29Si magic-angle spinning nuclear magnetic resonance (MAS-NMR), and mercury intrusion porosimetry (MIP), have been used to provide information on and insight in the evolution of the AASs structure.

MATERIALS & METHODS

AAS mortars with three w/b ratios of 0.35, 0.45 and 0.55 were produced from granulated blast furnace slag GGBFS (Ecocem Benelux), solid NaOH pellets (99% purity, VWR Chemicals), and solid sodium silicate from VWR Chemicals (consisting of 8.97% Na2O, 26.78% SiO2, 64.25% H2O). First, the activating solution was prepared by mixing NaOH, sodium silicate, and water until achieving a homogeneous activating solution, which was then stored during 24h in order to reach equilibrium prior to use. Then, GGBFS was mixed with the alkaline solution, extra water for adjusting the target w/b ratios, and finally river sand was added (<2 mm and a density of 2.67 g/cm3) as the fine aggregate. After casting, samples were cured for 28 days at 20 ℃ in a sealed condition, and then saturated in water under a reduced pressure for 24h prior to the leaching test. To proceed the leaching test, samples were immersed in the nitrate solution contained in leaching vessels. After 28 days of leaching, the leachate solution and specimens of “leached” AASs (within 3 mm from the exposed surface of samples) were subjected to characterization.

RESULTS & DISCUSSION

The main elements leached out of AASs were alkali (Na and K) and alkaline earth (Ca and Mg) elements (measured by ICP-OES). Sodium was the most leachable element of AASs instead of Ca as is the case for the leaching of OPC [5]. This attributes to the difference in chemical composition and phases between these materials. Once the pH of the pore solution drops due to the migration of H^+/NH_4^+ to the matrices, $Ca(OH)_2$ in OPC is initially dissolved and consequently released Ca to the surroundings [6], whereas Na in the pore solution of AAS is potentially leached out first. After 28 days of exposure, about 5 wt.%, 6 wt.%, and 8 wt.% of Na was leached from AAS with w/b ratios of 0.35, 0.45, and 0.55, respectively. In this study, the percentage of Ca leached from AAS, known as decalcification, was much lower than from OPC, approximately 2 wt.% from AAS 0.35 comparing to more than 6 wt.% from OPC [6] after 28 days of leaching under the same conditions. Notably, the amount of two main elements (Si and Al) structuring the C-A-S-H gel was very limited in the NH_4NO_3 solution, raising the question of whether the gel structure changes during leaching.

To understand the alteration of C-A-S-H gel induced by the leaching, ^{29}Si NMR measurements were applied on AAS mortars before (AAS) and after 28 days of leaching (L-AAS), as shown in Figure 15. Before leaching, the main Si sites of AAS samples were Q^1 as non-bridging silicates and Q^2 representing the paring conditions of the C-A-S-H gels. Observation of two separated Q^2 groups could be attributed to the difference in the chemical environment surrounding those Si sites. Furthermore, a limited amount of Q^3(1Al) groups at around -88 ppm indicated a less cross-linked C-A-S-H structure of the reference AASs. After 28 days of leaching, a significant shift to lower resonances (Q^3 and Q^4) was observed in all samples, in which the intensity of Q^3 and Q^4 in the leached AAS with higher w/b ratio was higher as indicated by deconvoluted ^{29}Si NMR, suggesting a much higher cross-linked structure of C-A-S-H. Multiple Q^2 groups, especially the presence of a new intense Q^2 at ~81 ppm, indicated a complicated chemical environment surrounding Q^2, potentially caused by a partial replacement of Na^+

and Ca^{2+} by H^+ and NH_4^+ in the charge balancing role for C-A-S-H gel.

As expected, the porosity and pore size distribution (PSD) of AAS in the meso-macro pore range were changed after leaching, as shown by MIP. A significant increase in the porosity of all samples due to the leaching was observed, i.e. an increase of 30% in AAS 0.45. The PSD also shifted to a larger pore size range, in which the gel pores fraction was reduced and replaced by the predominant capillary pores. The w/b ratio affected vastly on the microstructure of AAS, i.e. approximately two- and four-times higher porosity with the increase in w/b ratio from 0.35 to 0.45 and 0.55, respectively. Consequently, the later samples were coarser after leaching because the leaching was more accelerated in a higher w/b ratio AAS than the samples with a lower w/b ratio.

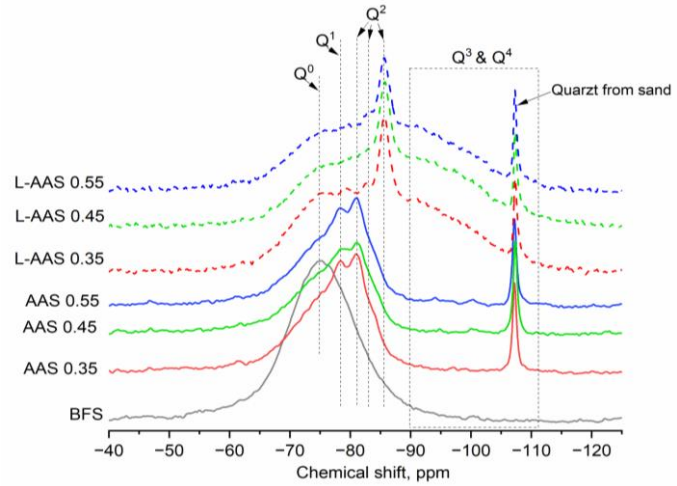

Figure 15. ^{29}Si NMR spectra of AASs with different w/b ratios before (AAS) and after 28 days of leaching (L-AAS) in 6M NH_4NO_3 solution for different w/b ratios

CONCLUSION

This study investigated the alteration of the nano-micro structure of AAS induced by leaching in a 6M NH_4NO_3 solution for 28 days, with a focus on the influence of the w/b ratio. The following conclusions were drawn:

- Sodium was the most leachable element in the AAS, but only ~5 wt.% of Na was leached out of AAS with a w/b ratio of 0.35 after 28 days of leaching.
- Decalcification of C-A-S-H gel resulted in a more cross-linked (siliceous) structure with a dominant Q^3 and Q^4 instead of Q^1 and Q^2 units. An increase in porosity and a shift to a larger pore size range of the pore size distribution were observed in all AASs.
- The impact of leaching became more intense in the AAS with a w/b ratio higher than 0.45.

ACKNOWLEDGEMENT

The authors would like to express our appreciation for the support of the European Union's Horizon 2020 research and innovation programme for Nuclear Fission and Radiation Protection Research (Call NFRP-2019-2020) under grant agreement No. 945098 (PREDIS). This work has also received funding (in parts) from the Belgian Energy Transition Fund (ASOF project) and IRSN (France).

REFERENCES

[1] Nguyen, T.N., Phung, Q.T., Yu, Z., Frederickx, L., Jacques, D., Sakellariou, D., Daurezes, A. and Pontikes, Y. Alteration in molecular structure of alkali activated slag with various water to binder ratios under accelerated carbonation. Scientific Reports 12(2022), 1-16.

[2] Aiken, T.A., Gu, L., Kwasny, J., Huseien, G.F., McPolin, D. and Sha, W. Acid resistance of alkali-activated binders: A review of performance, mechanisms of deterioration and testing procedures. Construction and Building Materials 342(2022).

[3] Komljenovic M.M., Bascarevic. Z., Marjanovic, N. and Nikolic, V. Decalcification resistance of alkali-activated slag. J Hazard Mater 233-234(2012),112-21.

[4] Varga, C., Alonso M.M., Mejía de Gutierrez, R., Mejía, J. and Puertas, F. Decalcification of alkali-activated slag pastes. Effect of the chemical composition of the slag. Materials and Structures 48(2014), 541-55.

[5] Phung, Q.T., Maes, N., Jacques, D., De Schutter, G. and Ye, G. Investigation of the changes in microstructure and transport properties of leached cement pastes accounting for mix composition. Cement and Concrete Research. 79(2015), 217-34.

[6] Jacques, D., Phung, Q.T., Perko. J., Seetharam, S.C., Maes, N. and Liu, S. Towards a scientific-based assessment of long-term durability and performance of cementitious materials for radioactive waste conditioning and disposal. Journal of Nuclear Materials (2021), 557.

3. Structural behaviour and design

LIST OF CONTRIBUTIONS

Keynote lecture:

Extended abstracts:

A future low-CO_2 cement industry shaped by industrial experience and research perspectives

Prof. Jannie S.J. van Deventer[1]

[1] Zeobond, AUSTRALIA. (E-mail: jannie@zeobond.com)

KEYNOTE SUMMARY

Zeobond has applied alkali-activated materials (AAMs) extensively in Australia from 2006 to 2018. It was possible to produce concrete with high durability, satisfactory workability, strength development and engineering properties. The key to success was the availability of the right source materials and proprietary admixtures, hence low additions of alkali activators were used. Excessive alkali addition leads to poor durability and high creep, even when satisfactory strength development can be achieved. Low reactivity of precursors should not be addressed by addition of concentrated alkalis, as is too often the case. Instead, strength development should be enhanced by reducing the potential across the electric double layer and by promoting nucleation through manipulation of the pore solution composition. With the focus on CO_2 reduction, AAM is attracting increasing attention, but researchers often under-estimate the complexity of the AAM system and the interplay between surface chemistry, rheology, the kinetics of dissolution of precursors and the formation of binding phases. AAM should not be viewed as a different class of binder; instead, it should be viewed as a continuum of other binders, including Portland cement (PC), blended cements, limestone-calcined clay cement (LC^3) and supersulphated cements.

In 2018, Zeobond was unable to source the right precursor materials and admixtures required to produce quality AAM. Subsequently, new binders have been developed that are compatible with source materials in the cementitious supply chain and that meet the existing standards and design codes. The CO_2 reduction compared with PC is still 80% for the cementitious content and 60% for reinforced precast concrete elements. Despite extensive testing, the market still questions the durability of new binders. The carbonation resistance of concrete containing high levels of supplementary cementitious material (SCM) is usually lower than for PC in accelerated tests, despite the beneficial chloride resistance. It remains a challenge to relate accelerated testing to steel corrosion and in-service performance, which also underpins the reluctance to widely adopt performance-based standards in place of the prescriptive standards that present a major obstacle to the adoption of low-CO_2 concrete. Substantial progress is being made in Australia to address these shortcomings.

The future of low-CO_2 cement lies in the synthesis of new SCMs from primary and secondary resources by adjusting their composition. Synthetic SCMs will create a new value chain by replacing the dwindling supplies of blast furnace slag and coal fly ash as the steel and energy sectors decarbonise. Zeobond is working towards the development of mobile electrically-enhanced supersonic shockwave reactors that produce powders directly without grinding. By rapid quenching through a venturi, the glassy phase is preserved that gives a high pozzolanic activity, with or without activation. This strategy to supply cementitious powder to concrete batching plants minimises loss of intellectual property compared with the blending of various components at concrete plants.

Influence of the fibre addition on shrinkage and pull-off bond strength of binary alkali-activated repair mortar made of blast furnace and copper slag

Ivana Krajnović[1], Stijn Matthys[1]

[1] Magnel-Vandepitte Laboratory for Structural Engineering and Building Materials, Ghent University, BELGIUM. (E-mail: ivana.krajnovic@ugent.be, stijn.matthys@ugent.be)

Keywords: alkali-activation, textile reinforcement, shrinkage mitigation, repair mortar

INTRODUCTION

Rehabilitation of structures in the built environment are of prime importance in many countries around the world, and relates amongst other to structural strengthening, restoration of serviceability and durability deficiencies, or improvement of the aesthetical appearance. Repair mortars widely used in rehabilitation are high-end products that come with significant costs and high amounts of Portland cement (PC) in comparison to regular mortars. With high amounts of cement comes also the increase in environmental footprint which is becoming more and more of concern for a sustainable society. In this respect, the interest in alkali-activated materials is increasing, given their potential for being environmentally friendly, as well as having high mechanical and durability performance. Relatively high shrinkage is one of the biggest obstacles for the utilisation of AAMs as repair mortar. In this paper different ways of reducing shrinkage of alkali-activated mixtures are adopted and their influence on autogenous and total shrinkage, as well as pull-off bond properties are examined.

MATERIALS AND METHODS

The precursors used in this study are blast furnace slag (type eco2cem, EcoCem) and iron-silicate slag (copper slag, type Koranell, Aurubis). Aggregate in this study is quartz sand (type M31, Sibelco). A combination of sodium silicate (45 wt% concentration, molar ratio (MS) 2.0 Crystall 112, PQ) and potassium hydroxide (with purity ≥ 85%, Brenntag), is used to prepare activating solution with MS of 1 and concentration of metal ions of 6.7% per weight of the precursors.

Table 11. Overview of the used materials.

	BFS [g]	ISS [g]	Sand [g]	Crystal 112 [g]	KOH [g]	Water [g]	addition
Mix 1	300	300	1200	96	31	172	-
Mix 1 + PPF	300	300	1200	96	31	172	PPF (0.5 vol%)
Mix 1 + GF	300	300	1200	96	31	172	GF (0.5 vol%)
Mix 1 + Glass Textile	300	300	1200	96	31	172	2 layers glass textile
Mix 1 + Carbon Textile	300	300	1200	96	31	172	1 layer carbon textile
Mix 2	270	270	1200	96	31	172	60g MK
Mix 1 + SRA	300	300	1200	96	31	172	SRA 3 (wt%)

The precursors used in this study are blast furnace slag (type eco2cem, EcoCem) and iron-silicate slag (copper slag, type Koranell, Aurubis). Aggregate in this study is quartz sand (type M31, Sibelco). A combination of sodium silicate (45 wt% concentration, molar ratio (MS) 2.0 Crystall 112, PQ) and potassium hydroxide (with purity ≥ 85%, Brenntag), is used to prepare activating solution with MS of 1 and concentration of metal ions of 6.7% per weight of the precursors.

Different variants of the alkali-activated mortar are compared, considering different potential ways to

improve the shrinkage, as indicated in Table 1. This included the addition of short fibres; 0,5 vol% polypropylene (length 6mm provided by SIKA) or glass fibres (length 6mm, type CEM FILL, provided by Owens Corning); the use of textile reinforcement (two layers of a balanced mesh of epoxy coated glass fibre textile or one layer of balanced carbon fibre mesh); the use of of a curing compound (type SIKA Antisol MP-10) applied on the surface; replacement of 10% of the blast furnace slag by a metakaolin (type Metastar 501, provided by Imeris); or the use of a shrinkage reducing admixture (SRA) (type SIKA control-50). This research used tiles of 300x300x10 mm to perform shrinkage measurements, by means of mechanical deformeters (type DEMEC) with gauge length of 200 mm.

These dimensions are chosen similar to the restrained shrinkage specimens (used for pull-off bond testing) that consisted of a 10 mm mortar layer on a sand blasted concrete substrate of 300 mm x 300 mm. Measurements were taken daily during 28 days after casting. In what follows, all specimens are tested on autogenous shrinkage (on sealed specimens) and total free shrinkage (on non-sealed specimens). The bond strength is tested by pull-off tests, to verify possible influence of the shrinkage on the bond quality between the overlay and the concrete substrate.

Specimens are cast within lab conditions, stored for one day at a relative humidity of 95% and a temperature of 20°C, demoulded after 24 hours and stored at 65% relative humidity and a temperature of 20°C. Shrinkage is then measured for 28 days. Three plates are cast for autogenous shrinkage and subsequently sealed in aluminium tape. Same procedure without sealing is followed for the total shrinkage plates. The restrained overlays are cast onto 5 months old substrates. The pull-off tests were done when specimens had an age of 56 days. Norm EN 1542 [1] is followed. 5 cores of diameter 50 mm are drilled on which dollies are glued with epoxy. Next, these cores are pulled from the substrate and the rupture stress and failure aspect are recorded.

RESULTS

1) Autogenous shrinkage

The results of the autogenous shrinkage tests are presented in Figure 16 a). SRA reduced shrinkage at 28 days for 21%, and that is the only reduction. As can be seen, basic mix (Mix1) shows lower autogenous shrinkage than most of the other mixes. Possible explanation for it can be that due to absorption and coating/film formation around the fibres or textiles less excessive liquid will be available to fill the microstructure of the binder matrix. This will lead to higher capillary pressure within the microstructure of the material, and ultimately to more contraction (shrinkage) of the material. Similar phenomena is earlier noted in PC fibre reinforced concrete with steel fibres [2]. It can be noted that the addition of the metakaolin actually increases shrinkage, which is in contrast with previously published work [3]. Metakaolin used in this study is a very fine high grade commercial additive for concrete (high purity amorphous pozzolan), which might be the reason for this difference. The mix with glass fibres tend to follow similar behaviour (after 14 days) compared to that of the mixes with embedded textiles, since the mass of fibres which are added is roughly the same (45g) to mass of textile added (46g). Mixes with the PP fibres shows the least shrinkage, but still higher autogenous shrinkage than the reference. This might be due to the combined effect of PP being of hydrophobic nature and the aforementioned film effect.

2) Total shrinkage

The results of total shrinkage can be seen in Figure 16b. Generally high shrinkage is noted, in the order of magnitude of 300 to 500 microstrain, similarly to [4]. The tile-shape of the shrinkage specimen and the way they were stored in the climatized room, caused uneven drying of the specimens. Due to the high evaporation rates, it might happen that specimens slightly curved, though this was not observed in a pronounced way. Given this difference between the autogenous and total shrinkage specimens, it was decided not to further express the drying shrinkage by subtracting the autogenous from the total shrinkage. In terms of total shrinkage the following is observed. The total shrinkage rate is highest at the early age of the material as can be noticed by the steepness of the curves. The shrinkage reducing admixture proves effective with 50% less total shrinkage compared to the reference mix at the age of

28 days. Furthermore, the trend indicates that shrinkage is almost fully achieved for the mix with SRA, while this is not the case e.g. for mixes Mix1, Mix1+PP, Mix1+GF. The mix with metakaolin shows the highest total shrinkage, extending on the high shrinkage trend also observed for the autogenous test. The mixes that contain short fibres show slightly (about 90 microstrain) higher total shrinkage than the reference mix, mainly in-line with their higher observed autogenous shrinkage. This can be explained by absorption and coating/film formation around the fibres, as also has been observed in other fibre reinforced mixes [5]. On the other hand, increased total shrinkage might also be associated to potential higher porosity of fibre mixes, that fosters higher shrinkage.

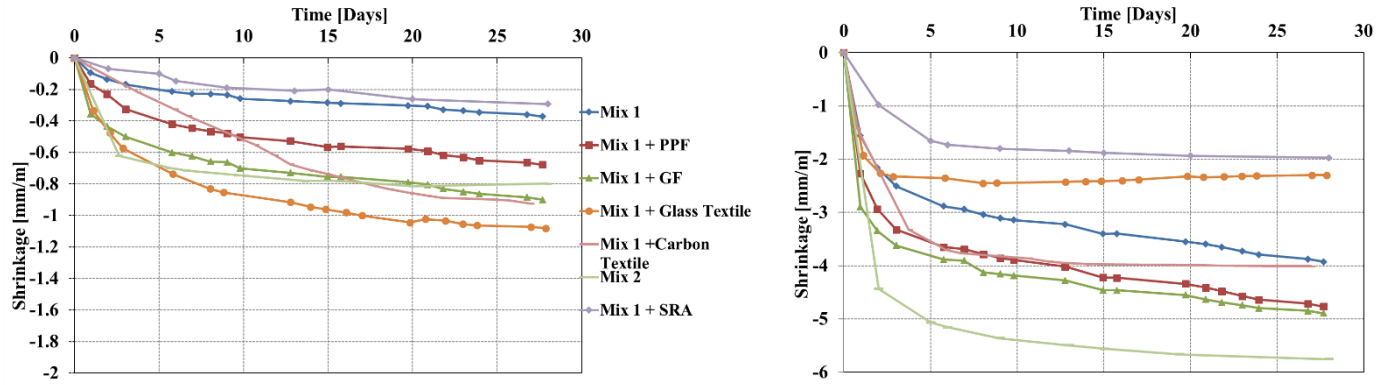

Figure 16. Autogenous (a), and total (b) shrinkage of AAM plates.

For both mixes with textiles the total shrinkage is close to that of the reference mix, which is opposite to the autogenous shrinkage. These mixes also seem to reach their ultimate shrinkage already after 2 weeks.

3) Pull-off bond strength

Results of the pull-off bond strength of the different mixes are presented in **Figure 17**. By adding fibres or textiles to the mix, improved bond strength has been observed, compared to the reference mix that had extremely low bond strength (the latter being compromised by restrained shrinkage induced stresses and cracking of the overlay). Due to introduction of fibres stress redistribution might take place, that positively influences the bond interaction. The failure plane occurred in the overlay for glass fibres, where the interface between overlay and substrate failed for the PP fibres. The mixes with textiles performed comparable to the glass fibre reinforced mixes and clearly better than the reference mix. Application of a curing compound on specimens for bond pull-off testing was observed to reduce the amount of restrained shrinkage induced cracking and associated bond strength of the reference mix. Except the reference and the mix with glass textile, the curing compound had rather a negative effect on bond strength. At the other hand, for the (ambient cured) mixes with fibres or textiles, a finer crack distribution was observed, indicating crack bridging behaviour and associated limitation of restrained shrinkage cracking.

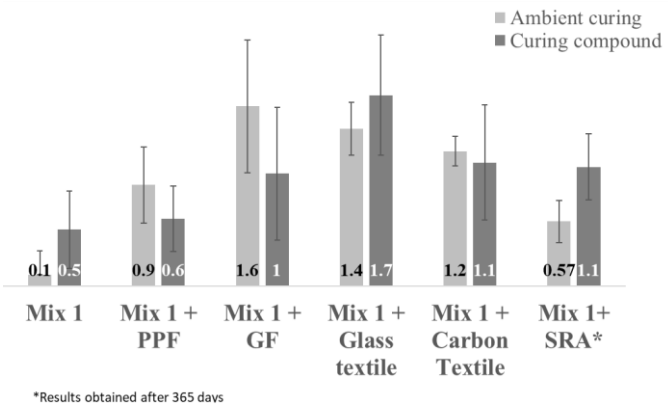

Figure 17. Pull-off bond strength test results (values in MPa).

CONCLUSIONS

The addition of fibres or textiles leads to a higher amount of autogenous shrinkage since less water is present in the system due to coating/absorption of the fibres. This leads to higher capillary pressure within the material, hence more shrinkage. In contrast to previous studies, the use of the particular metakaolin in this study lead to higher autogenous and total shrinkage. Usage of a shrinkage reducing admixture leads to lower autogenous and total shrinkage, that is beneficial to reduce restrained shrinkage induced stresses. Use of fibres might lead to lower workability. For thin overlays this may raise questions about the surface finishing. A more open structure is created through which more water can evaporate, thus higher overall shrinkage. Use of fibres leads to more smaller and distributed cracks, positively influencing the bond strength. Mix designs incorporating textiles observed similar trends as the mixes with short fibres, and were observed to have even more pronounced distributed cracking behaviour and associated restrained shrinkage crack bridging. Using a curing compound for the reference mix, appeared beneficial for the bond strength (due to reduced restrained shrinkage effects). Fibre or textile reinforced mixes in this study had however a more favourable effect on bond strength, and combination of curing compound and fibres/textiles was observed of no additional value.

ACKNOWLEDGEMENTS

This project has received funding from the European Union's Horizon 2020 research and innovation programme under grant agreement No 813596 DuRSAAM. Additionally, the authors wish to express their gratitude towards Ecocem, Aurubis, Sibelco, Owens Corning, Gavazzi, S&P reinforcement and Sika Belgium for providing materials used in this research.

REFERENCES

[1] "NBN EN 1542 - Products and systems for the protection and repair of concrete structures - Test methods - Measurement of bond strength by pull-off." 2003.

[2] Z. Al-Kamyani, F. P. Figueiredo, H. Hu, M. Guadagnini, and K. Pilakoutas, "Shrinkage and flexural behaviour of free and restrained hybrid steel fibre reinforced concrete," *Constr Build Mater*, vol. 189, pp. 1007–1018, Nov. 2018, doi: 10.1016/j.conbuildmat.2018.09.052.

[3] Z. Li, M. Nedeljković, B. Chen, and G. Ye, "Mitigating the autogenous shrinkage of alkali-activated slag by metakaolin," *Cem Concr Res*, vol. 122, no. March, pp. 30–41, 2019, doi: 10.1016/j.cemconres.2019.04.016.

[4] G. Ascensão, G. Beersaerts, M. Marchi, M. Segata, F. Faleschini, and Y. Pontikes, "Shrinkage and mitigation strategies to improve the dimensional stability of CaO-FeOx-Al2O3-SiO2 inorganic polymers," *Materials*, vol. 12, no. 22, Nov. 2019, doi: 10.3390/ma12223679.

[5] Noushini, K. Vessalas, G. Arabian, and B. Samali, "Drying shrinkage behaviour of fibre reinforced concrete incorporating polyvinyl alcohol fibres and fly ash," Advances in Civil Engineering, vol. 2014, 2014, doi: 10.1155/2014/836173

Stress-strain response of FRP-confined rubberised one-part alkali-activated concrete

Mohamed Elzeadani[1], Dan V. Bompa[1,2] and Ahmed Y. Elghazouli[1]

[1] Department of Civil and Environmental Engineering, Imperial College London, London, UNITED KINGDOM. (E-mail: m.el-zeadani20@imperial.ac.uk, a.elghazouli@imperial.ac.uk)

[2] Department of Civil and Environmental Engineering, University of Surrey, Guildford, UNITED KINGDOM. (E-mail: d.bompa@surrey.ac.uk)

HIGHLIGHTS

- Stress-strain response of aramid fibre reinforced polymer confined rubberised alkali-activated concrete.
- Effect of rubber content and fibre thickness on the stress-strain response is analysed.
- Volumetric behaviour due to different rubber content and fibre thickness is investigated.

Keywords: one-part alkali-activated materials, rubberised concrete, FRP confinement

INTRODUCTION

Practical developments in alkali-activated materials (AAMs) have led to the introduction of one-part AAMs, where a solid activator is used in the mix design instead of a caustic alkaline solution [1]. In such materials, the solid activator is mixed directly with the aluminosilicate precursors and any other dry materials, and then water is added to initiate the reaction. One-part AAMs present several benefits as compared to their traditional counterparts, including the possibility of packaging the activators and precursors together, and allowing for easier handling on site.

Rubberised concrete (RuC) has also received increased attention over the past two decades. In such materials, a proportion of the natural mineral aggregates is replaced with crumb rubber particles derived from worn out vehicle tyres. The softer nature of rubber particles causes changes in the mechanical properties of concrete, typically being a function of the rubber content. Well-observed improvements due to rubber addition include higher ductility, softer post-peak stress-strain response, and enhanced energy absorption capacity [2]. This comes at the expense of a reduction in the compressive strength, elastic modulus, splitting tensile strength and flexural strength [3]. To offset this reduction in mechanical properties and utilize the improved deformation merits of rubberised concrete, external confinement with fibre reinforced polymer (FRP) was investigated [4]. This proved to be extremely effective, allowing for some recovery of the strength lost and utilising more of the passive confinement due to higher concrete deformability.

While previous studies have looked at rubberised alkali-activated concrete (RuAAC), there is only limited work on rubberised one-part alkali-activated concrete (one-part RuAAC), and even less work on the confinement behaviour of one-part RuAAC [5]. As such, this study aims to investigate the compressive stress-strain response of aramid fibre reinforced polymer (AFRP) confined one-part RuAAC. Three different volumetric rubber replacement ratios of total natural aggregates were considered, including 0, 30 and 60% replacements. One to three layers of AFRP were also considered to quantify their effect on the stress-strain response.

MATERIALS & METHODS

The aluminosilicate precursors used were ground granulated blast furnace slag (GGBS) and low-calcium fly ash (FA). The solid activator employed was anhydrous sodium metasilicate with a silicate modulus of 0.92. Sodium tetraborate decahydrate-borax was added as a chemical admixture to improve the workability of the mix. The fine and coarse aggregates used were river sand and crushed gravel, respectively. Three different mixes were investigated: R00, R30 and R60, corresponding to 0, 30 and 60% replacement of total natural aggregates with crumb rubber particles, respectively. The mix design details are given in Table 1, where six different crumb rubber particle sizes were used to achieve optimum balance between loss of strength and workability.

Table 1. Concrete mix design.

		R00	R30	R60
Precursors (kg/m^3)	GGBS	480	480	480
	FA	120	120	120
Solid activator (kg/m^3)	Na_2SiO_3-anhydrous	72	72	72
Aggregates (kg/m^3)	Sand (0-5 mm)	675	472.5	270
	Gravel (5-10 mm)	825	577.5	330
Rubber (kg/m^3)	0-0.5 mm	0	8.1	16.3
	0.5-0.8 mm	0	8.1	16.3
	1-1.25 mm	0	24.4	48.8
	2-4 mm	0	32.6	65.1
	4-10 mm	0	16.3	32.6
	10-20 mm	0	73.3	146.5
Admixture (kg/m^3)	Borax	30	30	30
Water (L)		180	180	180

The AFRP layer thickness was 0.2 mm, and the elastic modulus, tensile strength and ultimate strain were 107 GPa, 2035 MPa and 1.9%, respectively. Specimens tested in compression were cylinders of Ø100×200 mm size, and the AFRP sheets, covering the entire width of the specimens, were attached using a wet lay-up procedure. The fibres were aligned along the transverse specimen direction, and all specimens were tested after 28-days of curing while allowing at least 7-days from the application of AFRP sheets to ensure that the bonding adhesive develops its full design strength.

RESULTS & DISCUSSION

Figure 1 shows the average stress-strain (σ-ε) response and volumetric behaviour of the considered specimens. The specimen reference adopts the format Rxx-Fy, where R indicates the mix design and F denotes the number of AFRP layers. Hence, R30-F2 refers to specimens made of mix R30 and confined with two AFRP layers. The results clearly indicate a reduction in the ultimate strength with higher rubber content, regardless of the number of AFRP layers. Increasing the number of AFRP layers consistently increased the ultimate compressive strength and ultimate strain. The shape of the σ-ε response was also different for the confined non-rubberised and rubberised specimens. For instance, all R00 specimens, regardless of the number of AFRP layers, experienced a softening and then hardening before eventual failure by AFRP rupture. Meanwhile, the rubberised specimens exhibited a

typical bi-linear response connected by a transition zone. The rubberised specimens also benefited more from AFRP confinement, experiencing higher confined-to-unconfined strength ratios. For example, R00-F1, R00-F2 and R00-F3 had confined-to-unconfined ratios of 1.2, 1.5 and 2.0, respectively. Meanwhile, R60-F1, R60-F2 and R60-F3 had confined-to-unconfined ratios of 2.9, 4.8 and 5.9, respectively.

The volumetric response, taken as εvol = εaxial + 2εlateral, was also different for the non-rubberised and rubberised specimens as shown in Figure 1. A positive εvol indicates volume reduction while a negative value indicates volume expansion. The non-rubberised R00 specimens mainly exhibited volume reduction up to almost 80-90% of the maximum load, and then experienced volume expansion. Rubberised specimens, on the other hand, exhibited this transition at a much lower rate, and for R60-F2 and R60-F3, volume reduction up to failure controlled the behaviour.

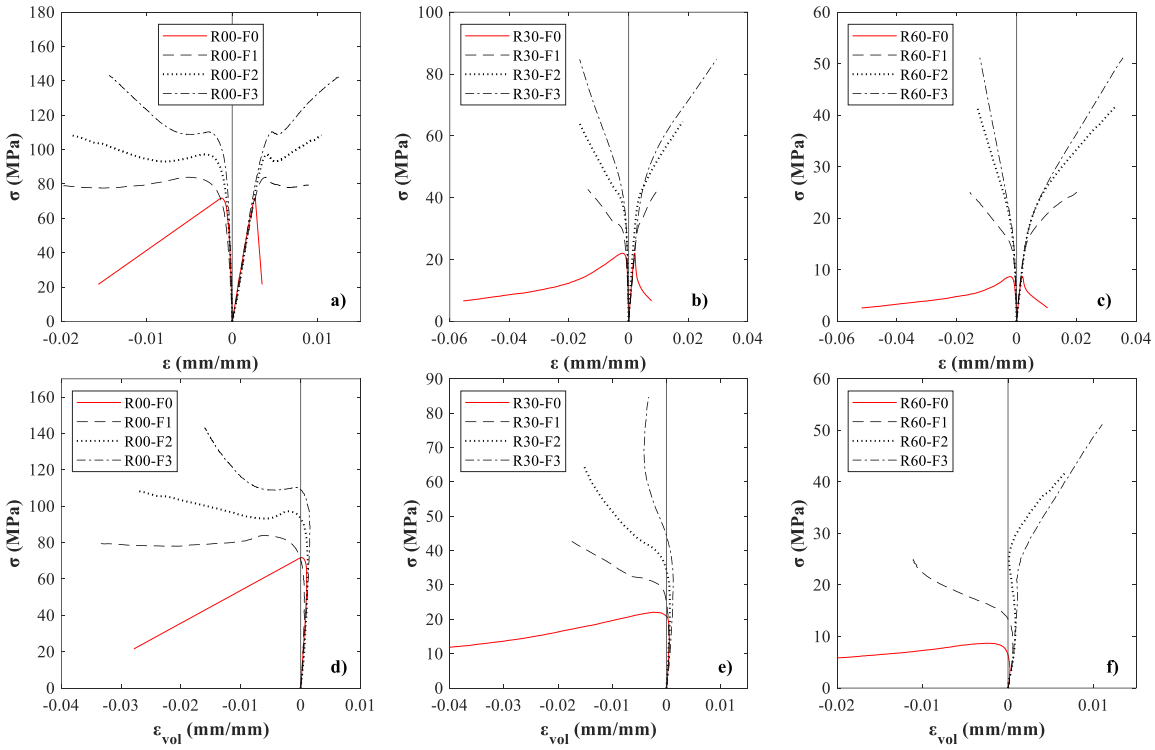

Figure 1. Stress-strain response and volumetric behaviour.

CONCLUSION

This study assessed the experimental stress-strain behaviour of AFRP-confined rubberised one-part alkali-activated materials. Three different volumetric rubber replacement ratios of total natural aggregates (0, 30 and 60%) and three AFRP layer thicknesses (1 to 3 layers) were investigated. The results clearly show that the stress-strain response is dependent on both the rubber content and AFRP layer thickness. The ratio of confined-to-unconfined strength and ultimate strain increased significantly with higher rubber content. The volumetric response of the tested specimens was also different indicating volume reduction and then expansion near the peak for the non-rubberised specimens, while the rubberised specimens experienced volumetric expansion at a much lower stress in comparison. The behaviour of R60 specimens with 2 and 3 layers of AFRP was predominantly controlled by volumetric reduction up to failure.

ACKNOWLEDGEMENT

The first author acknowledges the funding provided by the President's PhD Scholarship at Imperial College London for his research studies.

REFERENCES

[1] Elzeadani, M. Bompa, D. V., and Elghazouli, A. Y. One part alkali activated materials: A state-of-the-art review. *Journal of Building Engineering* 57 (2022), 104871.

[2] Elzeadani, M. Bompa, D. V., and Elghazouli, A. Y. Experimental assessment and constitutive modelling of rubberised one-part alkali-activated concrete. *Construction and Building Materials* 353 (2022), 129161.

[3] Bompa, D. V., Elghazouli, A. Y., Xu, B., Stafford, P. J., and Ruiz-Teran, A. M. Experimental assessment and constitutive modelling of rubberised concrete materials. *Construction and Building Materials* 137 (2017), 246-260.

[4] Bompa, D. V., and Elghazouli, A. Y. Stress-strain response and practical design expressions for FRP-confined recycled tyre rubber concrete. *Construction and Building Materials* 237 (2020), 117633.

[5] Elzeadani, M., Bompa, D. V., and Elghazouli, A. Y. Preparation and properties of rubberised geopolymer concrete: A review. *Construction and Building Materials* 313 (2021), 125504.

Seismic retrofitting of clay-brick masonry walls with AAM-TRM

Lazar D. Azdejkovic[1], Thanasis C. Triantafillou[2] and Catherine G. Papanicolaou[3]

[1, 2, 3] University of Patras, Patras, Greece.
(E-mail: lazar@upatras.gr, ttriant@upatras.gr, kpapanic@upatras.gr)

HIGHLIGHTS

- Utilization of AAM (geopolymer) mortar in TRM seismic and energy retrofitting of clay-brick masonry walls;
- Cyclic four-point bending testing of hollow clay-brick masonry walls;
- Achieved load capacity increase up to 72% and ductility increase up to 684%, depending on the retrofitting scheme.

Keywords: masonry, textile reinforced mortars, seismic retrofitting, alkali–activated materials, energy retrofitting.

INTRODUCTION

Despite the wide use of the robust, modern building materials (reinforced concrete, steel), the unreinforced masonry (URM) still remains the most prevailing building material in the existing building stock, worldwide. Most of the URM structures were constructed before the introduction of building codes, out of which some represent cultural heritage buildings while the vast majority is in everyday use (residential or commercial). More than 80% of the existing buildings in Europe are at least 30 years old while 40% of the buildings were constructed before 60's [1]. The current state of the existing building stock in European Union (EU) requires the systematic renovation that aims to improve the energy performance and reduce the environmental impact. Taking into account the seismic activity in southern Europe in combination with the energy retrofitting need emphasized in the EU "green deal" [2] resulted with the innovative solutions for combined seismic and energy upgrading of the existing masonry structures [3-4]. This paper investigates the seismic retrofitting of hollow clay-brick masonry walls with two textile reinforced mortar (TRM) configurations: in-house developed alkali activated (AAM) mortar mix [5] and a commercially available ordinary Portland cement (OPC)-based mortar, both combined with alkali-resistant (AR) glass-fiber textile (360 g/m2). Furthermore, the paper covers the integrated energy and seismic retrofitting system composed of extruded-polystyrene (XPS) thermal insulation boards (thickness t = 30 mm, elasticity modulus E = 20 MPa) and TRM jackets.

A ternary mix of precursors consisting of metakaolin, fly ash and ladle furnace slag was activated with potassium-based activators' solution. Short polyvinyl alcohol (PVA) fibers (6 mm) were added in a total amount of 0.25% per volume of fresh mortar. Standard siliceous river sand (0-2 mm) was used, keeping the aggregates-to-precursors weight ratio at 1.7. Detailed mix design of AAM-based mortar is presented in Table 1. Preparation of a polymer-modified commercial OPC-based mortar was carried out simply by adding water to the ready-made dry mortar mix according to the manufacturer's instruction (water to solid ratio of 0.2 per weight).

Table 12. AAM mortar mix design (in grams per dm^3 of fresh mortar).

KOH (90% pure)	K_2SiO_3, M_R = 2.4 (dry content 45%)	additional water	metakaolin	fly ash	ladle furnace slag	siliceous sand (d_{max} = 2 mm)	PVA fibers
62.5	350.0	225.0	343.8	212.5	100.0	1112.5	3.2

Mortar mechanical characteristics were obtained through three-point bending and compressive tests of mortar prisms after 28 days of age, according to EN196-1 (2016). Mean flexural and compressive strength of AAM-based mortar of 5.62 MPa and 43.78 MPa, respectively were obtained. On the other hand, mean flexural and compressive strength of OPC-based mortar were 4.19 MPa and 11.66 MPa, respectively.

The relative effectiveness of the seismic retrofitting and combined seismic and energy retrofitting with AAM-based TRM and XPS thermal insulating boards were studied through a set of experimental tests on spandrel-like masonry walls represented in Fig 1a. A total number of six single-leaf, hollow clay-brick masonry walls were constructed with a length and height of 1300 mm and 400 mm, respectively. The wall thickness was defined by an individual brick width, i.e. 90 mm. Support spacing was 1200 mm, while the in-plane cyclic loading was imposed at two points positioned 400 mm from each support (Figure 1).

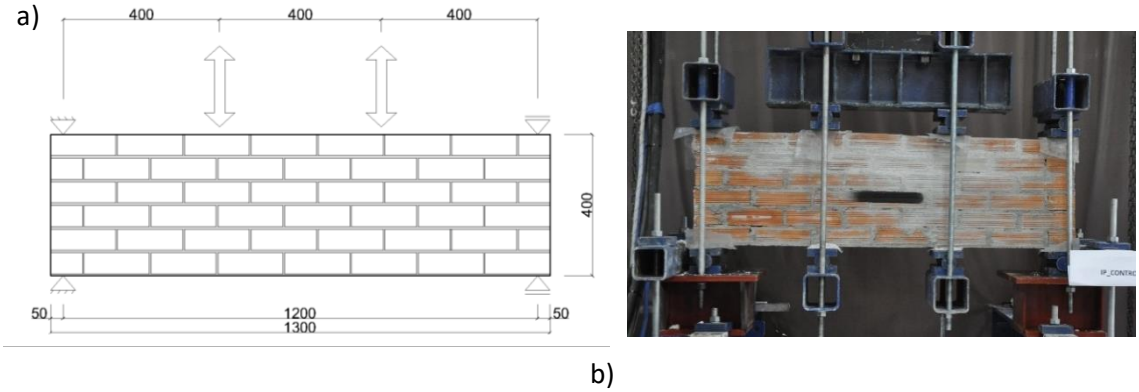

Figure 1. Four-point cyclic bending test setup (a) schematic and (b) photo representation.

Apart from testing of the unretrofitted (control) specimen, five specimens were strengthened 2 months after the construction, cured for additional 28 days and then tested. The three masonry walls were furnished with AAM-based TRMs in the following configurations: single layer placed at both sides (1L_AAM_1L), two layers applied on a single side (2L_AAM), XPS positioned between the two TRM layers applied on one side of the wall (AAM_1L_T_1L). For comparison reasons, one specimen was strengthened with the same strengthening scheme in which the AAM-based mortar was substituted with an OPC-based one (OPC_1L_T_1L). Finally, due to the fact that the stiffness of the applied XPS boards is not negligible, the specimen subjected to energy retrofitting only carried out by bonding the XPS board to the wall surface with the AAM mortar mix, was tested as well (Figure 2).

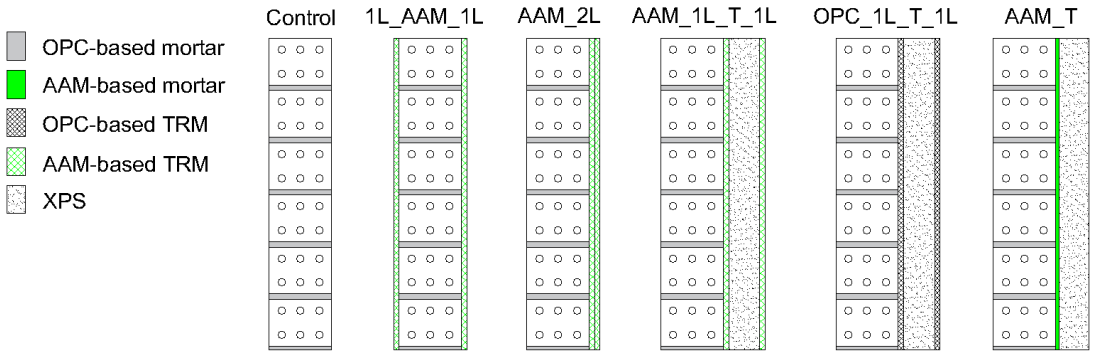

Figure 2. Retrofitting schemes with specimen ID's.

RESULTS & DISCUSSION

The displacements were measured continuously with a videoextensometer while the corresponding forces were acquired directly from the load cell. This way, the response functions presented in a hysteretic loop form were obtained for each specimen. Envelopes of load versus mid-span displacement functions are presented in Figure 3a. Cumulative energy dissipation graphs are presented in Figure 3b.

As expected, the unretrofitted specimen response was quite brittle. The first crack and, hence, the major stiffness reduction occurred during the first cycle in the pull direction, while the complete failure occurred during the third cycle (push direction). The failure occurred at the left shear span in the form of diagonal cracks along the mortar bed joints. AAM_T specimen sustained higher displacement capacity than the control specimen (49.4% and 109% in the push and pull direction, respectively) with a total energy dissipation increase of 140%, for the same number of cycles reached. The failure mode was changed since the specimen AAM_T failed in the vicinity of the mid-span. During testing of all other specimens, much higher peak load and displacement capacities were recorded. Specimen 1L_AAM_1L failed during the fourth cycle, while other retrofitted specimens failed during the sixth cycle. However, the application of a single layer of AAM-based TRM on each side of the wall resulted with an average load capacity increase of 72.7% (push and pull direction). The wall retrofitted with two AAM-based TRM layers placed on one side behaved significantly better in terms of the displacement and load capacity, with an average increase of 684% and 57%, respectively, compared to the unretrofitted one. Failure of both AAM_2L and 1L_AAM_1L specimens was determined with fibers' rupture near the mid-span. The total energy dissipated by AAM_2L wall was 262% higher than that of 1L_AAM_1L and 1387% higher than that of the control specimen.

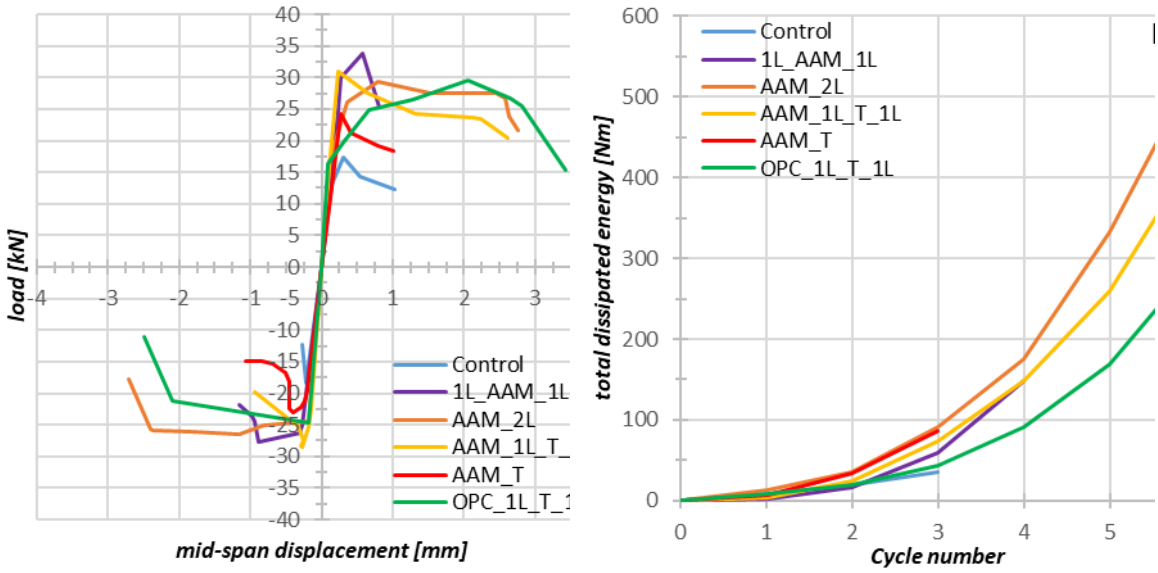

Figure 3. (a) Hysteretic loop envelopes, (b) Cumulative energy dissipation.

During testing of seismic and energy retrofitted specimens, the outer TRM layer was not fully activated because it was applied on a softer material (XPS). Thus, the maximum loads were slightly lower compared to the peak loads recorded during testing of AAM_2L and 1L_AAM_1L specimens. The total dissipated energy of the AAM_1L_T_1L specimen was 46% higher than its OPC-based counterpart in which partial debonding of the thermal insulation occurred during the second cycle. Failure of the OPC_1L_T_1L specimen was governed by fiber rupture of the inner TRM layer, while in the case of AAM_1L_T_1L, both TRM layers failed together with the XPS board. Debonding of the thermal insulating boards was not recorded in cases where the XPS was glued with AAM-based mortar to the walls.

CONCLUSION

A significant increase of the displacement and load capacity was achieved with the application of two layers of AAM-based TRM. The wall that was retrofitted with single-sided double-layer AAM-based TRM performed better -particularly in terms of displacement capacity- when compared to the specimen retrofitted on both sides with a single AAM-based TRM layer.

Combined seismic and energy retrofitting of the tested walls resulted with quite satisfying outcomes as well. AAM-based mortar showed better bond to XPS properties than the OPC-based one. However, the displacement capacity of AAM_1L_T_1L specimen was lower than that of OPC_1L_T_1L.

The aforementioned differences in the deformation capacity of the retrofitted walls aroused questions regarding the durability characteristics of the AR-glass textile embedded in a highly alkaline AAM mortar. Therefore, for addressing the potential durability issues, further research on styrene butadiene rubber (SBR)-coated AR glass textile embedded in the AAM mortar mix is currently being carried out.

ACKNOWLEDGEMENT

This research has received funding from the European Union's Horizon 2020 research and innovation programme under grant agreement No 813596 DuRSAAM.

The contents of this publication are the sole responsibility of the author and do not necessarily reflect the opinion of the European Union.

REFERENCES

[1] Economidou, M., Atanasiu, B., Despret, C., Maio, J., Nolte, I., Rapf, O., Laustsen, J., Ruyssevelt, P., Staniaszek, D., Strong, D. and Zinetti, S. Europe's buildings under the microscope. A country-by-country review of the energy performance of buildings. *Buildings Performance Institute Europe* (BPIE) (2011).

[2] The European green deal, 2019, final - communication from the commission to the European parliament, the European council, the council, the European economic and social committee and the committee of the regions. *European Commission*, Brussels (2019).

[3] Triantafillou, T.C., Karlos, K., Kefalou, K. and Argyropoulou, E. An innovative structural and energy retrofitting system for URM walls using textile reinforced mortars combined with thermal insulation: Mechanical and fire behavior. *Construction and Building Materials*, 133, pp.1-13 (2017).

[4] Triantafillou, T.C., Karlos, K., Kapsalis, P. and Georgiou, L. Innovative structural and energy retrofitting system for masonry walls using textile reinforced mortars combined with thermal insulation: In-plane mechanical behavior. *Journal of Composites for Construction*, 22(5), p.04018029 (2018).

[5] Askouni, P.D., Papanicolaou, C.G. and Azdejkovic L.A. Experimental Investigation of the TRM-to-Masonry Bond after Exposure to Elevated Temperatures: Cementitious and Alkali-Activated Matrices of Various Densities. *Materials 15, no. 1* (2021): 140.

Experimental investigation on long-term flexural behavior of prestressed Alkali-activated concrete (AaC) girders with cast-in-situ AAC topping

Zhenxu Qian[1], Guang Ye[2], Stijn Matthys[3] and Mladena Luković[4]

[1, 4] Engineering Structures, Delft University of Technology, Delft, The Netherlands. (E-mail: Z.Qian-2@tudelft.nl, M.Lukovic@tudelft.nl)

[2] Materials, Mechanics, Management & Design (3MD), Delft University of Technology, Delft, The Netherlands. (E-mail: g.ye@tudelft.nl)

[3] Department of Structural Engineering and Building Materials, Ghent University, Ghent, Belgium. (E-mail: Stijn.Matthys@UGent.be)

HIGHLIGHTS

- Higher shrinkage and creep effects, which do not reach plateau within 9 months, and relatively lower elastic modulus compared to conventional concrete, result in large prestress losses in AAC.
- Long-term material and structural tests are necessary to assess material properties, cracking moment and ultimate resistance for prestressed applications of AAC.
- Relying on test results at 28 days, like with conventional concrete, will result in an unsafe design of AAC.

Keywords: alkali-activated concrete (AAC), prestressed girder, long-term flexural behavior

INTRODUCTION

Alkali-activated concrete (AAC), in which the binder is formed by the chemical reaction between precursors and alkali activator, has emerged as a promising alternative to conventional concrete (CC). Despite the promising material properties of some AAC mixtures, the structural application is limited. Thus, researchers have shifted their target to AAC structures to establish fundamental knowledge for structural design. The focus of the research so far is on the short-term behavior of reinforced AAC elements. From the literature, it is concluded that reinforced AAC has similar short-term flexural and shear behavior with CC counterparts [1]. Few researchers gave insight into the feasibility of AAC in prestressed elements by studying their short-term flexural capacity and cracking behavior [2-3]. But prestressed AAC as well as its long-term performance has not been widely involved in the state of art. This paper aims to experimentally investigate the long-term flexural behavior of prestressed AAC girders with cast-in-situ AAC topping, which is a commonly used structural system in Dutch construction and therefore could promote the large-scale application of AAC.

In this experimental program, three individual girders with a nominal length of 7000mm, consisting of the precast girder and cast-in-situ topping were fabricated. Self-compacting AAC with the strength class of C45/C55, consisting of blast furnace slag (BFS) as the precursor and activated by a sodium-based alkaline activator, was developed to produce the precast girder [4]. Ready-mixed AAC provided by Cementbouw Betonmortel B.V. was used as cast-in-situ topping. The cross-sectional dimensions and the layout of prestressing strands/ reinforcement of precast girder and topping concrete are illustrated in Figure 1a and 1b, respectively. Prestress was introduced by cutting the strands at 2.75 days after casting of girders. The precast girders were covered with wet burlaps and plastic sheets for

30 days. Afterward, ready-mixed AAC was poured and the composite girders were made. One composite girder, covered with moist burlaps and plastic sheets until the testing age, was tested at the age of 28 days (short-term flexural test, STF). The other two composite girders, which were wrapped with plastic sheets for 3 days and exposed to lab condition for long-term monitoring, were tested at the age of 267 days and 274 days (long-term flexural tests: LTF and LTF_LS, respectively). One of them (LTF_LS) was subjected to sustained load until the testing age. The sustained loading regime consisted of point loads of 70kN applied for 158 days, and subsequently being increased to 130kN for 76 days. Four-point bending configuration was adopted in both monotonic and sustained loading tests (Figure 2). LVDTs were used to measure the midspan deflection. Digital Image Correlation (DIC) was applied to monitor the crack development in the constant moment zone.

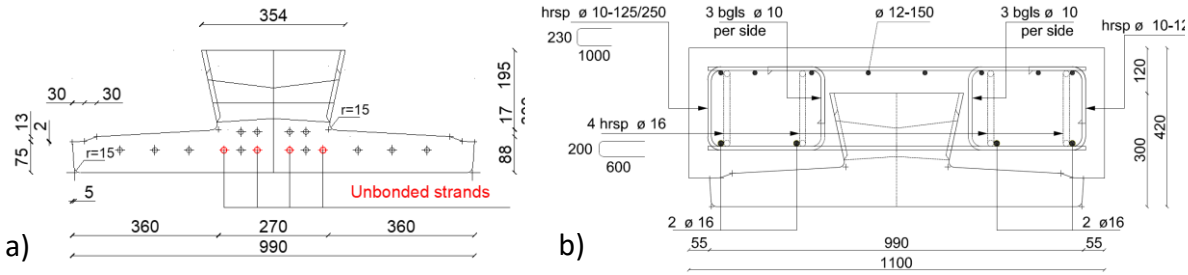

Figure 1. Cross-section of a) prestressed AAC girder with the layout of prestressing strands (16 strands ø12.9, 4 of them being debonded over a length of 1m) and b) composite girder with the layout of reinforcement in topping concrete.

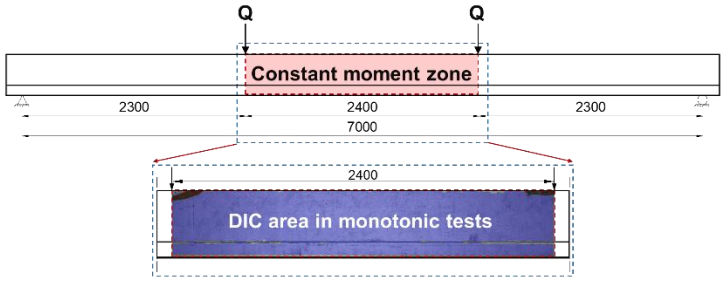

Figure 2. Position of (sustained) load in test setup.

RESULT & DISCUSSION

The long-term midspan deflection of specimen LTF and LTF_LS is plotted in Figure 3. Note that a negative value represents hogging trend of the girder while a positive value represents sagging trend. Almost the exactly same deflection development of two specimens was observed in the initial stage. The downward deflection of LTF_LS reached a plateau shortly after applying the load of 70kN. Once loaded with 130kN, the deflection increased and kept increasing gradually for the next three months. Minor flexural cracks were found at the soffit of LTF_LS within the constant moment region. The unloaded specimen (LTF) kept deforming upwards, which might be mainly attributed to the large creep effects. A horizontal crack between precast girder and topping concrete was observed for both specimens and resulted in the stiffness reduction.

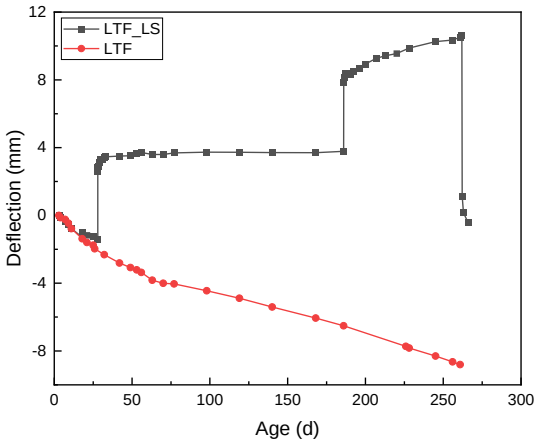

Figure 3. Long-term midspan deflection of LTF and LTF_LS.

In Figure 4, the load-deflection curves of all girders under four-point bending are shown. In the short-term test, although approaching the yielding of the prestressing strands, the maximum stroke of the jack was reached, and the specimen did not fail. The measured strain level in the concrete at the height of prestressing strands was 4.1mm/m, which was slightly lower compared to the yielding strain of 5mm/m.

On the other hand, in the long-term test girder (LTF), anchorage failure occurred at the loading level that was lower than the one in the short-term test. Finally, concrete crushing, as an indicator of flexural failure, was observed in LTF_LS. The change of failure mode might be related to the different bond capacities between strands and AAC, and different creep effects. The reduction of Hoyer effect due to creep and shrinkage causes the decrease of bond strength [5]. Since the application of sustained load results in a lower stress level in LTF_LS compared to LTF, the degradation of bond capacity in LTF_LS might be less significant.

Note that different loading schemes were applied in beams and significant nonlinearity after applying load cycles with high load levels was observed. Therefore, the focus of comparison of flexural test results of three girders was on the load-deflection relationship and cracking behavior until 195kN. At the same load level, LTF had the largest midspan deflection compared with the other specimens, indicating its lowest stiffness. Considering the cracking behavior, multiple cracks on the side surface of LTF were already observed at 130kN, unlike cracking in the other samples that first occurred at 160kN and 190kN for LTF_LS and STF, respectively. LTF showed both earlier cracking and larger cracks compared with LTF_LS (see Figure 5).

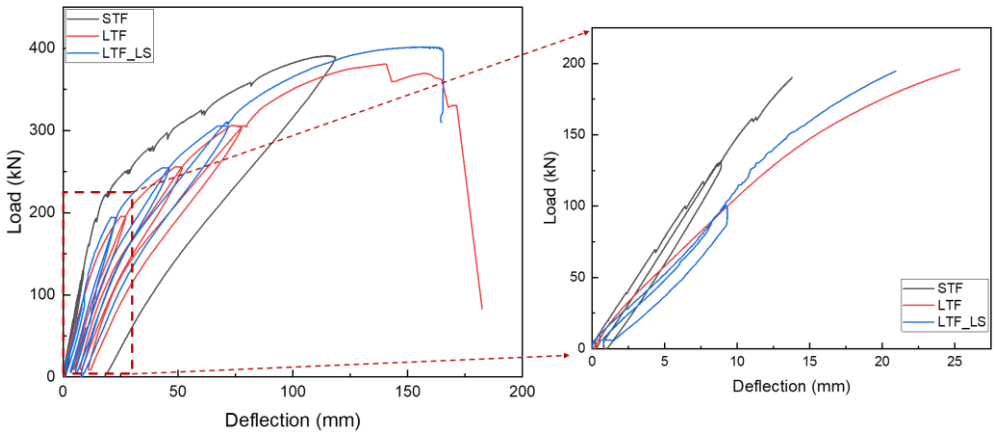

Figure 4. Load-deflection relationship of STF, LTF and LTF_LS.

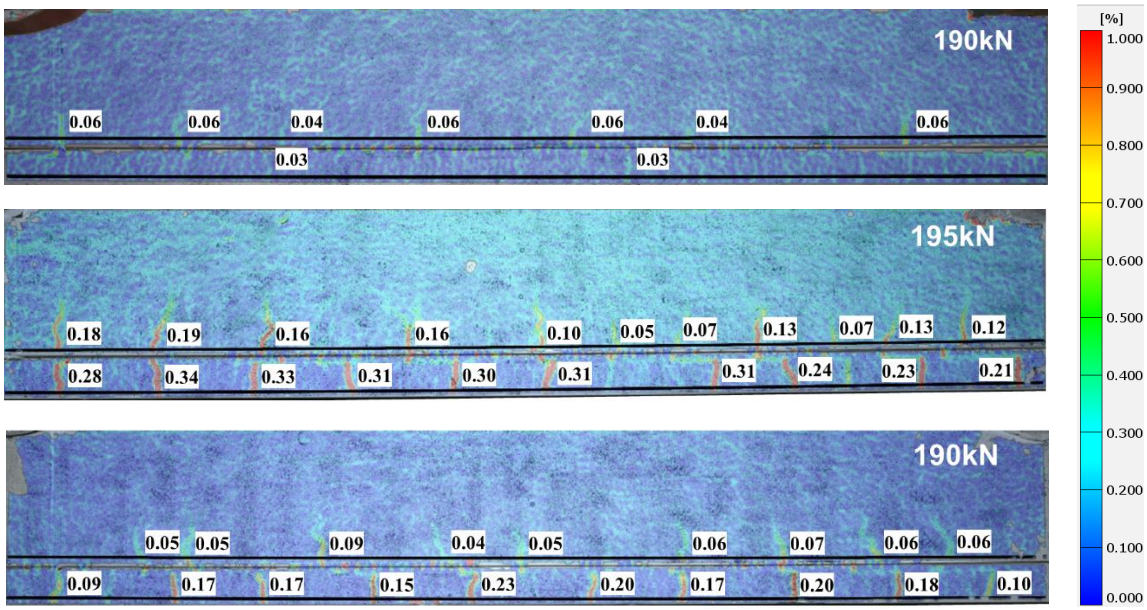

Figure 5. Crack pattern of STF, LTF and LTF_LS at around 190kN (measurement points in the tests).

The difference in the short-term and long-term flexural behavior of the three girders might result from the decrease of elastic modulus of AAC [4] and the significant prestress loss induced by pronounced shrinkage and creep effects [4]. The bond degradation also seems to play a role. Therefore, evaluating the structural resistance of AAC based on short-term test results, similar to CC, will lead to an unsafe prediction of ultimate capacity and cracking performance. Conducting long-term tests is necessary for AAC structural design.

CONCLUSION

This paper presents the experimental investigation of the long-term structural behavior of prestressed AAC girder with cast-in-situ AAC topping. Short-term and long-term flexural tests, including sustained loading tests and residual strength tests, were conducted. Based on the experimental results, the following conclusion could be drawn:

(1) Deflection of the specimen subjected to sustained load reached plateau while the unloaded specimen kept deforming upward, indicating the ongoing and pronounced creep effects.

(2) Compared with the specimen tested at 28 days, specimens tested at around 9 months showed lower stiffness and cracking resistance. Different creep effects induced by different stress levels play a role in structural behavior. This is in line with observations on the two girders exposed to different stress levels where sustained load has beneficial effects, thereby reducing stress level at the level of prestressing strands and reducing creep effects. Bond degradation also seems to play a role.

(3) It is of vital importance to investigate the long-term behavior of AAC structural members. Simply relying on the test results at 28 days will cause an unsafe structural design.

ACKNOWLEDGMENT

The authors would like to express their appreciation for the support of the sponsors with Project No CM2B17.

REFERENCES

[1] Mo, K. H., Alengaram, U. J. and Jumaat, M. Z. Structural performance of reinforced geopolymer concrete members: A review. *Construction and Building Materials* 120 (2016), 251-264.

[2] Liu, H., Lu, Z. and Peng, Z. Test research on prestressed beam of inorganic polymer concrete. *Materials and Structures* 48 (2015), 1919-1930.

[3] Sonal, T., Urmil, D. and Darshan, B. Behaviour of ambient cured prestressed and non-prestressed geopolymer concrete beams. *Case Studies in Construction Materials* 16 (2022), e00798.

[4] Zhang, S., Luković, M., Herder, H., Scharringa, A. and Ye, G., Geopolymeerbeton voor infrastructurele toepassingen (1): Ontwikkeling van zelfverdichtende mengsels. *Cement: vakblad voor de betonwereld* 2022(7), 42-50. https://www.cementonline.nl/geopolymeerbeton-voor-infrastructurele-toepassingen-1

[5] Barnes, R. W., Grove, J. W., and Burns, N. H. Experimental assessment of factors affecting transfer length. *Structural Journal* 100 (2003), 740-748.

Alkali-activated slag-based concrete incorporating single and multiple hooked-end steel fibres: mechanical behaviour and limitations to field applications

Laura Rossi[1,2] and Frank Dehn[1,2]

[1] Institute of Building Materials and Concrete Structures (IMB), Karlsruhe Institute of Technology (KIT), Karlsruhe, GERMANY.

[2] Materials Testing and Research Institute (MPA), Karlsruhe Institute of Technology (KIT), Karlsruhe, GERMANY. (E-mail: laura.rossi@kit.edu, frank.dehn@kit.edu)

HIGHLIGHTS

- Single and multiple hooked-end steel fibres can improve the brittleness of AASC
- AASC reinforced with Dramix® 3D, 4D and 5D fibres exhibits better mechanical performance compared to fibre-reinforced Portland cement concrete (FRPCC) with similar compressive strength
- The lack of analytical equations correlating the mechanical performance of FRAASC hinders its application in the construction industry as construction material

Keywords: alkali-activated concrete, hooked-end steel fibres, mechanical behaviour

INTRODUCTION

Alkali-activated slag-based concrete (AASC) has been demonstrated to exhibit higher mechanical and durability performance compared to traditional Portland cement concrete (PCC) [1–3]. However, the brittle behaviour of AASC hinders its application in construction works requiring high tensile strength and ductile post-cracking behaviour. The incorporation of single and multiple hooked-end steel fibres, designed to provide a higher fibre-matrix bond and improve the crack bridging ability of the fibres, enhance the mechanical performance of AASC [4], resulting in a more environmentally friendly performing construction material than PCC [5,6]. Despite the promising mechanical behaviour of steel fibre-reinforced AASC (FRAASC), its application is limited by the lack of performance-based design standards and building regulations. Current standards developed for PCC are not able to describe the behaviour of FRAASC, as they overestimate the modulus of elasticity, generally lower in AASC and FRAASC, and underestimate the tensile strength, as fibre geometry and dosage is not taken into account. New correlations need to be developed to facilitate the understanding of steel fibres in an alkali-activated matrix and the field implementation of FRAASC.

MATERIALS AND METHODS

Ground granulated blast furnace slag (GGBS) with a basicity coefficient $K_b = (CaO + MgO)/(SiO_2 + Al_2O_3)$ of 1.05 was used. Water, sodium hydroxide solution and waterglass with a silicate modulus $M_s = SiO_2/Na_2O$ [mol/mol] of 3.4 have been used to obtain an alkaline solution with a total concentration of Na_2O to binder [g/100g] of 5.3% and a SiO_2/Na_2O ratio of 0.5. River sand, fine and coarse aggregates have been used to cast the reference AASC to which different hooked-end steel fibres, i.e. Dramix® 3D, 4D and 5D fibres, with a length of 60 mm and aspect ratio of 65 have been added in different volume fractions, i.e. 0.25%, 0.50% and 0.75%. For each mixture, 12 cylinders (150 mm x 300 mm) and 6 beams (150 mm x 150 mm x 550 mm) have been cast to evaluate

the effect of fibre geometry and content on the compressive strength (EN 12390-3), modulus of elasticity (EN 12390-13:2014), splitting tensile strength (EN 12390-6) and flexural strength (EN 14651) of the composite. To evaluate the effect of fibre incorporation in different concrete matrices the same mixtures have been cast using Portland cement (CEM I 42.5R) as a binder. The same binder content, aggregate type and dosage have been used to obtain concretes with similar workability and compressive strength after 28 days. The mix proportions for both reference AASC and PCC are shown in Table 1.

Table 1. Mix proportions of AASC and PCC.

Mix	GGBS [kg/m^3]	CEM I [kg/m^3]	NaOH [kg/m^3]	Waterglass [kg/m^3]	Water [kg/m^3]	Sand [kg/m^3]	Fine aggregates (2-8 mm) [kg/m^3]	Coarse aggregates (8-16 mm) [kg/m^3]
AASC	425	-	50	36	154	660	495	495
PCC	-	425	-	-	229	660	495	495

RESULT & DISCUSSION

The 28-day compressive strength (CS), modulus of elasticity (MoE), splitting tensile strength (STS) and flexural strength (FS) of both AASC and PCC reinforced with Dramix® 3D, 4D and 5D fibres in different volume fractions are shown in Figure 1.

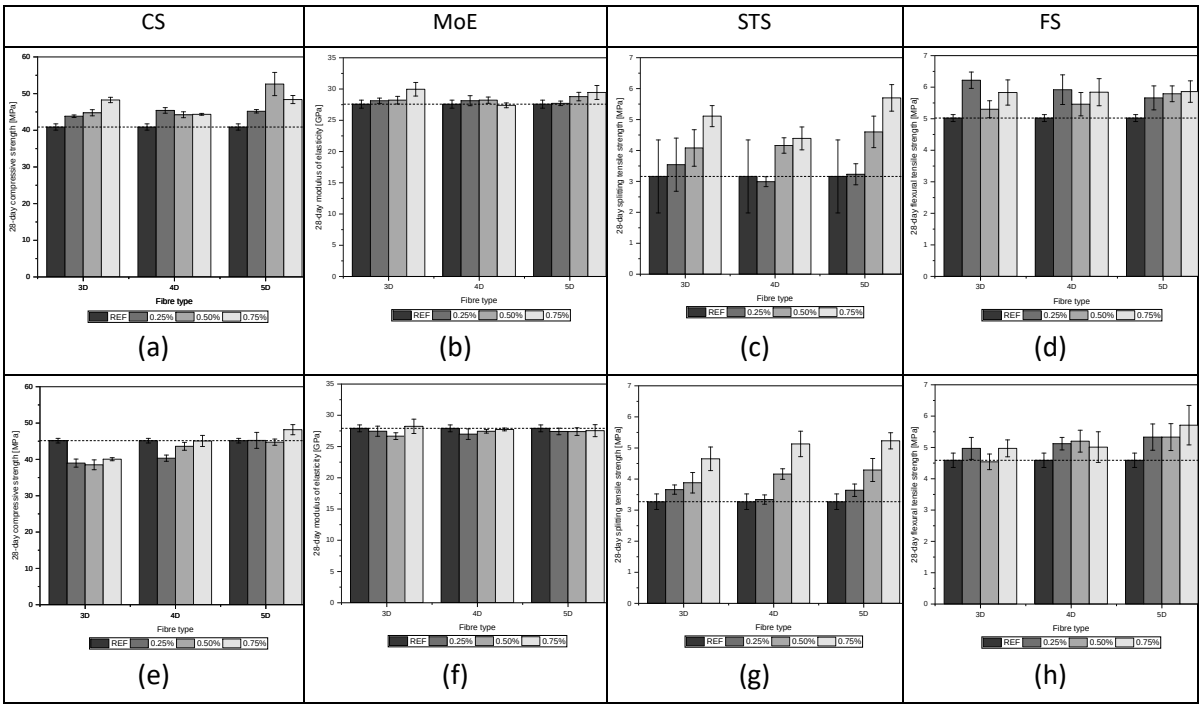

Figure 1. Results of the 28-day compressive strength, modulus of elastictiy, splitting and flexural tensile strength of FRAASC (a-d) and FRPCC (e-h).

If for PCC, the incorporation of hooked-end steel fibres, regardless of the fibre geometry and content, marginally affects the compressive strength and the modulus of elasticity, generally resulting in lower values than the reference mix, for AASC fibres enhance both CS and MoE, achieving the highest improvement compared to AASC-REF of 28.6% and 8.6%, respectively. Although AASC and PCC show comparable splitting and flexural tensile strength behaviour, FRAASC exhibits higher strength than PCC. The better behaviour of AASC incorporating hooked-end steel fibres compared to PCC can be due to the higher shrinkage of AASC, which leads to higher fibre-matrix bond and earlier activation of the fibre crack bridging capacity [7]. The results shown in Figure 1 demonstrate the potential of FRAASC as an alternative to PCC as a construction material. However, the current design analytical expressions provided by the fib Model Code 2010 to correlate the mechanical performance, i.e. modulus of

elasticity and indirect tensile strength, with the compressive strength of plain PCC are not able to predict the behaviour of AASC and FRAASC. As shown in Figure 2, AASC and FRAASC generally show a lower modulus of elasticity compared to PCC [6] as predicted by the fib Model Code 2010 (Figure 2a), since fibres' contribution to the composite performance under compressive loading is quite limited. On the other hand, the effect of steel fibres incorporation on the tensile strength of the composite cannot be neglected, as depending on the geometry and volume fraction, fibres enhance the tensile response of the composite, which is significantly underestimated by the current correlation developed for plain PCC (Figure 2b).

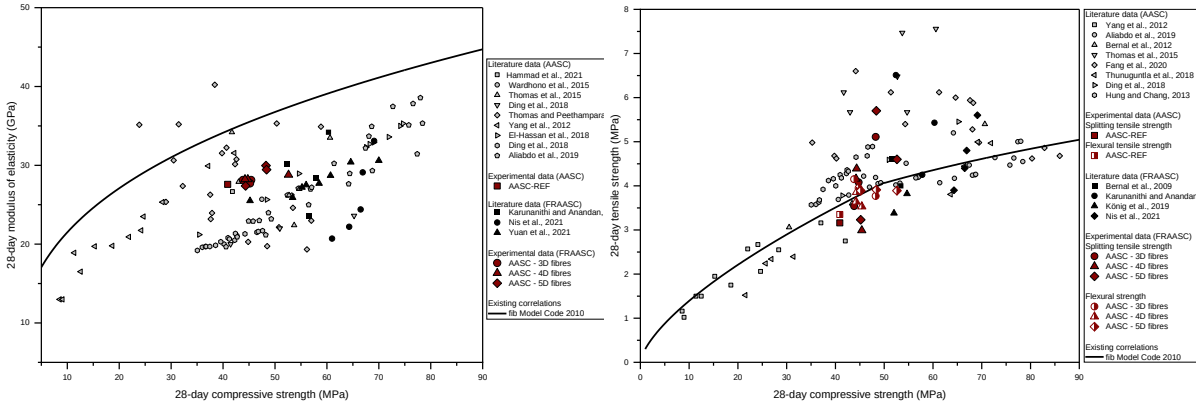

(a) (b)

Figure 2. Correlations between compressive strength and (a) modulus of elasticity and (b) indirect tensile strength for AASC and FRAASC and the current correlation proposed by the *fib* Model Code 2010.

CONCLUSION

This study evaluated the mechanical behaviour of AASC reinforced with different hooked-end steel fibres in volume fractions up to 0.75% and compared it to the same strength-grade PCC. Despite the limited effect of steel fibres on the 28-day compressive strength and modulus of elasticity of both AASC and PCC, the splitting and flexural tensile strength of FRAASC are significantly improved in comparison to the reference concrete and the corresponding PCC mixtures. The enhanced behaviour provided by the incorporation of steel fibres into the alkali-activated concrete matrix is the result of the better fibre-matrix bond properties givenfor instance by higher shrinkage characterising AASC in comparison to PCC. Although FRAASC exhibits improved mechanical behaviour under both compressive and tensile loading, its application in the construction industry is limited by the lack of design codes and performance-based standards able to predict its mechanical response. New analytical equations correlating the mechanical performance to the compressive strength of the composite are needed to facilitate the understanding of AASC incorporating steel fibres and increase its use as an alternative to PCC as a construction material.

ACKNOWLEDGEMENT

This project has received funding from the European Union's Horizon 2020 research and innovation programme under grant agreement No 813596 DuRSAAM. The opinions expressed in this document reflect only the author's view and reflect in no way the European Commission's opinions. The European Commission is not responsible for any use that may be made of the information it contains.

REFERENCES

[1] N.A. Farhan, M.N. Sheikh, M.N. Hadi, Investigation of engineering properties of normal and high strength fly ash based geopolymer and alkali-activated slag concrete compared to ordinary Portland cement concrete, Construction and Building Materials 196 (2019) 26–42.

[2] Y. Ding, J.-G. Dai, C.-J. Shi, Fracture properties of alkali-activated slag and ordinary Portland cement concrete and mortar, Construction and Building Materials 165 (2018) 310–320.

[3] M. Chi, Effects of dosage of alkali-activated solution and curing conditions on the properties and durability of alkali-activated slag concrete, Construction and Building Materials 35 (2012) 240–245.

[4] Niş, N.A. Eren, A. Çevik, Effects of nanosilica and steel fibers on the impact resistance of slag based self-compacting alkali-activated concrete, Ceramics International 47 (2021) 23905–23918.

[5] Amer, M. Kohail, M.S. El-Feky, A. Rashad, M.A. Khalaf, A review on alkali-activated slag concrete, Ain Shams Engineering Journal 12 (2021) 1475–1499.

[6] R.J. Thomas, S. Peethamparan, Alkali-activated concrete: Engineering properties and stress–strain behavior, Construction and Building Materials 93 (2015) 49–56.

[7] Beglarigale, S. Aydın, C. Kızılırmak, Fiber-Matrix Bond Characteristics of Alkali-Activated Slag Cement–Based Composites, J. Mater. Civ. Eng. 28 (2016)

Performance at load-bearing reinforced concrete with treated Cu slag as cement replacement

Pithchai Sivakumar[1,2], Muhammad Arslan Yaqub[1] and Stijn Matthys[1]

[1] Magnel-Vandepitte Laboratory for Structural Engineering and Building Materials, Ghent University, Ghent, BELGIUM. (E-mail: pithchaipandian.sivakumar@ugent.be, muhammadarslan.yaqub@ugent.be, Stijn.Matthys@UGent.be)

[2] R&D Department, Aurubis Beerse (N.V), Beerse, BELGIUM. (E-mail: p.sivakumar@aurubis.com)

HIGHLIGHTS

- Large-scale reinforced concrete slabs made with treated Cu slag as cement replacement were designed and fabricated.
- 4-point bending tests until failure were performed to assess the structural performance of the novel concrete with treated Cu slag.

Keywords: treated Cu slag, cement replacement, structural performance

INTRODUCTION

The use of Cu slag as a construction mineral, either as an artificial aggregate for sand replacement or in the milled form as a secondary cementitious material, is of growing interest. This interest originates from the perspective of lowering the environmental impact of concrete, reducing the use of primary raw materials, as well as implementing a circular economy. Furthermore, the use of this novel concrete with treated Cu slag as a structural material is an open question. As a first tentative answer to this question, the flexural behaviour of reinforced concrete slabs has been investigated, whereby the slabs have been cast at a ready-mix concrete plant using MFS (treated Cu) slag-based concrete formulations.

To the best knowledge of the authors, the flexural performance of reinforced concrete (RC) structural elements, whereby the concrete is based on MFS or treated Cu slag, has not yet been investigated. However, a few attempts have been made to understand the influence of pozzolanic slags that were quite comparable to MFS [1,2]. Considering that an MFS slag-based concrete mix is designed, amongst others, for a specific concrete strength suited for structural applications and as RC design is to a large extent driven by the concrete class (with compressive strength as the main parameter), the structural behaviour of RC members with MFS based concrete should be close to the conventional concrete. However, for structural engineers to decide about the application of novel concrete mix designs, it is important to know how RC design and performance of MFS based concrete differs with respect to a conventional concrete mix.

MATERIALS AND METHODS

Two mix compositions have been used, a reference mix based on CEM III/A 42.5 N and a concrete mix with 30% MFS cement replacement and natural aggregates were cast at the ready mix concrete plant. Hereby, two different types of cement were used to make the concrete batches. For reference concrete, CEM III/A 42.5 N-type cement was used, whereas, SCM concrete was made with a blend of MFS slag and CEM I 52.5 R. Two different grades of natural sand and gravel have been used.

Four point bending tests were performed on the slabs with a total length of 4300 mm, whereas, the height and width were 150 mm and 400 mm, respectively. The slabs were supported over a span of

4000 mm. The slabs were subjected to two concentrated loads placed symmetrically with a steel profile over the top and a 50 kN load cell, whereas the distance between the two loading points was 1500 mm. Longitudinal reinforcement is placed at the bottom with a clear concrete cover of 25 mm, whereas, the transverse reinforcement is positioned above the longitudinal bars. The steel reinforcement has a diameter of 10 mm, where the distance between both the longitudinal and transverse rebars was 100 mm. The steel reinforcement used was class S500, with a characteristic yield strength of 500 N/mm².

After 28 days of concrete curing (temperature: 13 C ± 5 C; RH: 84.6%), the specimens were loaded up to failure in a displacement-controlled way (stroke rate 0.1 mm/min). During testing the following measurements have been recorded:

- Applied total load, using a 50 kN load cell
- Midspan deflection, using a potentiometric and various linear variable displacement transducers
- Concrete strains in the constant moment region (between the point loads), using strain stirrups. Strain stirrups are provided at the top of the specimen to assess the average concrete strain at the top (designated as "C"). Similar, stirrups are provided at the level of the longitudinal tensile reinforcement to assess the average concrete strain(designated as "T").

RESULTS & DISCUSSION

The overviewof the test results of the 2 tested slabs are given in Table 1, in terms of ultimate load capacity, midspan deflection at failure and failure aspect. The behaviour of the MFS slag-based specimens was very similar to that of the reference slab. All specimens failed, as designed for, by yielding of the steel followed by concrete crushing. The failure load of the both specimens was very similar and large midspan deflections at the ultimate limit state are obtained for both specimens.

Although some limited differences in concrete strength properties are observed between the 2 mixes, this appears not to significantly influence the test results. This is because the flexural behaviour of these slabs is mainly driven by the internal reinforcement (which is identical for the 2 specimens) and to a lower extent by the concrete compressive strength.

Table 1. Summary of main results of the 4-point bending test on slabs.

Specimen designation	Maximum load (kN)	Maximum deflection (mm)	Failure aspect*
SCM 1	24.35	426.7	YS/CC
SCM 2	24.86	272.2	YS/CC

* YS/CC: yielding of the steel reinforcement followed by concrete crushing at the top

In Eurocode 2 [3–5] equations are given to estimate the concrete tensile strength and modulus of elasticity, corresponding to a specific concrete compressive strength. Table 2 shows a comparison between these calculated values and those experimentally observed. As input for the calculation, each time the experimental mean concrete compressive cube strength is considered (which is first converted into a concrete compressive cylinder strength, nearly equal to 0,8 times the cube strength). It is clear from Table 2 that the f_{ctm} (flexural tensile strength), f_{ct_sp} (splitting strength) and E_{cm} (E-modulus) of all the concrete mixes are underestimated using the EC2 equations. It can be concluded that applying EC2 relations valid for more traditional concrete gives an underestimation of the mechanical strength of MFS Cu based concrete. The order of magnitude of the underestimation appeared similar between the 2 concrete types used in the slab tests.

Furthermore, in Table 3 a comparison is given between the predicted failure load and the experimental failure load of the 2 slabs. The flexural load resistance calculation of the slabs has been done following EC2, yet assuming all safety factors equal to 1, considering the f_{cm} following Table 2, and assuming a mean strength of the steel equal to 530 N/mm². For the concrete constitutive model, the parabolic-

rectangular design model has been used, which assumes concrete crushing at 3.5 mm/m. This confirms that EC2 calculation remains suited to predict the flexural capacity of the slabs based on MFS concrete, similar to the reference specimen.

Table 2. Mechanical properties according to Eurocode 2 (SCM 1 and SCM 2).

Test	SCM 1			SCM 2		
	Exp	Pred	Exp/Pred [-]	Exp	Pred	Exp/Pred [-]
f_{cm} cubes	51.50	N/A	-	46.80	N/A	-
f_{cm} = 0.8* fcm_{cub}	40.60	41.20	0.98	37.9	37.4	1.01
f_{ctm} = 2.12 * ln(1+ fcm/10)	4.91	3.46	1.41	4.1	3.3	1.24
f_{ctsp} = fctm/0.9	5.11	3.85	1.32	4.9	3.7	1.32
E_{cm} = 22000 $(fcm/10)^{0.3}$	41045.87	33642.78	1.22	39870	32690	1.21

Table 3. Failure load according to Eurocode 2 (SCM 1 and SCM 2).

Specimen designation	Exp. [kN]	Pred. [kN]	Exp/Pred [-]
SCM 1	24.35	25.8	0.94
SCM 2	24.38	25.7	0.94

CONCLUSION

In short, the results discussed give the first confirmation that concrete based on MFS slag can indeed be used for structural applications. From the perspective of easy availability of raw materials and material flow balance matching the available volume of MFS with possible demand by ready mix plants, practical applicability has been confirmed. From the perspective of design engineers, this preliminary investigation with respect to design and flexural performance gave very interesting overview with respect to standard practices.

It should however be noted that the practical-oriented reflections in this chapter are based on limited data and testing of only 2 specimens, in terms of isostatic one-way loaded slabs. To extend this conclusion to a broader range of structural members, loading conditions and further optimized MFS slag-based mix designs might be needed. Therefore, during the development stage of this novel concrete, design by testing approaches could be considered to support practical structural applications.

ACKNOWLEDGEMENT

The authors would like to express their appreciation for the support by the SIM MARES program (DUSC project), grant number HBC.2017.0607.

REFERENCES

[1] G. Fathifazl, A.G. Razaqpur, O.B. Isgor, A. Abbas, B. Fournier, S. Foo, Flexural performance of steel-reinforced recycled concrete beams, ACI Struct. J. 106 (2009) 858–867. https://doi.org/10.14359/51663187.

[2] S. Seara-Paz, B. González-Fonteboa, F. Martínez-Abella, J. Eiras-López, Flexural performance of reinforced concrete beams made with recycled concrete coarse aggregate, Eng. Struct. 156 (2018) 32–45. https://doi.org/10.1016/j.engstruct.2017.11.015.

[3] C. Arya, Eurocode 2: Design of concrete structures, in: Des. Struct. Elem., 2015. https://doi.org/10.1201/b18121-18.

[4] G. Toniolo, M. Di Prisco, Reinforced concrete design to eurocode 2, in: Springer Tracts Civ. Eng., 2017. https://doi.org/10.1201/b15266.

[5] C. Nwoji, A. Ugwu, COMPARATIVE STUDY OF BS 8110 AND EUROCODE 2 IN STRUCTURAL DESIGN AND ANALYSIS, Niger. J. Technol. 36 (2017). https://doi.org/10.4314/njt.v36i3.14.

4. Service life and life cycle assessment

LIST OF CONTRIBUTIONS

Greening concrete with circular practices: environmental, toxicological, and economic benefits and challenges

Prof. José Dinis Silvestre[1]

[1] Department of Civil Engineering, Architecture and Georesources, Instituto Superior Tecnico - Universidade de Lisboa, PORTUGAL. (E-mail: jose.silvestre@tecnico.ulisboa.pt)

KEYNOTE SUMMARY

The construction, use and rehabilitation of buildings generate substantial environmental impacts, namely due to the significant consumption of energy resources and environmental emissions. Life Cycle Assessment (LCA) is an important tool to identify, quantify and prevent these impacts.

This lecture will focus on the environmental LCA methodology, and on how it can support eco-innovation and the implementation of a circular economy in the construction sector, and particularly in the concrete value chain.

The application of LCA to the construction materials' industries makes manufacturers look at the processes from the production stage until the end-of-life of a product, and acknowledge and reduce their global environmental, but also social and/or economic, impacts. Besides improving their processes, manufacturers are also challenged to choose more sustainable raw materials and energy sources, to reduce transportation distances, and to improve their products' performance at installation, during operation and at end-of-life. The eco-design (ecologic design) of products and the stimulus for the use of more ecologic products should be motivated since both can mitigate climate change. The implementation of this strategy at a European level is giving rise to the birth of criteria for ecologic purchases (green procurement).

The use of subproducts or secondary resources in concrete can increase the efficiency of resource use, reduce pressure to landfills and generate revenues and new business opportunities. Nevertheless, these advantages substantially depend on the thoughtful evaluation of the potential toxicological risks and of the increased transportation needs of these practices.

Researchers from the PositiveCycle group from CERIS (Civil Engineering Research and Innovation for Sustainability) centre at Instituto Superior Técnico - Universidade de Lisboa, Portugal (positivecycle.pt), already made important contributions for this body of knowledge, including cement-based and composite construction materials with recycled or bio-based content. This lecture will present some of these results, and available data and tools at the international level for the sustainability assessment of these construction materials

Sensitivity analysis for a probabilistic service life prediction of alkali-activated concrete

Tamara Janey Chidiac[1], Neven Ukrainczyk[2], Dale P. Prentice[3,4], Zhidong Zhang[5], Tim Soetens[6], Bjorn Van Belleghem[6], John L. Provis[1]

[1]Department of Materials Science and Engineering, University of Sheffield, Sheffield, UK. (t.chidiac@sheffield.ac.uk, j.provis@sheffield.ac.uk)

[2]Institute of Construction and Building Materials, Technische Universität Darmstadt, Germany.

[3]Laboratory for the Chemistry of Construction Materials, UCLA, USA.

[4]Institute for Carbon Management (ICM), University of California, Los Angeles, USA

[5]Department of Civil, Environment, and Geomatic Engineering. ETH Zürich, Switzerland.

[6]Sanacon bv Merelbeke, Belgium. (Bjorn.VanBelleghem@sanacon.be, tim.soetens@sanacon.be)

HIGHLIGHTS

- A reactive transport model (RTM) has been proposed in order to couple the effects of carbonation and relative humidity on chloride ingress, and thus predict service life, of alkali-activated concrete.
- Resistivity measurements are performed on alkali-activated and Portland cement-based mortars that have been exposed for 120 days in three different laboratory climate chambers. The data obtained are used to estimate the evolution of the formation factor, as a function of time, and implement its effects on transport properties in the RTM.
- The RTM has been validated with service data and sensitivity analysis has been conducted to indicate the most prominent variables in the model that impact service life calculations.

Keywords: reactive transport model, service life, sensitivity analysis

INTRODUCTION

The time taken to reach the serviceability limit state of a structure exposed in corrosive environments has often been calculated by service life models (SLM) solely based on Fick's second law for chloride diffusion [1]. The main limitation of this type of model is that it does not account for the modes of transport and reaction that occur when the concrete is exposed in unsaturated conditions. In this state, moisture egress, chloride ingress and carbonation reactions can occur at the same time and aggravate the durability of the structure. Therefore, the focus of this research is: to first validate a developed reactive transport model (RTM) with real chloride profile data, and then to probabilistically calculate the service life of alkali-activated concrete, AAC, through sensitivity analysis.

MATERIALS AND METHODS

In this research, a link between chloride data in laboratory and service conditions is made, to predict the chloride profiles in AAMs for the same number of years that a PC based structure is exposed in a real marine environment. For this outcome to be estimated, the following steps have been

implemented. First, periodic resistivity measurements, through embedded electrode method [2], have been performed on alkali-activated and Portland cement-based mortars submerged in water for 120 days at three different testing temperature conditions: 10,20 and 30°C. The following table describes the mix design of the mortars.

Table 13 Mix design of alkali-activated and Portland cement mortars

Sample	Na_2O (Wt.% of Binder)	Mr ($nSiO_2/nNa_2O$)	water/binder	Sand/binder
100%Slag	4	1.5	0.5	3
CEMII	-	-	0.5	3

Next, the data obtained is used to estimate the time evolution of formation factor of the mortars that is needed to calculate the aging factor and be included in the effective diffusion of chloride ions. This aging factor represents the extent of cement hydration resulting from pozzolanic activity. The third step is comparison between the chloride profile of laboratory PC concrete predicted after 25 years and the chloride profile, obtained from literature, of a PC structure exposed for the same number of years [3]. Based on differences between these results, the chloride aging model for PC has been readjusted to incorporate effects of real service conditions on the durability of the concrete. Finally, combining the real service chloride profile of PC-concrete and comparison factor of chloride profile between AAM and PC-based mortars, obtained in laboratory conditions, the chloride profile of AAM-concrete in real conditions after 25 years is predicted. The data will be used to validate the proposed reactive transport service life model.

FUNDAMENTAL RELATIONS

Concrete is described as a reactive porous medium with a variable moisture state that is dependent on the environmental relative humidity. The pore saturation degree governs the effect of carbonation on chloride ingress only when its value is in low and medium ranges, whereas in complete saturation only the chloride ingress would take place [4]. The pore saturation degree, SL, is considered as the volumetric fraction of the liquid phase in pores of the concrete as follows,

$$s_l = \frac{\phi_L}{\phi} \tag{1}$$

Where ϕ is the total porosity, containing a fraction of the gas phase ϕ_G and fraction of the liquid phase ϕ_L.

The following system of partial differential equations is described as follows:

Eq.2.a; couples the moisture, $\boldsymbol{\varepsilon}$, via anomalous transport due to moisture hysteresis effect present in the cementitious system, with dissolved ions, chlorides and carbonates, that result from chloride ingress and carbonation reactions.

Eq.2.b; defines the ingress of chloride ions, Cl-, in the aqueous state, along with chloride binding by the formed cement hydrates.

Eq.2.c; describes the diffusion of carbon dioxide in the gaseous phase of the capillary pores of the concrete and its dissolution into the pore solution in the form of carbonate ions, CO_3^{2-}.

Eq.2.d; links the transport of formed carbonate ions with their consumption via the formation of the carbonate phase calcite, CaCO3.

Eq.2.e; calculates the congruent dissolution of calcium-containing cement hydrates and precipitation of calcium carbonate, dependent on the content of free carbonate ions in the pore solution

$$\begin{cases} (c_{Cl}+c_{CO_3^{2-}})\dfrac{\partial \varepsilon}{\partial t}=\left(D_{Cl}c_{Cl}+D_{CO_3^{2-}}c_{CO_3^{2-}}\right)\dfrac{\partial^2 \varepsilon}{\partial x^2}+\nu(c_{Cl}+c_{CO_3^{2-}})\dfrac{\partial \varepsilon}{\partial x}+(c_{Cl}+c_{CO_3^{2-}})\Gamma_w & (2.a)\\ \varepsilon\dfrac{\partial C_{Cl}}{\partial t}=\varepsilon D_e\dfrac{\partial^2 C_{Cl}}{\partial x^2}+\nu\varepsilon\dfrac{\partial C_{Cl}}{\partial x}-\dfrac{\partial q_{cl}}{\partial t} & (2.b)\\ (1-\varepsilon)\dfrac{\partial C_{CO_2}}{\partial t}=D_{CO_2}(1-\varepsilon)\dfrac{\partial^2 C_{CO_2}}{\partial x^2}+g(1-\varepsilon)\dfrac{\partial C_{CO_2}}{\partial x}-rCO_{2(aq)} & (2.c)\\ \varepsilon\dfrac{\partial C_{CO_3^{2-}}}{\partial t}=D_{CO_3^{2-}}\varepsilon\dfrac{\partial^2 C_{CO_3^{2-}}}{\partial x^2}+\nu(\varepsilon)\dfrac{\partial C_{CO_3^{2-}}}{\partial x}+rCO_3^{2-}-rC & (2.d)\\ \dfrac{\partial m}{\partial t}=Ak\left(\dfrac{a(Ca^{2+})aCO3^{2-}}{Ksp_{CaCO_3}}\right) & (2.e) \end{cases}$$

RESULTS & DISCUSSION

The effective chloride diffusion with the aging factor of slag based alkali-activated concrete, in laboratory conditions, has been calculated and modelled through a power function as shown in figure 1 A. This model with the extent of aging set until 1 year based on negligible change in chloride diffusion shown after 1 year according to figure 1 B has been included in equation 2.b in order to predict the total chloride profile after 25 years as shown in figure 2. In addition, the effect of temperature is also included in the chloride transport by using the following Arrhenius equation with activation energy, Ea, calculated to be 10,000 J.mol-1.K-1;

$$D_{Cl}=D_{eff}\times e^{\frac{E_a}{R}\times\left(\frac{1}{T_e}-\frac{1}{T_0}\right)} \qquad (3)$$

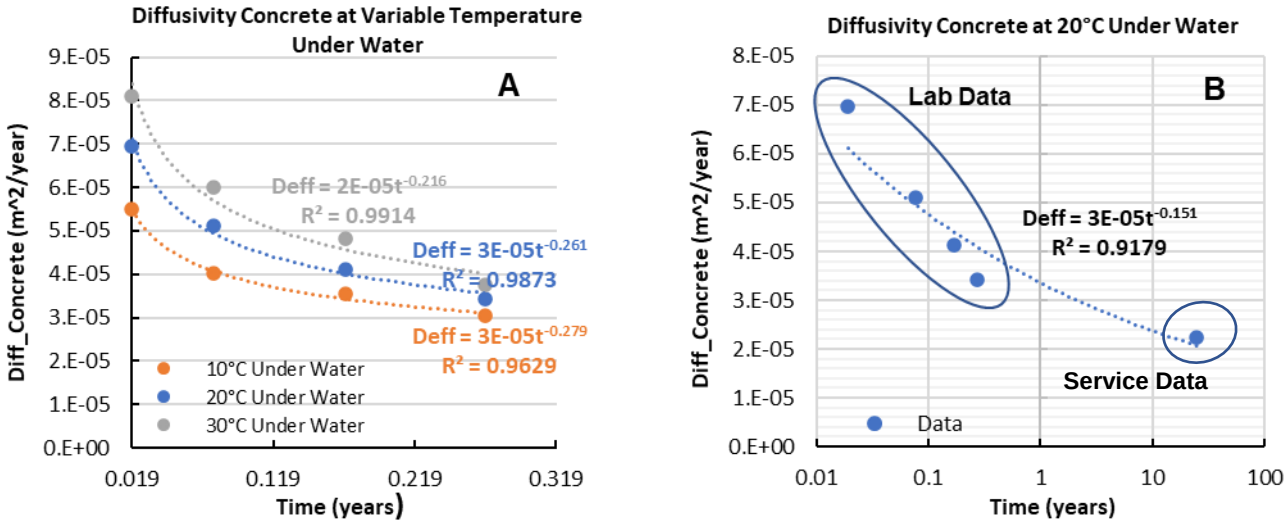

Figure 18. Effective chloride diffusion in alkali-activated slag concrete submerged in water at different temperatures (A) and extent of chloride diffusion after 25 years of exposure (B).

Figure 2 shows that the predicted chloride profile from the RTM has been validated with the estimated chloride profile of slag based alkali-activated concrete exposed for 25 years in real service conditions. In addition, with the conversion factor from mol/l to wt.% of binder, by ≅1.5, figure 3 depicts the accumulation of chloride content, in wt.% of binder, after 100 years across the rebar located at 50 mm cover depth as a function of the percentage of chloride binding. It can be deduced that the effect of

activating solution and mineralogical composition of the cement, that control the percentage of chloride binding, have a great impact on service life of alkali-activated slag concrete. The presence of chloride binding can lower the 50% risk of corrosion, to a minimal risk of 25%, after 100 years, when the type of slag used contains high calcium and magnesium oxide content in its mineralogical composition and the mix design of the concrete has a low alkali-dosage.

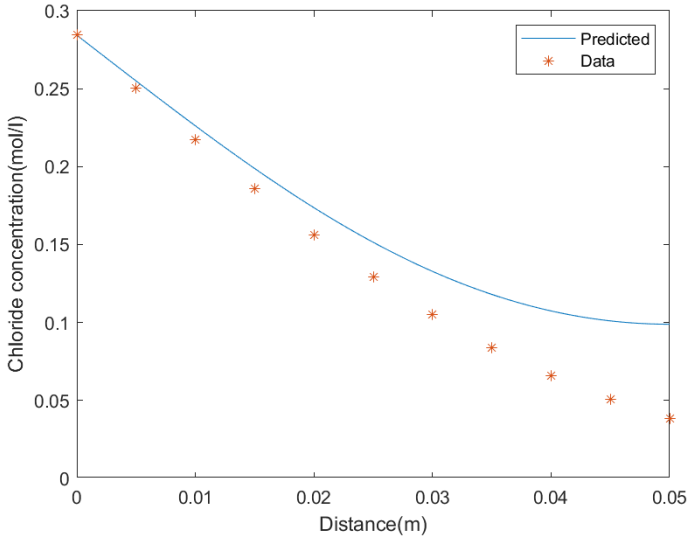

Figure 19. Predicted chloride profile (solid line) compared to real service chloride data (∗) of alkali-activated slag concrete exposed for 25 years in a marine environment. Data for PC-concrete from reference [3].

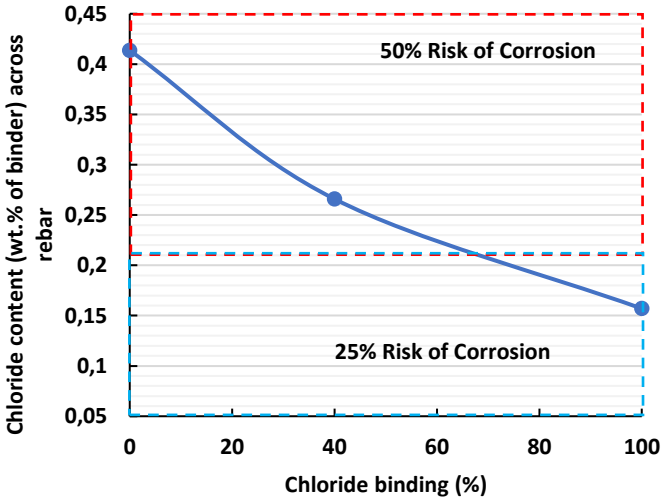

Figure 20. Impact of chloride binding in alkali-activated slag-based concrete (cement = 400 kg/m^3, water/binder=0.5, Na_2O=4 wt.%Binder,Mr=2, sand/aggregate=0.662).

CONCLUSION

The importance of the developed RTM is that it can be used as an efficient decision-making tool in material design of concrete for the suitable structural application and with low environmental impact. The outcome is the estimated uncertainty values for the calculated service life of AAC and the assessment of the main mix variable and durability parameters that have the most impact on the serviceability limit state.

ACKNOWLEDGEMENTS

Research presented in this paper was performed within the DuRSAAM project, which has received funding from the European Union's Horizon 2020 research and innovation programme under the grant

agreement No 813596.

REFERENCE

[1] J. M. Frederiksen, L. Mejlbro, and L.-O. Nilsson, "Fick's 2nd law-Complete solutions for chloride ingress into concrete–with focus on time dependent diffusivity and boundary condition," 2009.

[2] M. M. a. T. S. Bjorn Van Belleghem, "Resistivity of repair materials for concrete repair prior to the application of a cathodic protection system," presented at the 75th RILEM Annual Week-International Conference on Advances in Sustainable Construction Materials and Structures, 2021.

[3] I. Stipanovic Oslakovic, D. Bjegovic, and D. Mikulic, "Evaluation of service life design models on concrete structures exposed to marine environment," *Materials and Structures,* vol. 43, no. 10, pp. 1397-1412, 2010, doi: 10.1617/s11527-010-9590-z.

[4] J. Shen, P. Dangla, and M. Thiery, "Reactive transport modeling of CO2 through cementitious materials under CO2 geological storage conditions," *International Journal of Greenhouse Gas Control,* vol. 18, pp. 75-87, 2013.

The environmental impacts of alkali activated concretes: examining contribution of variability in constituents and of service life time to the uncertainty of LCA

Anastasija Komkova[1], Tamara Janey Chidiac[2], John Provis[2] and Guillaume Habert[1]

[1]Chair of Sustainable Construction, ETH Zurich, Zurich, Switzerland.
(komkova@ibi.baug.ethz.ch, habert@ibi.baug.ethz.ch)

[2]Department of Materials Science and Engineering, University of Sheffield, Sheffield, UK.
(t.chidiac@sheffield.ac.uk, j.provis@sheffield.ac.uk)

HIGHLIGHTS

- The estimates of probabilistic service life time model are included in the LCA of alkali-activated concretes to examine environmental impacts within the target service life time for concrete structures.
- The variability in mix constituents and uncertainty associated with data quality are analysed, along with uncertainty in predicted service life.
- For the FA- and GBFS-FA-based alkali-activated concretes examined, uncertainty associated with service life time is the major contributor to the total variance of the LCA model.

Keywords: life cycle assessment, service life time model, uncertainty

INTRODUCTION

Alkali activated materials (AAMs) are considered to be an alternative to conventional Portland cement (PC) with lower CO2 eq. emissions throughout their life cycle [1]. The published life cycle assessment (LCA) studies often focus on the cradle-to-gate framework, in the absence of key data on durability properties of analyzed mixes, and the rehabilitation and repair of concrete structures are often not included within the scope of the analyses. In this study, we incorporate results of probabilistic service life time modeling into the LCA of steel-reinforced alkali-activated concretes, in order to examine environmental impacts over a 100 year target service life for infrastructure objects.

MATERIALS AND METHODS

In this study we examine AAM concrete mixes with granulated blast furnace slag (GBFS) and fly ash (FA) as single precursors, as well as blends between the two (Table 1). The system boundaries include mix constituent production, and because manufacturing and curing are considered to be conducted under ambient temperatures, the environmental impacts of these processes are assumed to be identical between the mixes, and therefore are not examined within the scope of the LCA. Furthermore, the service life time model estimates time to chloride ingress-induced corrosion, allowing us to calculate concrete cover replacements within the target service life of 100 years. The service life time model follows the 2006 fib Model Code. The functional unit is defined as 1 m3 of steel-reinforced concrete, where concrete cover thickness depends on the mix design. The life cycle inventory has been collected from the Ecoinvent database v3.4. and from the relevant environmental product declarations (EPDs), and analysis is performed using SimaPro software. CML IA method has

been used to quantify GWP100.

Table 1. Mix design parameters per 1 m^3 of concrete.

Mix	GBFS	FA	NaOH	Sodium silicate	Sand	Gravel	Water	Density	Compressive strength	Ref.
	(kg)	(kg)	(kg)	(kg)	(kg)	(kg)	(kg)	(kg/m^3)	(MPA)	
AAS	357		11	5	729	1093	153	2347	35	[2]
AAF		425	25	70	729	1093	110	2453	42	[2]
AASF	205	205	5	36	859	1050	136	1682	47	[3]

The variability in production processes of precursors and activators, along with uncertainty associated with sand, gravel and water data quality in the Ecoinvent database, have been examined using a Monte Carlo simulation in Matlab. Furthermore, the Monte Carlo simulation has also been performed for the service life time model, allowing us to quantify uncertainty associated with time to concrete cover replacement. The global sensitivity analysis has been performed using the UQLab framework to examine the contribution of the each model parameter to the total variance of the model, by quantifying Sobol indices [4].

RESULTS & DISCUSSION

Results of the Monte Carlo simulation for the mixes examined are presented in Figure 1. AAF has the lowest estimated service life-time of average 55 years (SD=4 years), and with concrete cover replacement being required within the target service life of 100 years, it leads to highest environmental impacts among examined mixes, being 483kg $CO_{2\ eq}$ (SD=48kg $CO_{2\ eq}$). The AAS mix has a predicted service life time of 114 years (SD=6 years) and has the lowest GWP among three mixes with the most robust estimates, with a mean of 148kg $CO_{2\ eq}$ (SD=4.9kg $CO_{2\ eq.}$). The blend of slag and fly ash has 101 years of life time with an SD of 4 years, where uncertainty associated with the number of concrete cover replacements is reflected in the peaks of the obtained distribution for AASF as observed in Figure 1.

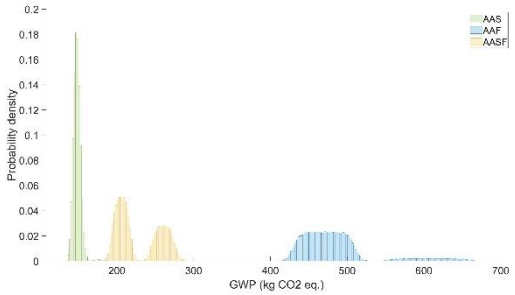

Figure 1. GWP over 100 years of target service life time.

Figure 2a shows that for GWP of AAS, the main source of uncertainty is the data quality for gravel production, followed by variability in blast furnace slag production processes and uncertainty associated with predicted service life time. The major contributor to the uncertainty associated with the estimated GWP of AAF concrete is service life time, followed by the variability in sodium silicate production (Figure 2b). This also holds for the AASF concrete mix design (Figure 2c).

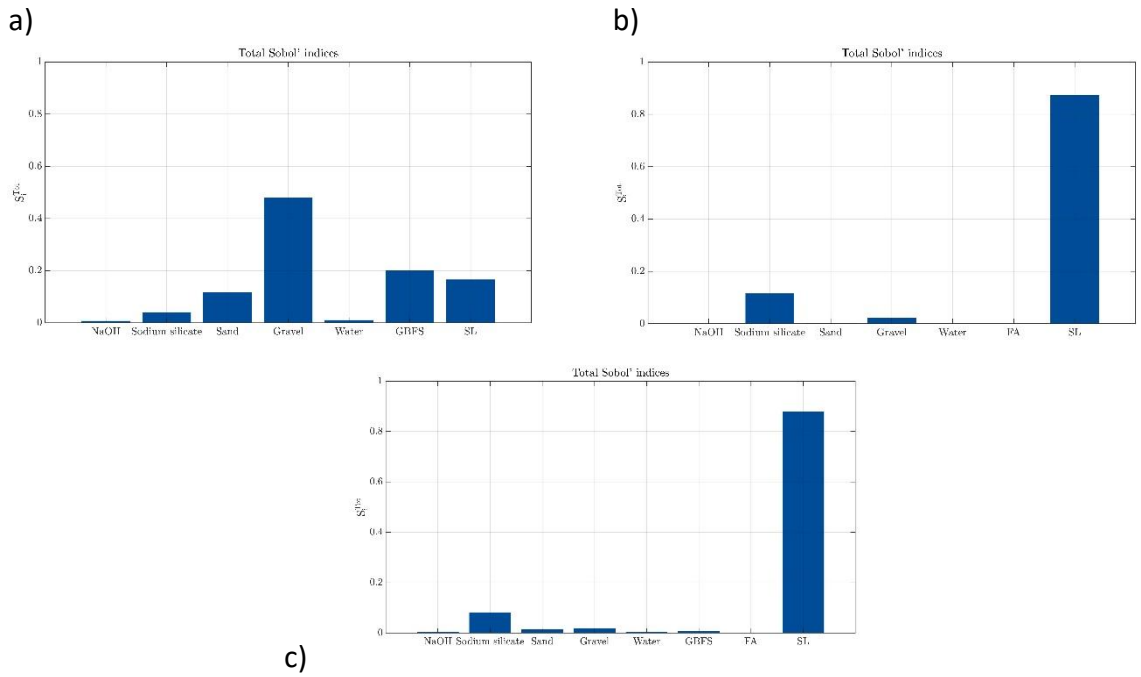

Figure 2. Contribution of uncertainty associated with input parameters to the total variance in GWP of (a) AAS, (b) AAF, and (c) AASF concretes.

CONCLUSIONS

A probabilistic service life time model has been used to predict the time to concrete cover replacement within the target service life time of 100 years. Among the mixes examined in this study, the GBFS-based AA concretes have highest estimated service life time and lower CO2 eq. emissions, compared to the FA-based AAMs and GBFS-FA blends. Uncertainty associated with the service life time has the highest contribution to the total uncertainty of LCA results of the examined FA-based AA concrete mixes and hybrid GBFS-FA concrete mixes, meaning that durability properties have to be considered when comparing the environmental impacts of alternative materials. Therefore, service life time can have a crucial impact on the total LCA outcomes of AAM mixes and therefore can become a determining factor in the choice of optimal mix design for concrete structures.

ACKNOWLEDGEMENT

This project has received funding from the European Union's Horizon 2020 research and innovation programme under grant agreement No. 813596 DuRSAAM. The opinions expressed in this document reflect only the author's view and reflects in no way the European Commission's opinions. The European Commission is not responsible for any use that may be made of the information it contains.

REFERENCES

[1] A. Komkova and G. Habert, "Environmental impact assessment of alkali-activated materials: Examining impacts of variability in constituent production processes and transportation," Constr. Build. Mater., vol. 363, #129032, 2023.

[2] L. Provis et al., "RILEM TC 247-DTA Round Robin Test: Mix design and reproducibility of compressive strength of alkali-activated concretes," Mater. Struct., vol.52, #99, 2019.

[3] A.Noushini, Q. D. Nguyen, and A. Castel, "Assessing alkali-activated concrete performance in chloride environments using NT Build 492," Mater. Struct., vol. 54, #57, 2021.

[4] F. Belizario-Silva et al., "Stakeholder influence on global warming potential of reinforced concrete structure," J. Build. Eng., vol. 44, #102979, 2021.

5. Industry perspective and application cases

LIST OF CONTRIBUTIONS

Keynote lecture:

Extended abstracts:

Industry perspective and application cases

Dr. Vilma Ducman[1]

[1] Laboratory for Cements, Mortars and Ceramics, ZAG, SLOVENIA. (E-mail: vilma.ducman@zag.si)

KEYNOTE SUMMARY

The construction sector in Europe is strictly regulated by the Construction Products Regulation (CPR, 305/2011), which sets technical requirements and legal procedures for placing construction products on the EU market. This strict regulation aims to ensure the safety, stability and sustainability of construction works by properly fulfilling seven basic requirements:

1. Mechanical resistance and stability
2. Safety in case of a fire
3. Hygiene, health and the environment
4. Safety and accessibility in use
5. Protection against noise
6. Energy economy and heat retention
7. Sustainable use of natural resources

A product that is labelled by CE mark meets the basic requirements that are important for its intended use. The procedures for meeting the requirements from the CPD are detailed in the harmonised European standards (hEN) for most construction products; such standards exist for practically all traditional construction products from bricks and cement to aggregates, concrete, roof tiles, etc. Most of the EN standards are so-called "material-based" rather than "performance-based" standards, which means that it matters what materials the product is made of. Such an approach presents some obstacles, as newly developed products are often not covered by harmonised standards. For example, there are no standards for alkali-activated materials, and the standards for cement-based (OPC) materials cannot be used directly for alkali-activated products. Therefore, a different route must be taken: either the procedure established by EOTA (European Organisation for Technical Approval) or a national procedure, which may vary from country to country. Some EU-funded projects (H2020 InnoWEE, H2020 Wool2Loop, EraMIn FLOW...) have already recognised that a lack of standardisation in the field of alkali-activated products could hinder or slow down their successful positioning on the market, and therefore procedures have been elaborated to address these regulatory issues. This approach and some potentially problematic technical aspects (including leaching) will be presented at the workshop.

Design and tendering experiences of a geopolymer concrete bridge

C.B.M. Blom[1], W.D. Schutte[2], A.P. Allaart[3], J.L.M. van Leeuwen[4]

[1, 2, 3, 4] City of Rotterdam, Engineering department, Rotterdam, THE NETHERLANDS. (E-mail: cbm.blom@rotterdam.nl, w.schutte@rotterdam.nl, ap.allaart@rotterdam.nl, jlm.vanleeuwen@rotterdam.nl)

HIGHLIGHTS

- Lessons from an actual tendering project with Geopolymer Concrete.
- How clients could apply Geopolymer Concrete as structural concrete.

Keywords: geopolymer, concrete, client, AAM, GPC, Eurocode, full-scale, test

INTRODUCTION

The city of Rotterdam is a local governmental organization. A major task is to develop and maintain infrastructures (e.g. transportation, sewers, water barriers) and buildings which involve concrete. The tasks should obey political ambitions, including the reduction of CO2e (equivalent) exhausts and usage of raw material resources.

Figure 1. Impression of the test project for URBCON concrete.

The Interreg project URBCON (2019 – 2023) serves the goal to reduce CO2 (equivalents) production and limiting raw material resources in the process to create concrete. Rotterdam participates in this project to include the role of clients. On the one hand is the development of concrete types without (or limited use of) Ordinary Portland Cements (OPC) by use of Alkali Activated Materials (Geopolymer Concrete, GPC) and the use of a considerable amount of secondary (mined) raw materials like sands and aggregates. On the other hand, the society is willing to use these new types of concrete. Clients evidently play an important role.

Many research projects on new concrete developments have several scales, from molecular, nano, micro to macro levels. From the client's perspective it should be understood that projects involve design, funding, verification, tendering, procurement, permits, project management, construction, usage, maintenance, etc. In a regular tendering process the procedures are quite efficient and based on known track records (risk control) and sets of regulations (e.g. Eurocodes, certifications, protocols), which are not valid and available for the newly developed concretes. The inclusion of 'clients needs' is an additional scale level that is included in the URBCON project.

To clients it is of interest what (tendering) processes should look like in projects in order to make use of the developments. The Rotterdam participation in URBCON includes the actual realization of a concrete pedestrian bridge, which is a structure that normally would fit the standard procedures (see figure 1).

NEW CONCRETE FROM THE CLIENTS POINT OF VIEW

During the URBCON project some interesting lessons are learnt.

1. **The client prescribes the basic performance parameters for the concrete, based on terms**

known from Eurocode 2.

It turned out that the basic performance parameters could be described as 'equivalent to': strength class C45/55, environmental classes XD3/XF4 and consistence class S4. The client was able to formulate this based on a regular preliminary design of the bridge structure. As a result to the client, these performance parameters are now basic assumptions and should therefore be guaranteed to be fulfilled in the project.

2. **The scientists develop the new concrete and perform a wide range of tests that show the properties.**

The scientists developed geopolymer concrete mixes based on AAM based on the default research scales (paste, mortar, concrete). During the process the client was requested to express their preference for an expected successful preliminary concrete mix design. In this case the amount of secondary raw aggregates has been of choice. Higher amounts has a drawback on properties but has benefits to the Environmental Cost Indicator (ECI) and the client deals with the trade off in this decision.

3. **The scientists prove that the basic performance parameters are obeyed.**

A structured test plan was used to execute tests at different ages of the concrete. All participants contributed to this plan and results were discussed. To the client it became clear that additional attention should be needed to describe matters in tendering documents and the constructor should be supported to use the newly developed concrete mix.

4. **The scientists provide information about anomalies that influence the design, building, use or maintenance of the structure.**

Some anomalies became clear form the tests (in comparison with regular EC2 concrete):

(a) More sensitive to creep and frost-thaw. As a consequence the bridge design has been adjusted (shape that compensates for creep deformation, sealing of the up facing sides and increased concrete cover).

(b) Strict prescription of secondary raw materials. It turns out that the mix quality is sensitive to the used secondary raw materials. Therefor the client exactly prescribes which material must be used by the contractor.

5. **The scientists provide the recipe and mix specification (and education) to the contractor.**

At this point Intellectual Property (IP) became of interest. The concrete mix developing is a very knowledge intensive process and the IP should be respected. The tender includes not the specific recipe, but it explains that a new type of concrete mix has to be used. The actual recipe will be provided after procurement to the winning contractor of the tender. Also, the winning contractor guarantees the client, issued by the concrete developer, that for future (other) projects this mix will only be used with respect to the IP. Another issue is that the scientists will be stand by to the contractor by actual preparing the concrete mix at the supplier factory. In case of upscaling concrete from lab to practice it is known that sometimes adjustments are required to mix order or doses.

6. **Tests are needed to prove that (structural) verification rules from Eurocode 2 are accepted.**

The new concrete doesn't fulfill the EN206 requirements. Therefore EC2 is basically not applicable. The question is how to provide evidence that the structure is structurally safe. The concept of (Eurocode 0) 'design by testing' is used: next to tests on pastes, mortars and (small) concrete specimens, the client (also in agreement with local permit departments) requires fundamental element tests (i.e. large specimen 4 point bending and shear testing). From these tests it became clear that for this concrete mix design it is expected that EC2 basic rules for ULS could be applied. The bridge itself will be monitored for a long time, to provide information on long term behavior and properties. Finally the bridge has to be full-scale tested up to design load. To this final test the consequence is that the bridge

will be loaded beyond service level and extended cracking would be expected, which is a drawback to durability. Therefor the bridge design has been adjusted to limit crack development in case of this full-scale test.

CONCLUSION

Reduction of CO2e exhausts and usage of secondary raw material resources lead to new concrete types which are of interest to clients. The city of Rotterdam is a local governmental organization willing to use the new concrete types. Rotterdam joined the URBCON project to learn and experience how the new concrete mixes could be used in actual projects and what it means to traditional tendering processes. It is concluded that the cooperation between researcher, industry and clients in URBCON is very valuable. Many lessons have been learnt to all participants.

The URBCON project finalizes in 2023 and results will be published.

ACKNOWLEDGEMENT

The authors would like to express their appreciation for the support of the European Interreg-program North-West Europe and the URBCON project. City of Ghent (administrative coordinator), Ghent University (technical coordinator), City of Rotterdam, TU Delft, FDN Engineering, University of Sheffield, Imertech, ResourceFull, CWARE, Kamp C, TU Kaiserslautern, ArcelorMittal BE.

REFERENCES

http://www.nweurope.eu/urbcon

Removal of ammonium from wastewater with metakaolin based-geopolymer sorbents

M. Otero[1], L. Freire[1], S. Gómez-Cuervo[1], P. Villar[1]

[1] AIMEN Technology Centre, O Porriño, SPAIN. (E-mail: miguel.otero@aimen.es, lorena.freire@aimen.es, santiago.cuervo@aimen.es, pvillar@aimen.es)

HIGHLIGHTS

- Metakaolin based geopolymer was manufactured as ammonium adsorbent.
- Characterization through batch and continuous tests.
- Implementation of a wastewater treatment plant with adsorbent geopolymer.

Keywords: geopolymer, sorbent material, metakaolin, NH_4^+ removal

INTRODUCTION

Ammonium (NH4+) is the most dominant form of nitrogen pollution in the aquatic environment. Elevated NH4+ concentrations in untreated waterways contribute to eutrophication and dissolved oxygen depletion, which causes severe degradation of water quality. Untreated wastewater containing high organic and nitrogen contents poses serious environmental problems if those pollutants are improperly managed. Anaerobic treatment technology is commonly adopted to treat piggery wastewater especially in developing countries with only emphasis on removing organic matter. However, the NH4+removal in anaerobic systems were limited.

The commonly methods used for NH4+ removal include microbial nitrification–denitrification reactions, breakpoint chlorination, air extraction, reverse osmosis, ionic exchange and sorption. The most widely used method to remove nitrogen from wastewater is microbial nitrification–denitrification reactions. However, nitrification rate drops sharply as temperature of wastewater decreases [1]. Adsorption or ion-exchange-based approaches offer a more robust alternative method for NH4+ removal. It was demonstrated by a simulation that anaerobic digestion followed by zeolite-based ion-exchange had lower operational costs and better nitrogen-removal [2].

One of the main problems with zeolites is in their production, which requires high synthesis temperatures. Geopolymers have emerged as a promising alternative. Geopolymer is an inorganic polymer with excellent mechanical and physical properties and can be synthesized by alkaline activation of aluminosilicate materials from natural minerals or inorganic waste. Like zeolite, geopolymer has negative charges on the aluminosilicate structure where the exchangeable cations are located in the voids. The geopolymer could be synthesized at room temperature, resulting in lower energy consumption. To reduce the consumption of non-renewable resources in line with the circular economy principle, attempts have been made to convert industrial waste into useful products, including geopolymer. These materials do not require high synthesis temperatures, and their raw materials are available locally and at a relatively low cost. In addition, its adsorption capacities are even slightly higher than zeolites [1].

In our study, a porous metakaolin based-geopolymer was manufactured. Batch and continuous experiments were carried out to study ammonium removal capacity. After laboratory tests, the produced geopolymer with optimal characteristics is taken to a real industrial wastewater, located in Spain in order to validate the capacity adsorption.

Metakaolin geopolymers were manufactured at room temperature using waste from the granite industry. Commercial sodium silicate solution (Na2SiO3) containing 25,6 wt% SiO2, 7,9 wt% Na2O and 66,5 wt% H2O; and sodium hydroxide solution (NaOH) were used as alkaline activator with different silicate modulus (Ms). H2O2 was added as foaming agent in a range between 0.5% - 3%. The material was crushed and sieved to obtain particle sizes of 4 - 8 mm.

The adsorbent characteristics play an essential role in the adsorption process. This research characterized and compared the physical properties (e.g., bulk density, apparent porosity) of the synthesized geopolymer adsorbents. Batch experiments were carried out in 250 mL Erlenmeyer flasks using deionized water with known ammonium concentrations and geopolymer weights (generally for 24 h, pH = 6,50 mg NH4+/L and 5 g/L of geopolymer). The effect of variables was measured, including initial water pH, adsorbent dose, contact time and initial concentration. The experimental data will be adjusted to the isotherm model and kinetic equation that present a greater goodness. Column tests were also carried out with a pollutant flow of 6ml/min to determine the adsorbent capacity of ammonium of the produced material.

As a final validation, the optimal formulation obtained from the laboratory results was taken to a Spanish landfill, where two wastewater systems were designed and data on the decrease in ammonium concentration, pH and conductivity were collected.

RESULT & DISCUSSION

Several geopolymer formulations were studied, being the following one, the most promising as adsorbent material (Table 1).

Table 14: Most promising geopolymer formulation.

Silicate modulus	NaOH (M)	Si_2O_3/NaOH (molar ratio)	Granite waste substitution	% H_2O_2	Setting time (h)	Curing T (°C)
1,5	10	1,2	20	1	24	Room temperature

The effect of pH was examined, and it was observed that the adsorption increased slightly the more acid. Regarding the dose of adsorbent, the highest was found at 5g/L with similar results at higher doses. The 1h contact time is when the highest slope of elimination occurs. At longer times the slope becomes smaller. Finally, the initial ammonium concentration tests show that the maximum adsorbent capacity (qm) is 23mg of ammonium per gram of geopolymer.

The isotherm that best fits the data is the Redlich–Peterson isotherm (Figure 1). The rate equation with the best fit is the Weber-Morris equation (Figure 2).

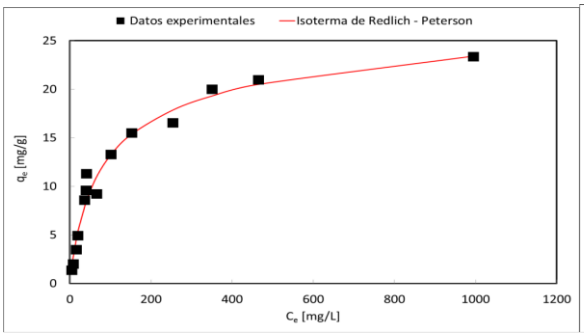

Figure 21: Redlich–Peterson isotherm

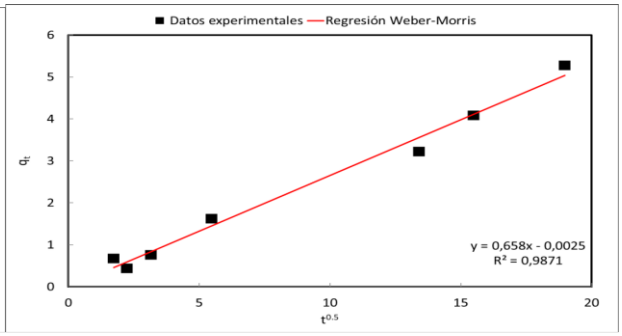

Figure 22: Linear regression fit of the WM equation.

The results of continuous tests performed in columns show how at short times the NH4+ elimination is maximum, but from 120h the geopolymer becomes saturated and the contaminant concentration does not decrease (Figure 3).

Once the laboratory tests were finished, the selected geopolymer were conformed in form of cylinders (3cm diameter, 5 cm height) and in form of gravel (4mm-8mm sizes) as shown in Figures 4 and 5. These pieces were located at the wastewater plant in order to test the adsorbent material in real operating conditions. The results obtained for the ammonium removal in this industrial wastewater plant was up to 80%. However, the pH of the effluent increased from 9 to almost 12 at the outlet of the treatment. This issue needs to be studied in future works.

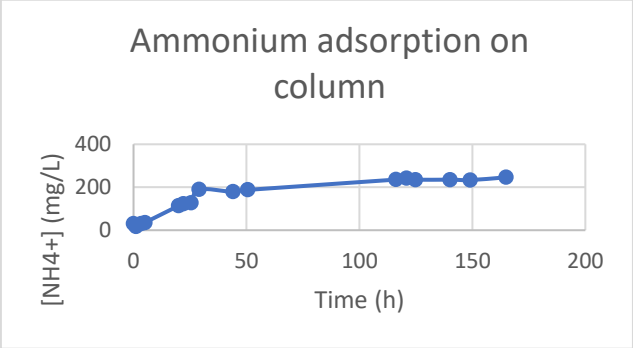

Figure 23. Continuous column tests.

Figure 24. Geopolymer in cilynder format.

Figure 5. Geopolymer in gravel format.

CONCLUSIONS

Preliminary results have shown a high sorption capacity of the geopolymer, obtaining removal efficiencies up to 80% and a maximum adsorption capacity (qm) of about 23 mg/g. This value is similar to that reported for natural and synthetic zeolite [1]. When the geopolymer is implemented in a wastewater treatment plant, the adsorption capacity maintains above 80%.

According to these results, this material can be an alternative adsorbent due to its simple synthesis conditions and low operational costs. In addition, it shows good workability in different climates.

However, more studies are required to increase the NH4+ removal. It is priority to control the adsorption mechanism and the alkali leachate in order to implement the material at industrial scale.

ACKNOWLEDGEMENT

The project LIFE GREENADAPT has received funding from the LIFE Programme of the European Union under the Grant Agreement no LIFE20 CCA/ES/001795.

REFERENCES

[1] Giorgia, F., Janne, P., Tero, L., Chengying, B., Paolo, S., Renata, B., Sara, C., Murilo, I. and Paolo, C. Removal of Ammonium from Wastewater with Geopolymer Sorbents Fabricated via Additive Manufacturing. *Materials and Mechanics* 195 (2020), 109006.

[2] Lin Y, Guo M, Shah N, et al. Economic and environmental evaluation of nitrogen removal and recovery methods from wastewater. *Bioresour Technol*. 215 (2016), 227–238.

Disclaimer: The contents of this publication are the sole responsibility of LIFE GREENADAPT and do not necessarily reflect the opinion of the European Union.

Additive manufacturing of geopolymer-stones to replicate natural sandstones with low availability

St. Partschefeld[1], A. Tutal[1] and A. Osburg[1]

[1] Chair of Construction Chemistry and Polymer Materials, F.A. Finger Institute for Building Materials Science, Weimar, Germany. (E-mail: stephan.partschefeld@uni-weimar.de, adrian.tutal@uni-weimar.de, andrea.osburg@uni-weimar.de)

HIGHLIGHTS

- Development of a geopolymer fine mortar for additive manufacturing with high durability
- Natural sandstones with low availability can be replicate
- Complicated structures can be easily produced

Keywords: additive manufacturing, geopolymer, metakaolin, sandstone replicas

INTRODUCTION

Additive manufacturing with plastics, metals, ceramics and building materials such as concrete is opening more and more areas of application and has achieved a high level of public awareness. The driving force in construction materials industry to establish additive manufacturing, is to increase productivity [1]. Three advantages of additive manufacturing are worth highlighting: Additive processes are material-efficient and resource-saving. To produce a component, only the material that is contained in the component is consumed. Thus, no significant waste is produced during manufacturing. In addition, additive manufacturing offers a maximum in geometric freedom. Shaping is not limited by a necessary demold ability. This means that almost any geometries can be created [2, 3]. Extrusion-based 3D printing is the most popular form of additive manufacturing in construction industry. The material is extruded through a nozzle and applied layer by layer to form an object [1, 2, 4]. Portland cement is usually used as binder for additively manufactured concrete components. However, the binder content is higher than for conventionally molded components [5]. Due to the high CO2 emissions associated with the production of cement, attempts have been made to replace Portland cement with more environmentally friendly geopolymers [6, 7, 8] in additive manufacturing. In recent years, research has also begun into the potential applications of additive manufacturing processes in restoration, conservation, and historic preservation [9] and testing of materials available on the market [10]. In general, the potential applications of additive manufacturing processes in conservation and restoration lie primarily in the production of replicas, customized support structures and precisely fitting additions. Furthermore, 3D models and 3D printing can be used to produce design drawings for new workpieces that are to be integrated into a listed building and avoid faulty designs in advance. The aim of this study was to recreate an often-used weather-sensitive sandstone ("Bebertaler Sandstone"), which is hardly available anymore due to the closure of quarries, by additive manufacturing with a low calcium geopolymer fine mortar.

RESULT & DISCUSSION

For the development of the geopolymer fine mortar, it was necessary to determine the material properties of the Bebertaler sandstone beforehand. For this purpose, the compressive and flexural strength, the particle size, the capillary water absorption, and the bulk density were determined. In addition, the coloration in dry and wet condition was investigated. It plays a special role from the

viewpoint of monument preservation, so that the developed geopolymer fine mortar should correspond to it as far as possible. Furthermore, the additive manufactured geopolymer fine mortar must be workable by stonemasons 'methods like grinding, cutting, and scraping. Table 1 shows the mechanical properties and bulk density of the Bebertaler sandstone as well the capillary water absorption. Due to the high capillary water absorption, frost damage occurs in historic structures made from this sandstone.

Table 1. Material parameters of the Bebertaler sandstone.

Compressive Strength [MPa]	**Flexural Strength** [MPa]	**Bulk Density** [g/cm³]	**Water Absorption** [kg/m²·h^{0,5}]
81.6 ± 5.5	7.8 ± 0.8	2.4	1.6

For the development of the geopolymer fine mortar, a metakaolin from NEWCHEM GmbH (Austria) was used. The metakaolin was characterized in terms of its chemical and mineralogical composition by ICP-OES and XRD analysis. In addition, the pozzolanic reactivity was characterized with the modified Chapelle-test described in the French norm NF P 18-513, Annexe A and the particle size measured by laser granulometry. The determined material properties of the used metakaolin are given in table 2.

Table 2. Material parameters of the used metakaolin.

SiO_2 [%]	**Al_2O_3** [%]	**TiO_2** [%]	**K_2O** [%]	**Si/Al** [-]	**Amorphous content** [%]	**Kaolinite** [%]	**Quartz** [%]	**Reactivity** [mg/g]	**Particle Size** **d_{10}; d_{50}; d_{90}** [µm]
52.1	47.3	0.47	0.49	1:1	71.7	24	2.5	1275	0.75; 8.2; 20.2

A sodium silicate solution made by Woellner GmbH (Germany) was used as an alkaline activator. The SiO2/Na2O ratio of the solution was adjusted to 1.6 by adding NaOH pellets. Due to the high shrinkage of the geopolymer binder of 5.2 mm/m, a granite based crushed sand was used as a filler for mortar preparation to decrease the shrinkage to 0.7 mm/m. A low amount of iron pigment was added to achieve the coloration of the Bebertaler sandstone. The composition of the geopolymer fine mortar used for additive manufacturing is shown in table 1.

Table 3. Composition of the geopolymer fine mortar for additive manufacturing to replicate natural sandstones.

Sodium silicate solution (Module 1.6)	**Metakaolin**	**Granite based crushed sand** (particle size 0 – 0.5 mm)	**Water**	**Fe_2O_3 pigment content** based on the solids content
18.7 %	20.6 %	58.8 %	4.5 %	0.1 %

The developed geopolymer fine mortar exhibits rheological properties suitable for 3D printing in that it liquefies when force is applied and exhibits a stable and resilient base structure when no force is applied. It is also characterized by the fact that no organic additives are required to adjust the consistency. Solidification of the geopolymer fine mortar starts after approx. 5 h at 20 °C and can be significantly accelerated by moderate thermal treatment of 60 °C to 30 min. The project partner WZR ceramic solutions GmbH (Germany) developed a special dual-purpose mixing-extruder for this material

and started by printing prismatic samples with dimensions of 50 × 70 × 200 mm. The printed specimens exhibited a compressive strength of approx. 80 MPa and a flexural tensile strength of approx. 13 MPa, so that comparable mechanical properties to the Bebertaler sandstone were achieved. Climate change storage tests and eluate investigations showed that the developed geopolymer fine mortar has a high durability. The last objective of this study was the creation of an additive manufactured sandstone replica of a complex shaped sandstone specimen which should be reworked in a stonemasonry way with only a small effort. Figure 1 shows the shape of the sandstone to be replicated as a CAD model (left), extrusion printing of the replica with the geopolymer fine mortar (middle), and the demonstrator component with one half reworked in a stonemasonry manner (right).

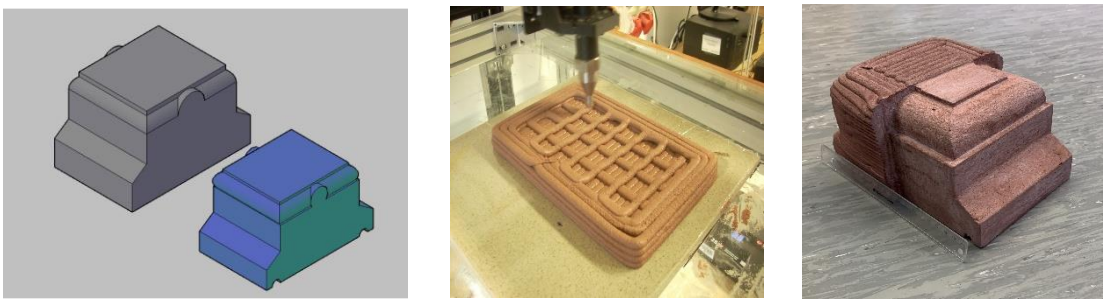

Figure 1. CAD-Model (left), 3D-printing of geopolymer fine mortar (middle) and demonstrator of the replicate sandstone (right).

CONCLUSION

The aim of this study was to recreate an often-used weather-sensitive sandstone ("Bebertaler Sandstone"), which is hardly available anymore due to the closure of quarries, by additive manufacturing with a geopolymer fine mortar. The developed geopolymer fine mortar showed excellent rheological properties for additive manufacturing and high durability especially under different climate conditions.

ACKNOWLEDGEMENT

The authors would like to express their appreciation for the support of the federal ministry of economics and climate protection of Germany, the AiF-Project GmbH and the project partners Opus Denkmalpflege GmbH and WZR ceramics solutions GmbH.

REFERENCES

[1] T. Wangler, N. Roussel, F.P. Bos, T.A.M. Salet, R.J. Flatt. Digital concrete: a review. Cement Concr. Res. 123 (2019) 105780.

[2] M.K. Mohan, A.V. Rahul, G. De Schutter, K. Van Tittelboom. Extrusion-based concrete 3D printing from a material perspective: a state-of-the-art review. Cement Concr. Compos. 115 (2021) 103855.

[3] T.D. Ngo, A. Kashani, G. Imbalzano, K.T.Q. Nguyen, D. Hui. Additive manufacturing (3D printing): a review of materials, methods, applications and challenges. Compos. B Eng. 143 (2018) 172–196.

[4] R.A. Buswell, W.R. Leal de Silva, S.Z. Jones, J. Dirrenberger, 3D printing using concrete extrusion: a roadmap for research, Cement Concr. Res. 112 (2018) 37–49.

[5] C. Zhang, V.N. Nerella, A. Krishna, S. Wang, Y. Zhang, V. Mechtcherine, N. Banthia, Mix design concepts for 3D printable concrete: a review, Cement Concr. Compos. 122 (2021) 104155.

[6] S. Bhattacherjee, A.S. Basavaraj, A.V. Rahul, M. Santhanam, R. Gettu, B. Panda, E. Schlangen, Y. Chen, O. Copuroglu, G. Ma, L. Wang, M.A. Basit Beigh, V. Mechtcherine. Sustainable materials for 3D concrete printing. Cement Concr. Compos. 122 (2021) 104156.

[7] B. Panda, S.C. Paul, L.J. Hui, Y.W.D. Tay, M.J. Tan, Additive manufacturing of geopolymer for

sustainable built environment, J. Clean. Prod. 167 (2017) 281–288.

[8] B. Panda, C. Unluer, M.J. Tan, Investigation of the rheology and strength of geopolymer mixtures for extrusion-based 3D printing, Cement Concr. Compos. 94 (2018) 307–314.

[9] Hergestell, E. 3D-Druck: Recherchen zu Möglichkeiten und Grenzen des Einsatzes für Konservierungs- und Restaurierungsarbeiten. HAWK Hildesheim, Bachelor-Thesis. 2014

[10] Pamer, I. Anwendungsmöglichkeiten des Fused Deposition Modeling (FDM) 3D-Druckverfahrens in der Restaurierung: Materialanalyse und Adaption. HTW Berlin, Master Thesis. 2015

Self-compacting alkali-activated concrete (AAC) for precast prestressed bridge girders - from lab research to industrial production

Shizhe Zhang[1], Mladena Luković[2], Yuguang Yang[3], Hendrik Herder[4], Arend Scharringa[5], Guang Ye[6]

[1, 6] Microlab, Faculty of Civil Engineering and Geosciences, Delft University of Technology, Delft, the Netherlands. (E-mail: shizhe.zhang@tudelft.nl, g.ye@tudelft.nl)

[2, 3] Section Concrete Structures, Faculty of Civil Engineering and Geosciences, Delft University of Technology, Delft, the Netherlands. (Email: M.Lukovic@tudelft.nl, Yuguang.Yang@tudelft.nl)

[4]Haitsma Beton, Kootstertille, the Netherlands. (Email: h.herder@haitsma.nl)

[5]Provincie Fryslân, Leeuwarden, the Netherlands. (Email: a.scharringa@fryslan.frl)

HIGHLIGHTS

- For the first time, the self-compacting AAC was applied to produce a precast prestressed bridge girders in an industrial scale environment, pushing TRL to 8.
- The self-compacting AAC has good flowability and rapid strength development at early age.
- The self-compacting AAC does not show intensive heat release.

Keywords: alkali-activated concrete (AAC), self-compacting, slag, precast, structural application

INTRODUCTION

Using the technology developed at TU Delft, the prestressed precast bridge girders have been produced using self-compacting alkali-activated concrete (AAC) with strength class C45/55 in Haitsma Beton to be tested before the possible real-scale application in the bridge. This is the first time that cement-free AAC has been made for prestressed structural elements for bridges. The binder precursor is blast furnace slag, which is activated using a liquid sodium silicate activator. The fine and coarse aggregates are the same as the ones in conventional concrete. The developed self-compacting AAC performs in a comparable way to conventional ones based on CEM III/B, concerning both fresh properties and mechanical properties. More importantly, when considered per one m3, it reduces the CO2 emission by 70% and the total environmental impact by 50% compared to the self-compacting concrete based on CEM III/B.

This research targets the gap between lab research and industrial production toward broader and large-scale applications of alkali-activated concrete. The fresh properties and mechanical properties of the alkali-activated concrete were determined. The temperature history and the early-age volume stability of the bridge girders were also evaluated. Smart aggregate and fiber optic sensors have been installed inside the girder for monitoring the girders in the later phases of the structural testing and long-term monitoring.

CASTING AND CURING

The mixture design of the self-compacting AAC used are given in Table 15. Noting that a fit-for-purpose retarding admixture effective in AAC mixes were applied in order to meet the requirements of the open time for industrial-scale production.

Table 15. Self-compacting AAC mixture design for bridge girders.

Binder	Blast furnace slag: 550 kg/m^3
Alkaline activator	Sodium-based silicate solution
Admixture	Superplasticizer/retarder
Aggregate	Sand 0-4 mm:, coarse aggregate 4-16 mm

The bridge girder is 7350 mm in length, 990 mm in width, and 300 mm in height. The maximum prestress applied is around 20 MPa for all the girders. The prestress at the anchorage is 20.15 MPa due to the small influence of self-weight. The prestress at the middle of the span is 19.5 MPa.

The casting procedure is similar to the production of conventional self-compacting concrete. The precursors and aggregate were firstly mixed dry for 4 to 5 min before the activator was pumped upwards and added to the mixer. The alkaline activator was added within 2 to 3 min. The retarder was then subsequently added to the mixer within 30 seconds. The mixture was then allowed to mix for another 10 min before it was transferred to the casting hall using a rail system. One trial mixing was conducted on Aug 25. Eight bridge girders were cast separately on Aug 27, Sept 10, and Sep 17, 2021. After demolding, the curing of the girders was done using wet burlaps to cover the surface of the specimen and then seal it with the plastic film (see Figure 26). The successful production has pushed the technology readiness levels (TRL) to 8.

Figure 25. Casting of the bridge girders.

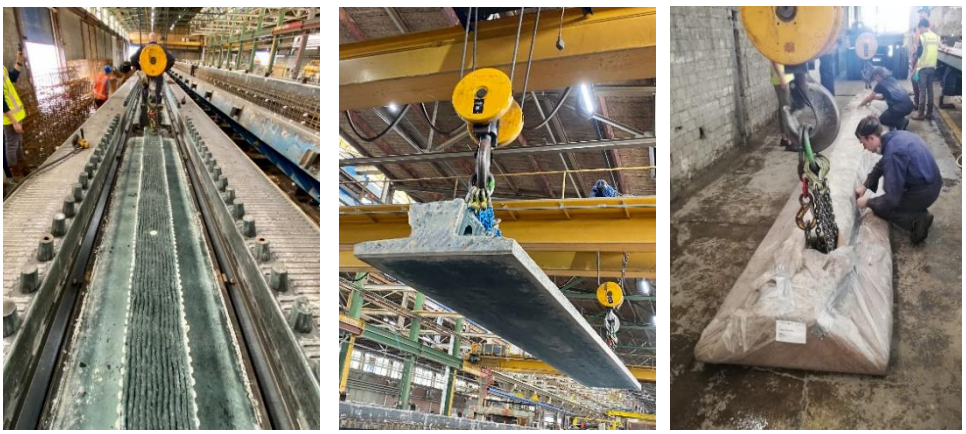

Figure 26. Casting, demoulding and curing of the bridge girders.

RESULT & DISCUSSION

Fresh properties

The Fresh properties of the AAC prepared by an industrial-scale mixer are summarized in Table 16. The followability is tested with J-ring on a flow table according to EN 12350-12. At about 40 min after mixing, the J-ring slump lies in between 560 to 600 mm and the J-ring blocking step is about 15-16.5 mm. These values fulfil the slump-flow class SF1 and the minimum requirement of the blocking-step (BJ=15 mm, an empirical value determined in the lab for AAC). The fresh mixtures seem to be more viscous than conventional Portland cement (PC) concrete, but the mixture can flow nicely without any segregation. Notably, the V-funnel time lies between 3.5 to 4.4 seconds. This value is considerably lower than the self-compacting PC concrete of a similar strength class (6 to 8 seconds). The density of the mixture is very close to the design value of 2300 kg/m3.

Table 16. Fresh properties of the AAC mixture for the casting of the bridge girder.

Casting date	J-ring flowability (mm)	V-funnel time (s)	J-ring blocking-step (mm)	Mixture density (kg/m^3)
Aug 25	600	3.6	15.0	2288
Aug 27	570	3.7	-	2288
Sep 10	560	3.6	16.5	2288
Sep 17	580	4.4	-	2311

Heat evolution and temperature history

The temperature in one of the girders was monitored using 4 temperature sensors. Sensors 1 to 3 were placed in the middle of the girder: 1) near the top surface, 2) in the core and 3) near the bottom surface. Sensor 4 was placed in the core at the end of the girder. The result of the sensors together with the ambient temperature of the manufacturing hall is shown in Figure 27. The AAC hardens under ambient temperature from 19 to 26 ºC in the first three days. Even with the reaction being the most intensive in the first days, the trend of temperature change in AAC, indicating that no large temperature differences between ambient temperature and the girder during hardening were generated, thereby reducing the risk of cracking at the early age. In fact, no cracking was observed during the production.

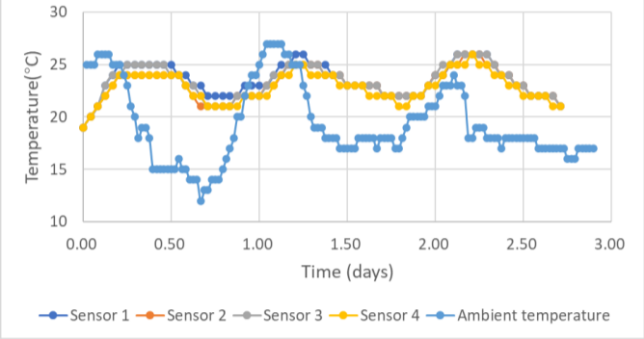

Figure 27. Temperature history of the girder in the first three days.

Mechanical properties

The compressive strength (fc) and elastic modulus (Em) of the AAC is given in Table 17. After 2.5 days of curing, the fc determined using cubic samples (150 x 150 x 150 mm3) is about 50 MPa. The strength development is very fast considering that 85% of 28-day strength has been reached within 7 days. The average elastic modulus (Em) tested for different testing batches, increases from 24.1 GPa at 2.5 days to 35.6 GPa at 28 days. Notably, the 28-day Em is higher than that of the samples prepared in the lab

of TU Delft (30 GPa). This is most likely due to the different types of coarse aggregate used when preparing AAC in Haitsma. In comparison to the pebble aggregate used in the lab of TU Delft, crushed limestone aggregate were adopted during the AAC production in Haitsma. Further tests on the 56-day mechanical properties indicate that both fc and Em is still increasing from 28 days to 56 days when cured under RH>95%.

Table 17. Mechanical properties of the AAC for the casting of the bridge girders.

Age of mixtures	Compressive strength (MPa)			Elastic modulus (GPa)		
	Aug 27	Sep 10	Sep 17	Aug 27	Sep 10	Sep 17
2.5 days	47.5	50.6	49.6	24.1	27.1	25.04
7 days	53.4	53.7	53.5	-	-	-
28 days	63.6	63.4	59.4	35.5	35.6	-
56 days	67.6	64.3	62.8	-	34.2	-

CONCLUSION

- Self-compacting AAC can be produced in a very similar way to conventional concrete on an industrial scale. The current facilities for the production of conventional concrete can also be used for the production of AAC.
- The self-compacting AAC has good flowability. Satisfactory flowability can be maintained for more than 45 min. This makes the casting and processing easy to control.
- The strength development of self-compacting AAC at ambient temperature is very fast and reaches 85% of its designed strength within 7 days.
- The AAC does not show intensive heat release during the early ages. This indicates AAC has a low potential for thermal ingredient-induced cracking.
- The current mixtures of self-compacting AAC reach TRL 8 and can be already applied on an industrial scale for the production of structural precast elements.

ACKNOWLEDGEMENT

The authors would like to thank Microlab, Faculty of Civil Engineering and Geosciences, Delft University of Technology, and Haitsma Beton B.V. for the support throughout the project. The financial support from the Province of Friesland is also gratefully acknowledged.

URBCON - By-products for sustainable concrete in the urban environment

Wouter Crijns[1]

[1] ResourceFull, Belgium (E-mail: wouter.crijns@resourcefull.eu)

ABSTRACT

URBCON reduces the use of raw materials and CO_2 emissions from construction and maintenance of buildings and infrastructure in cities. The URBCON project targets the use of eco-friendly concrete as a building material. With the focus on the metropolitan areas of Ghent and Rotterdam, as well as the region of Westerlo, by-products such as metallic slags and incineration ashes are used as alternative raw materials for the production of concrete. Replacing primary raw materials with by-products could save an estimated 84 million tonnes of mineral building materials per year.

As an URBCON partner, ResourceFull has a long-term vision to drop worldwide CO_2 by 1%. ResourceFull is in close collaboration with multiple academic institutions and metallurgical players and in contact with a large group of innovative architects and construction companies. Over the years and through different applications, amongst other in Leuven, Gent and Westerlo, 4 kinds of sustainable concretes have been applied: (1) low impact binder combined with primary aggregates, major part of the Portland cement binder being replaced with alkali-activated ground granulated blast furnace slag (GGBFS); (2) low impact binder combined with secondary aggregates; (3) eco-friendly binder combined with primary aggregates, whereby the Portland cement is fully replaced with GGBFS; (4) eco-friendly binder with a blended AAM formulation applying different kinds of precursors to partially replace GGBFS.

Remarkable is the recently built fire escape stair case at the Zonnepoort school in the City of Ghent. This realisation is visited during the last afternoon of the DuRSAAM symposium.

Awards

Two best oral presenters have been recognized publicly at the end of the conference, one award by a jury of selected scientific committee members and one public award.

Considered selection criteria for the awards were as follows: presenters showcasing expertise in (an aspect of) AAMs, being passionate and convincing about the technology, and having a presentation memorable in advancing AAMs.

Best Presenter Jury Award to:

Luiz Miranda de lima Jr. *– "Influence of temperature on the kinetics of formation of sodium aluminosilicate hydrate gel" 6*

Best Presenter Public Award to:

C.B.M (Kees) Blom *– "Design and tendering experiences of a geopolymer concrete bridge" 184*

Partners

https://www.fib-international.org/

https://www.rilem.net/

https://www.fwo.be/en/

https://www.ugent.be/en

https://stad.gent/en

https://dursaam.ugent.be/

https://www.nweurope.eu/urbcon

Author index

About DuRSAAM

DuRSAAM is a collaborative PhD framework creating a critical mass of experts skilled in innovative alkali-activated material (AAM) concrete, as a key enabling technology for a sustainable and resilient built environment. AAM technology presents a new generation of materials, ideally conceived to respond to the need for more efficient, durable, eco-friendly and reliable construction, and utilizing by-product resources as raw materials. Modern concrete will be produced with low carbon footprint (CO2 emissions reduced by 80%), lower energy consumption and reduced use of primary resources (>1.5 t raw materials are quarried per t Portland cement clinker; this will be reduced by >60%), and with an addressable market for AAM binders of 5 B€/yr. DuRSAAM answers unmet industry demands, to facilitate emerging AAM technology for continued market entry and to unlock its potential in society.

The consortium brings together 7 academic (Ghent University, Delft University of Technology, Karlsruhe Institute of Technology, University of Sheffield, University of Zagreb, University of Patras, ETH Zurich) and 16 non-academic partners (Flemish Ministry of Public Works (MOW), FDN Engineering, City of Rotterdam, CRH, Bekaert, Owens Corning, T.EPI.KAT., LafargeHolcim, Argos, Aurubis, Gradmont, ResourceFull, Sanacon, Arcelor Mittal, CWare, City of Ghent), to excel in the scientific development and exploitation of AAM concrete, advancing design, modelling and practice beyond the state-of-the-art. It holds a unique focus on: (1) today's concerns of users and engineers that the durability and sustainability of AAM concrete is yet insufficiently quantified; and (2) provision of an AAM technology for rehabilitation of structures to meet the growing demand for renovation, to be developed in parallel with AAM for new concrete structures.

DuRSAAM runs from 2018 till 2023 and delivers world-leading training in this multidisciplinary field through 13 PhDs in interrelated aspects of AAM concrete, fibre reinforced high-performance concrete, and textile-reinforced mortar, as well as sustainability assessment. The outcomes will be instrumental in delivering a sustainable future in Europe's construction industry, which is increasingly driven by the growing demand for durable yet cost-effective solutions, driving a greater focus on reliable and comprehensive eco-efficient material technologies such as AAM.

The PhD Training Network on Durable, Reliable and Sustainable Structures with Alkali-Activated Materials

This project has received funding from the European Union's Horizon 2020 research and innovation programme under grant agreement No 813596 DuRSAAM.

DuRSAAM Symposium

Co-sponsorships:

fib CEB-FIP

rilem

fwo

Parking building with AAM
Photo by Nele & Jan

Advancing Alkali-Activated Materials

DuRSAAM 2023 Symposium | February 8-10, 2023 | Ghent, Belgium

Marie Curie Innovative Training Network
H2020-MSCA-ITN-2018-813596

Ghent University · TU Delft · KIT Karlsruhe Institute of Technology · The University of Sheffield · University of Patras · ETH zürich